



# Modelling and Simulation of Long-Term Dynamics in Power Systems

Taulant Kërçi

17203097

A thesis submitted to University College Dublin  
in fulfilment of the requirements for the degree of

**Doctor of Philosophy**

College of Engineering and Architecture  
School of Electrical & Electronic Engineering  
*Head of School:* Prof. John T. Sheridan

*Supervisor:* Prof. Federico Milano

November 2021

I hereby certify that the submitted work is my own work, was completed while registered as a candidate for the degree stated on the Title Page, and I have not obtained a degree elsewhere on the basis of the research presented in this submitted work.

© Taulant Kërçi, 2021. All Rights Reserved.

# Acknowledgements

First and foremost, I would like to thank my supervisor, Prof. Federico Milano, for giving me the opportunity to pursue a PhD at University College Dublin. I have been very fortunate to have him as a supervisor. His continuous support, help, motivation and feedback have contributed to the successful completion of this thesis. In particular, I wish to thank him for always finding the time for our weekly meetings and my questions. Working with him has been a pleasure and a challenge at the same time. A pleasure for two reasons: (i) his immense knowledge of power systems and other related and non-related fields have served as a great learning process; and (ii) he always supported me to implement my research ideas. A challenge because he always expects the best from you, and as such, it pushes you to the limits.

Second, I would like to thank Science Foundation Ireland for making this PhD work possible by funding me under project ESIPP, Grant No. SFI/15/SPP/E3125.

Next, I would like to thank all my colleagues at UCD for their invaluable help and for sharing everyday life on and off-campus. In particular, I want to thank Dr. Mohammed Ahsan Adib Murad, Dr. Georgios Tzounas, Dr. Ioannis Dassios, and Weilin Zhong for their friendship and excellent collaboration. I also wish to thank my Albanian friends in Ireland, Alban, Evis, Elida, Andi, Anisa, Ledi and Ola, and those back in Albania, Mariglen, Erlin, Donard, Andi, Pjerin and Grisild for being great friends.

Finally, I am grateful to my family and relatives. Thank you to my parents Sulejman and Sheqere, my wonderful wife Marina, my sister Arvenola, my brother Qazim, my nephew Eldjon, my niece Anduena and my brother and sister-in-law Ndriçim and Denada. They have always been my biggest supporters during this long journey with many ups and downs (of course, more downs) and given me unconditional love and encouragement.

*Taulant Kërçi*

*Dublin, November 2021*

*Familjes sime.*

# Abstract

A reliable and cost-effective operation of power systems involves different tasks over different time horizons ranging from tens of milliseconds (protection) to years (planning). Generally, power system operators routinely check the effectiveness of these tasks separately (depending on time constants) through computer studies based on mathematical models. While the modelling and simulation of short-term dynamics of power systems (e.g. electromagnetic and transient simulation) have received tremendous attention in the literature, that is not the case for long-term dynamics.

In this context, this thesis aims to assist power system operators in addressing the modelling and simulation of long-term dynamics in modern power systems (minutes to years). To do so, the thesis presents novel mathematical and software tools that allow studying the long-term impact interactions between different short-term electricity markets models and power systems, and the impact of energy policy incentives on the evolution of Renewable Energy Sources (RESs) technologies, particularly that of solar Photovoltaics (PVs).

Short-term electricity markets are essential tools to guarantee the reliable operation of the power system. They are moving closer to real-time and using finer time resolutions (e.g. 5 minutes) in response to the large-scale integration of variable RESs. This means that their dynamics evolve with a timescale similar to some long-term power system dynamics, e.g. the Automatic Generation Control (AGC). Consequently, assessing the impact interactions between such markets and the dynamic response of the power grid becomes increasingly important. The contributions on this topic are as follows:

(i) Investigate the effect of real-time electricity markets modelled as a sort of discrete AGC or Market-based Automatic Generation Control (MAGC) on power system dynamics. In particular, a thorough analysis using Time Domain Simulations (TDSs) is provided.

(ii) Propose a short-term dynamic electricity market model that includes the memory effect of market participants. Particularly, the effect of the memory of suppliers on the decision-making (generator schedules) and dynamic response of the grid is discussed.

(iii) Investigate the impact interactions between sub-hourly deterministic Unit Commitment (d-UC) and stochastic Unit Commitment (s-UC) and the power grid.

Furthermore, the thesis also proposes a dynamic model based on nonlinear delay Differential-Algebraic Equations (DAEs) able to predict the evolution of PV installations for different countries. This model is a valuable tool that can help policymakers in the decision-making process, such as the definition of the Feed-in Tariff (FIT) price and the duration of the incentives.

Finally, the proposed models and tools are duly validated throughout the thesis by means of numerical tests based on benchmark test systems.

# Contents

<b>List of Figures</b>	<b>ix</b>
<b>List of Tables</b>	<b>xv</b>
<b>Acronyms</b>	<b>xvii</b>
<b>1 Introduction</b>	<b>1</b>
1.1 Context and Research Motivation . . . . .	1
1.1.1 Subject Matter and Scope . . . . .	3
1.2 Thesis Overview . . . . .	4
1.2.1 Contributions . . . . .	4
1.2.2 Organization . . . . .	7
1.2.3 Publications . . . . .	8
<b>2 Impact of Discrete Secondary Controllers on Power System Dynamics</b>	<b>12</b>
2.1 Introduction . . . . .	12
2.2 Hybrid Power System Model . . . . .	12
2.3 Conventional AGC . . . . .	14
2.3.1 Illustrative Example on the AGC . . . . .	16
2.4 Market-based AGC . . . . .	22
2.4.1 Dynamic Electricity Market Model . . . . .	22
2.4.2 Analogy between AGC and MAGC . . . . .	23
2.4.3 Illustrative Example on the MAGC . . . . .	24
2.4.4 Inclusion of Non-Synchronous Devices . . . . .	29
2.5 Case Study 1: Contribution of ESSs to Long-Term Power System Dynamic Performance . . . . .	32

2.5.1	WSCC 9-bus System . . . . .	33
2.6	Case Study 2: Impact of the Aggregate Response of DERs . . . . .	38
2.6.1	AGC-based VPP . . . . .	39
2.6.2	MILP-based VPP . . . . .	39
2.6.3	Comparison between AGC-based and MILP-based VPP . . . . .	41
2.7	Conclusions . . . . .	42
<b>3</b>	<b>A Short-Term Dynamic Electricity Market Model with Memory Effect</b>	<b>44</b>
3.1	Introduction . . . . .	44
3.2	Modelling Economic Processes with Memory . . . . .	45
3.3	Proposed fractional-order electricity market model . . . . .	47
3.3.1	Modelling . . . . .	47
3.4	Solutions investigation . . . . .	52
3.5	Examples . . . . .	56
3.5.1	Example 1 . . . . .	56
3.5.2	Example 2 . . . . .	57
3.6	Concluding remarks . . . . .	62
<b>4</b>	<b>Interaction between Deterministic Sub-Hourly Unit Commitment and Power System Dynamics</b>	<b>65</b>
4.1	Introduction . . . . .	65
4.2	Need for Sub-hourly Modelling . . . . .	65
4.3	Deterministic Unit Commitment Formulation . . . . .	66
4.4	Interaction between d-UC and HDAEs . . . . .	70
4.5	Case Study 1: Impact of Different Scheduling Time Periods of d-UC . . . . .	71
4.6	Case Study 2: Impact of Different Net-Load Volatility and Control/Machine parameters . . . . .	77
4.7	Conclusions . . . . .	79
<b>5</b>	<b>Interaction between Stochastic Sub-Hourly Unit Commitment and Power System Dynamics</b>	<b>81</b>
5.1	Introduction . . . . .	81
5.2	Stochastic Long-Term Power System Model . . . . .	82
5.2.1	Modelling of stochastic processes . . . . .	83

5.3	Complete Stochastic Unit Commitment Formulation . . . . .	84
5.4	Simplified Stochastic Unit Commitment Formulation . . . . .	90
5.5	Alternative Stochastic Unit Commitment Formulation . . . . .	91
5.6	Interaction between s-UC and SDAEs . . . . .	92
5.7	Case Study 1: Impact of Different Scheduling Time Periods . . . . .	94
5.8	Case Study 2: Impact of Different s-UC and Frequency Controllers/Machine Parameters . . . . .	108
5.9	Conclusions . . . . .	116
<b>6</b>	<b>A Dynamic Behavioral Model of the Long-Term Development of Solar Photovoltaic Generation driven by Feed-in Tariffs</b>	<b>119</b>
6.1	Introduction . . . . .	119
6.2	FiT Evolution in Italy and Germany . . . . .	120
6.3	Proposed Model . . . . .	121
6.4	Model Validation . . . . .	126
6.5	Sensitivity Analysis . . . . .	133
6.6	Conclusions and Policy Implications . . . . .	143
<b>7</b>	<b>Conclusions and Future Work</b>	<b>146</b>
	<b>Appendices</b>	<b>149</b>
	<b>A Data</b>	<b>150</b>
A.1	Chapters 2 and 3 . . . . .	150
A.2	Chapters 4 and 5 . . . . .	151
A.3	Chapter 6 . . . . .	152
	<b>Bibliography</b>	<b>157</b>

# List of Figures

1.1	Tasks by timescales in power system operation [46]. . . . .	2
2.1	AGC control diagram. . . . .	15
2.2	Turbine governor control diagram. . . . .	16
2.3	Single line diagram of the IEEE Western Systems Coordinating Council (WSCC) 3-machine 9-bus system. . . . .	16
2.4	Transient response of $\omega_{CoI}(t)$ of the WSCC 9-bus system for different AGCgains. . . . .	17
2.5	Transient response of $\omega_{CoI}(t)$ of the WSCC 9-bus system for different AGCgains. . . . .	18
2.6	Transient response of $\omega_{CoI}(t)$ for different AGC time intervals. . . . .	18
2.7	Transient response of $\omega_{CoI}(t)$ for different AGC time intervals. . . . .	19
2.8	Transient response of $\Delta p(t)$ for different AGC time intervals. . . . .	19
2.9	Transient response of $\omega_{CoI}(t)$ for different AGC time intervals and with Rate of Change of Frequency (ROCOF) dead-band. . . . .	21
2.10	Transient response of $\omega_{CoI}(t)$ for different $\Delta p(t)$ limits. . . . .	21
2.11	MAGC control diagram. . . . .	23
2.12	Transient response of $\omega_{CoI}(t)$ for different MAGC time intervals. . . . .	25
2.13	Transient response of the electricity price $\rho(t)$ for different MAGC time intervals. . . . .	26
2.14	Transient response of $\omega_{CoI}(t)$ for different $\rho(t)$ limits. . . . .	27
2.15	Transient response of $\omega_{CoI}(t)$ using the AGC and MAGC. . . . .	27
2.16	Secondary frequency controller signals for the scenarios with MAGC only and with both MAGC and AGC. . . . .	28

2.17	Profit of generator 1 for the scenarios with MAGC only and with both MAGC and AGC. . . . .	29
2.18	Transient response of $\omega_{CoI}(t)$ for different wind power shares. . . . .	31
2.19	Transient response of the $\omega_{CoI}(t)$ for WPPs included and not included in to the MAGC, respectively. . . . .	32
2.20	The frequency control scheme of an Energy Storage System (ESS). . . . .	33
2.21	Transient response of $\omega_{CoI}(t)$ following a 10% instantaneous load increase without ESSs limits. . . . .	34
2.22	Transient response of $\omega_{CoI}(t)$ following a 10% instantaneous load increase with ESSs limits. . . . .	35
2.23	Transient response of $\omega_{CoI}(t)$ following a 10% instantaneous load increase with zero droop and without ESSs limits. . . . .	36
2.24	Transient response of $\omega_{CoI}(t)$ following a 10% instantaneous load increase with zero droop and with ESSs limits. . . . .	37
2.25	Transient response of $\omega_{CoI}(t)$ following a 10% instantaneous load increase with non-zero droop and without ESSs limits. . . . .	38
2.26	Transient response of $\omega_{CoI}(t)$ following a 10% instantaneous load increase with non-zero droop and with ESSs limits. . . . .	38
2.27	Transient response of ESS active power following a 10% instantaneous load increase with non-zero droop and with ESSs limits. . . . .	39
2.28	Basic AGC control scheme for active power regulation of Virtual Power Plants (VPPs). . . . .	40
2.29	Comparison of the impact of AGC-based and Mixed-Integer Linear Programming (MILP)-based VPP. . . . .	42
3.1	Oustaloup's recursive approximation block diagram. . . . .	58
3.2	<a href="#">Updated turbine governor control diagram with the AGC and MAGC outputs.</a>	58
3.3	Trajectories of the frequency of the CoI. . . . .	59
3.4	Trajectories of the MAGC active power schedules of generator 1. . . . .	59
3.5	Trajectories of the AGC active power set-point of generator 1. . . . .	60
3.6	Comparison of the trajectories of the frequency of the CoI as obtained with the I-MAGC and F-MAGC. . . . .	61
3.7	Trajectories of the MAGC active power schedules of generator 1. . . . .	62

3.8	Trajectories of the AGC active power set-point of generator 1. . . . .	62
3.9	Trajectories of the MAGC active power schedules of generator 1. . . . .	63
3.10	Trajectories of the AGC active power set-point of generator 1. . . . .	63
4.1	Interaction between the d-UC problem, AGC, Turbine Governors (TGs), synchronous machines and the grid. . . . .	70
4.2	Mechanical power of two relevant machines for the 15 minute scheduling period. . . . .	72
4.3	Frequency of the center of inertia for 15-minute scheduling period. . . . .	73
4.4	Frequency of the center of inertia for the 10 minute Unit Commitment (UC) scheduling period. . . . .	73
4.5	Frequency of the center of inertia for 7.5-minute d-UC scheduling period. . . . .	74
4.6	Frequency of the center of inertia for 3.75-minute scheduling period. . . . .	74
4.7	Mechanical power of the relevant machines for 15-minute scheduling and noise. . . . .	75
4.8	Frequency of the center of inertia for 15-minutes scheduling and noise. . . . .	75
4.9	Frequency of two synchronous machines following a contingency for the 15-minute scheduling. . . . .	76
4.10	Frequency of two synchronous machines following a contingency for the 3.75-minute scheduling. . . . .	76
5.1	Wind power 15min rate of change for 12 typical day in the Irish system in 2018. . . . .	88
5.2	Wind power profile for two typical days (Jan, Jul) in the Irish system in 2018. . . . .	89
5.3	Interaction between the s-UC problem, AGC, TGs, synchronous machines and the grid. . . . .	93
5.4	15-minute scheduling – Trajectories of $\omega_{CoI}(t)$ for 12h. . . . .	96
5.5	15-minute scheduling – Trajectories of wind speeds for 12h. Dashed lines indicate the high, medium and low scenarios, respectively, while black line indicate the same scenarios with inclusion of volatility. . . . .	96
5.6	15-minute scheduling – $\sigma_{CoI}$ as a function of wind uncertainty and volatility. . . . .	99
5.7	15-minute scheduling – Expected cost as a function of wind uncertainty and volatility. . . . .	99

5.8	5-minute scheduling – Trajectories of $\omega_{CoI}(t)$ for 12h. . . . .	101
5.9	5-minute scheduling – Trajectories of wind speeds for 12h. Dashed lines indicate the high, medium and low scenarios, respectively, while black line indicate the same scenarios with inclusion of volatility. . . . .	101
5.10	5-minute scheduling – $\sigma_{CoI}$ as a function of wind uncertainty and volatility.	103
5.11	5-min scheduling – Expected cost as a function of wind uncertainty and volatility. . . . .	103
5.12	s-UC and 25% wind penetration – Trajectories of the rotor speed of relevant machines following a contingency. . . . .	104
5.13	d-UC and 25% wind penetration – Trajectories of the rotor speed of relevant machines following a contingency. . . . .	104
5.14	s-UC and 50% wind penetration – Trajectories of the rotor speed of relevant machines following a contingency. . . . .	105
5.15	d-UC and 50% wind penetration – Trajectories of the rotor speed of relevant machines following a contingency. . . . .	105
5.16	15-minute scheduling – Trajectories of $\omega_{CoI}(t)$ for 10 s-UC wind power scenarios. . . . .	107
5.17	15-minute time period – $\sigma_{CoI}$ as a function of different frequency controllers/machine parameters using the complete s-UC and d-UC models.	110
5.18	15-minute time period – $\sigma_{CoI}$ as a function of different frequency controllers/machine parameters using the simplified and alternative s-UC models. . . . .	112
5.19	5-minute time period – $\sigma_{CoI}$ as a function of different frequency controllers/machine parameters. . . . .	112
5.20	Trajectories of $\omega_{CoI}(t)$ for 15-minute time period and complete s-UC. . .	113
5.21	Trajectories of $\omega_{CoI}(t)$ for 15-minute time period and simplified s-UC. . .	113
5.22	Trajectories of $\omega_{CoI}(t)$ for 15-minute time period and alternative s-UC model.	114
5.23	Mechanical power of synchronous generators 1, 2 and 4, for 15-minute time period and complete s-UC model. . . . .	115
5.24	Mechanical power of synchronous generators 1, 2 and 4, for 15-minute time period and simplified s-UC model. . . . .	115

5.25	Mechanical power synchronous generators 1, 2 and 4, for 15-minute time period and alternative s-UC model. . . . .	116
6.1	Italian case: Cumulative solar PV installations. . . . .	127
6.2	Italian case: Cumulative solar PV generation. . . . .	127
6.3	Italian case: Cumulative FiT fund. . . . .	128
6.4	Italian case: Solar PV cost. . . . .	128
6.5	Italian case: Solar PV FiT price. . . . .	129
6.6	Italian case: Willingness of people to install solar PVs. . . . .	129
6.7	German case: Cumulative solar PV installed. . . . .	130
6.8	German case: Cumulative solar PV generation. . . . .	130
6.9	German case: Solar PV cost. . . . .	131
6.10	German case: Cumulative FiT fund. . . . .	132
6.11	German case: Solar PV feed-in tariff price. . . . .	132
6.12	German case: Willingness of people to install solar PVs. . . . .	133
6.13	Italian case: Cumulative solar PV installed. . . . .	134
6.14	Italian case: Cumulative solar PV generation. . . . .	134
6.15	Italian case: Cumulative solar PV installed. . . . .	135
6.16	Italian case: Cumulative solar PV generation. . . . .	135
6.17	Italian case: Cumulative solar PV installed. . . . .	136
6.18	Italian case: Cumulative solar PV generation. . . . .	136
6.19	Italian case: Cumulative solar PV installed. . . . .	137
6.20	Italian case: Cumulative solar PV generation. . . . .	138
6.21	Italian case: Cumulative solar PV installed. . . . .	138
6.22	Italian case: Cumulative solar PV generation. . . . .	139
6.23	Italian case: Cumulative solar PV installed. . . . .	140
6.24	Italian case: Cumulative solar PV generation. . . . .	140
6.25	Italian case: Cumulative FiT fund. . . . .	141
6.26	Italian case: Solar PV FiT. . . . .	141
6.27	Italian case: Cumulative solar PV installed. . . . .	142
6.28	Italian case: Cumulative solar PV generation. . . . .	142
6.29	Italian case: Cumulative solar PV installed. . . . .	143
6.30	Italian case: Cumulative solar PV generation. . . . .	143

6.31 Italian case: Cumulative solar PV installed. . . . .	144
6.32 Italian case: Cumulative solar PV generation. . . . .	144

# List of Tables

4.1	15-minute scheduling with high noise – Standard deviation $\sigma$ of the frequency for different control/machine parameters . . . . .	78
4.2	15-minute scheduling with low noise – Standard deviations $\sigma$ of the frequency for different control/machine parameters . . . . .	78
4.3	5-minute scheduling with high noise – Standard deviations $\sigma$ of the frequency for different control/machine parameters . . . . .	79
4.4	5-minute scheduling with low noise – Standard deviations $\sigma$ of the frequency for different control/machine parameters . . . . .	79
5.1	15-minute scheduling – $\sigma_{CoI}$ for different s-UC probabilities with $j = 10\%$ .	97
5.2	15-minute scheduling – $\sigma_{CoI}$ for different s-UC probabilities and different $j$ .	98
5.3	15-minute scheduling – $\sigma_{CoI}$ for different stochastic unit commitment probabilities with $j = 10\%$ . . . . .	98
5.4	5-minute scheduling – $\sigma_{CoI}$ for different s-UC probabilities with $j = 3.333\%$ .	102
5.5	5-minute scheduling – $\sigma_{CoI}$ for different s-UC probabilities with $j = 3.333\%$ .	102
5.6	15-minute scheduling – $\sigma_{CoI}$ for different s-UC probabilities with $j = 10\%$ and 50% wind penetration. . . . .	107
5.7	15-minute scheduling – Different s-UC probabilities with $j = 10\%$ and 10 wind power scenarios. . . . .	108
5.8	15-minute scheduling – $\sigma_{CoI}$ for different s-UC probabilities with $j = 10\%$ and 10 wind power scenarios. . . . .	108
A.1	DERs data for the MILP-based VPP. Based on [14]. . . . .	150
A.2	Parameters for AGC and MAGC. Based on [6]. . . . .	151
A.3	d-UC and s-UC parameters. Based on [18, 19]. . . . .	151
A.4	Variables . . . . .	152

A.5	Parameter values, Italy. Based on this work and [1,104,112]. . . . .	153
A.6	PV historical data, Italy. Based on this work and [59,80,112]. . . . .	154
A.7	Parameter values, Germany. Based on this work and [41,53,103]. . . . .	155
A.8	PV historical data, Germany. Based on this work and [7,10,103]. . . . .	156

# List of Acronyms and Abbreviations

<b>AGC</b>	Automatic Generation Control
<b>AVR</b>	Automatic Voltage Regulator
<b>CoI</b>	Center of Inertia
<b>d-UC</b>	deterministic Unit Commitment
<b>DAE</b>	Differential-Algebraic Equation
<b>DER</b>	Distributed Energy Resource
<b>ESS</b>	Energy Storage System
<b>ENTSO-E</b>	European Network of Transmission System Operators for Electricity
<b>FiT</b>	Feed-in Tariff
<b>F-MAGC</b>	Fractional-Order MAGC
<b>HDAE</b>	Hybrid Differential-Algebraic Equation
<b>I-MAGC</b>	Integer-Order MAGC
<b>LPF</b>	Low-Pass Filter
<b>MAGC</b>	Market-based Automatic Generation Control
<b>MILP</b>	Mixed-Integer Linear Programming
<b>MC</b>	Monte Carlo Method
<b>ORA</b>	Oustaloup's Recursive Approximation
<b>PV</b>	Photovoltaic

<b>PSS</b>	Power System Stabilizer
<b>PFC</b>	Primary Frequency Control
<b>PI</b>	Proportional Integral
<b>RES</b>	Renewable Energy Source
<b>RoCoF</b>	Rate of Change of Frequency
<b>SFC</b>	Secondary Frequency Control
<b>SDAE</b>	Stochastic Differential-Algebraic Equation
<b>SDE</b>	Stochastic Differential Equation
<b>s-UC</b>	stochastic Unit Commitment
<b>TDS</b>	Time Domain Simulation
<b>TSO</b>	Transmission System Operator
<b>TG</b>	Turbine Governor
<b>UC</b>	Unit Commitment
<b>VPP</b>	Virtual Power Plant
<b>WSCC</b>	Western Systems Coordinating Council

# Notation

This section states the notation adopted throughout the thesis.

## Vectors and Matrices

$a, A$	scalar
$\mathbf{a}, \mathbf{a}$	vector
$\mathbf{A}, \mathbf{A}$	matrix
$\mathbf{I}_n$	identity matrix of dimensions $n \times n$
$\mathbf{0}_{n_x, n_y}$	zero matrix of dimensions $n_x \times n_y$

## Sets and Units

$\mathcal{C}^n$	$n$ time continuously differentiable functions
$\mathbb{C}$	complex numbers
$\mathcal{D}$	set of demands $l$
$\mathcal{F}$	set of transmission lines
$\mathcal{G}$	set of dispatchable generators $g$
$\mathcal{K}$	set of stochastic power production units $k$
$\mathcal{M}$	set of nodes $m \in \mathcal{N}$ that are connected to node $n$ by a transmission line
$\mathcal{N}$	set of nodes $n$
$\mathbb{N}$	natural numbers
$\mathbb{R}$	real numbers
$\mathcal{T}$	set of time periods $t$
$\mathbb{Z}$	integer numbers
$\mathcal{S}$	set of scenarios $\xi$

## Time and Frequency Domain

$a(t)$	time domain quantity
--------	----------------------

$\dot{a}(t)$	first order derivative
$\ddot{a}(t)$	second order derivative
$a^{(n)}(t)$	$n$ -th order derivative (of fractional order or of integer order $\geq 3$ )
$a(s)$	Laplace domain quantity
$\mathcal{L}$	Laplace transform
$s$	complex Laplace variable

## Eigenvalues and Eigenvectors

$\mathbf{V}$	right eigenvector matrix
$\mathbf{W}$	left eigenvector matrix
$\mu$	multiplicity of infinite eigenvalue
$\nu$	number of finite eigenvalues
$\lambda$	eigenvalue

## Parameters

$b$	fixed bid coefficient
$B$	susceptance
$c$	proportional bid coefficient
$C$	production cost constant
$E_C$	total energy consumption
$E_G$	total energy generation
$h$	time step size
$H$	inertia constant
$I$	reference PV yield
$\mathcal{I}_d$	integral deviation coefficient
$K$	control gain
$L_R$	learning rate
$L_P$	levy constant
$M$	mechanical starting time
$P_R$	performance ratio
$R$	generator response time
$R$	generator ramp
$\mathcal{R}$	droop constant of primary frequency control
$T$	time constant

$X$	reactance
$\alpha$	fractional-order
$\beta$	learning parameter
$\pi_\xi$	probability of scenario $\xi$
$\tau$	time delay

### Variables and Functions

$d$	load demand
$e_s$	supply for goods
$e_d$	demand for goods
$p$	active power
$q$	stock
$r$	active power reserve
$t$	time
$u$	input signal
$v$	wind speed
$w$	willingness of people
$W$	wind power penetration level
$x$	state variable
$y$	algebraic variable
$z$	discrete variable
$\gamma$	memory function
$\Gamma$	gamma function
$\delta$	angular position
$\Delta p$	output of AGC/MAGC controller
$\varepsilon$	cumulative revenues
$\zeta$	white noise
$\eta$	stochastic variable
$\theta$	voltage phase angle
$\Theta$	FiT price
$\vartheta$	PV cost
$\iota$	mean reversion speed
$\varpi$	goods price
$\rho$	electricity price

$\sigma$	standard deviation
$v$	cumulative solar PV generation
$\phi$	decreasing function for FiT
$\Phi$	number of PV MW installed
$\varphi$	solar PV generation
$\chi$	cumulative expenses
$\omega$	angular speed

### Superscripts and Subscripts

Alt	alternative
$C$	consumption
$d$	demand
D	decrease in the active power output
$D$	deterministic
$F$	fixed variable production cost
$g$	generator
$G$	generation
$h$	high
$l$	low
$L$	involuntary load curtailment
$m$	medium
m	mechanical
min	minimum
max	maximum
$o$	initial condition
$pv$	photovoltaic
ref	reference
$s$	supply
$S$	stochastic
$SH$	load that is involuntarily shed
Sim	simplified
$SU$	start-up
$SD$	shut-down
U	increase in the active power output

$V$  variable production cost

# Chapter 1

## Introduction

### 1.1 Context and Research Motivation

Modern power systems have dramatically evolved over the last decades. In particular, two significant changes have been taking place, namely the deregulation of the energy industry and the replacement of conventional large-scale power plants with converter-based RESs (e.g. wind and solar) and Distributed Energy Resources (DERs) (e.g. ESSs and flexible loads). The changes are mainly driven by economic and environmental factors, respectively. Among the deregulation activities, it is worth mentioning the liberalisation of the electricity markets and the separation of generation, transmission and distribution. These transformations have brought massive challenges to power system operators to ensure a reliable electricity supply.

A reliable and cost-effective electricity supply involves different tasks over different time horizons. Figure 1.1 shows the main tasks by timescales in power system operation [46]. Transmission System Operators (TSOs) need to ensure the continuous balance between generation and demand through various frequency control strategies like, for example, the AGC (minutes timescale). Furthermore, system operators need to establish the generation schedules through a day-ahead market clearing mechanism (e.g. UC). TSOs also are responsible for the continuous development of the high voltage grid infrastructure to deal with, for example, the integration of highly variable and uncertain RESs (years timescale). On the other hand, wholesale electricity markets need to provide adequate investment signals to invest in or expand generation capacity (years timescale). Finally,

governments need to introduce incentive policies to support the development of various RESs technologies like, for example, wind and solar PVs (years timescale).

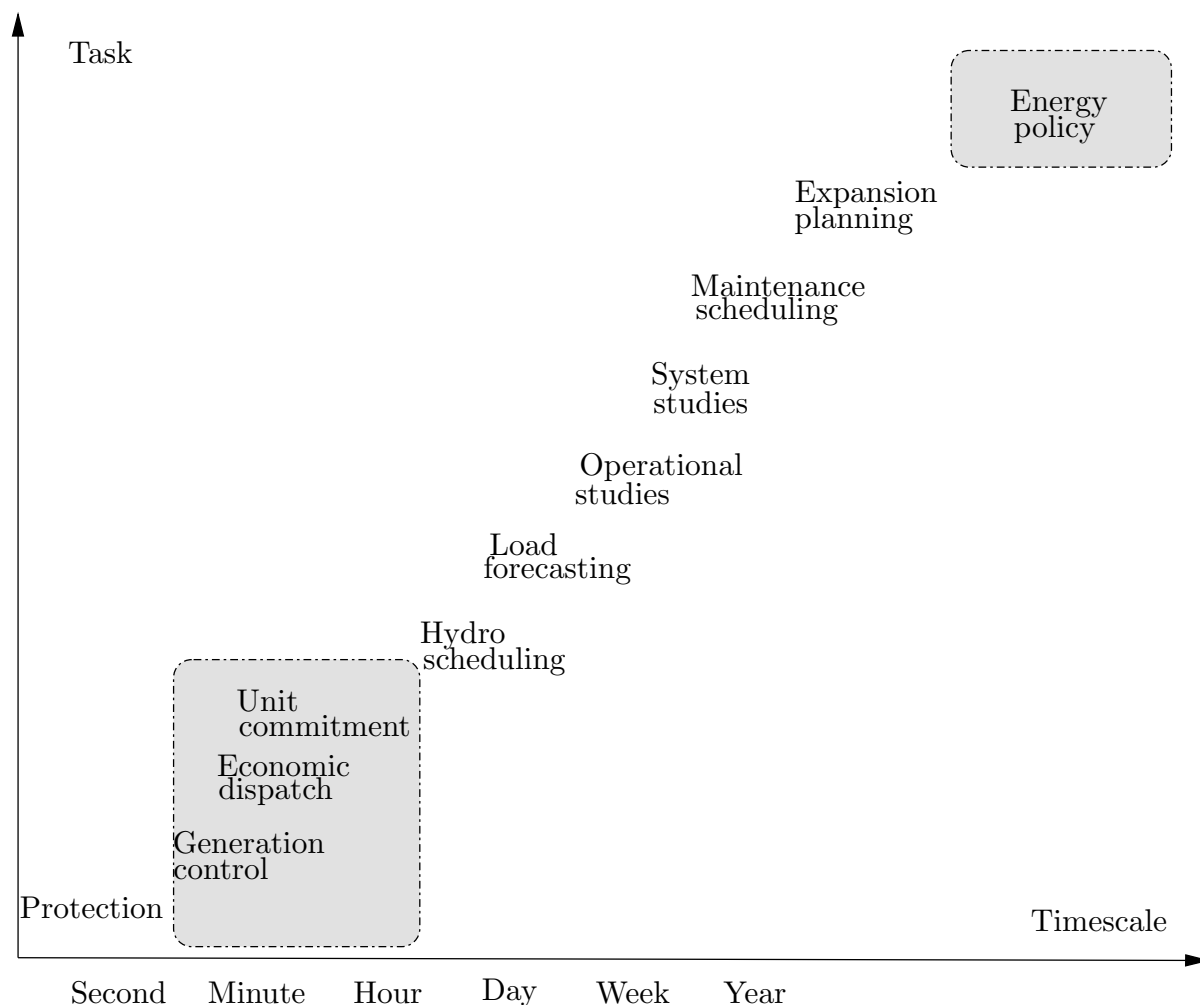


Figure 1.1: Tasks by timescales in power system operation [46].

Power system operators ensure a safe, secure and reliable electricity supply by conducting detailed analyses and simulations of each of the above tasks. Any analysis and simulation have to be performed by means of a mathematical model, which, based on a set of equations, allows us to know their behavior under different conditions [46]. However, a mathematical model that includes all tasks in Fig. 1.1 is intractable in practice due to computational issues. For this reason, TSOs necessarily employ a study time segmentation of tasks based on time scales. While the modelling and simulation of short-term dynamics of power systems (e.g. electromagnetic and transient simulation) have received tremendous attention, that is not the case of the long-term dynamics [55]. This thesis attempts to fill this gap.

### 1.1.1 Subject Matter and Scope

This thesis addresses two main research questions: (i) how to systematically study the long-term impact interactions between short-term electricity markets and the power grid; (ii) how to assess the impact of RESs incentives on their long-term development. To tackle these research questions, the thesis presents novel tools to help TSOs and policymakers address the modelling and simulation of the long-term dynamics in modern power systems. In particular, the dissertation focuses on the modelling and simulation of the AGC, sub-hourly UC, and the energy policy (see the shaded areas in Fig. 1.1). This choice is motivated by the fact that there is a concern on the coupling between the dynamic response of the power system and short-term electricity markets because of the similar timescales.

Such markets, e.g. balancing (real-time) markets, currently operate in time intervals as short as 5-15 minutes in order to offer additional operational flexibility [71, 82]. The utilization of sub-hourly time intervals as opposed to the conventional hourly intervals is a trend that is expected to further continue in power system markets with high penetration of RESs [37, 78]. For example, the European Network of Transmission System Operators for Electricity (ENTSO-E) has recommended that in order to tackle the phenomena of deterministic frequency deviation in the European power systems the following measures have to be taken: *Introduction of 15-minute market schedules and balancing; Introduction of 15-minute period imbalance settlement in each balancing area* [38]. Likewise, the Australian energy market operator plans to use a 5-minute imbalance period by 2021 [3]. Sub-hourly modelling is thus to be preferred compared to the conventional hourly dispatch.

However, as aforementioned, sub-hourly electricity markets, e.g. 5-minute resolution, can overlap with long-term power system dynamics. The first studies that have looked at this problem date back to around two decades ago when Alvarado used first-order differential equations to describe the dynamics of a short-term electricity market model [5]. Since then, numerous works have studied the same problem in the literature, for example, we cite [105] and [20].

On the other hand, a powerful way to understand the long-term behavior of incentive policies and capture the interactions among their variable components, is to construct proper dynamic models and simulate their response over different scenarios. To this aim, the thesis proposes a novel mathematical tool to help understand the coupling between

incentives and the actual installed capacity of PV panels. This is considered key for the design of policies under different scenarios [92].

Finally, throughout the thesis, the proposed software and mathematical tools are tested by means of computer-based simulations.

## 1.2 Thesis Overview

### 1.2.1 Contributions

The goal of this dissertation is twofold: (i) provide TSOs useful software and mathematical tools to evaluate possible interactions between different short-term electricity market formulations and power system dynamic response; (ii) provide a useful mathematical tool to energy policymakers to predict the evolution of RESs technologies, particularly that of PVs. In particular, the contributions of the thesis are in three directions, namely assess the effect of discrete AGC/MAGC on power system dynamics, study the interactions between the sub-hourly UC and the power grid, and understand the coupling between incentives and the actual installed capacity of PVs.

### Automatic Generation Control

The AGC is an essential component in the secure operation of the power system. Installed in the control centers of TSOs, it coordinates dispatchable generating units to ensure the power balance in real-time. This thesis uses the AGC approach in four ways: (i) by studying the impact of discrete AGC and MAGC on power system dynamics; (ii) by exploring the effectiveness of ESS in mitigating the long-term frequency deviations caused by large MAGC time intervals; (iii) by presenting an AGC-based approach for the coordination of DERs that form a VPP and comparing its performance to a MILP-based scheduling approach; and (iv) by proposing a MAGC model with the inclusion of memory effect of market participants, particularly that of suppliers.

#### 1. *AGC and MAGC:*

The AGC coordination consists in a set of set-points sent to the generators every 2-6 s. So far, this time interval has shown to be adequate to return the frequency to the target value and has not created any stability issue. The first part of Chapter 2

indicates a range of values, from few tens of seconds to few minutes, of the execution cycles of conventional AGC that leads to a limit cycle. This result serves as a motivation to study the same phenomenon when considering real-time electricity markets with short trading intervals. With this aim, a formal analogy between the AGC and real-time electricity markets modeled as a sort of MAGC is provided. Such an analogy then serves to study the impact of discrete MAGC time intervals on power system dynamics.

## 2. *Converter-interfaced ESSs:*

Converter-interfaced ESSs are an emerging technology of modern power systems. They have gained high interest in recent years due to their ability to add increased flexibility to power systems by smoothing the variable output of non-dispatchable power production such as RESs.

This thesis explores the potential application of the converter-interfaced ESS and its control parameters in removing long-term power system frequency deviations caused by large MAGC time intervals. A comprehensive analysis of the performance of ESSs show that, while ESSs can significantly reduce the frequency oscillations, two parameters of the ESS primary frequency control, namely deadband and droop, have to be carefully designed to avoid undesirable fluctuations of the frequency.

## 3. *AGC-based VPP:*

The penetration of DERs creates additional challenges for TSOs mainly due to their uncertain and variable nature and the lack of visibility (i.e. mostly connected on the distribution level). For this reason, it is essential to manage DERs to better contribute to electricity markets and system operation. A way to address this problem is to make use of the VPP concept. A VPP is generally composed of different DERs technologies, including conventional (e.g. gas power plants) and non-conventional (e.g. wind power plants) generating units, ESSs and flexible loads, and operates as a single transmission-connected generator.

This thesis proposes a simple yet efficient AGC approach for VPPs. The proposed approach is compared to that of the VPPs based on MILP scheduling. It is shown that the AGC-based approach leads to a better dynamic performance of the system.

#### 4. *Fractional MAGC:*

Considering the memory of market participants is of utmost importance in economic processes as they can remember the changes of economic indicators and factors in the past. To this aim, the thesis proposes a short-term dynamic electricity market model with the inclusion of memory effect. The memory is represented through fractional-order derivatives. Chapter 3 presents an in-depth comparison of the impact of fractional and integer-order market models on the decision-making process of suppliers and on the overall dynamic performance of the grid.

#### **Unit Commitment**

The short-term scheduling of power generation, often known as the UC, is a crucial decision-making component in the operation of power systems. This is because the scheduling of generators determines the level of system inertia in the system and the amount of available reserves. This thesis presents a software framework to include the UC problem into TDS. The proposed framework models the UC problem as a slow “discrete controller” that responds to the time-varying loading condition of the grid by changing the power order set-points of the TGs of the power plants. Such a framework is a valuable tool for TSOs to understand the impact interactions of different UC formulations, including sub-hourly d-UC and s-UC with the actual dynamic response of the grid.

#### **PV Energy Policy**

The development of RESs technologies like wind and solar PV is directly related to incentives policies introduced by governments. For example, the solar PV market has seen a significant increase over the past two decades due to extremely favorable incentives policies and installation cost reduction. This thesis presents a simple yet accurate dynamic model for the long-term development of solar PV generation. A simple and practical model, in fact, is much more likely to be implemented and used in practice by policymakers. The model uses the *learning-by-doing* concept, FIT budget and people’s willingness to install PVs to predict the evolution of PV installations. In particular, the *learning-by-doing* concept to model the PV cost and consequently the PV development is proposed for the first time in this thesis. Further, the thesis provides a thorough validation of the proposed model through the Italian and German cases. This is considered an advantage

of the current dynamic model compared to others proposed in the literature that only focus on one PV market.

\* \* \*

All models developed in the course of this thesis are implemented and simulations are carried out using the Python-based power system analysis software tool Dome [85]. In addition, the optimization problems considered in this thesis, e.g. d-UC and s-UC, are implemented in the Python language and solved using Gurobi [49].

## 1.2.2 Organization

The remainder of the thesis is organized as follows.

Chapter 2 provides a systematic study on the impact of discrete secondary frequency controllers on the dynamic response of power systems. At first, the deterministic power system model based on Hybrid Differential-Algebraic Equations (HDAEs) is presented. Then, the effect of conventional discrete AGC and MAGC is discussed through various illustrative examples using the well-known WSCC test system. In addition, Chapter 2 examines the potential application of converter-interfaced ESS in removing the long-term frequency deviations originated by the MAGC. Finally, the chapter compares the dynamic performance of two VPP secondary frequency controllers, namely AGC-based VPP and MILP-based VPP.

Chapter 3 presents a short-term dynamic electricity market model with memory effect. First, the chapter describes the modelling of economic processes with memory using fractional calculus. Subsequently, the proposed fractional-order market model and its solutions is presented. The WSCC 3-machine 9-bus system is then employed to compare the impact of integer and fractional market models on suppliers' decision-making and power system dynamics.

Chapter 4 focuses on the interactions between sub-hourly d-UC and power system dynamics. The need for sub-hourly modelling in power systems is first discussed. Subsequently, a conventional MILP d-UC problem is introduced. Next, Chapter 4 proposes a software framework to embed the d-UC problem into the TDS routine of Dome. Finally, two case studies are carried out employing the IEEE 39-bus system

to assess the impact of different scheduling periods of the d-UC and different net-load volatility and control/machine parameters.

Chapter 5 focuses on the interactions between sub-hourly s-UC and power system dynamics. With this aim, the chapter presents the stochastic long-term power system model based on Stochastic Differential-Algebraic Equations (SDAEs). Next, Chapter 5 introduces different s-UC formulations, namely complete, simplified, and alternative. Then, the chapter provides a modified version of the proposed software framework that embeds various s-UC problems into the TDS routine of Dome. Similar to Chapter 4, two case studies are then carried out by means of the IEEE 39-bus system to assess the impact of different scheduling periods and different s-UC formulations.

Chapter 6 proposes a dynamic behavioral model of the long-term development of solar PV generation driven by FITs. First, the chapter provides a background of FITs schemes in two of the biggest PV markets in the world, namely Italy and Germany. The proposed dynamic model is then validated against historical data of the two PV markets. Finally, a parametric analysis is carried out using the Italian case, where crucial parameters of the model are identified.

Finally, Chapter 7 concludes the thesis, summarizes the most relevant conclusions, and suggests directions for future work.

### 1.2.3 Publications

This section provides the list of publications that gave rise to the work presented in this thesis.

#### Journal papers

##### (Published)

1. I. Dassios, **T. Kërçi**, and F. Milano, Fractional-order dynamical model for electricity markets, *Mathematical Methods in the Applied Sciences*, Wiley, accepted on Sep. 2021, in press.
2. **T. Kërçi**, M. A. A. Murad, I. Dassios, and F. Milano, On the Impact of Discrete Secondary Controllers on Power System Dynamics, *IEEE Transactions on Power Systems*, vol. 36, no. 5, pp. 4400-4409, Sept. 2021. DOI: 10.1109/TPWRS.2021.3061584.

3. **T. Kërçi**, J. Giraldo, and F. Milano, Analysis of the impact of sub-hourly unit commitment on power system dynamics, *International Journal of Electrical Power & Energy Systems*, vol. 119, pp. 105819, Jan. 2020. DOI: 10.1016/j.ijepes.2020.105819.
4. **T. Kërçi**, J. Giraldo, and F. Milano, Sensitivity analysis of the impact of the sub-hourly stochastic unit commitment on power system dynamics, *Energies*, MDPI, *Special Issue: Power System Simulation, Control and Optimization*, vol. 13, no. 6, Mar. 2020. DOI: 10.3390/en13061468.

(Submitted)

5. **T. Kërçi**, G. Tzounas, and F. Milano, A Dynamic Behavioral Model of the Long-Term Development of Solar Photovoltaic Generation driven by Feed-in Tariffs, *Energy*, Elsevier, submitted in Sep. 2021.

## Book Chapters

6. **T. Kërçi**, W. Zhong, A. Moghassemi, F. Milano and P. Moutis, *Frequency Control and Regulating Reserves by VPPs*, in *Scheduling and Operation of Virtual Power Plants*, Elsevier, expected date of publication in Nov. 2021.

## Technical Reports

7. G. Tzounas, J. Chen, **T. Kërçi**, W. Zhong, and F. Milano, Frequency Control Concepts for Current VPPs in Large Scale Deployment, edgeFLEX, Mar. 2021. [Online]. Available: [https://www.edgeflex-h2020.eu/files/content-edgeflex/Content\\_Pages/Progress/Deliverables/edgeFLEX\\_883710\\_D2.2.pdf](https://www.edgeflex-h2020.eu/files/content-edgeflex/Content_Pages/Progress/Deliverables/edgeFLEX_883710_D2.2.pdf)
8. G. Tzounas, F. Milano, J. Chen, **T. Kërçi**, W. Zhong, D. Nouti, and G. Lipari, Scenario Description for Frequency and Inertia Response Control for VPPs, edgeFLEX, Mar. 2021. [Online]. Available: [https://www.edgeflex-h2020.eu/files/content-edgeflex/Content\\_Pages/Progress/Deliverables/edgeFLEX\\_883710\\_D2.1.pdf](https://www.edgeflex-h2020.eu/files/content-edgeflex/Content_Pages/Progress/Deliverables/edgeFLEX_883710_D2.1.pdf)

## Conference Papers

9. **T. Kërçi**, G. Tzounas, I. Dassios, M. A. A. Murad, and F. Milano, A Short-Term Dynamic Electricity Market Model with Memory Effect, IEEE PES General Meeting, Washington, DC, on-line event, 25-29 July 2021.
10. **T. Kërçi**, M. A. A. Murad, I. Dassios, and F. Milano, Contribution of Energy Storage Systems to Long-Term Power System Dynamic Performance, PowerTech, Madrid, Spain, on-line event, 27 June - 2 July 2021.
11. **T. Kërçi**, M. T. Devine, M. A. A. Murad, and F. Milano, Impact of the Aggregate Response of Distributed Energy Resources on Power System Dynamics, IEEE PES General Meeting, Montreal, QC, on-line event, 2-6 August 2020. **The paper was included in the session Best Conference Papers on Power System Dynamics, Control, and Protection.**
12. **T. Kërçi**, and F. Milano, Sensitivity Analysis of the Interaction between Power System Dynamics and Unit Commitment, PowerTech, Milano, Italy, 23-27 June 2019.
13. **T. Kërçi**, and F. Milano, A Framework to embed the Unit Commitment Problem into Time Domain Simulations, 19th International Conference on Environmental and Electrical Engineering (EEEIC), Genova, Italy, 11-14 June 2019.
14. P. Beagon, M. D. Bustamante, M. T. Devine, S. Fennell, J. Grant-Peters, C. Hall, Róisín Hill, **T. Kërçi**, and G. O'Keefe, Optimal scheduling of distributed generation to achieve linear aggregate response, Proceedings from the 141st European Study Group with Industry, University College Dublin, Ireland, 25-29 June 2018.

### (Other publications)

15. F. Milano, G. Tzounas, I. Dassios, **T. Kërçi**, Applications of the Frenet Frame to Electric Circuits, IEEE Transactions on Circuits and Systems I: Regular Papers, submitted in Sep. 2021.
16. W. Zhong, **T. Kërçi**, and F. Milano, On the Impact of Topology on the Primary Frequency Control of Virtual Power Plants, PowerTech, Madrid, Spain, on-line event, 27 June - 2 July 2021.

17. J. McMahon, **T. Kërçi**, and F. Milano, Combining Flexible Loads with Energy Storage Systems to provide Frequency Control, IEEE PES IGST-Asia 2021, submitted in May. 2021.
18. J. Giraldo, M. A. A. Murad, **T. Kërçi**, and F. Milano, Impact of Decentralized Microgrids Optimal Energy Management on Power System Dynamics, 22nd Power Systems Computation Conference, Porto, Portugal - June 27 - July 1, 2022, in preparation.
19. M. Adeen, **T. Kërçi**, and F. Milano, On the Impact of Correlated Stochastic Disturbances on Automatic Generation Control Systems, IEEE PES General Meeting, Denver, CO, USA, 17-21 July, 2022, in preparation.
20. **T. Kërçi**, M. A. A. Murad, G. Tzounas, J. C. Olives-Camps, and F. Milano, Validation of the Novel Concept of Geometric Frequency, IEEE PES General Meeting, Denver, CO, USA, 17-21 July, 2022, in preparation.

# Chapter 2

## Impact of Discrete Secondary Controllers on Power System Dynamics

### 2.1 Introduction

This chapter provides a comprehensive analysis of the impact of various secondary frequency controllers, namely AGC, MAGC, AGC-based VPP, and MILP-based VPP, on the dynamic response of power systems. The chapter is organized as follows. Section 2.2 presents the dynamic model of power systems based on HDAEs. Section 2.3 and 2.4 discuss the impact of discrete AGC and MAGC on power system dynamics through various illustrative examples. Section 2.5 provides a case study regarding the contribution of ESSs to long-term power system dynamic performance. Section 2.6 compares AGC-based VPP and MILP-based VPP dynamic performance through a case study on the IEEE 39-bus system. Finally, conclusions are drawn in Section 2.7.

### 2.2 Hybrid Power System Model

Power systems are intrinsically hybrid dynamical systems due to interactions between continuous dynamics and discrete events. They can be formulated as a set of nonlinear

HDAEs [84], as follows:

$$\begin{aligned}\dot{\mathbf{x}} &= \mathbf{f}(\mathbf{x}, \mathbf{y}, \mathbf{u}, \mathbf{z}), \\ \mathbf{0}_{n_y,1} &= \mathbf{g}(\mathbf{x}, \mathbf{y}, \mathbf{u}, \mathbf{z}),\end{aligned}\tag{2.1}$$

where  $\mathbf{f}$  are the differential equations,  $\mathbf{g}$  are the algebraic equations,  $\mathbf{x}, \mathbf{x} \in \mathbb{R}^{n_x}$  are the state variables, e.g. generator rotor speeds, and  $\mathbf{y}, \mathbf{y} \in \mathbb{R}^{n_y}$ , are the algebraic variables, e.g. bus voltage angles;  $\mathbf{u}, \mathbf{u} \in \mathbb{R}^{n_u}$ , are the inputs, e.g. load forecast, generator bids; and  $\mathbf{z}, \mathbf{z} \in \mathbb{N}^{n_z}$ , are the discrete variables, e.g. status of the machines. The functions  $\mathbf{f}, \mathbf{g}$  are at least  $C^1$ .

The set of nonlinear HDAEs (2.1) is a special case of a singular system of nonlinear hybrid differential equations in the following form:

$$\mathbf{E}\dot{\boldsymbol{\psi}} = \mathbf{F}(\boldsymbol{\psi}, \mathbf{u}, \mathbf{z}),\tag{2.2}$$

where

$$\mathbf{E} = \begin{bmatrix} \mathbf{I}_{n_x} & \mathbf{0}_{n_x, n_y} \\ \mathbf{0}_{n_y, n_x} & \mathbf{0}_{n_y, n_y} \end{bmatrix}, \quad \boldsymbol{\psi} = \begin{bmatrix} \mathbf{x}(t) \\ \mathbf{y}(t) \end{bmatrix},$$

and

$$\mathbf{F}(\boldsymbol{\psi}, \mathbf{u}, \mathbf{z}) = \begin{bmatrix} \mathbf{f}(\mathbf{x}, \mathbf{y}, \mathbf{u}, \mathbf{z}) \\ \mathbf{g}(\mathbf{x}, \mathbf{y}, \mathbf{u}, \mathbf{z}) \end{bmatrix}.$$

An hybrid system is a set of systems of differential equations where transition conditions from one system to another in that set of systems play an important role. This can be easily seen from the following example. Let  $\mathbf{z} \in \{\mathbf{z}_1, \mathbf{z}_2\}$ ,  $\mathbf{z}_1, \mathbf{z}_2$  constant vectors in  $\mathbb{N}^{n_z}$ ;  $\mathbf{z}_1, \mathbf{z}_2$  can then be considered as two different modes and (2.2) can be split into two systems:

$$\mathbf{E}\dot{\boldsymbol{\psi}} = \mathbf{F}(\boldsymbol{\psi}, \mathbf{u}, \mathbf{z}_1), \quad \mathbf{E}\dot{\boldsymbol{\psi}} = \mathbf{F}(\boldsymbol{\psi}, \mathbf{u}, \mathbf{z}_2).$$

In this case, there will be two systems of singular non-linear differential equations. However, the index set of the mode transitions as well as the transition conditions should be taken into account and defined. In general, (2.2) can be rewritten as  $\mathbf{E}\dot{\boldsymbol{\psi}} = \mathbf{F}(\boldsymbol{\psi}, \mathbf{u}, \mathbf{z}_i)$ ,  $i = 0, 1, 2, \dots, N$ ,  $\mathbf{z}_i$  constant. Then each singular nonlinear system is only defined in a certain interval  $t \in [t_i, t_{i+1})$ ,  $i = 0, 1, 2, \dots, N$ .

Equations (2.1) and (2.2) are utilized to emulate the transient behavior of power systems. These equations include the dynamic models of synchronous machines, TGs,

Automatic Voltage Regulators (AVRs), Power System Stabilizers (PSSs) and the discrete model of the AGC and MAGC, to name a few.

It is important to note that tools for the stability analysis of nonlinear hybrid dynamical systems are quite limited. The nonlinearity prevents the use of methods that require a linear set of equations and this eliminates the vast majority of available techniques. The Lyapunov stability theory has been widely utilized for the analysis of nonlinear systems, including power systems. However, due to the dissipative nature of power systems, even assuming that a Lyapunov function can be found, the Lyapunov theory would not provide sufficient and necessary conditions and is thus of limited practical use. The only fully general approach to study the stability of power systems that does not require shortcuts or simplifications is the TDS. This is the approach utilized in this thesis.

## 2.3 Conventional AGC

The Secondary Frequency Control (SFC), also known as AGC (in ENTSO-E terminology known as the frequency restoration process), is a centralized secondary regulator implemented in the control centers of TSOs. It follows and reinstates frequency to the nominal value, while it may also restore power exchanges between different areas to their scheduled values. This action is achieved through continuously monitoring the MW output of the controllable generating units. Typically, AGC dynamics take place in the time scale of minutes, e.g. 10 minutes [86]. In practice, the AGC is implemented in a discrete form. That is, the AGC sends power signals to participating generating units at fixed intervals, e.g. every 2-6 seconds [9, 95]. This time interval has shown to be adequate in managing real-time power mismatches and has not caused any power system instability.

Figure 2.1 shows a standard control scheme of an AGC. The input of the controller is the difference between the reference frequency  $\omega^{\text{ref}}$  and the measured frequency  $\omega_{\text{CoI}}(t)$ , that is, the Center of Inertia (CoI). Note that in practice TSOs use the frequency of a pilot bus of the system as an input for the AGC. Next, the main controller of the AGC is an integral control with gain  $K_o$ , as follows:

$$\Delta p(t) = K_o(\omega^{\text{ref}} - \omega_{\text{CoI}}(t)), \quad (2.3)$$

where  $\Delta p(t)$  is the output of the integrator. The integral term is needed to perfect tracking the reference frequency and nullify the steady-state frequency error introduced by the Primary Frequency Control (PFC) (in ENTSO-E terminology known as frequency containment process). In general, TSOs use AGC based on Proportional Integral (PI) controller that includes other functionalities, among others, filtering and heuristics in order to reduce the area control error [99]. However, the fact that  $\omega_{CoI}(t)$  is used as an input for the controller represents actually a sort of filter (i.e. it filters local frequency oscillations due to its weighted nature). The output of the continuous integrator is discretized at given fixed-time intervals and sent to each TG. These signals ( $\Delta p_i$ ) are proportional to

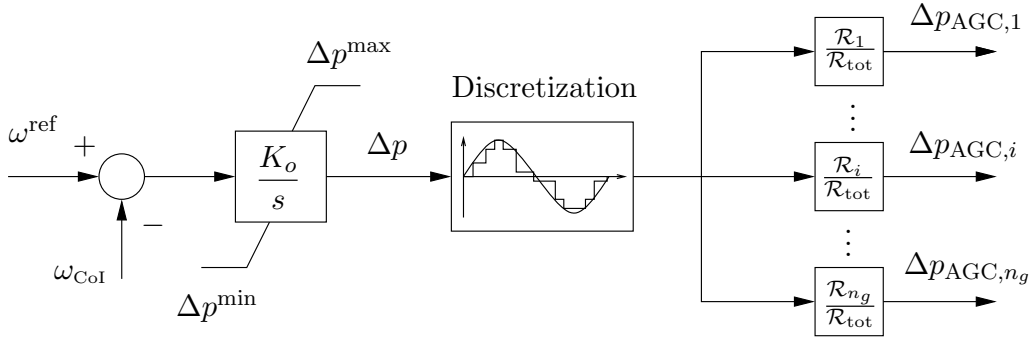


Figure 2.1: AGC control diagram.

the capacity of the machines and the TG droops ( $\mathcal{R}_i$ ) and normalized with respect to the total droop of the system:

$$\mathcal{R}_{\text{tot}} = \sum_{i=1}^{n_g} \mathcal{R}_i. \quad (2.4)$$

The model of the TG considered in this chapter is depicted in Fig. 2.2. It is composed of a droop  $\mathcal{R}_i$  and a lead lag transfer function.  $T_{1,i}$  and  $T_{2,i}$  represent the transient gain and governor time constant, respectively.  $p_{\text{ord},i}$  represent the power order set-point as obtained by the electricity market. This model is suitable for transient stability analysis [84].

In practice, the output of the AGC is limited by the secondary regulation reserve [95]. Therefore, the active power output of the integrator block of the AGC (see  $\Delta p(t)$  in

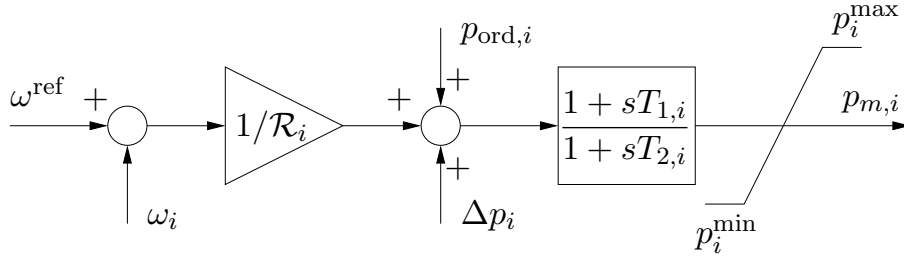


Figure 2.2: Turbine governor control diagram.

Fig. 2.1) is limited [96], in this case, through an anti-windup (AW) limiter, as follows:

$$\begin{aligned}
 &\text{if } \Delta p(t) \geq \Delta p^{\max} \ \& \ \Delta \dot{p}(t) \geq 0 : \Delta p(t) = \Delta p^{\max} \ \& \ \Delta \dot{p}(t) = 0, \\
 &\text{if } \Delta p(t) \leq \Delta p^{\min} \ \& \ \Delta \dot{p}(t) \leq 0 : \Delta p(t) = \Delta p^{\min} \ \& \ \Delta \dot{p}(t) = 0, \\
 &\text{otherwise : } \Delta \dot{p}(t) = K_o(\omega^{\text{ref}} - \omega_{\text{CoI}}(t)).
 \end{aligned} \tag{2.5}$$

The AW limiter is needed to limit the windup phenomenon of the integrator state variable ( $\Delta p(t)$ ).

### 2.3.1 Illustrative Example on the AGC

In this section, we present an illustrative example on the impact of discrete AGC on power system stability. The IEEE WSCC 9-bus system (see Fig. 2.3) is utilized to show the effect of different AGC time intervals. The base case data of this IEEE benchmark network can be found in [58].

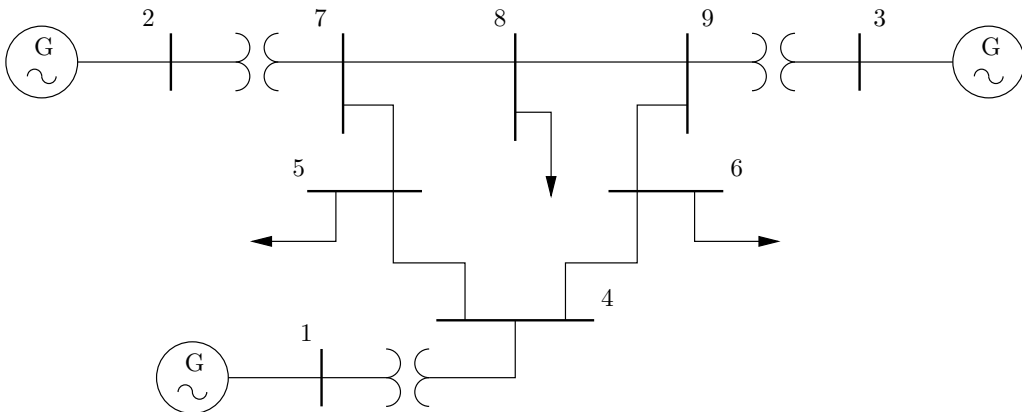


Figure 2.3: Single line diagram of the IEEE WSCC 3-machine 9-bus system.

Since the original benchmark system does not include an AGC, we have included in the model the AGC described in the previous section. In the simulation results below, the disturbance consists in the disconnection of the load at bus 6 at  $t = 1$  s.

### Sensitivity analysis with respect to $K_o$

We first consider the effect of  $K_o$  with a continuous AGC model. It is well-known that a high gain of the AGC may lead to power system instability due to the coupling between the dynamics of the PFC and AGC. Figure 2.4 shows the transient behavior of  $\omega_{CoI}(t)$  for  $K_o = \{5, 20, 50\}$  without considering the AW limiter; and for  $K_o = 100$  with inclusion of the AW limiter on  $\Delta p(t)$  (40% of the total generation capacity). As expected, the system is unstable for high values of  $K_o$ , in this case, for  $K_o > 20$ . On the other hand, low gain values keep the system stable (see Fig. 2.5). However, the dynamic response with this small value of  $K_o$  is very slow, and consequently the controller is not effective. Finally, imposing a limiter on  $\Delta p(t)$  leads to a limit cycle.

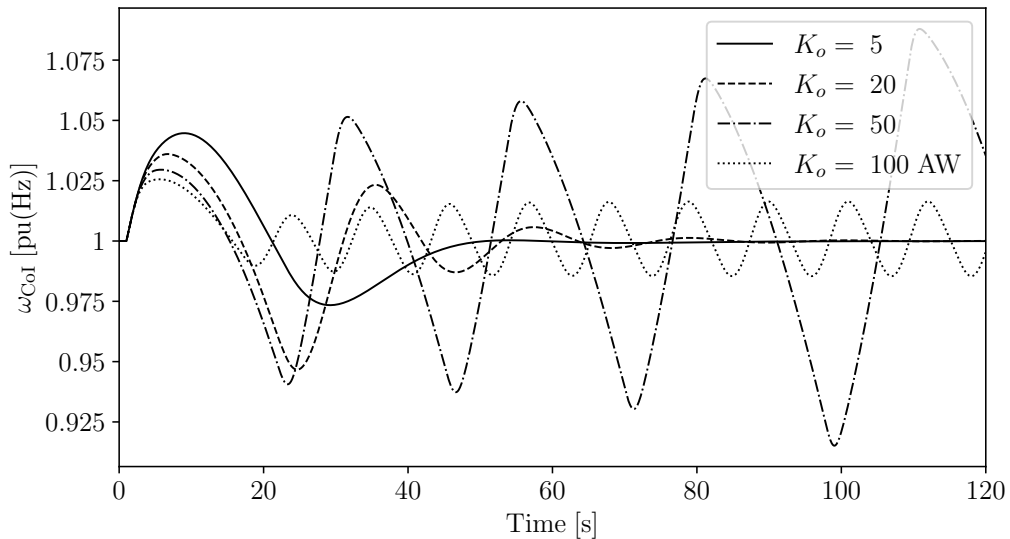


Figure 2.4: Transient response of  $\omega_{CoI}(t)$  of the WSCC 9-bus system for different AGC gains.

### Impact of different AGC time intervals

First we show qualitatively that the impact of different values of  $K_o$  of continuous AGC is equivalent to different time intervals of a discrete AGC. Let us discretize the first-order

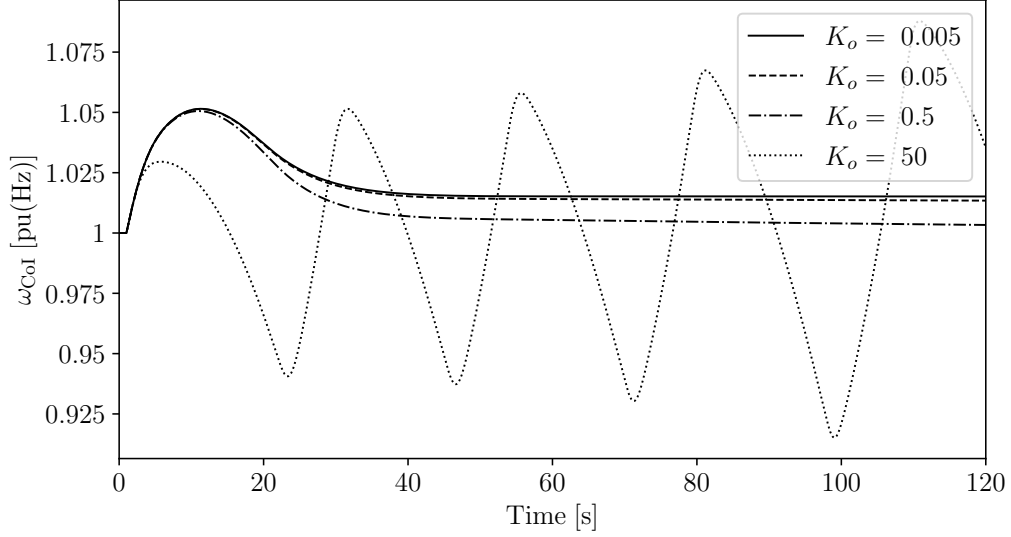


Figure 2.5: Transient response of  $\omega_{CoI}(t)$  of the WSCC 9-bus system for different AGC gains.

differential equation (2.3) using the forward Euler method. The  $k$ -th integration step is:

$$\Delta p^{(k+1)} = K_o \Delta t (\omega^{\text{ref}} - \omega_{CoI}(t)) + \Delta p^{(k)}, \quad (2.6)$$

where  $\Delta p^{(k+1)}$  and  $\Delta p^{(k)}$  are the next and present value of  $\Delta p(t)$ , respectively;  $\Delta t$  is the integration time interval. From (2.6), it is apparent that increasing  $\Delta t$  is equivalent to increasing  $K_o$ .

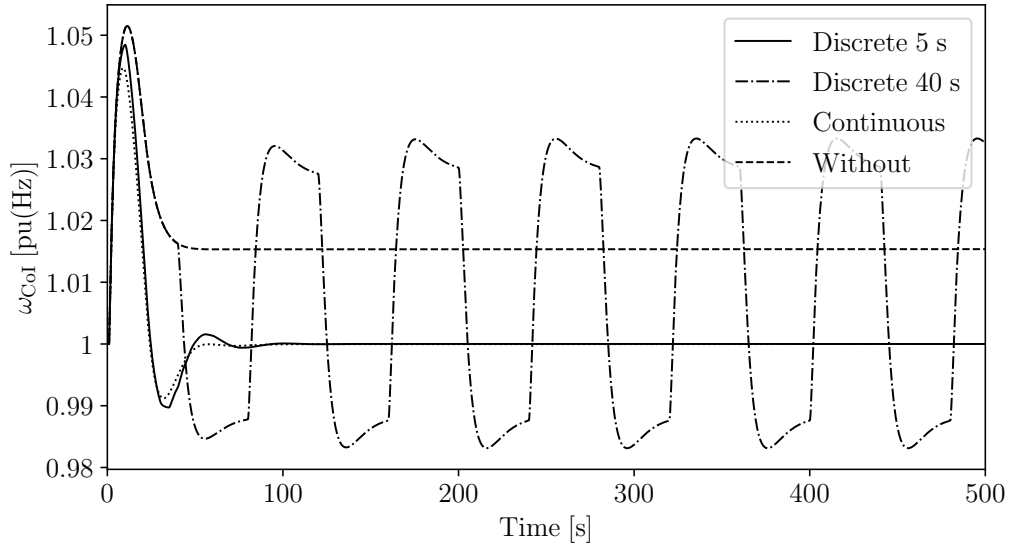


Figure 2.6: Transient response of  $\omega_{CoI}(t)$  for different AGC time intervals.

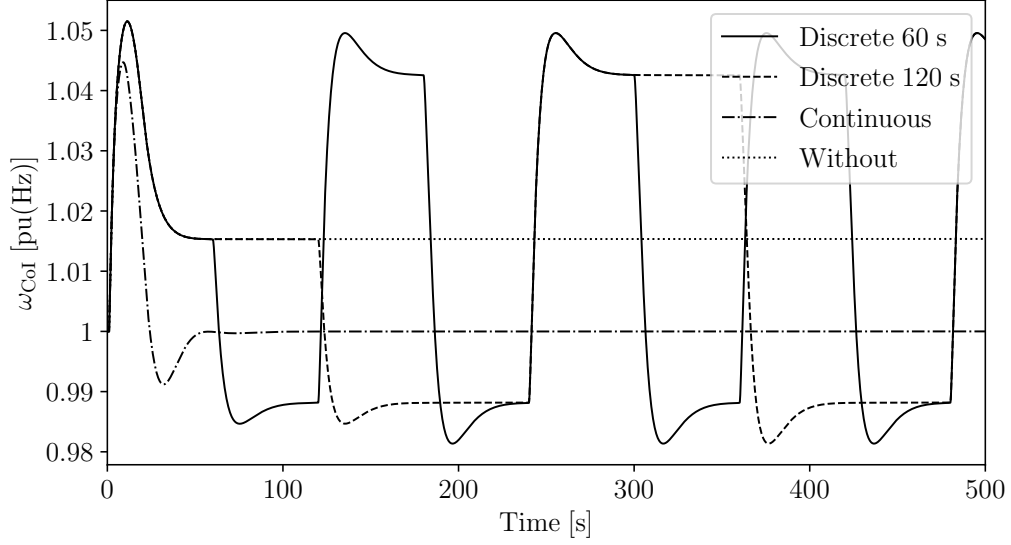


Figure 2.7: Transient response of  $\omega_{CoI}(t)$  for different AGC time intervals.

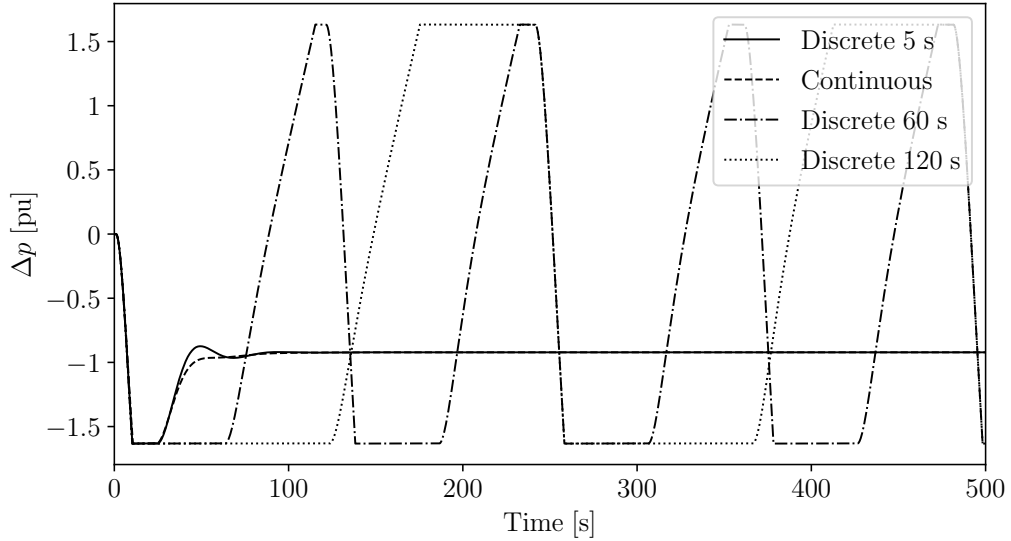


Figure 2.8: Transient response of  $\Delta p(t)$  for different AGC time intervals.

Figures 2.6 and 2.7 depict the transient response of the  $\omega_{CoI}(t)$  for different AGC time intervals. Observe that using a continuous AGC and a discrete AGC with a time interval of 5, the system is stable as the controller is fast enough to bring back the frequency to the nominal value. On the other hand, the results without an AGC show a stable transient response with a steady state-frequency error. For AGC time intervals equal or greater than 40 s, the system enters into a limit cycle. As expected from the discussion above, large discretization time intervals lead to unstable system dynamics. For this reason, in

practice, the AGC time interval is in the range of (2, 6) s, which is small enough not to originate any limit cycle.

Figure 2.8 shows the transient behavior of the state variable of the AGC ( $\Delta p(t)$ ) for some relevant AGC time intervals. The limit cycle occurs whenever the AGC time interval is big enough (e.g. 120 s) to allow  $\Delta p(t)$  to go to the other extreme value (limit) and saturate. Other factors that determine the period of the limit cycle are related to how fast is the AGC controller as well as the type of the contingency. Note that for very long-time intervals, e.g. > 10 minutes, the AGC controller is not effective anymore and other mechanisms are in place to compensate the power unbalance e.g. short-term optimal power flow.

### RoCoF dead-band

A way to remove the bang-bang phenomena shown in the previous section is to consider a dead-band on the RoCoF. In this chapter, the RoCoF is calculated using the following expression:

$$\text{RoCoF} = \frac{\omega_{\text{CoI}}^{(k-1)} - \omega_{\text{CoI}}^{(k)}}{\Delta t}, \quad (2.7)$$

where  $\omega_{\text{CoI}}^{(k-1)}$  and  $\omega_{\text{CoI}}^{(k)}$  correspond to the values of  $\omega_{\text{CoI}}(t)$  at the previous interval (e.g. 5 seconds) and the current time, respectively. While  $\Delta t$  represents the AGC time interval. Note that controlling the frequency of the CoI is not viable in practice. One can, however, implement RoCoF dead-bands in the primary frequency controllers of the power plants. These will affect the variation of the rotor speeds of the synchronous machines and, in turn, of the frequency of the CoI. The model considered in the chapter is thus an approximation but it is sufficient to show the effect of this dead-band.

Figure 2.9 depicts the transient behavior of the  $\omega_{\text{CoI}}(t)$  with RoCoF dead-band of 0.0002 pu(Hz/s). The RoCoF dead-band successfully removes the limit cycle, however, it leads to a frequency steady-state error. Clearly, this is not desirable because the AGC cannot serve its main purpose.

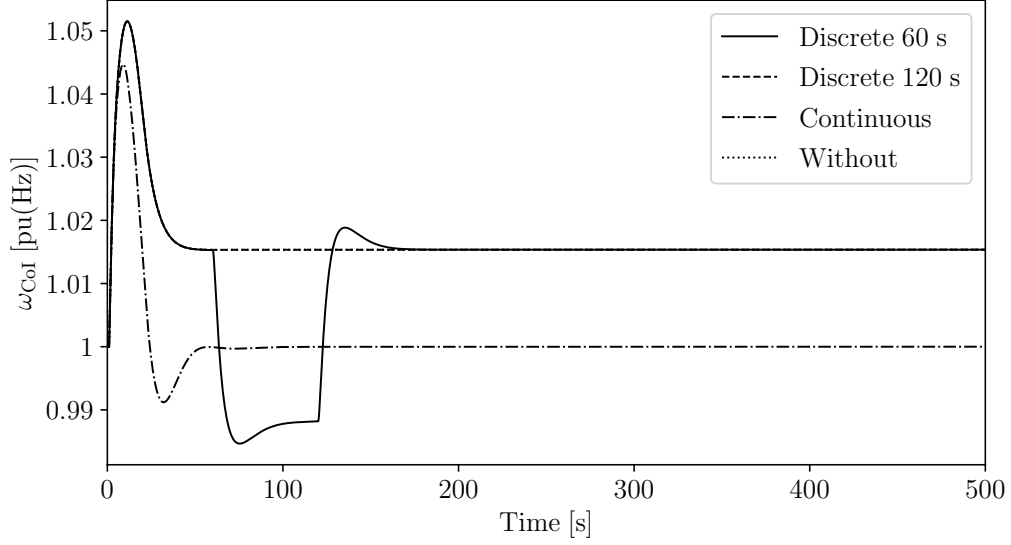


Figure 2.9: Transient response of  $\omega_{CoI}(t)$  for different AGC time intervals and with RoCoF dead-band.

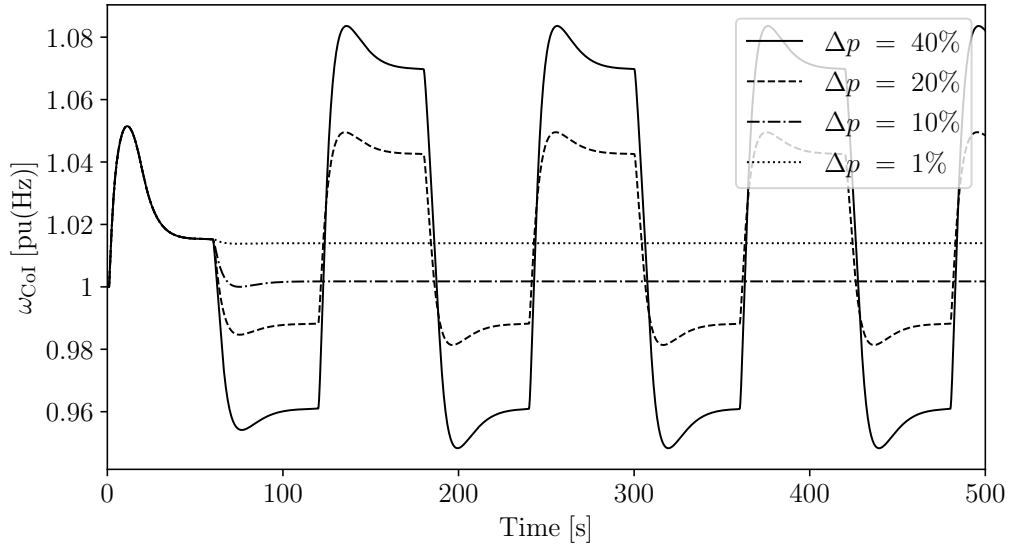


Figure 2.10: Transient response of  $\omega_{CoI}(t)$  for different  $\Delta p(t)$  limits.

### Sensitivity analysis with respect to $\Delta p(t)$

Another solution to prevent the bang-bang phenomena is to limit the variation of the internal state variable of the AGC, namely  $\Delta p(t)$ . The limit case, of course, is when the limit of  $\Delta p^{\max} = \Delta p^{\min} = 0$ , which basically opens the control loop. Figure 2.10 depicts the transient behavior of the  $\omega_{CoI}(t)$  for a variation of  $\Delta p(t)$  from 40% up to 1% and for an AGC time interval of 60 seconds. As expected, limiting  $\Delta p(t)$  makes the AGC controller

less effective. For example, allowing  $\Delta p(t)$  to vary just 1% of the total generation capacity, is almost equivalent to disabling the AGC.

Based on the simulation results above, we conclude that the only effective solution to avoid the limit cycle phenomena caused by the discretization of the AGC is to impose a sufficiently small  $\Delta t$ .

## 2.4 Market-based AGC

The previous section shows that there is a range of values, from few tens of seconds to few minutes, of the execution cycles of conventional AGC that leads to a limit cycle. Such a result serves as a motivation to study the same phenomenon when considering real-time electricity markets. These markets are currently moving to 5 minutes or even faster trading intervals to facilitate the integration of weather-dependent RESs into power systems [2]. These time scales are comparable with those of the AGC. Motivated by this fact and by the observation that real-time market can be modeled as a sort of discrete AGC, we make use of a dynamic electricity market model proposed in [6] and discretize it to represent different trading intervals. Then, we investigate the impact of the MAGC on the power system stability when using different trading intervals and different shares of renewable generation.

### 2.4.1 Dynamic Electricity Market Model

Alvarado started to study the dynamics of electricity markets after similar works were performed by economists in their respective fields [5]. The main idea behind his studies on this topic was to be able to manage the real-time balance between power demand and supply through a continuous price signal sent to both loads and generators.

In this model, it is assumed that when a generator sees that the electricity price, say,  $\rho(t)$ , is higher/lower than the corresponding marginal cost, then the generator will increase/decrease its production until the cost matches the price. These assumptions lead to the following dynamic electricity market model [6]:

$$T_\rho \dot{\rho}(t) = K_E(\omega^{\text{ref}} - \omega_{\text{Col}}(t)) - \mathcal{I}_d \rho(t), \quad (2.8)$$

$$T_{g,i} \Delta \dot{p}_{g,i}(t) = \rho(t) - c_{g,i} \Delta p_{g,i}(t) - b_{g,i}, \quad i = 1, \dots, n_g, \quad (2.9)$$

where  $\Delta p_{g,i}(t)$  represent the active power order set points ( $p_{\text{ord},i}$ ) of the TGs (see Fig. 2.2);  $c_{g,i}$  and  $b_{g,i}$  are the parameters of the marginal cost of the generators.  $T_\rho$  and  $T_{g,i}$  are the time constants; and  $K_E$  is the feedback gain.  $\mathcal{I}_d$  is the deviation with respect to a perfect tracking integrator and for a Low-Pass Filter (LPF) is  $\mathcal{I}_d = 1$ . Finally, the mismatch  $\omega^{\text{ref}} - \omega_{\text{CoI}}(t)$  is utilized as an indirect estimation of the real-time energy imbalance in the system.

In [6], loads responds similarly to generators with respect to the electricity price  $\rho(t)$  but with opposite strategy, i.e. load bids increase as the electricity price decreases. In this chapter, however, loads are assumed to be inelastic and do not participate in the MAGC. Such an assumption is consistent with the current situation in most of the electricity markets where loads (effectively) do not respond to changes in the wholesale electricity prices. In fact, it has been shown in the literature that making loads price responsive as well will further deteriorate the stability of the system [93].

Note that the use of this electricity market model (2.8)-(2.9) is considered adequate for real-time markets with short dispatch periods [6]. As mentioned above, some systems already use these markets and they will be more common in future power systems.

## 2.4.2 Analogy between AGC and MAGC

The structure of the equations (2.8)-(2.9) is formally similar to the structure of the AGC shown in Fig. 2.1. For comparison, the “control” diagram of (2.8)-(2.9) is depicted in Fig. 2.11. The AGC and the MAGC have exactly the same structure for  $\mathcal{I}_d = b_{g,i} = T_{g,i} = 0$ . The MAGC can be thus seen as a generalized secondary frequency controller.

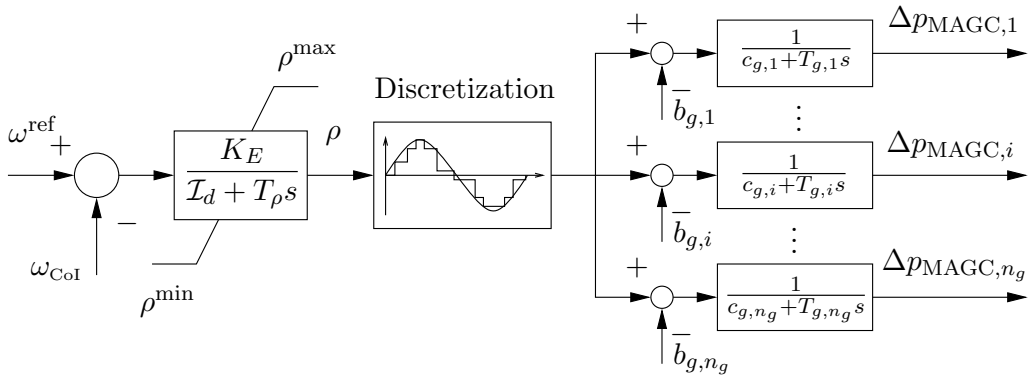


Figure 2.11: MAGC control diagram.

A substantial difference between the two controllers concerns the meaning of the state variables, namely  $\Delta p(t)$  and  $\rho(t)$ . In the MAGC,  $\rho(t)$  is a price, which does not carry any information on the energy involved in the system, as opposed to  $\Delta p(t)$ , which is a power reserve. Nevertheless, the market model (2.8)-(2.9) makes  $\rho(t)$  a “physical quantity” of the system.

### Anti-Windup Limiter on $\rho(t)$

Similar to the AW limiter on  $\Delta p(t)$ , one can limit the state variable of the MAGC, namely  $\rho(t)$  in Fig. 2.11. Enforcing a limit on  $\rho(t)$  might be desirable in order to limit the electricity price spikes. This happens, for example, in most of the European electricity markets [39]. The AW limiter on  $\rho(t)$  is as follows:

$$\begin{aligned} &\text{if } \rho(t) \geq \rho^{\max} \ \& \ \dot{\rho}(t) \geq 0 : \rho(t) = \rho^{\max} \ \& \ \dot{\rho}(t) = 0 , \\ &\text{if } \rho(t) \leq \rho^{\min} \ \& \ \dot{\rho}(t) \leq 0 : \rho(t) = \rho^{\min} \ \& \ \dot{\rho}(t) = 0 , \\ &\text{otherwise : equation (2.8) .} \end{aligned} \tag{2.10}$$

### 2.4.3 Illustrative Example on the MAGC

The analogy discussed above allows us simulating real-time electricity markets as an equivalent AGC. In this case, however, the time interval matters because in practice electricity markets use dispatch periods of the order of minutes, not seconds as in the conventional AGC.

For a fair comparison between the AGC and MAGC, we use again the IEEE WSCC 9-bus system and we assume that the three generators have the same market data as the first three generators in the IEEE 39-bus system [6]. Unless stated otherwise, for simulation purposes, the maximum and minimum limit of  $\rho(t)$  is set to 4,000 and 0 \$/MWh, respectively. The contingency is the outage of the load at bus 6 at  $t = 1$  s.

#### Systems with MAGC only

In this first scenario, it is assumed that the system includes only the MAGC controller, i.e. there is no AGC. This scenario corresponds to power systems that do not include an AGC, but instead use some sort of offline and/or “manual” generation control [99]. The

goal is to investigate whether the idea of controlling power systems exclusively based on market mechanism is feasible.

Figures 2.12 and 2.13 show the transient behavior of  $\omega_{CoI}(t)$  and  $\rho(t)$ , respectively. The discrete MAGC leads to limit cycles similar to the case of the AGC. Specifically, the limit cycle appears for a MAGC time interval equal or above 120 s. Compared to the AGC, this phenomenon appears for longer time intervals. This is due to the parameters of the MAGC control scheme. It is important to note, however, that the limit cycles always appear for a certain range of  $\Delta t$ , independently from the parameters of the secondary controller.

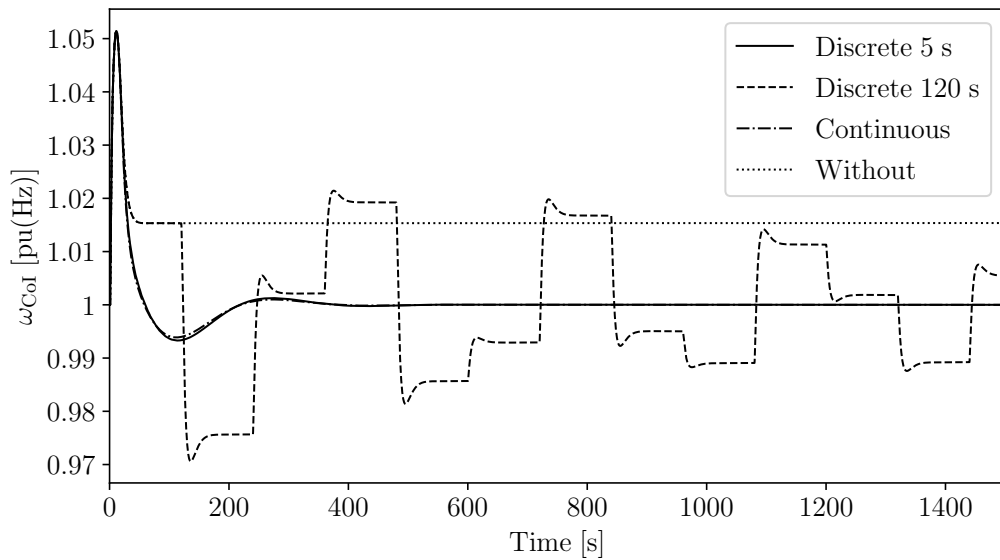


Figure 2.12: Transient response of  $\omega_{CoI}(t)$  for different MAGC time intervals.

There are two ways to avoid the limit cycles. One is to use “short” time periods, for example, 5 s in Fig. 2.12. The other one is to use “long” time periods, for example, 10 minutes [34]. In this case, the MAGC approximation does not hold and is effectively decoupled from the dynamics of the system, and thus it does not cause the occurrence of instability. Figure 2.12 also suggests that real-time electricity markets with very short periods, e.g. 5 s, can, in principle, substitute the AGC provided that they have the same features.

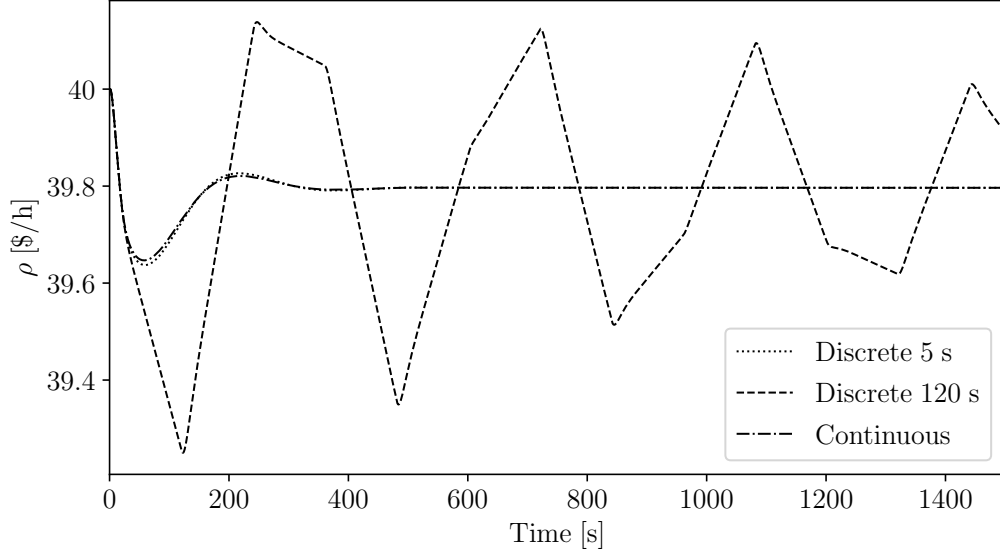


Figure 2.13: Transient response of the electricity price  $\rho(t)$  for different MAGC time intervals.

### Sensitivity analysis with respect to $\rho(t)$

As discussed earlier in the chapter, a solution to remove the limit cycle is to limit the variation of the state variable of the AGC controller, in this case, that of MAGC controller. In this context, Fig. 2.14 shows the transient response of the system for different  $\rho(t)$  limits. As expected, limiting the variation of the state variable removes the limit cycle. For example, allowing  $\rho(t)$  to vary just 0.75% from its nominal value (40 \$/MWh) appears to be able to remove the instability, however, it leads to a steady state frequency error. Further limiting the variation of  $\rho(t)$ , e.g. 0.125%, makes the controller even less effective, i.e. almost an open loop. The interested reader is referred to [66] for such an example. As for the case of the AGC, the best solution appears to be that of using short dispatch intervals.

### Systems with AGC and MAGC

This scenario considers a common scenario, i.e. power systems equipped with both an AGC and a real-time electricity market. The AGC considered here has a time interval of 4 s. Simulations are solved considering the same load outage as in the previous section.

The transient response of the system following the contingency is depicted in Fig. 2.15. The inclusion of the AGC removes the limit cycle. It appears that, if the system includes an AGC, then the discretization of the real-time market does not cause instability issues.

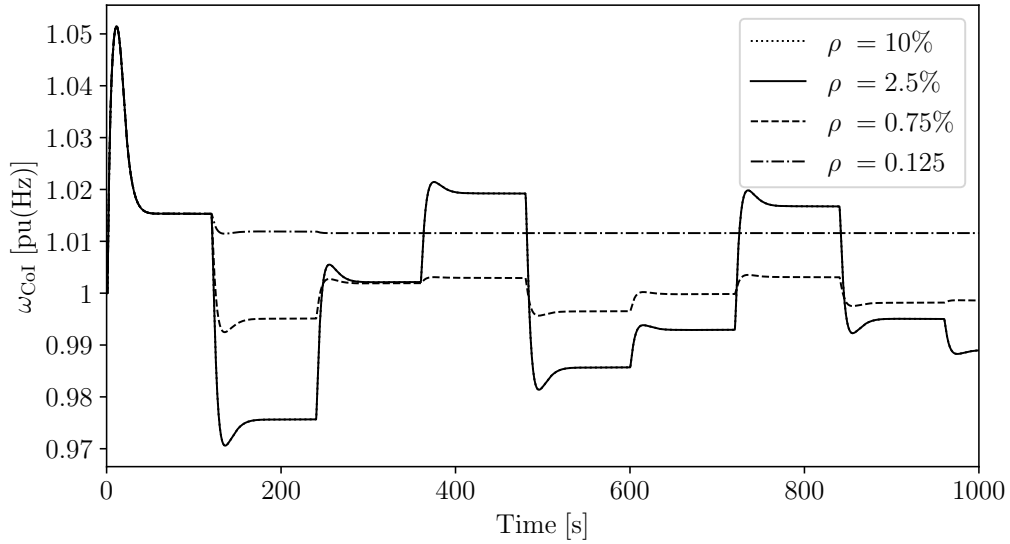


Figure 2.14: Transient response of  $\omega_{CoI}(t)$  for different  $\rho(t)$  limits.

It is also interesting to note that using a continuous MAGC leads to a lower frequency nadir. This is due to the dynamic coupling between the dynamics of the MAGC and the AGC. Depending on the severity of the frequency variations, the system operator may have to implement corrective actions, e.g. load shedding. However, a discussion on corrective actions is outside the scope of this chapter.

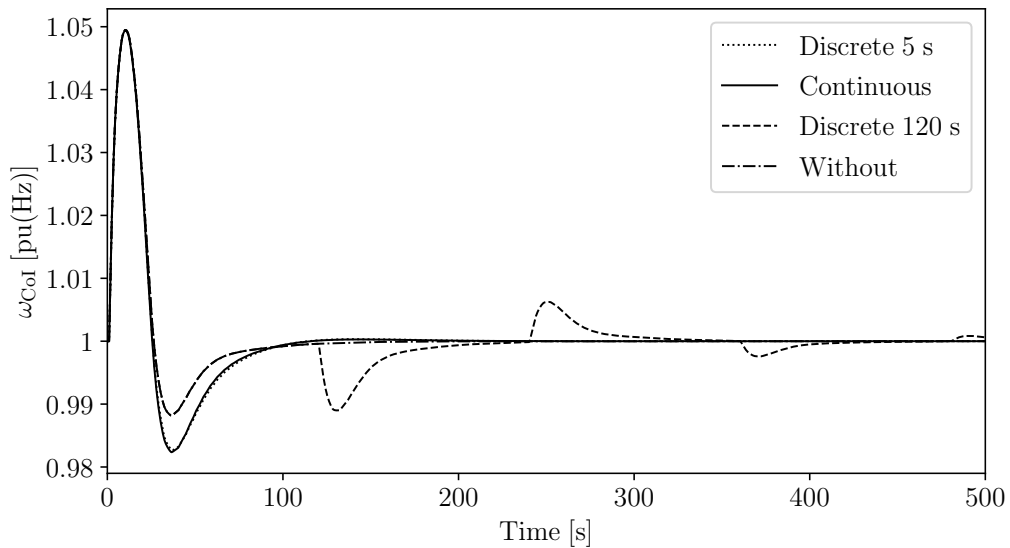


Figure 2.15: Transient response of  $\omega_{CoI}(t)$  using the AGC and MAGC.

## Economic impact of systems with and without an AGC

This scenario discusses the differences with respect to the profit of the generating units that are part of systems that include only MAGC controller, and both AGC and MAGC. We assume that both MAGC controllers utilizes a time interval of 60 s, whereas the AGC utilizes a time interval of 4 seconds. Figure 2.16 shows the outputs of the controllers for the generator at bus 1, for the scenarios with MAGC only, and with both AGC and MAGC.

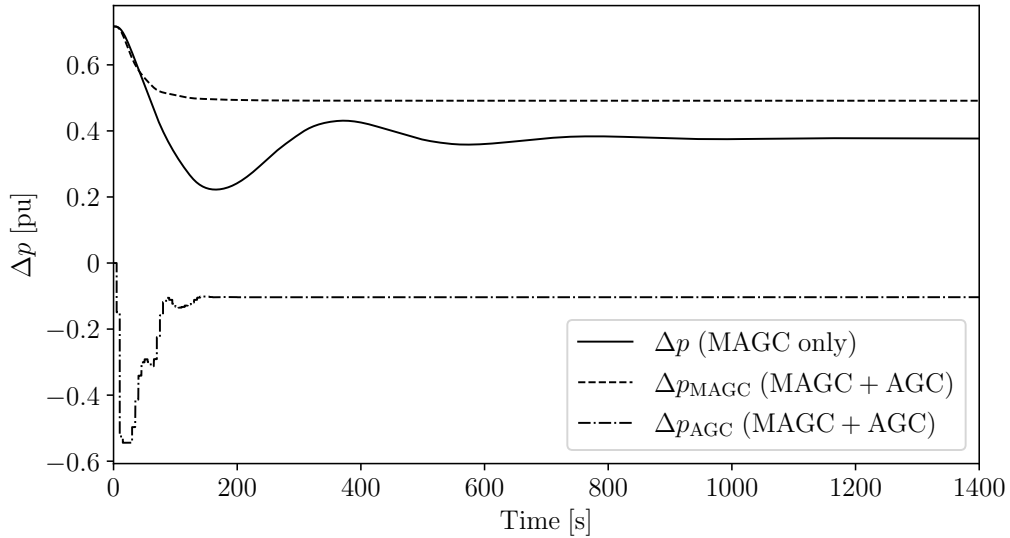


Figure 2.16: Secondary frequency controller signals for the scenarios with MAGC only and with both MAGC and AGC.

It is interesting to see that the MAGC only controller contributes more (by decreasing more its output in response to the contingency) compared to the same controller when the system includes both MAGC and AGC. This is due to the fact that in the scenario that includes both controllers, the AGC is the dominant controller (being faster) and takes care of power mismatches. For this reason, the profit of generating units that participate in the MAGC only is less compared to the profit of the same generating units that are part of power systems with MAGC and AGC (the other way round is true if a generator is lost). This is better shown in Fig. 2.17 where the income of the first generator is depicted for both scenarios considered in this section.

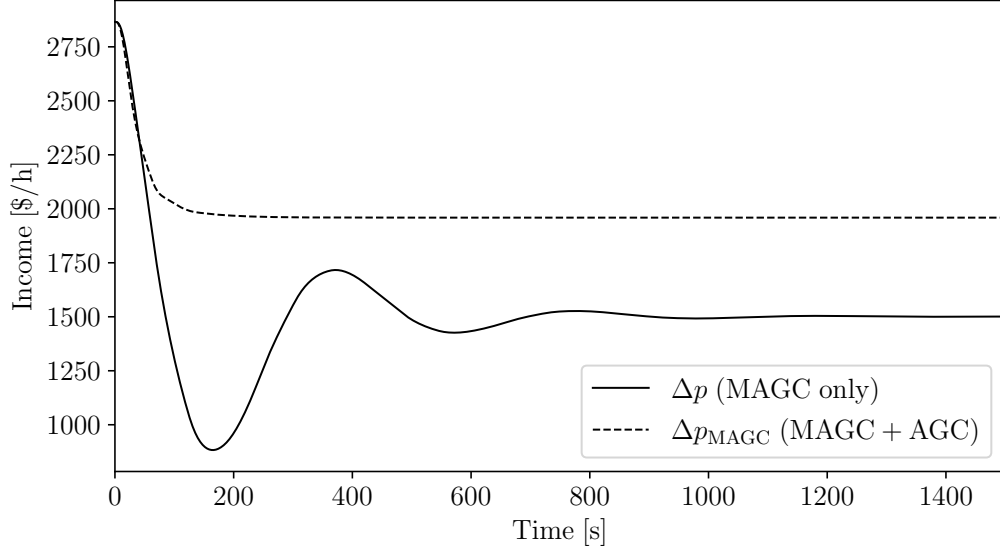


Figure 2.17: Profit of generator 1 for the scenarios with MAGC only and with both MAGC and AGC.

#### 2.4.4 Inclusion of Non-Synchronous Devices

So far we have studied the impact of discrete AGC and MAGC using conventional power systems. However, it is also relevant to study such an impact on power systems with high shares of non-synchronous devices. The impact of wind power penetration is considered. With this aim, the New England IEEE 39-bus system [57] is utilized along with the market data taken from [6]. The contingency is the outage at  $t = 1$  s of the load located at bus 3. For simulation purposes a MAGC with a time interval of 120 s (chosen on purpose as it is the worse case scenario) and gain  $K_E = 15$  are used. Whereas for the AGC a time interval of 4 s and gain  $K_o = 2$  is used. The focus is on the transient response of the COI following the contingency. Three scenarios are considered: (i) base case with conventional generation; (ii) 25% penetration of wind generation; and (iii) 50% penetration of wind generation. For a fair comparison, all scenarios have same loading level, control and network topology.

### Wind Power Modelling in Real-Time Electricity Markets

Nowadays, in most electricity markets worldwide, wind power producers bid in the same way and follow same rules as conventional power plants. For instance, wind power plants are responsible for power deviations with respect to the values scheduled in day-ahead

market. In this context, following the structure of the original dynamic market model in (2.8)-(2.9), one can write the equation that models wind power plants (WPPs) behavior with respect to their marginal cost and the price  $\rho(t)$ , as follows:

$$T_{w,k} \dot{p}_{w,k}(t) = \rho(t) - c_{w,k} p_{w,k}(t) - b_{w,k}, \quad k = 1, \dots, n_w, \quad (2.11)$$

where  $p_{w,k}(t)$ ,  $T_{w,k}$ ,  $c_{w,k}$ ,  $b_{w,k}$  have same meaning as in (2.9).

### Marginal cost of wind power equal to zero

In general, the marginal cost of wind is assumed to be zero, i.e.:

$$c_{w,k} p_{w,k}(t) - b_{w,k} = 0,$$

and, from (2.11), we have:

$$T_{w,k} \dot{p}_{w,k}(t) = \rho(t). \quad (2.12)$$

Equation (2.12) is a pure integrator. This means that the WPPs will try to dynamically integrate and set the price  $\rho(t) = 0$ . As shown earlier in the chapter, a pure integrator tends to be unstable. Thus, the WPPs will integrate until their output reaches a maximum power limit. In the same vein, if:

$$c_{w,k} p_{w,k}(t) + b_{w,k} < 0,$$

i.e. the WPPs bid negative prices, then from the dynamic point of view their market secondary control is unstable. However, this does not mean that WPPs drives the system to instability, but just that they are going to generate their maximum power all the time.

To simulate this case, we assume that the system includes both AGC and MAGC and show the transient behavior of  $\omega_{CoI}(t)$  in Fig. 2.18. The scenarios with non-synchronous devices, i.e. the scenarios with inclusion of wind generation, worsen the performance of both AGC/MAGC controllers, and consequently the dynamic performance of the system. These results indicate that future power systems with high shares of wind power will

require much shorter dispatch periods compared to, for example, conventional power systems to avoid possible instabilities.

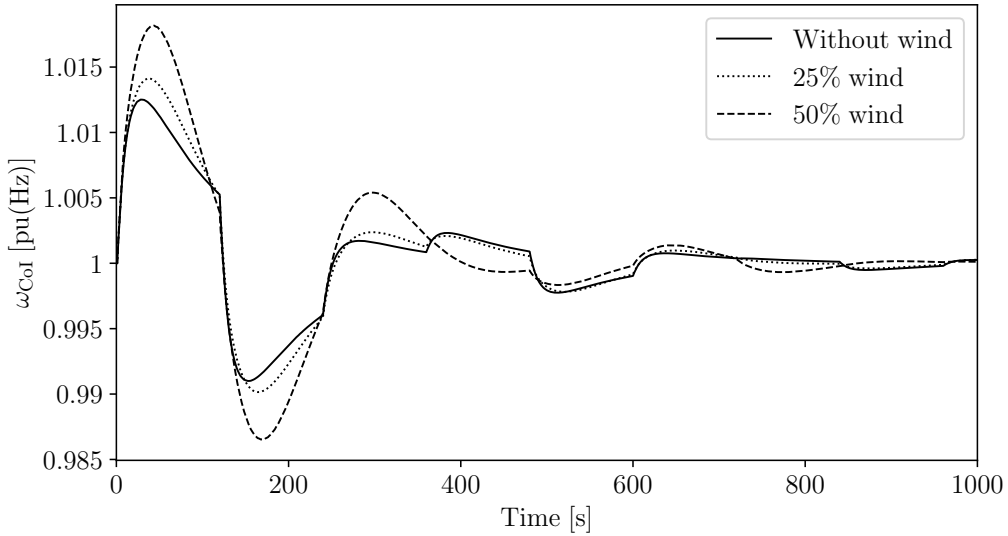


Figure 2.18: Transient response of  $\omega_{CoI}(t)$  for different wind power shares.

### Marginal cost of wind power different from zero

If the share of WPPs in the electricity market increases, WPPs may consider acting strategically (i.e. price maker) in order to increase their own profits through intentionally altering the market clearing price. This scenario has been well discussed in the literature, e.g. in reference [31]. In order to become a price maker, WPPs will have to be sufficiently big (otherwise they will be limited), and with a marginal cost that is in the same range as that of other conventional generators. In this scenario, WPPs will participate in the real-time electricity market according to (2.11), i.e. will be part of the MAGC shown in Fig. 2.11.

Note that, if they are not coupled with ESSs or include some mechanism to provide power reserve, the WPPs can only provide down regulating service, that is, will only decrease their power production. To simulate this scenario, we consider a 25% wind power penetration, i.e. replace 3 conventional generators with WPPs. Furthermore, we assume that the WPPs have the same bids and market data as the conventional power plants. The Spanish electricity market is a real-world example where RESs and conventional power plants bid together [12]. We also assume that the systems includes both AGC and MAGC.

Figure 2.19 shows the results for this scenario. It appears that the participation of WPPs in real-time electricity markets does not make a huge difference with respect to the transient response of the system. This is due to the fact that the AGC is the dominant secondary controller, as it is faster than the MAGC and thus contributes more after the occurrence of the contingency (see Fig. 2.16). We can conclude that, in this scenario, the participation of WPPs in real-time electricity markets does not make a significant contribution to long-term power system dynamics.

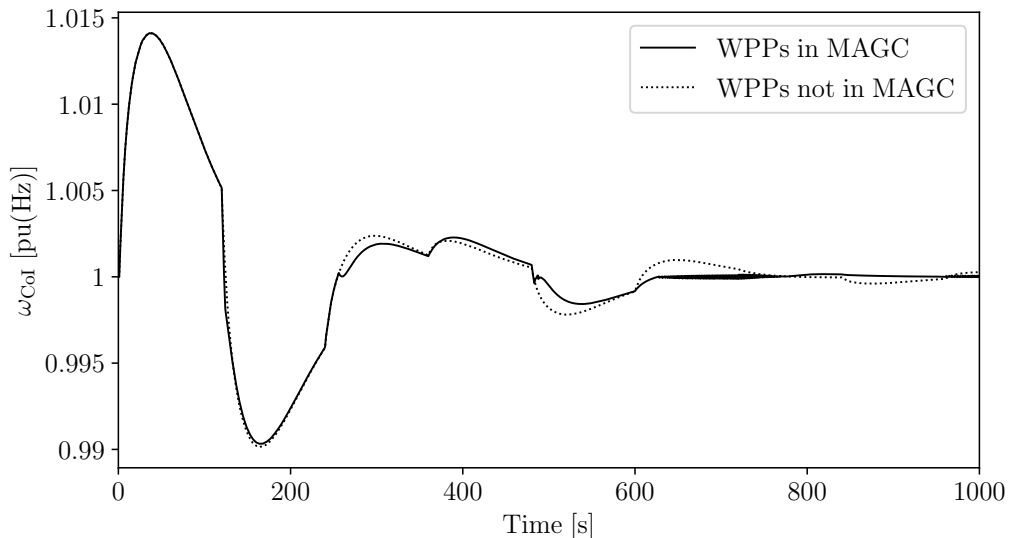


Figure 2.19: Transient response of the  $\omega_{CoI}(t)$  for WPPs included and not included in to the MAGC, respectively.

## 2.5 Case Study 1: Contribution of ESSs to Long-Term Power System Dynamic Performance

The performance of the converter-interfaced ESSs in mitigating the long-term oscillatory behavior of the frequency caused by the electricity market (see Fig. 2.12) is illustrated in this case study. Such an application of the ESSs is motivated by the fact that they can be used for many power system applications, including the safe integration of intermittent RESs, PFC and SFC, voltage support, and RoCoF control, to mention some [88]. With this aim, we assume that ESSs do not participate in the electricity markets, i.e. are not part of the MAGC in Fig. 2.11, but instead are paid for the frequency containment support that they provide. Here, we utilize the simplified ESS model presented in [94]. The ESS

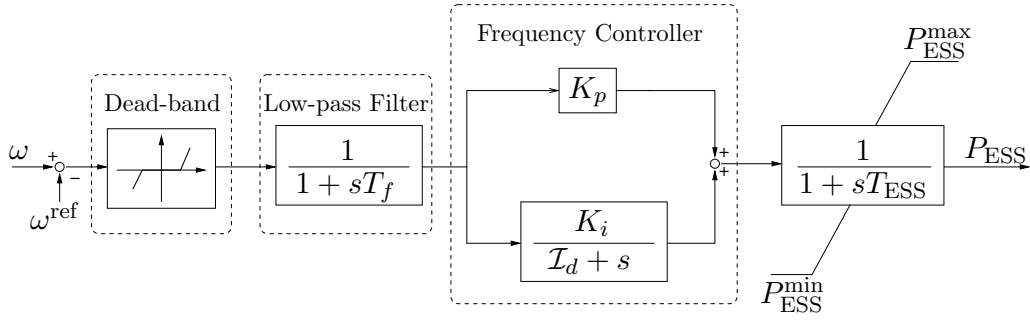


Figure 2.20: The frequency control scheme of an ESS.

frequency control diagram is depicted in Fig. 2.20. In this case, the controller's input is the difference between the measured ( $\omega$ ) and reference frequency ( $\omega^{\text{ref}}$ ). The frequency is measured through a phase-locked loop device. Next, the ESS control scheme includes a deadband and a LPF to make the controller less sensitive to small frequency deviations and filter out noises, respectively. Then, it includes a PI regulator with  $K_p$  being the proportional gain and  $K_i$  being the integral gain. In the control scheme shown in Fig. 2.20, the droop coefficient is obtained indirectly through the integral deviation coefficient  $\mathcal{I}_d$ . For  $\mathcal{I}_d = 0$  the controller is a PI and hence the droop coefficient is  $\mathcal{R} = 0$ , whereas for  $\mathcal{I}_d \neq 0$ , the controller becomes a lead-lag filter, with droop coefficient  $\mathcal{R} = \mathcal{I}_d / (K_i + K_p \mathcal{I}_d)$ . Finally, the ESS is represented by an anti-windup first-order lag filter with time constant  $T_{ESS}$ .

### 2.5.1 WSCC 9-bus System

The effectiveness of ESS is studied by means of a modified WSCC 9-bus system where a MAGC time interval of 120 seconds is considered. Furthermore, the contingency is a 10% instantaneous load increase (approximately 32 MW) at  $t = 1$  s.

ESS devices are connected to different buses of the system, and their impact on the long-term frequency deviations is duly discussed. Three scenarios are considered, as follows:

- Without ESSs limits;
- With ESSs limits; and
- Comparison of the impact of droop and deadband parameters.

All scenarios above are compared with the base case, i.e. without ESSs (see Fig. 2.12).

## ESSs without Capacity Limits

This first scenario discusses the effect of ESSs on long-term power system dynamics without considering the capacity limits of the ESS. This scenario is relevant for microgrids where the storage capacity can be relatively large with respect to the total installed power capacity. For simulation purposes,  $\mathcal{I}_d = 0.7$  is used, and the deadband is set to zero. Figure 2.21 shows the transient response of  $\omega_{CoI}(t)$  for three scenarios, namely with one ESS connected at bus 9, three ESSs connected at buses 7, 8, and 9, and when no storage is included in the system.

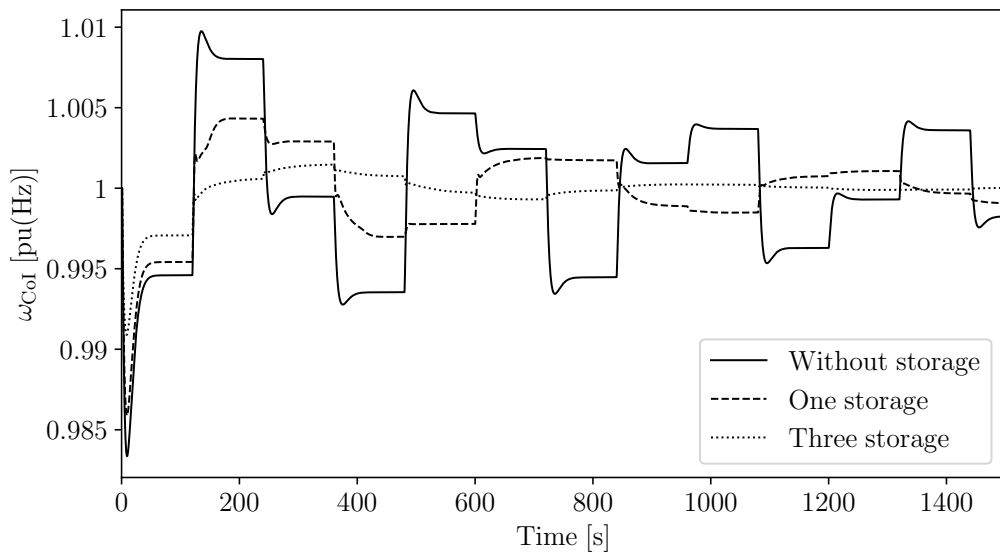


Figure 2.21: Transient response of  $\omega_{CoI}(t)$  following a 10% instantaneous load increase without ESSs limits.

Simulation results indicate that the ESSs help reduce the frequency variations caused by large MAGC time intervals and, hence, considerably improve the system's dynamic performance. Moreover, the case with three ESSs leads to significantly lower frequency variations than the case with one ESS. This result indicates that, from the dynamic point of view of the system, it is better to install ESSs in different locations of the network rather than installing them in one location.

## ESSs with Capacity Limits

This section considers the same system and contingency as in the previous scenario but taking into account the ESS capacity limits. In particular, each ESS device is now

assumed to have a 10 MW capacity. Thus, the case with three ESSs represents almost the 10% instantaneous load increase (32 MW). Figure 2.22 depicts the transient response of  $\omega_{CoI}(t)$ . The case with three ESSs leads to a similar dynamic behaviour where no limits are considered (Fig. 2.21). In contrast, the case when one ESS is connected in the system is unable to solve the problem caused by the MAGC discretization. These results indicate that, as expected, the performance of the ESS is greatly impacted by its capacity.

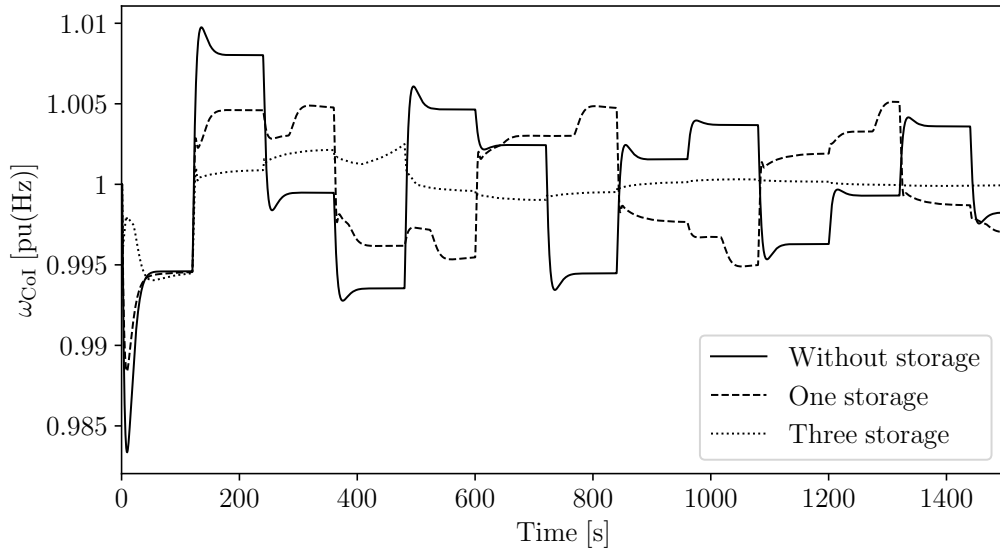


Figure 2.22: Transient response of  $\omega_{CoI}(t)$  following a 10% instantaneous load increase with ESSs limits.

## Impact of Droop and Deadband

Deadband and droop coefficient are two relevant parameters that can reduce the sensitivity of a controller to small frequency variations and noise. In the context of this chapter, we are interested to understand what is the impact of these control parameters on the overall dynamic performance of the system. With this aim, four cases are considered, as follows:

1. Zero droop and without ESSs limits.
2. Zero droop and with ESSs limits.
3. Non-zero droop and without ESSs limits.
4. Non-zero droop and with ESSs limits.

When non-zero values are utilized, a deadband value of  $db = 0.0006$  pu(Hz) and  $\mathcal{I}_d = 0.7$  are used. Furthermore, only the case when three ESSs connected at buses 7, 8, and 9 is considered below.

### Zero droop without ESS limits

Figure 2.23 shows the trajectories of the  $\omega_{CoI}(t)$  for three scenarios, namely without storage, with storage and without deadband, and with storage and with deadband. The aim is to evaluate the impact of the deadband on the frequency error when ESS capacity limits are not considered. Interestingly, the case with a non-zero deadband leads to a worse dynamic behaviour compared to the case without. This result leads to conclude that it is better not to include a deadband on the frequency error.

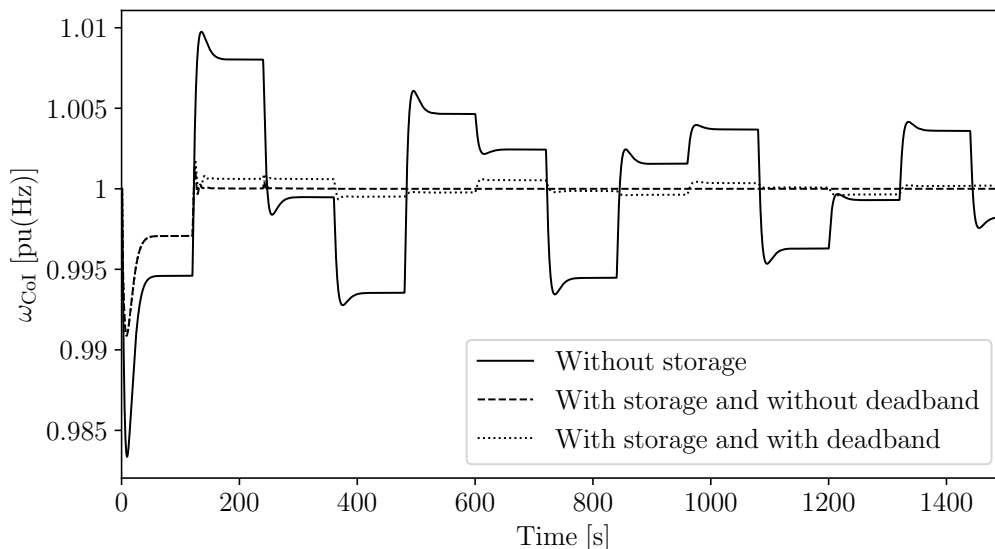


Figure 2.23: Transient response of  $\omega_{CoI}(t)$  following a 10% instantaneous load increase with zero droop and without ESSs limits.

### Zero droop with ESS capacity limits

The results of this scenario are shown in Fig. 2.24. If the ESSs limits are taken into account and the droop is set to zero ( $\mathcal{I}_d = 0$ ), the inclusion of the ESSs does not necessarily improve the system's dynamic behaviour. Moreover, introducing or not a deadband on the frequency error does not improve the overall dynamic response of the system. These results indicate that a PI controller is not the most adequate set-up to mitigate the long-term frequency variations caused by the market.

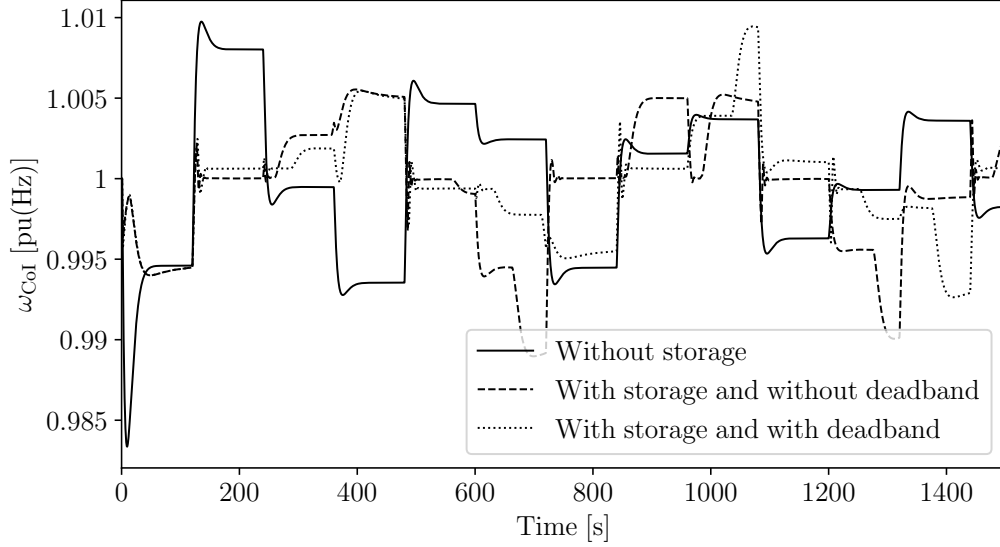


Figure 2.24: Transient response of  $\omega_{CoI}(t)$  following a 10% instantaneous load increase with zero droop and with ESSs limits.

### Non-zero droop without ESS capacity limits

This scenario considers a system setup similar to the case with zero droop without ESS limits except for the value of the integral deviation coefficient assumed to be  $\mathcal{I}_d = 0.7$ . Figure 2.25 shows that the frequency deviations for this scenario are similar to those obtained in Fig. 2.23. Also, in this case, the inclusion of the deadband on the frequency error leads to a worse dynamic behaviour of the system as compared to the case without deadband.

### Non-zero droop with ESS capacity limits

This last scenario considers ESS controllers with a non-zero droop and with and without a deadband in a scenario where ESS capacity limits are binding.

Results shown in Fig. 2.26 allow concluding that, also in this scenario, the inclusion of the deadband deteriorates the dynamic behaviour of the system. Figure 2.27 shows the effect of the deadband on the active power of an ESS. When deadband is not zero, the ESS reaches its active power limit, which gives rise to a sort of *bang-bang* phenomenon. These results indicate that depending on the set-up of the real-time electricity market, the values of the droop and deadband of the ESS frequency controller have to be carefully chosen.

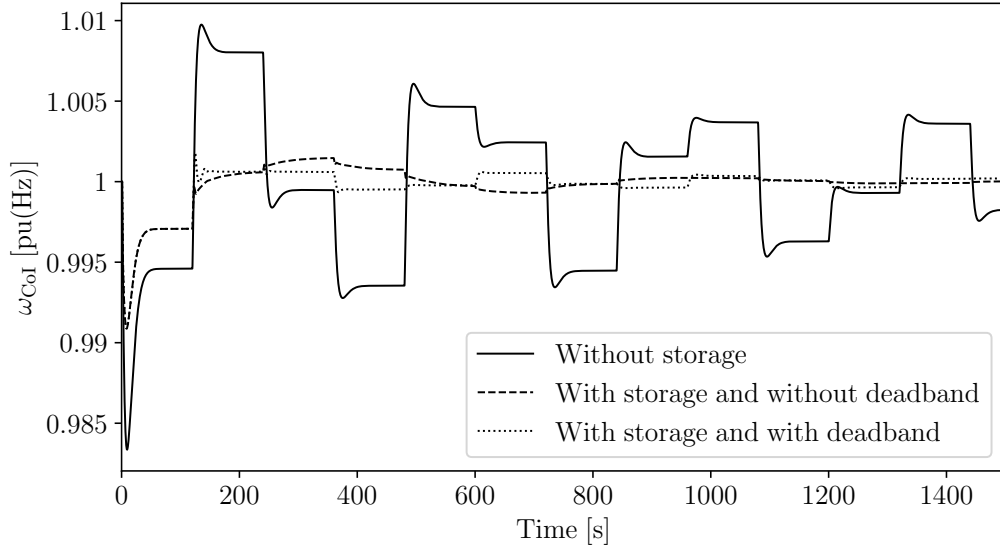


Figure 2.25: Transient response of  $\omega_{CoI}(t)$  following a 10% instantaneous load increase with non-zero droop and without ESSs limits.

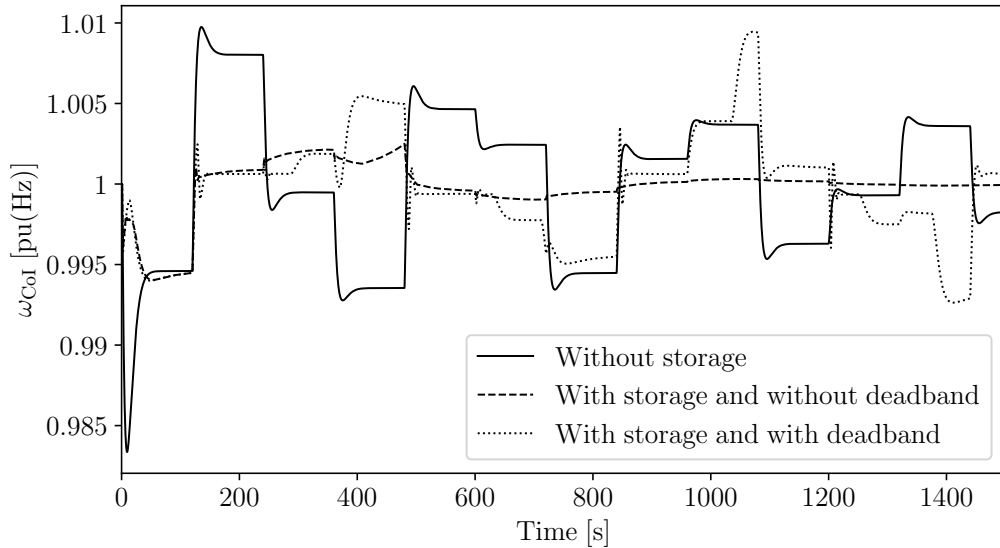


Figure 2.26: Transient response of  $\omega_{CoI}(t)$  following a 10% instantaneous load increase with non-zero droop and with ESSs limits.

## 2.6 Case Study 2: Impact of the Aggregate Response of DERs

This case study uses the AGC approach discussed in the previous sections to coordinate the DERs included in the VPP. The proposed approach aims to address a current concern of the Irish TSO, namely the impact of linear aggregate response of DERs on the

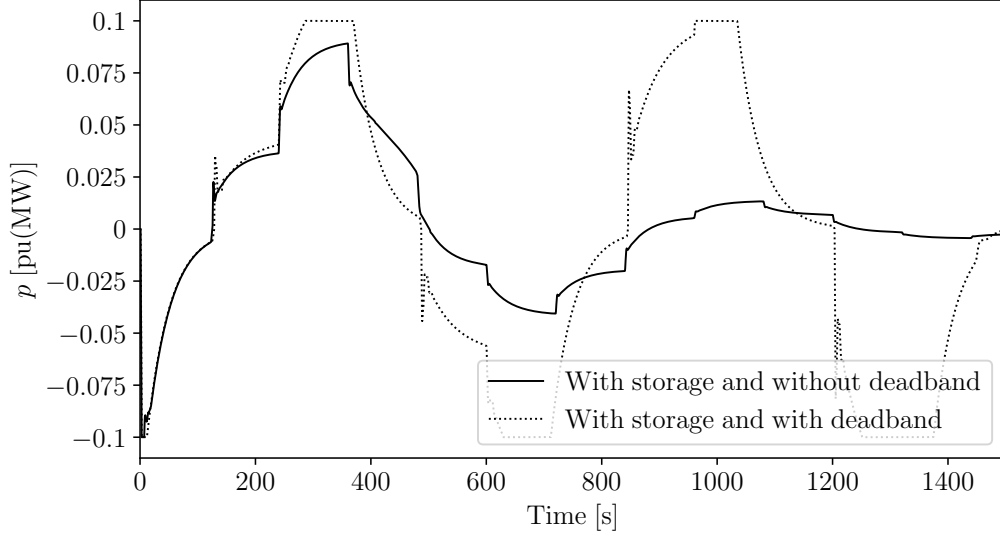


Figure 2.27: Transient response of ESS active power following a 10% instantaneous load increase with non-zero droop and with ESSs limits.

dynamic behavior of transmission systems [14]. Furthermore, its performance is compared with that of a MILP problem that optimally schedules the DERs that compose the VPP. To do so, the MILP is embedded into a TDS by means of software framework in order to study its impact on the dynamic response of the system [61]. Simulations on the IEEE 39-bus system serve to illustrate the features and dynamic behaviour of the proposed approaches.

### 2.6.1 AGC-based VPP

In this section, we propose an AGC scheme for the VPP that instead of regulating the frequency, regulates the total active power of the VPP. The proposed AGC control scheme is shown in Fig. 2.28 [68]. The signal  $p_{VPP}^{ref}$  is the reference power signal sent by the TSO to the VPP, and  $p_{VPP}$  is the sum of the measured active power of the DERs included in the VPP. An integrator block is then included to reduce the steady-state error to zero, with  $K_o$  being its gain. Finally, the AGC coordinates each TG of the generators proportionally to their droop, i.e.  $\mathcal{R}_g/\mathcal{R}_{tot}$ , where  $\mathcal{R}_{tot} = \sum_{g=1}^n \mathcal{R}_g$ .

### 2.6.2 MILP-based VPP

TSOs commonly utilize MILP to solve power system operation (e.g. UC) and planning problems. These analyses are facilitated by the significant improvements in the efficiency

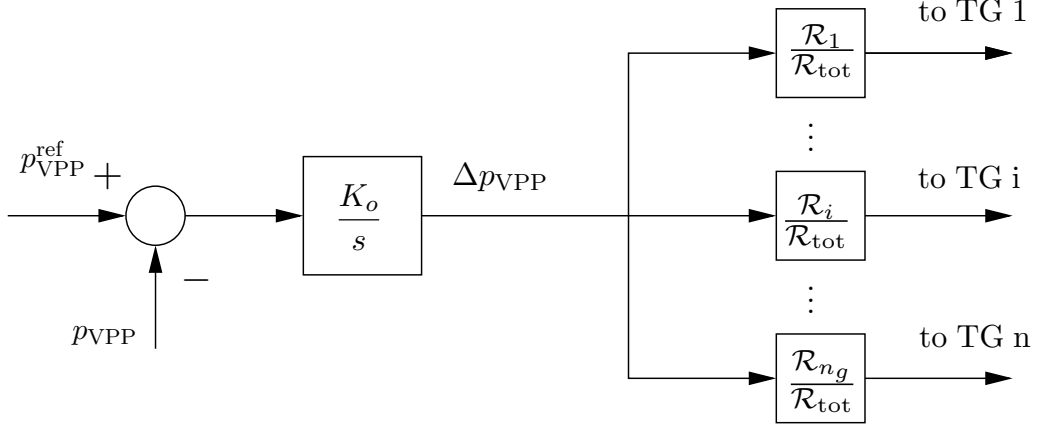


Figure 2.28: Basic AGC control scheme for active power regulation of VPPs.

and robustness of MILP solvers in recent years [91]. In this section, we use the MILP model proposed in [14] to optimally schedule the single generators of the VPP and obtain a ramping rate that is as close to linear as possible. The mathematical formulation of such a problem is as follows.

$$\min \sum_t (p_{a,t} + K p_{b,t}), \quad (2.13)$$

such that

$$p_{g,t} \leq p_g^{\max}, \quad \forall g, t, \quad (2.14)$$

$$p_{g,t} = p_{g,t-1} + R_g(z_{g,t} - \bar{z}_{g,t}), \quad \forall g, t, \quad (2.15)$$

$$z_{g,t} \geq z_{g,t-1}, \quad \forall g, t, \quad (2.16)$$

$$\bar{z}_{g,t} \geq \bar{z}_{g,t-1}, \quad \forall g, t, \quad (2.17)$$

$$\sum_t (z_{g,t} - \bar{z}_{g,t}) = \Upsilon_g, \quad \forall g, \quad (2.18)$$

$$\sum_g p_{g,t} + p_{b,t} - p_{a,t} = \frac{t \sum_g p_g^{\max}}{|\tilde{T}|}, \quad \forall t, \quad (2.19)$$

$$z_{g,t}, \bar{z}_{g,t} \in \{0, 1\}, \quad \forall g, t, \quad (2.20)$$

$$p_{g,t}, p_{a,t}, p_{b,t} \geq 0, \quad \forall g, t. \quad (2.21)$$

where  $p_{a,t}$  and  $p_{b,t}$  represent continuous variables that model the distances above and below the target linear characteristic (e.g. represented by the power generated by a single large power plant, see [61]) at time  $t$ , respectively.  $K$  represents a penalty multiplier when

the actual ramping rate is below the target line, i.e. this is needed as the VPP is penalized if it provides less power but that is not true for the other way round. In this chapter, a value of  $K = 10$  is considered. Equations (2.14) model the capacity limits of single small generators, where  $p_{g,t}$  represents the active power generation of the  $g$ -th generator at time period  $t$ . Equalities (2.15) model the ramping limits of generating units, where the binary variables  $z_{g,t}$  model the status of generating units when they are generating (1 if producing and 0 otherwise), while the binary variables  $\bar{z}_{g,t}$  model the status of generating units when they are generating at maximum capacity (1 if true and 0 otherwise). Equations (2.16) and (2.17) model the logic of the binary variables. Equations (2.18) model the generators ramp time ( $\Upsilon_g$ ), i.e. the sum of the differences  $z_{g,t} - \bar{z}_{g,t}$  must equal  $\Upsilon_g$ . Equations (2.19) model the target ramping line, i.e.  $\frac{t \sum_g p_g^{\max}}{|\tilde{T}|}$ , with  $|\tilde{T}|$  representing the total number of time periods. Finally, equations (2.20) and (2.21) represent variable declarations.

### 2.6.3 Comparison between AGC-based and MILP-based VPP

This section compares the performance of the AGC described in Section 2.6.1 and assumes a 20% penetration of VPPs. With this aim, it is assumed that at  $t = 1$  s there is a 20% instantaneous load increase. Because of this contingency, it is assumed that the TSO sends a signal to the VPP to start the production and cover the increase of the load within 15 minutes. The gain of the AGC is set to  $K_o = 50$ . The data of the VPP are given in Table A.1. To simulate the VPP, we connect ten small generators at buses 10-19. In the following, we assume that the VPP is only composed of non-renewable generation, i.e. small gas power plants, as is the case in the Irish system. The focus is on the first 15 minutes of the planning horizon that is the relevant time window for the aggregated response of DERs.

Figure 2.29 shows the results for two scenarios, namely MILP-based VPP and AGC-based VPP. The AGC-based VPP leads to better dynamic behaviour in the long-term than the MILP-based approach and achieves a null steady-state frequency error. **This is because the AGC-based approach has a slightly faster response than the MILP-based one.** Since the MILP-based control starts up the generators one by one (e.g. starting from the cheapest one) until they reach the set-point sent by the TSO, it cannot track perfectly the reference frequency. Moreover, The MILP-based approach causes several “ripples” in the frequency that correspond to the start-up of the units included in the VPP.

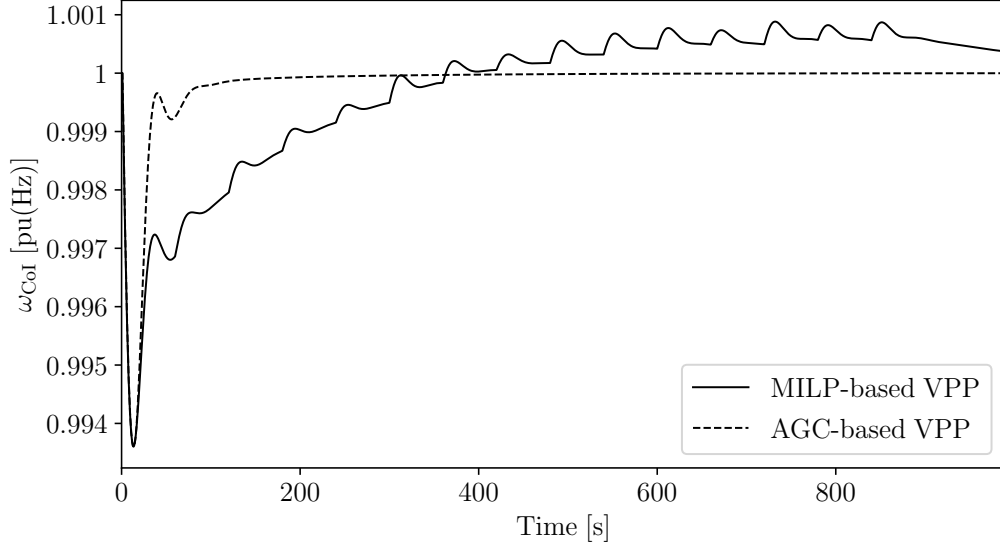


Figure 2.29: Comparison of the impact of AGC-based and MILP-based VPP.

The AGC-based VPP, on the other hand, starts up the DERs all at the same time and then smoothly increase their power output. From a system operator point of view, thus, the AGC-based VPP is preferable with respect to the conventional scheduling based on a MILP problem.

## 2.7 Conclusions

This chapter studies the impact of discrete secondary frequency controllers on power system dynamic behavior. In the first part, the chapter considers the impact of AGC and MAGC on the dynamic response of the system. The AGC is a controller installed in most of the control centers of TSOs, while the MAGC is a model that reproduces the behavior of real-time electricity markets with short dispatch periods. The illustrative examples suggest that increasing too much the execution cycles of the AGC leads to a limit cycle or bang-bang phenomena. It is shown that the only effective solution to remove this issue is to keep as short as possible the AGC execution cycles. The formal analogy between the AGC and MAGC and the results of the illustrative example indicate that if future real-time electricity markets will be based on the power imbalance to update the electricity price and use dispatch periods that range from some tens of seconds up to few minutes then these markets might lead to some sort of limit-cycles and/or power system instability.

The first part of the chapter also shows that: (i) integrating more wind power generation into power systems worsen the performance of both AGC controllers, and consequently, the power system dynamic performance; and (ii) the inclusion of WPPs in MAGC (real-time electricity markets) does not necessarily mean an improvement in the system's dynamic performance.

In the second part, the chapter evaluates the ability of converter-interfaced ESSs to mitigate long-term power system frequency deviations caused by quasi-real-time electricity markets. The main conclusion is that ESSs play an essential role in reducing the frequency deviations caused by the market. However, the ESS frequency control parameters, namely the droop coefficient and the deadband on the frequency error, have to be carefully chosen not to deteriorate the system's overall dynamic performance.

Finally, the chapter considers the problem of VPP linear ramping response and compares the performance of two approaches to coordinate the DERs, namely AGC-based and MILP-based VPP. While both methods achieve the main goal which is that of providing a linear ramping response of VPP, that is not the case for their dynamic performance. Specifically, Section 2.6.3 shows that an AGC-based VPP is to be preferred compared to scheduling based on an optimization problem as it leads to lower frequency variations of the system in the long-term. This is because the AGC-based VPP starts-up the generators simultaneously, whereas the MILP-based VPP starts-up the generators one by one (e.g. starting from the cheapest one) until they reach the set-point sent by the TSO. Despite the advantage of the AGC-based VPP, TSOs should pay special attention to possible interactions between the AGC-based VPP and conventional AGC. In other words, the control parameters of the two SFC controllers have to be carefully chosen to avoid possible dynamic couplings.

# Chapter 3

## A Short-Term Dynamic Electricity Market Model with Memory Effect

### 3.1 Introduction

In this chapter, an approach to include in the dynamic model [5] a specific aspect of the behavior of the market participants such as suppliers, namely the “memory effect”, is proposed. This aspect is absent in the several variants of the dynamic market model proposed so far in the literature. These models, in fact, are all based on conventional integer-order time derivatives. These consider an infinitely small neighborhood of the “present” time, i.e. the time at which the derivatives are computed [107]. This means that, by definition, the processes that are modelled through conventional differential equations have infinitely fast “amnesia.” However, taking into account the memory of market participants is of utmost importance in economic processes as they can remember the changes of economic indicators and factors in the past [108]. These changes can then impact their behavior and decisions. For example, it is shown that market participants can use available market information to form price expectations and to exploit arbitrage opportunities [97]. Therefore, modelling such a behaviour is critical in current and future electricity markets.

An effective and powerful tool to model the memory effects of a dynamic system is fractional calculus, which deals with the analysis of non-integer order differentials and integrals [110]. The ability of fractional derivatives to capture physical processes better than traditional integer-order derivatives has been shown for several systems in physics

and engineering [11]. For example, reference [106] provides a review of the application of fractional calculus in science and engineering. The recent work in [109] proposes a new economic model of the price dynamics of goods that considers the memory of the market agents. Using the work in [109] as a source of inspiration, this chapter takes into account for the first time the memory of the participants, in particular, suppliers, in power system markets.

The main goal of this chapter is to provide a short-term dynamic electricity market model with the inclusion of the memory effect. The model is a generalized system of differential equations of fractional order [28, 65]. It is highly realistic since it successfully describes the dynamic aspects of systems and incorporates the desired memory into the electricity market model by adding the essential information on how the memory of market participants, namely suppliers and consumers, impacts their behavior, i.e. on their bids.

The remainder of the chapter is organized as follows. Section 3.2 describes the modelling of economic processes with memory using fractional calculus. Section 3.3 presents the proposed fractional-order market model. Section 3.4 presents solutions of the proposed model and provides closed formulas of solutions. Section 3.5 provides an example using the obtained formula of solutions and a comparison between the integer and fractional market models on suppliers' decision-making and on power system dynamics. Finally, conclusions and future work are discussed in Section 3.6.

## 3.2 Modelling Economic Processes with Memory

A mathematical tool that allows modelling the memory effects of market agents is fractional-order differential equations. The recent work [109] extends the well-known Evans model – that describes the price dynamics of goods [40] – to take into account the memory of market participants. Based on this theoretical background, this section shows the mathematical steps that lead to the proposed fractional market model.

The Evans model of price dynamics is as follows:

$$\dot{\varpi}(t) = -\gamma\dot{q}(t), \quad (3.1)$$

where  $\varpi(t)$  represents the price of goods;  $\gamma$  is a proportional coefficient that represents the speed of response; and  $q(t)$  represents the stocks. The change in stocks is defined by

the following differential equation:

$$\dot{q}(t) = e_s(t) - e_d(t), \quad (3.2)$$

where  $e_s(t)$  and  $e_d(t)$  represent the supply and demand for goods, respectively. Using equation (3.2), equation (3.1) can be rewritten as:

$$\dot{\varpi}(t) = -\gamma(e_s(t) - e_d(t)). \quad (3.3)$$

The supply and demand are described by the following equations:

$$\begin{aligned} e_s(t) &= b_s + c_s \varpi(t), \\ e_d(t) &= b_d + c_d \varpi(t), \end{aligned} \quad (3.4)$$

where  $c_d, c_s, b_s, b_d$  are constant parameters. In particular,  $b_s$  and  $b_d$  represent the supply and demand, respectively, and do not depend on the price  $\varpi(t)$ . In general, it is assumed that  $c_d < 0$  and  $c_s > 0$ . Using equation (3.4), equation (3.3) of price dynamics can be rewritten, as follows:

$$\dot{\varpi}(t) + \gamma(c_s - c_d)\varpi(t) = \gamma(b_d - b_s). \quad (3.5)$$

Equation (3.5) is a first-order differential equation. It cannot account for the memory of the market participants. With this aim, one has to consider not only the difference  $e_s(t) - e_d(t)$ , but also the ‘‘history’’ of changes of the differences  $e_s(\tau) - e_d(\tau)$  on a finite time interval  $\tau \in [0, t]$ . Such a dependence of  $\varpi(t)$  can be described by the following equation:

$$\begin{aligned} \dot{\varpi}(t) &= - \int_0^t \gamma(t - \tau) \frac{dq(\tau)}{d\tau} d\tau \\ &= - \int_0^t \gamma(t - \tau) (e_s(\tau) - e_d(\tau)) d\tau, \end{aligned} \quad (3.6)$$

where  $\gamma(t)$  represents the memory function. Assuming a power-law fading memory, the function  $\gamma(t)$  can be written as follows:

$$\gamma(t - \tau) = \frac{\gamma}{\Gamma(\alpha)} (t - \tau)^{\alpha-1}, \quad (3.7)$$

where  $\Gamma(\alpha)$  is the gamma function;  $0 < \alpha < 1$  is the fractional-order; and  $t > \tau$ . Using (3.7), (3.6) can be rewritten as:

$$\begin{aligned}\dot{\varpi}(t) &= -\gamma \left( I_{RL;0+}^{\alpha} q^{(1)} \right) (t) \\ &= -\gamma \left( I_{RL;0+}^{\alpha} (e_s - e_d) \right) (t),\end{aligned}\tag{3.8}$$

where  $I_{RL;0+}$  is the Riemann-Liouville fractional integral defined as:

$$I_{RL;0+}^{\alpha} f(t) = \frac{1}{\Gamma(\alpha)} \int_0^t (t - \tau)^{\alpha-1} f(\tau) d\tau,\tag{3.9}$$

where the function  $f(\tau)$  is measurable on the interval  $(0, t)$  and has the property  $\int_0^t |f(\tau)| d\tau < \infty$ . Since we are interested to obtain a differential equation for the price dynamics, we act on equation (3.8) by the left-sided Caputo derivative of order  $\alpha > 0$  defined as follows:

$$\frac{d^{\alpha}}{dt^{\alpha} C;0+} f(t) = \frac{1}{\Gamma(n - \alpha)} \int_0^t (t - \tau)^{n-\alpha-1} f^{(n)}(\tau) d\tau,\tag{3.10}$$

and obtain the following fractional differential equation:

$$\frac{d^{\alpha+1}}{dt^{\alpha+1} C;0+} \varpi(t) = -\gamma(e_s(t) - e_d(t)),\tag{3.11}$$

where  $n - 1 < \alpha + 1 \leq 1$  and  $n \in \mathbb{N}$ . It can be seen that for  $\alpha = 0$ , equation (3.11) takes the form of the equation (3.5), while for  $\alpha = 1$ , equation (3.11) takes the form of the second-order differential equation of the Evans model [109].

## 3.3 Proposed fractional-order electricity market model

### 3.3.1 Modelling

The original version of the Alvarado model proposes a dynamic market model to study the couplings between the dynamics of the power network and the short-term electricity market, see [6]. It is based on the following equations:

- The first equation accounts for the system power imbalance indirectly, i.e. through the deviation frequency of the COI with respect to the reference frequency:

$$T_\rho \dot{\rho}(t) = -\mathcal{I}_d \rho(t) + K_E (\omega^{\text{ref}} - \omega_{\text{CoI}}(t)), \quad (3.12)$$

where  $\rho(t)$  is the electricity price;  $\omega^{\text{ref}}$  represents the reference frequency;  $\omega_{\text{CoI}}(t)$  represents the frequency of the COI, i.e.  $\omega^{\text{ref}} - \omega_{\text{CoI}}(t)$  is the deviation frequency of the COI with respect to the reference frequency;  $T_\rho$  is the time constant;  $\mathcal{I}_d$  is the deviation with respect to a perfect tracking integrator and for a LPF it is  $\mathcal{I}_d = 1$ ; and  $K_E$  can be written as  $K \cdot \rho(t)$  and be used as feedback gain.

- The second equation assumes that a generator will increase its power production if the electricity price is higher than its marginal cost:

$$T_{gi} \Delta \dot{p}_{gi}(t) = \rho(t) - c_{gi} \Delta p_{gi}(t) - b_{gi}, \quad (3.13)$$

where  $\Delta p_{gi}(t)$  is the generator active power;  $c_{gi}$ ,  $b_{gi}$  are the parameters of the marginal cost of the generator; and  $T_{gi}$  is the time constant.

- The third equation assumes that a load will decrease its power consumption if the electricity price  $\rho(t)$  is higher than its marginal benefit.

$$T_{di} \Delta \dot{p}_{di}(t) = -\rho(t) + c_{di} \Delta p_{di}(t) + b_{di}, \quad (3.14)$$

where  $\Delta p_{di}(t)$  is the load active power;  $c_{di}$ ,  $b_{di}$  are the parameters of the benefit of the load;  $T_{di}$  is the time constant.

If one assumes loads to be inelastic (i.e. not considering (3.14)), then the market model (3.12)-(3.13) has a very similar structure to that of a conventional SFC, i.e. the AGC [64] (see Fig. 2.1 and Fig. 2.11).

Equations (3.12)-(3.14) can be written as a matrix equation and form the following generalized system of differential equations:

$$\mathbf{E} \mathbf{x}'(t) = \mathbf{A} \mathbf{x}(t) + \boldsymbol{\omega}(t). \quad (3.15)$$

Where

$$\mathbf{E} = \begin{bmatrix} T_\rho & 0 & 0 \\ 0 & T_{gi} & 0 \\ 0 & 0 & T_{di} \end{bmatrix}, \quad \mathbf{A} = \begin{bmatrix} -\mathcal{I}_d & 0 & 0 \\ 1 & -c_{gi} & 0 \\ -1 & 0 & c_{di} \end{bmatrix}, \quad \mathbf{x}(t) = \begin{bmatrix} \rho(t) \\ \Delta p_{gi}(t) \\ \Delta P_{di}(t) \end{bmatrix},$$

and

$$\mathbf{B} = \begin{bmatrix} \omega^{\text{ref}} - \omega_{\text{CoI}}(t) & 0 & 0 \\ 0 & 1 & 0 \\ 0 & 0 & 1 \end{bmatrix}, \quad \mathbf{u} = \begin{bmatrix} K_E \\ -b_{gi} \\ b_{di} \end{bmatrix}, \quad \boldsymbol{\omega} = \mathbf{B}\mathbf{u}.$$

Next, we will define the Caputo fractional derivative that we will use as a tool for our model. Note that there exist several other definitions of fractional derivatives. We chose the Caputo fractional derivative because the initial conditions required are of the integer-order rather than the fractional order. This aspect is critical in engineering because we only have information about integer-order initial conditions and not fractional ones [115].

**Definition 3.1.** (see [13], [27]) Let  $Y : [0, +\infty) \rightarrow \mathbb{R}^{m \times 1}$ ,  $t \rightarrow Y$ , denote a column of continuous and differentiable functions. Then, the Caputo ( $C$ ) fractional derivative of order  $a$ ,  $0 < a < 1$ , is defined by:

$$\mathbf{Y}_C^{(a)}(t) := \mathbf{Y}^{(a)}(t) = \frac{1}{\Gamma(1-a)} \int_0^t [(t-x)^{-a} \mathbf{Y}'(x)] dx.$$

In order to simply explain why the proposed fractional derivative and its memory effect will relate to our model, we will use the discrete version of (3.15). An alternative way to represent this system, formed through (3.12)-(3.14), is the following generalized discrete time system:

$$\mathbf{E} \mathbf{x}_{k+1} = \mathbf{A} \mathbf{x}_k + \boldsymbol{\omega}_k, \quad k \in \mathbb{N}. \quad (3.16)$$

Where

$$\mathbf{E} = \begin{bmatrix} T_\rho & 0 & 0 \\ 0 & T_{gi} & 0 \\ 0 & 0 & T_{di} \end{bmatrix}, \quad \mathbf{A} = \begin{bmatrix} -\mathcal{I}_d & 0 & 0 \\ 1 & -c_{gi} & 0 \\ -1 & 0 & c_{di} \end{bmatrix}, \quad \mathbf{x}_k = \begin{bmatrix} \rho_k \\ \Delta p_{gi_k} \\ \Delta p_{di_k} \end{bmatrix}.$$

and

$$\mathbf{B} = \begin{bmatrix} \omega^{\text{ref}} - \omega_{\text{Col}}(t) & 0 & 0 \\ 0 & 1 & 0 \\ 0 & 0 & 1 \end{bmatrix}, \quad \mathbf{u} = \begin{bmatrix} K_{Ek} \\ -b_{gi} \\ b_{di} \end{bmatrix}, \quad \boldsymbol{\omega} = \mathbf{B}\mathbf{u}_k.$$

Equation (3.16) is a first-order matrix difference equation. It cannot account for the memory of the market participants. The term  $\mathbf{x}_{k+1}$  is only related to just a previous step in time namely the term  $\mathbf{x}_k$ . Hence, when using (3.16), we obtain the values of  $\rho_{k+1}$ ,  $\Delta p_{gi_{k+1}}$ ,  $\Delta p_{di_{k+1}}$  by only absorbing information from just a previous step in time  $k$ , and not considering all the ‘‘history’’ of changes at times  $k-1$ ,  $k-2$ , ...,  $k_0$ , where  $k_0$  the initial time step which can be assumed zero, i.e.  $k_0 = 0$ . To include the information from all these time steps we will use the fractional nabla operator.

To define this fractional operator and how it is formed, we initially have to define the backward difference operator of first order, denoted by  $\nabla$  (nabla operator), which when applied to a vector of sequences  $\mathbf{Y}_k : \mathbb{N} \rightarrow \mathbb{C}^m$  it produces the following result:

$$\nabla \mathbf{Y}_k = \mathbf{Y}_k - \mathbf{Y}_{k-1};$$

while the backward difference operator of second order, denoted by  $\nabla^2$ , is defined by:

$$\nabla^2 \mathbf{Y}_k = \nabla(\nabla \mathbf{Y}_k) = \mathbf{Y}_k - 2\mathbf{Y}_{k-1} + \mathbf{Y}_{k-2};$$

Similarly, the  $\nu^{\text{th}}$  backward difference operator,  $\nabla^\nu$ , is defined by:

$$\nabla^\nu \mathbf{Y}_k = \frac{1}{\Gamma(\nu+1)} \sum_{j=0}^{\nu} (-1)^j \frac{1}{\Gamma(j+1)\Gamma(\nu-j+1)} \mathbf{Y}_{k-j}, \quad \nu \in \mathbb{N}.$$

Where  $\Gamma(\cdot)$  is the Gamma function. In order to define the fractional nabla operator, see [26], we set:

$$\nabla^\nu \mathbf{Y}_k = \mathbf{f}_k.$$

Where  $\mathbf{f}_k$ , known vector of sequences. By solving for  $\mathbf{Y}_k$  we get:

$$\mathbf{Y}_k = \frac{1}{\Gamma(\nu)} \sum_{j=\alpha}^k (k-j+1)^{\overline{\nu-1}} \mathbf{f}_j = \nabla^{-\nu} \mathbf{f}_k.$$

Based on this expression, i.e.  $\nabla^{-\nu} \mathbf{f}_k = \frac{1}{\Gamma(\nu)} \sum_{j=\alpha}^k (k-j+1)^{\overline{\nu-1}} \mathbf{f}_j$ , if we define  $\mathbb{N}_\alpha$  by  $\mathbb{N}_\alpha = \{\alpha, \alpha+1, \alpha+2, \dots\}$ ,  $\alpha$  positive integer, and  $n$  fractional then the nabla fractional operator of  $n$ -th order for any  $\mathbf{Y}_k : \mathbb{N}_\alpha \rightarrow \mathbb{C}^m$  is defined by:

$$\nabla_\alpha^{-n} \mathbf{Y}_k = \sum_{j=\alpha}^k b_{k-j} \mathbf{Y}_j,$$

where  $b_{k-j} = \frac{1}{\Gamma(n)} (k-j+1)^{\overline{n-1}}$ ,  $j = \alpha, \alpha+1, \dots, k-1, k$ .

As already written, one has to consider not only one time step to absorb information from the past but also the “history” of changes throughout the timeline  $0, 1, \dots, k-1, k$ . This should be applied to three equations that form system (3.16) and have a different effect in each case:

$$\begin{aligned} T_\rho \rho_{k+1} &= \sum_{j=0}^k \gamma_{1,k-j} \left\{ -\mathcal{I}_d \rho_j + K_E (\omega^{\text{ref}} - \omega_{\text{CoI}}(t)_j) \right\} \\ T_{gi} \Delta p_{gi_{k+1}} &= \sum_{j=0}^k \gamma_{2,k-j} \left\{ \rho_j - c_{gi} \Delta p_{gi_j} - b_{gi} \right\} \\ T_{di} \Delta p_{di_{k+1}} &= \sum_{j=0}^k \gamma_{3,k-j} \left\{ -\rho_j + c_{di} \Delta p_{di_j} + b_{di} \right\}, \end{aligned}$$

where  $\gamma_{i,k-j}$ ,  $i = 1, 2, 3$ , represents the memory functions. Assuming a power-law fading memory, the functions  $\gamma(t)$  can be written as follows:

$$\gamma_{i,k-j} = \frac{1}{\Gamma(n_i)} (k-j+1)^{\overline{n_i-1}}, \quad j = 0, 1, \dots, k-1, k,$$

where  $\Gamma(n_i)$  are gamma functions; Equivalently we then have:

$$\begin{aligned} T_\rho \nabla_\alpha^{n_1} \rho_{k+1} &= -\mathcal{I}_d \rho_k + K_E (\omega^{\text{ref}} - \omega_{\text{CoI}}(t)_k) \\ T_{gi} \nabla_\alpha^{n_2} \Delta p_{gi_{k+1}} &= \rho_k - c_{gi} \Delta p_{gi_k} - b_{gi} \\ T_{di} \nabla_\alpha^{n_3} \Delta p_{di_{k+1}} &= -\rho_k + c_{di} \Delta p_{di_k} + b_{di}. \end{aligned} \tag{3.17}$$

Where  $0 \leq n_i \leq 1$  are the fractional-orders of the nabla discrete operator; Returning to the continues time system (3.15), and by using the previous discussion, we propose the

following fractional-order version of the dynamic electricity market model:

$$T_\rho \rho^{(n_1)}(t) = -\mathcal{I}_d \rho(t) + K_E(\omega^{\text{ref}} - \omega_{\text{Col}}(t)), \quad (3.18)$$

$$T_{gi} \Delta p_{gi}^{(n_2)}(t) = \rho(t) - c_{gi} \Delta p_{gi}(t) - b_{gi}, \quad (3.19)$$

$$T_{di} \Delta p_{di}^{(n_3)}(t) = -\rho(t) + c_{di} \Delta p_{di}(t) + b_{di}, \quad (3.20)$$

where  $0 \leq n_i \leq 1$  are the orders of the fractional derivatives. It's matrix form is:

$$\mathbf{E} \mathbf{x}^\Psi(t) = \mathbf{A} \mathbf{x}(t) + \boldsymbol{\omega}(t), \quad \mathbf{x}^\Psi = \begin{bmatrix} \rho^{(n_1)}(t) \\ \Delta p_{gi}^{(n_2)}(t) \\ \Delta p_{di}^{(n_3)}(t) \end{bmatrix}. \quad (3.21)$$

Where  $\mathbf{E}$ ,  $\mathbf{A}$ ,  $\mathbf{x}(t)$ ,  $\mathbf{B}$ ,  $\mathbf{u}$  as defined in (3.15). The pencil of the system is equal to, see [29]:

$$\begin{aligned} \begin{bmatrix} s^{n_1} & 0 & 0 \\ 0 & s^{n_2} & 0 \\ 0 & 0 & s^{n_3} \end{bmatrix} \mathbf{E} - \mathbf{A} &= \begin{bmatrix} s^{n_1} & 0 & 0 \\ 0 & s^{n_2} & 0 \\ 0 & 0 & s^{n_3} \end{bmatrix} \begin{bmatrix} T_\rho & 0 & 0 \\ 0 & T_{gi} & 0 \\ 0 & 0 & T_{di} \end{bmatrix} - \begin{bmatrix} -\mathcal{I}_d & 0 & 0 \\ 1 & -c_{gi} & 0 \\ -1 & 0 & c_{di} \end{bmatrix} \\ &= \begin{bmatrix} s^{n_1} T_\rho + \mathcal{I}_d & 0 & 0 \\ -1 & s^{n_2} T_{gi} + c_{gi} & 0 \\ 1 & 0 & s^{n_3} T_{di} - c_{di} \end{bmatrix}. \end{aligned}$$

The determinant of the pencil is equal to  $(s^{n_1} T_\rho + \mathcal{I}_d)(s^{n_2} T_{gi} + c_{gi})(s^{n_3} T_{di} - c_{di})$  which means that the pencil of this system is regular, though the system can be singular if at least one of the elements  $T_\rho$ ,  $T_{gi}$ ,  $T_{di}$  is zero or tends to be close to zero.

### 3.4 Solutions investigation

Since the pencil of system (3.21) is regular there exist solutions for the system, see [27], and in addition  $s\mathbf{E} - \mathbf{A}$  is also a regular pencil, see [29]. Because of the structure of  $\mathbf{E}$  there exist invariants of the following type:

- $\kappa$  finite eigenvalues of algebraic multiplicity  $\nu_i$ ,  $i = 1, \dots, \kappa, \dots, 3$ ;
- an infinite eigenvalue of algebraic multiplicity  $\mu$ ,

where  $\sum_{i=1}^{\kappa} \nu_i = \nu$ ,  $\nu + \mu = 3$ . There exist non-singular matrices  $\mathbf{W}, \mathbf{V} \in \mathbb{C}^{3 \times 3}$  such that, see [45]:

$$\mathbf{WEV} = \mathbf{I}_{\nu} \oplus \mathbf{H}_{\mu}, \quad \mathbf{WAV} = \mathbf{J}_{\nu} \oplus \mathbf{I}_{\mu}, \quad (3.22)$$

where  $\mathbf{J}_{\nu} \in \mathbb{C}^{\nu \times \nu}$  is Jordan matrix, constructed by the finite eigenvalues of the pencil and their algebraic multiplicity,  $\mathbf{H}_{\mu} \in \mathbb{C}^{\mu \times \mu}$  is a nilpotent matrix with index  $\mu_*$ , constructed by using the algebraic multiplicity of the infinite eigenvalue. We have the following cases:

1. The pencil of (3.21) to have all its eigenvalues finite. This is the most realistic case since it would mean that  $T_{\rho}, T_{gi}, T_{di}$  are all non-zero. In this case let

$$\mathbf{W} = \begin{bmatrix} \mathbf{W}_{1,n_1} \\ \mathbf{W}_{1,n_2} \\ \mathbf{W}_{1,n_3} \end{bmatrix}, \quad \mathbf{V} = \begin{bmatrix} \mathbf{V}_{\nu,n_1} & \mathbf{V}_{\nu,n_2} & \mathbf{V}_{\nu,n_3} \end{bmatrix},$$

where  $\mathbf{W}_{1,n_1} \in \mathbb{C}^{1 \times 3}$ ,  $\mathbf{W}_{1,n_2} \in \mathbb{C}^{1 \times 3}$ ,  $\mathbf{W}_{1,n_3} \in \mathbb{C}^{1 \times 3}$ , and  $\mathbf{V}_{\nu,n_1} \in \mathbb{C}^{3 \times 1}$ ,  $\mathbf{V}_{\nu,n_2} \in \mathbb{C}^{3 \times 1}$ ,  $\mathbf{V}_{\nu,n_3} \in \mathbb{C}^{3 \times 1}$ . Then (3.22) will take the form:

$$\mathbf{WEV} = \mathbf{I}_{\nu}, \quad \mathbf{WAV} = \mathbf{J}_{\nu}.$$

We can write (3.21) in the form:

$$\begin{bmatrix} \frac{d^{n_1}}{dt^{n_1}} & 0 & 0 \\ 0 & \frac{d^{n_2}}{dt^{n_2}} & 0 \\ 0 & 0 & \frac{d^{n_3}}{dt^{n_3}} \end{bmatrix} \mathbf{E}\mathbf{x} = \mathbf{A}\mathbf{x} + \boldsymbol{\omega}.$$

By using the transformation  $\mathbf{x} = \mathbf{V}\mathbf{z}$ , then multiplying by  $\mathbf{W}$  and using the above notation and (3.22) we get:

$$\mathbf{z}_{\hat{\nu}}^{(n_1)}(t) = \mathbf{J}_{\hat{\nu}} \mathbf{z}_{\hat{\nu}}(t) + \mathbf{W}_{1,n_1} \boldsymbol{\omega}(t);$$

$$\mathbf{z}_{\hat{\nu}}^{(n_2)}(t) = \mathbf{J}_{\hat{\nu}} \mathbf{z}_{\hat{\nu}}(t) + \mathbf{W}_{1,n_2} \boldsymbol{\omega}(t);$$

$$\mathbf{z}_{\hat{\nu}}^{(n_3)}(t) = \mathbf{J}_{\hat{\nu}} \mathbf{z}_{\hat{\nu}}(t) + \mathbf{W}_{1,n_3} \boldsymbol{\omega}(t),$$

where

$$\mathbf{z}(t) = \begin{bmatrix} \mathbf{z}_{\hat{\nu}}(t) \\ \mathbf{z}_{\bar{\nu}}(t) \\ \mathbf{z}_{\bar{\nu}}(t) \end{bmatrix}, \quad \mathbf{J}_p = \mathbf{J}_{\hat{\nu}} \oplus \mathbf{J}_{\bar{\nu}} \oplus \mathbf{J}_{\bar{\nu}}.$$

We consider the first equation. By applying the Laplace transform  $\mathcal{L}$  we get:

$$\mathcal{L}\{\mathbf{z}_{\hat{\nu}}^{(n_1)}(t)\} = \mathbf{J}_{\hat{\nu}}\mathcal{L}\{\mathbf{z}_{\hat{\nu}}(t)\} + \mathbf{W}_{1,n_1}\mathcal{L}\{\boldsymbol{\omega}(t)\}.$$

Let  $\mathcal{L}\{\mathbf{z}_{\hat{\nu}}(t)\} = \mathbf{w}_{\hat{\nu}}(s)$ . Then:

$$(s^{n_1}\mathbf{I}_{\hat{\nu}} - \mathbf{J}_{\hat{\nu}})\mathbf{w}_{\hat{\nu}}(s) = s^{n_1-1}C_1 + \mathbf{W}_{1,n_1}\mathcal{L}\{\boldsymbol{\omega}(t)\},$$

or, equivalently,

$$\mathbf{w}_{\hat{\nu}}(s) = s^{\gamma-1}(s^{n_1}\mathbf{I}_{\hat{\nu}} - \mathbf{J}_{\hat{\nu}})^{-1}C_1 + (s^{n_1}\mathbf{I}_{\hat{\nu}} - \mathbf{J}_{\hat{\nu}})^{-1}\mathbf{W}_{1,n_1}\mathcal{L}\{\boldsymbol{\omega}(t)\}.$$

By taking into account that  $(s^{n_1}\mathbf{I}_{\hat{\nu}} - \mathbf{J}_{\hat{\nu}})^{-1} = \sum_{k=0}^{\infty} s^{-(k+1)n_1} \mathbf{J}_{\hat{\nu}}^k$  we have:

$$\mathbf{w}_{\hat{\nu}}(s) = \sum_{k=0}^{\infty} s^{-n_1k-1} \mathbf{J}_{\hat{\nu}}^k C_1 + \sum_{k=0}^{\infty} s^{-(k+1)n_1} \mathbf{J}_{\hat{\nu}}^k \mathbf{W}_{1,n_1} \mathcal{L}\{\boldsymbol{\omega}(t)\}.$$

Then:

$$\mathbf{z}_{\hat{\nu}}(t) = \sum_{k=0}^{\infty} \frac{t^{n_1k}}{\Gamma(kn_1 + 1)} \mathbf{J}_{\hat{\nu}}^k C_1 + \int_0^t \frac{(t-\tau)^{(k+1)n_1-1}}{\Gamma(kn_1 + n_1)} \mathbf{J}_{\hat{\nu}}^k \boldsymbol{\omega}(\tau) d\tau.$$

To conclude, by similarly solving the other two equations we arrive at the general solution of (3.21) for this case:

$$\mathbf{x}(t) = \mathbf{V}\mathbf{z}(t) = \sum_{i=1}^3 \mathbf{V}_{\nu,n_i} \left[ \sum_{k=0}^{\infty} \frac{t^{n_i k}}{\Gamma(kn_i + 1)} \mathbf{J}_i^k C_i + \int_0^t \frac{(t-\tau)^{(k+1)n_i-1}}{\Gamma(kn_i + n_i)} \mathbf{J}_i^k \boldsymbol{\omega}(\tau) d\tau \right]. \quad (3.23)$$

Where  $\mathbf{J}_1 = \mathbf{J}_{\hat{\nu}}$ ,  $\mathbf{J}_2 = \mathbf{J}_{\bar{\nu}}$ ,  $\mathbf{J}_3 = \mathbf{J}_{\bar{\nu}}$ .

2. The second case is the pencil of (3.21) to have an infinite eigenvalue. This means that at least one of the terms  $T_\rho$ ,  $T_{gi}$ ,  $T_{di}$  is zero or tends to zero. The number of terms that are zero is the algebraic multiplicity  $q$  of the infinite eigenvalue. Let  $T_{di}$  be the term that is zero but let  $T_\rho$ ,  $T_{gi}$  be strictly non-zero. Then the algebraic

multiplicity  $q$  of the infinite eigenvalue is 1. Let:

$$\mathbf{W} = \begin{bmatrix} \mathbf{W}_{1,n_1} \\ \mathbf{W}_{1,n_2} \\ \mathbf{W}_{2,n_3} \end{bmatrix}, \quad \mathbf{V} = \begin{bmatrix} \mathbf{V}_{\nu,n_1} & \mathbf{V}_{\nu,n_2} & \mathbf{V}_{\nu,n_3} \end{bmatrix},$$

where  $\mathbf{W}_{1,n_1} \in \mathbb{C}^{1 \times 3}$ ,  $\mathbf{W}_{1,n_2} \in \mathbb{C}^{1 \times 3}$ ,  $\mathbf{W}_{1,n_3} \in \mathbb{C}^{1 \times 3}$ , and  $\mathbf{V}_{\nu,n_1} \in \mathbb{C}^{3 \times 1}$ ,  $\mathbf{V}_{\nu,n_2} \in \mathbb{C}^{3 \times 1}$ ,  $\mathbf{V}_{\nu,n_3} \in \mathbb{C}^{3 \times 1}$ . The equations in (3.22) will take the form:

$$\mathbf{W}\mathbf{F}\mathbf{V} = \mathbf{I}_{\hat{\nu}} \oplus \mathbf{I}_{\bar{\nu}} \oplus \mathbf{0}, \quad \mathbf{W}\mathbf{G}\mathbf{V} = \mathbf{J}_{\hat{\nu}} \oplus \mathbf{J}_{\bar{\nu}} \oplus \mathbf{1}.$$

We can write (3.21) in the form:

$$\begin{bmatrix} \frac{d^{n_1}}{dt^{n_1}} & 0 & 0 \\ 0 & \frac{d^{n_2}}{dt^{n_2}} & 0 \\ 0 & 0 & \frac{d^{n_3}}{dt^{n_3}} \end{bmatrix} \mathbf{E}\mathbf{x} = \mathbf{A}\mathbf{x} + \boldsymbol{\omega}.$$

By using the transformation  $\mathbf{x} = \mathbf{V}\mathbf{z}$ , then multiplying by  $\mathbf{W}$  and using (3.22) we get:

$$\mathbf{z}_{\hat{\nu}}^{(n_1)}(t) = \mathbf{J}_{\hat{\nu}}\mathbf{z}_{\hat{\nu}}(t) + \mathbf{W}_{1,n_1}\boldsymbol{\omega}(t);$$

$$\mathbf{z}_{\bar{\nu}}^{(n_2)}(t) = \mathbf{J}_{\bar{\nu}}\mathbf{z}_{\bar{\nu}}(t) + \mathbf{W}_{1,n_2}\boldsymbol{\omega}(t);$$

$$0 = \mathbf{z}_{\bar{q}}(t) + \mathbf{W}_{2,n_3}\boldsymbol{\omega}(t),$$

where

$$\mathbf{z}(t) = \begin{bmatrix} \mathbf{z}_{\hat{\nu}}(t) \\ \mathbf{z}_{\bar{\nu}}(t) \\ \mathbf{z}_{\bar{q}}(t) \end{bmatrix}.$$

The first two equations have same solutions as in case 1. The third equation has solution:

$$\mathbf{z}_{\bar{q}}(t) = -\mathbf{W}_{2,n_3}\boldsymbol{\omega}(t).$$

To conclude, by using  $\mathbf{x}(t) = \mathbf{V}\mathbf{z}(t)$ , we arrive at the general solution of (3.21) for this case:

$$\mathbf{x}(t) =$$

$$\sum_{i=1}^2 \mathbf{V}_{\nu, n_i} \left[ \sum_{k=0}^{\infty} \frac{t^{n_i k}}{\Gamma(k n_i + 1)} \mathbf{J}_i^k C_i + \int_0^t \frac{(t-\tau)^{(k+1)n_i-1}}{\Gamma(k n_i + n_i)} \mathbf{J}_i^k \omega(\tau) d\tau \right] - \mathbf{V}_{\nu, n_3} \mathbf{W}_{2, n_3} \omega(t) . \quad (3.24)$$

Where  $\mathbf{J}_1 = \mathbf{J}_{\hat{\nu}}$ ,  $\mathbf{J}_2 = \mathbf{J}_{\bar{\nu}}$ .

We proved the following theorem:

**Theorem 3.1.** Using the spectrum of the pencil  $s\mathbf{E} - \mathbf{A}$ , the general solution of the fractional order system (3.21) is given by:

$$\begin{aligned} \mathbf{x}(t) = & \sum_{i=1}^3 f(T_i) \mathbf{V}_{\nu, n_i} \left[ \sum_{k=0}^{\infty} \frac{t^{n_i k}}{\Gamma(k n_i + 1)} \mathbf{J}_i^k C_i + \int_0^t \sum_{k=0}^{\infty} \frac{(t-\tau)^{(k+1)n_i-1}}{\Gamma(k n_i + n_i)} \mathbf{J}_i^k \omega(\tau) d\tau \right] - \\ & \sum_{i=1}^3 g(T_i) \mathbf{V}_{q, n_i} \mathbf{W}_{2, n_i} \omega(t) . \end{aligned} \quad (3.25)$$

Where  $T_1 = T_{\rho}$ ,  $T_2 = T_{g_i}$ ,  $T_3 = T_{d_i}$ . The matrices  $J_1, J_2, J_3$  are Jordan matrices defined in (3.22), (3.23), (3.24), and constructed by the finite eigenvalues of the pencil  $s\mathbf{E} - \mathbf{A}$ , and their algebraic multiplicity, while  $\mathbf{V}_{\nu, n_i} \in \mathbb{C}^{3 \times \nu}$  are the matrices constructed by the linear independent eigenvectors related to the finite eigenvalues of the pencil.  $C_i \in \mathbb{C}^{\nu \times 1}$  are constant vectors. The matrices  $\mathbf{V}_{\nu, n_i}, \mathbf{W}_{2, n_i}$  are matrices with left and right eigenvectors of the infinite eigenvalue. Finally

$$f(T_i) = \begin{cases} 1, & T_i \neq 0 \\ 0, & T_i = 0 \end{cases}, \quad g(T_i) = 1 - f(T_i).$$

## 3.5 Examples

### 3.5.1 Example 1

As a first example we assume system (3.21) with  $T_{\rho} = H_{\mu} = c_{g_i} = 1$ ,  $T_{g_i} = -c_{d_i} = \frac{1}{2}$ ,  $T_{d_i} = \frac{1}{6}$ . The pencil  $s\mathbf{E} - \mathbf{A}$  has three finite eigenvalues  $\lambda_1 = -1$ ,  $\lambda_2 = -2$ ,  $\lambda_3 = -3$  with eigenvectors

$$\mathbf{V}_{\nu, n_1} = \begin{bmatrix} 1 \\ 1 \\ -3 \end{bmatrix}, \quad \mathbf{V}_{\nu, n_2} = \begin{bmatrix} 0 \\ 1 \\ 0 \end{bmatrix}, \quad \mathbf{V}_{\nu, n_3} = \begin{bmatrix} 0 \\ 0 \\ 1 \end{bmatrix},$$

respectively. Hence the solution of the system is equal to:

$$\mathbf{x}(t) = \begin{bmatrix} 1 \\ 1 \\ -3 \\ 0 \\ 1 \\ 0 \\ 0 \\ 0 \\ 0 \\ 1 \end{bmatrix} \begin{bmatrix} [\sum_{k=0}^{\infty} \frac{t^{n_1 k}}{\Gamma(kn_1+1)} (-1)^k C_1 + \int_0^t \sum_{k=0}^{\infty} \frac{(t-\tau)^{(k+1)n_1-1}}{\Gamma(kn_1+n_1)} (-1)^k \omega(\tau) d\tau] + \\ [\sum_{k=0}^{\infty} \frac{t^{n_2 k}}{\Gamma(kn_2+1)} (-2)^k C_2 + \int_0^t \sum_{k=0}^{\infty} \frac{(t-\tau)^{(k+1)n_2-1}}{\Gamma(kn_2+n_2)} (-2)^k \omega(\tau) d\tau] + \\ [\sum_{k=0}^{\infty} \frac{t^{n_3 k}}{\Gamma(kn_3+1)} (-3)^k C_3 + \int_0^t \sum_{k=0}^{\infty} \frac{(t-\tau)^{(k+1)n_3-1}}{\Gamma(kn_3+n_3)} (-3)^k \omega(\tau) d\tau] . \end{bmatrix}$$

### 3.5.2 Example 2

In this second example, we provide a comparison between the conventional Integer-Order MAGC (I-MAGC) (3.12)-(3.13),  $n_1 = n_2 = 1$ , and the Fractional-Order MAGC (F-MAGC) (3.18)-(3.19) with  $n_1 = 1$ ,  $n_2 = \alpha$ . The objective is to evaluate the impact of these models on the behavior of market participants, e.g. generator schedules, and on the overall dynamic response of the power system.

The comparison is based on a modified version of the well-known WSCC 9-bus test system, whose details are provided in [64]. A 10% sudden load increase is considered as a contingency.

#### Oustaloup's Recursive Approximation

In order to implement or simulate in practice the proposed fractional market model (3.18)-(3.19), one needs to approximate the fractional dynamics using appropriate rational order transfer functions. In this chapter, we use the Oustaloup's Recursive Approximation (ORA) method which is widely utilized as a continuous approximation technique. The generalized ORA of a fractional derivative of order  $\alpha$  is defined as [89]:

$$s^\alpha \approx \omega_h^\alpha \prod_{k=1}^N \frac{s + \omega'_k}{s + \omega_k}, \quad (3.26)$$

where  $\omega'_k = \omega_b \omega_v^{(2k-1-\alpha)/N}$ ,  $\omega_k = \omega_b \omega_v^{(2k-1+\alpha)/N}$ ,  $\omega_v = \sqrt{\omega_h/\omega_b}$ . In the above expressions,  $[\omega_b, \omega_h]$  is the frequency range for which the approximation is designed to be valid;  $N$  is the order of the polynomial approximation. The term “generalized” means that, in (3.26),  $N$  can be either even or odd [89], while the term “recursive” implies that the values of  $\omega'_k$ ,  $\omega_k$  result from a set of recursive equations. The block diagram of ORA is shown in Fig. 3.1. Further details on the ORA method and its accuracy can be found in [115] and references therein.

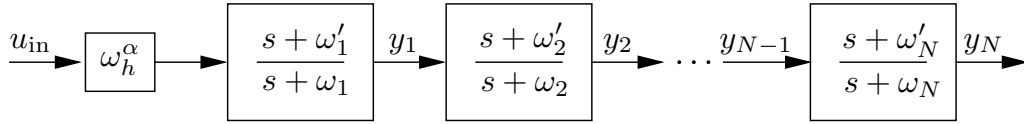


Figure 3.1: Oustaloup's recursive approximation block diagram.

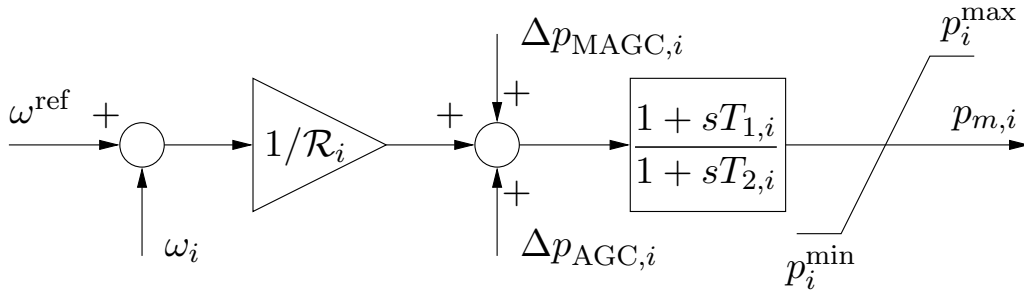


Figure 3.2: Updated turbine governor control diagram with the AGC and MAGC outputs.

## Impact of the Frequency of Price Updates

Some long-term power system dynamics, e.g. the dynamics of the AGC, evolve with a timescale similar to today's short-term market dynamics [122]. For this reason, it is essential to understand how the frequency with which the market price is updated impacts the decision-making process of market participants and on power system dynamics. In the continuous market models considered in this chapter, the information on how often the price is updated is contained in the value of the gain  $K_E$  in (3.12). Hence, this section presents a sensitivity analysis with respect to the variations of the  $K_E$ .

Figure 3.3 shows that the value of  $K_E$  has a negligible impact on the overall dynamic of the system, i.e. the frequency nadir is the same in all cases. [This was expected as the MAGC is slow with respect to the PFC \(see the model of the TGs and the respective](#)

interactions in Fig. 3.2). Figure 3.4, on the other hand, shows that the schedules of generator active power are by the value of  $K_E$ . Specifically, the faster the price updates, i.e. the higher  $K_E$ , the faster the generator response and consequently the higher the generator schedules. This phenomenon is called *price chasing* [124]. These results indicate that how often the market updates the price (which in this continuous model is modelled by means of  $K_E$ ) impacts the schedule of the suppliers or generators.

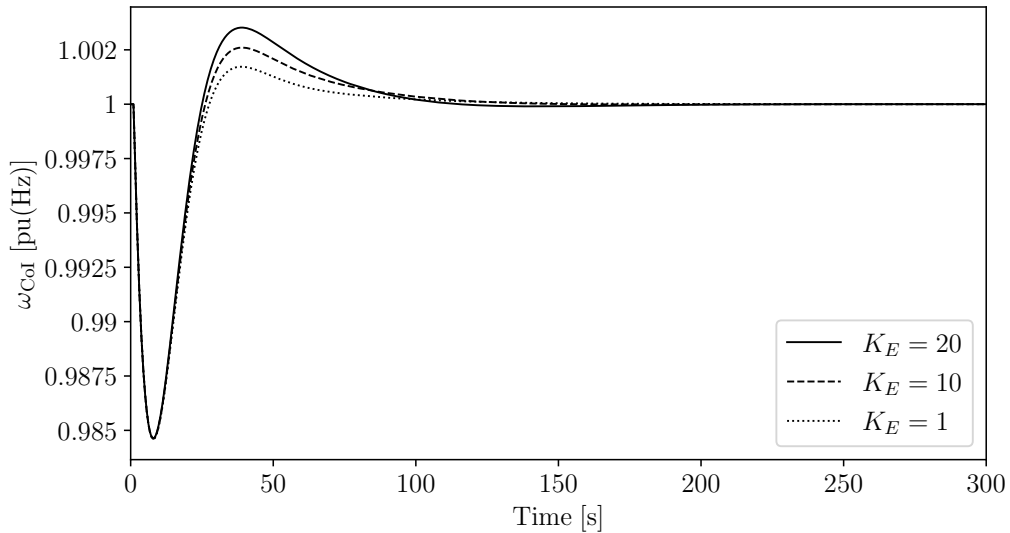


Figure 3.3: Trajectories of the frequency of the CoI.

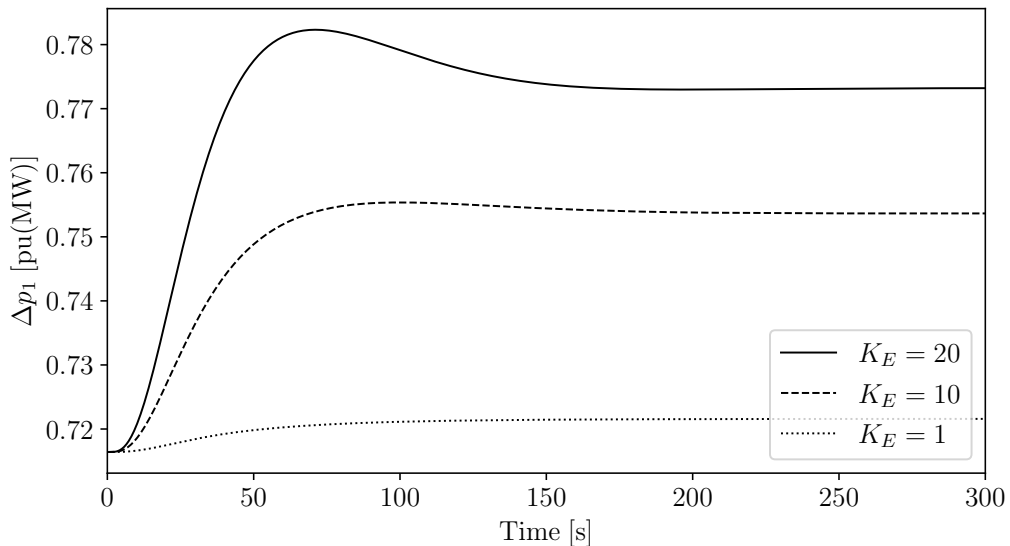


Figure 3.4: Trajectories of the MAGC active power schedules of generator 1.

The trajectories of the AGC set-point  $\Delta p_1$  of generator 1 are shown in Fig. 3.5. Higher gain values – and hence faster price updates – lead to faster AGC response and lower

AGC set-points. This has to be expected as the AGC has to compensate the difference in the market schedules since at the end the total power output of the generator has to be the same. These results imply that, depending on the market design and rewards of the ancillary services, generators may prefer to compensate power imbalances through the short-term market or through the SFC.

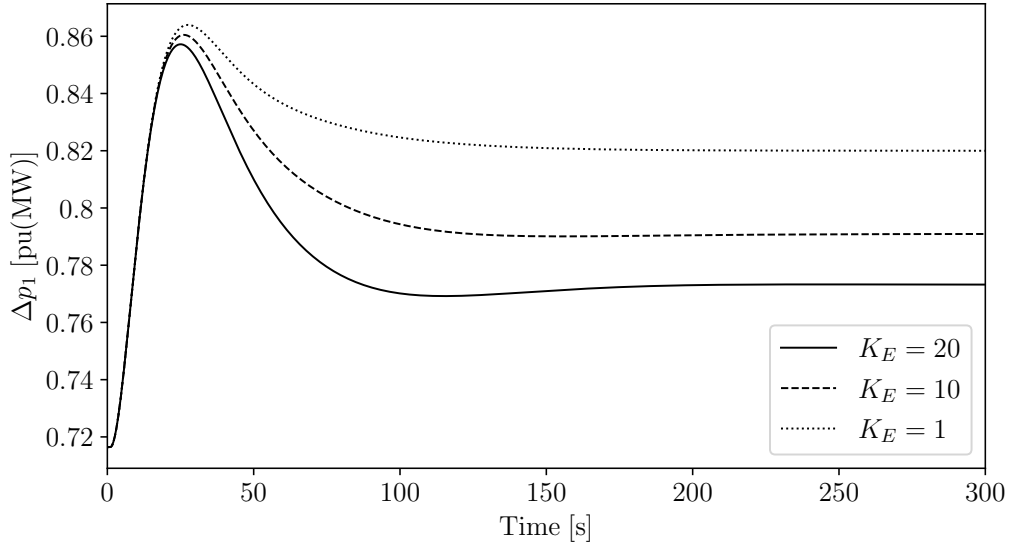


Figure 3.5: Trajectories of the AGC active power set-point of generator 1.

### Sensitivity Analysis

This section presents a sensitivity analysis with respect to the fractional-order  $\alpha$  of the F-MAGC and compares the results with the ones obtained using the conventional integer-order market model. For fair comparison, all other parameters, namely time constants and gains, of both market models, (3.12)-(3.13) and (3.18)-(3.19), are kept the same.

First, we compare the impact of I-MAGC and F-MAGC on power system dynamics. Figure 3.6 shows the trajectories of  $\omega_{CoI}(t)$  for both models. It is interesting to observe that both the I-MAGC and F-MAGC lead to the same frequency nadir and very similar frequency overshoots. The memory of market participants, thus, does not have a relevant impact on the overall power system dynamics. These results are consistent with those shown in Fig. 3.3.

Next, we compare the effect that different values of  $\alpha$  have on the behavior of the generators. Figure 3.7 shows that the F-MAGC leads to different (in this case, lower) market schedules compared to that of the I-MAGC. This result suggests that the

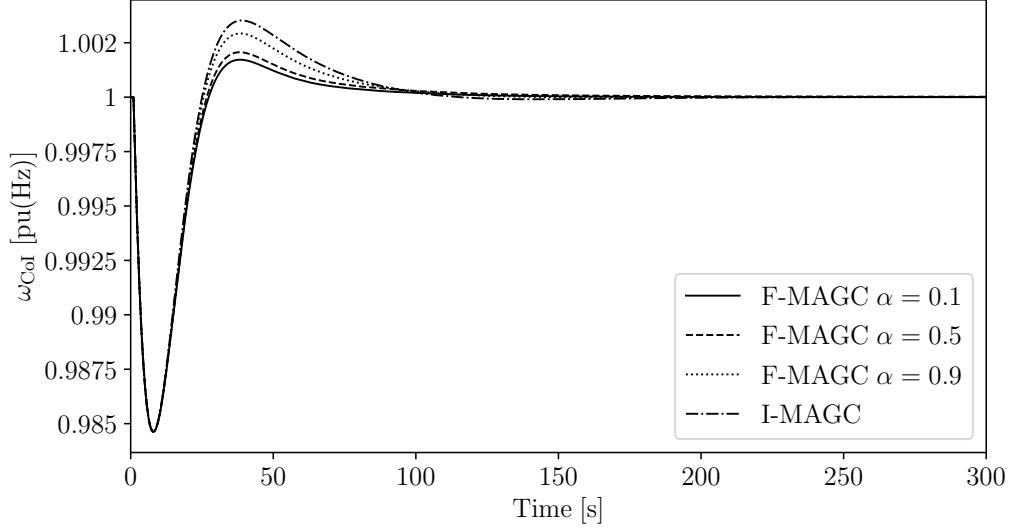


Figure 3.6: Comparison of the trajectories of the frequency of the CoI as obtained with the I-MAGC and F-MAGC.

F-MAGC is less prone to price changes. In other words, taking into account the memory of market participants makes them more conservative. Furthermore, the higher the fractional-order  $\alpha$ , the faster the generator response, and consequently, the higher the generator market schedules. This conclusion is supported by Fig. 3.8. This figure shows that the AGC set-point for the fractional market is less prone to changes compared to the conventional market. Observe that, in steady-state, the total active power generation depends only on the variation of the load consumption. However,  $\alpha$  changes the quota of active power produced by each machine. The dependency of the steady-state on  $\alpha$  is evident in Fig. 3.7. However, for  $\alpha > 0.9$  and  $\alpha \rightarrow 1$ , the steady-state operating point of each machine varies very little.

### Impact of a Sudden Load Decrease

In this final example, we compare the impact on the performance of I-MAGC and F-MAGC of a 10% sudden load decrease occurring at  $t = 1$  s.

Figure 3.9 shows that the F-MAGC is again less prone to price changes compared to the I-MAGC. For the considered contingency, such a behavior leads the market to schedule higher generator powers.

Figure 3.10 shows the AGC power output and indicates that the I-MAGC case responds faster than the F-MAGC to the contingency. This result is consistent with that obtained in the previous section, i.e. the memory effect makes the generators less sensitive

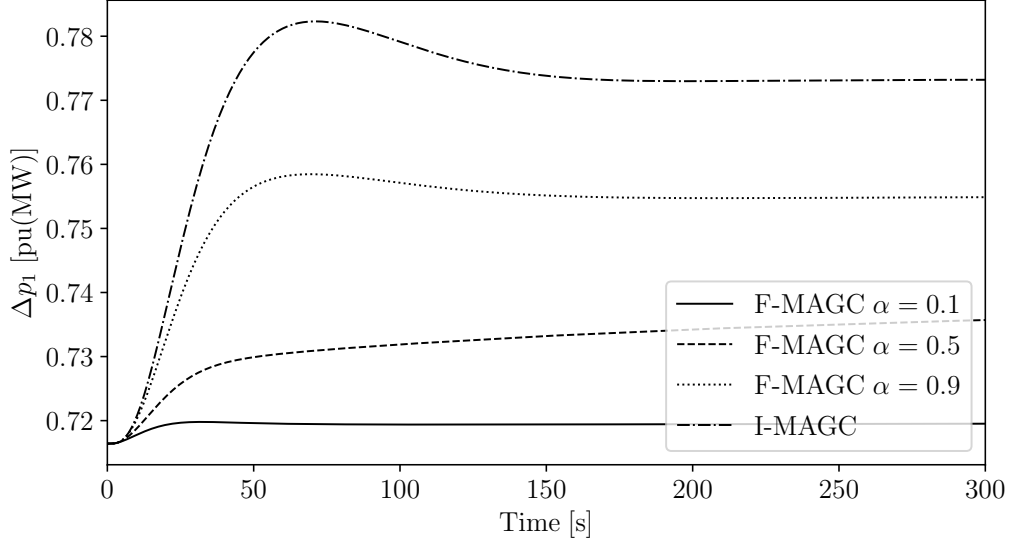


Figure 3.7: Trajectories of the MAGC active power schedules of generator 1.

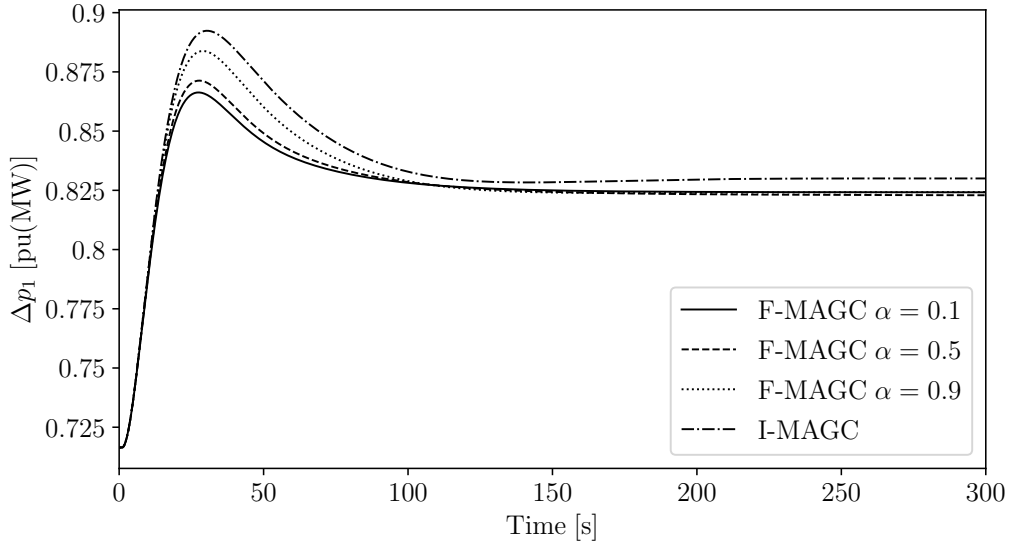


Figure 3.8: Trajectories of the AGC active power set-point of generator 1.

to changes in the operating point of the grid. This conservativeness, however, has to be compensated, at least in the short term, by the secondary frequency regulation.

### 3.6 Concluding remarks

This chapter contributes to the application of fractional calculus in power systems by proposing a dynamic model for electricity markets based on differential equations of fractional order. This is the first attempt to model the behavior of market participants

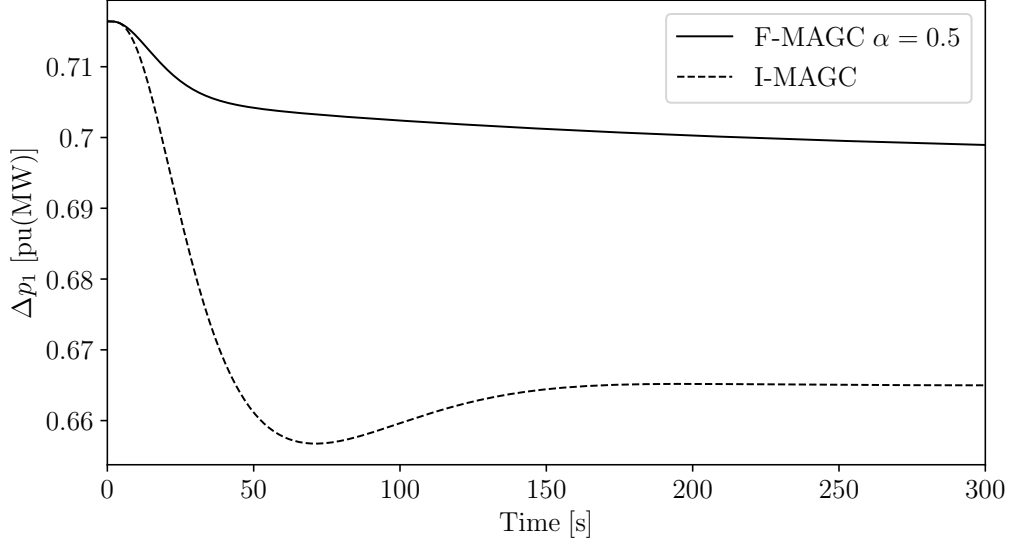


Figure 3.9: Trajectories of the MAGC active power schedules of generator 1.

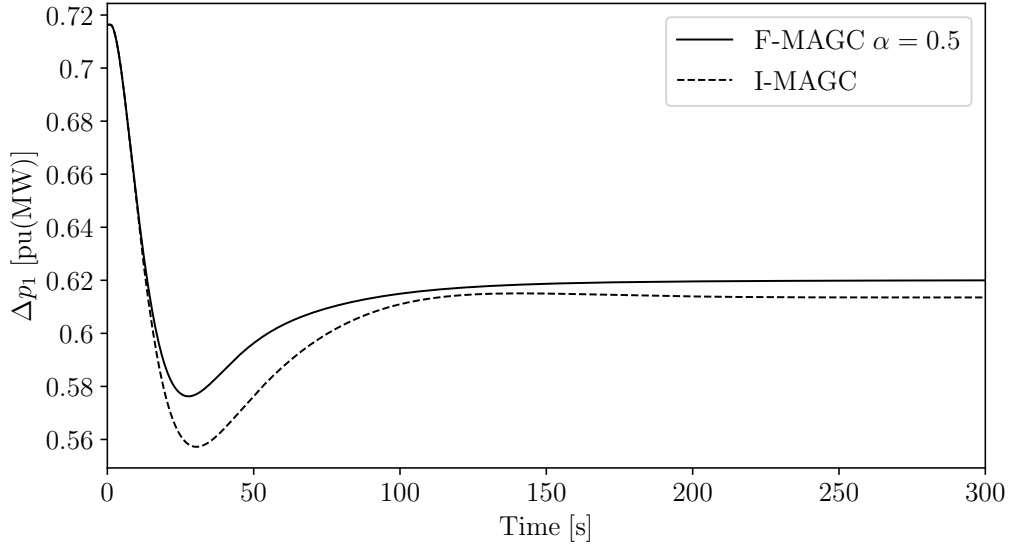


Figure 3.10: Trajectories of the AGC active power set-point of generator 1.

and its impact on their decisions and power system dynamics. As such, we believe it is an exciting research topic and necessarily yet to be fully understood.

First, it is shown how to model economic processes with memory by applying fractional calculus to the Evans model that describes the price dynamics of goods. Using such an application as a motivation, a short-term fractional dynamic electricity market model is then proposed. Next, we study its solutions and provide analytical and numerical examples, including comparing a model of integer order differential equations. In particular, for the numerical example, we employ the ORA method to approximate the fractional dynamics. This is critical if one needs to implement in practice such a model in a software tool.

The second example demonstrates that taking into account the memory of suppliers has a negligible impact on the dynamic behaviour of power systems. This has to be expected as such an aspect of market participates intrinsically has a long timescale compared to power system dynamics. In contrast, the memory effect leads to a conservative behavior of suppliers and their decisions. Specifically, different fractional order  $\alpha$  lead to different market schedules. Therefore, accounting for the memory effect in future electricity markets is of utmost importance.

# Chapter 4

## Interaction between Deterministic Sub-Hourly Unit Commitment and Power System Dynamics

### 4.1 Introduction

This chapter states the need for sub-hourly modelling in power systems and discusses the impact interactions between the sub-hourly d-UC and power system dynamics through a recently proposed software framework. The remainder of the chapter is organized as follows. Section 4.2 motivates the use of sub-hourly timescales in power system scheduling. Section 4.3 describes the mathematical formulation of d-UC. Section 4.4 presents the proposed software framework for studying the interactions between d-UC and HDAEs. Two case studies are presented in Section 4.5 and Section 4.6 that focus on the effect of different scheduling periods and different net-load volatility and control/machine parameters on the system's dynamic response. Finally, conclusions are drawn in Section 4.7.

### 4.2 Need for Sub-hourly Modelling

The UC problem plays a crucial role in the secure operation of power systems. Most of the electric utilities in the US clear the markets using a d-UC [42]. The level of system security in these models is mainly defined by network constraints equations (e.g. line flow limits) and the amount of scheduled reserves. Traditionally, these models are solved with

an hourly time period [43]. This time scale is well decoupled from relevant power system dynamics. However, a sub-hourly UC is to be preferred in systems with high penetration of variable RESs [117, 128] as these increase variability and uncertainty and at the same time decrease the overall inertia of the system [86].

Furthermore, sub-hourly scheduling is a way to increase flexibility without investing in physical assets [51, 76]. Reference [30] shows that sub-hourly modelling allows to better capture the costs and the ramping capability of generators. A more recent paper [44] demonstrates that sub-hourly dispatch results in lower costs and lower reserves. The importance of sub-hourly modelling is also shown in [113], where the authors conclude that sub-hourly modelling reveals significant power plant cycling in the form of ramping and start-ups. Moreover, reference [67] shows that using a sub-hourly UC with a rolling horizon approach, i.e. scheduling the system more frequently using a forecast moving window, the required reserves can be decreased.

A sub-hourly UC, e.g. 5-minute resolution, can overlap with long-term dynamics. There exist several attempts to include simplified dynamic constraints into the UC problem, for example [4, 25, 33, 73, 77, 100, 111]. However, the main limitation of these approaches is that the dynamics of the system are oversimplified and linearized. On the other hand, embedding the UC problem into a fully-fledged transient stability analysis software tool has not been thoroughly discussed so far.

### 4.3 Deterministic Unit Commitment Formulation

The main objective of the UC problem is to minimize the total operating cost and determine for a given planning horizon the ON/OFF status of the generating units needed to match the demand. It is common practice to formulate the UC as a MILP problem thanks to the good performance of the available commercial solvers [18]. In this chapter, a conventional MILP d-UC problem is used [22]. The mathematical formulation is recalled below.

## Objective function

The objective function of the d-UC to be minimized consists of the fixed, variable, start-up and shut-down costs of the generating units, as follows:

$$\sum_{t \in \mathcal{T}} \sum_{g \in \mathcal{G}} (C_g^F z_{g,t}^F + C_g^V p_{g,t} + C_g^{SU} z_{g,t}^{SU} + C_g^{SD} z_{g,t}^{SD}) \quad (4.1)$$

where  $t$  is the index for the time period;  $g$  is the index for the generating units;  $\mathcal{T}$  is the set of time periods, e.g.  $\{1, \dots, 24\}$  hours;  $\mathcal{G}$  is the set of generating units;  $z_{g,t}^F$  is the binary variable that represents the status of the units in time period  $t$ , e.g. 1 if ON;  $z_{g,t}^{SU}$  and  $z_{g,t}^{SD}$  are the binary variables that represent the status of the units at the beginning of time period  $t$ , i.e.  $z_{g,t}^{SU} = 1, z_{g,t}^{SD} = 0$  if the generator is up and  $z_{g,t}^{SU} = 0, z_{g,t}^{SD} = 1$  if the generator is down; and  $p_{g,t}$  is the continuous variable representing the active power production during time period  $t$ .

## Binary variable constraints

These constraints are needed to ensure the consistency of the logic of binary variables. For example, if a unit is ON in a given period  $t$ , then it can only be switched OFF but not started-up in the following period. The constraints are:

$$z_{g,t}^{SU} - z_{g,t}^{SD} = z_{g,t}^F - z_{g,t-1}^F, \quad \forall g \in \mathcal{G}, \forall t \in \mathcal{T}, \quad (4.2)$$

$$z_{g,t}^{SU} + z_{g,t}^{SD} \leq 1, \quad \forall g \in \mathcal{G}, \forall t \in \mathcal{T}, \quad (4.3)$$

$$z_{g,t}^F, z_{g,t}^{SU}, z_{g,t}^{SD} \in \{0, 1\} \quad \forall g \in \mathcal{G}, \forall t \in \mathcal{T} \quad (4.4)$$

Note that the sum of the start-up and shut-down binary variables cannot be greater than one. Note also that for the first time period, the initial status of the unit, namely  $z_{g,0}^F$  has to be known in (4.2) and is thus an input datum. When the model steps forward (i.e. rolling horizon) the status of the units at the end of the horizon serve as an initial status for the next planning horizon, and so on.

## Power bounds

Typical technical constraints of the generating units include their upper and lower limits:

$$P_g^{\min} z_{g,t}^F \leq p_{g,t} \leq P_g^{\max} z_{g,t}^F, \quad \forall g \in \mathcal{G}, \forall t \in \mathcal{T}, \quad (4.5)$$

where,  $P_g^{\min}$  and  $P_g^{\max}$  are the minimum and maximum active power limits, respectively.

## Ramping limits

Other important constraints of generation units are the so-called ramping limits. For instance, between two successive time periods, a unit output is bounded by a maximum value called the ramping-up limit. Also, a start-up limit is applied to the unit power output during its start-up time. Similar considerations apply to the ramping-down and shut-down ramping limits. The ramping limit constraints are:

$$p_{g,t} - p_{g,t-1} \leq R_g^U z_{g,t-1}^F + R_g^{SU} z_{g,t}^{SU}, \quad \forall g \in \mathcal{G}, \forall t \in \mathcal{T}, \quad (4.6)$$

$$p_{g,t-1} - p_{g,t} \leq R_g^D z_{g,t}^F + R_g^{SD} z_{g,t}^{SD}, \quad \forall g \in \mathcal{G}, \forall t \in \mathcal{T}, \quad (4.7)$$

where,  $R_g^U, R_g^{SU}, R_g^D, R_g^{SD}$  are the ramping-up, start-up ramping, ramping-down and shut-down ramping limits, respectively. Since ramping limits are generally given in per hour, we divide the hourly data by the relevant sub-hourly scheduling interval, e.g. by 4 in the 15 min case. Again,  $z_{g,0}^F$  has to be assigned for the first time period.

## Power balance

The following constraints ensures the active power balance at every node of the network:

$$\begin{aligned} \sum_{g \in \mathcal{G}_n} p_{g,t} - \sum_{l \in \mathcal{D}_n} d_{l,t} = \\ \sum_{m \in \mathcal{F}_n} B_{nm} (\theta_{n,t} - \theta_{m,t}), \quad \forall n \in \mathcal{F}, \quad \forall t \in \mathcal{T}, \end{aligned} \quad (4.8)$$

where  $d_{l,t}$  is the forecasted demand located at node  $n$ ;  $\mathcal{F}$  is the set of all branches;  $B_{nm}$  is the susceptance of transmission line  $n - m$ ; and  $\theta_{n,t}$  and  $\theta_{m,t}$  are the voltage phase angles at nodes  $n$  and  $m$ , respectively. The set  $\mathcal{G}_n$  indicates the generators connected to bus  $n$ . Similarly,  $\mathcal{D}_n$  and  $\mathcal{F}_n$  are the demands and lines, respectively, connected to bus  $n$ .

### Transmission lines limits

Generally, the power through a transmission line is limited by its thermal limit:

$$\begin{aligned} -P_{nm}^{\max} &\leq B_{nm}(\theta_{nt} - \theta_{mt}) \leq P_{nm}^{\max}, \\ \forall n, \forall m \in \mathcal{F}_n, \forall t, \end{aligned} \tag{4.9}$$

where,  $P_{nm}^{\max}$  is the capacity limit of the line.

### Security constraints

System operators usually schedule some spinning reserves in order to cope with unforeseen events, e.g. an unscheduled outage. So, for all time periods, the total generation available online has to be greater than the actual demand:

$$\sum_{g \in \mathcal{G}_i} P_g^{\max} z_{g,t}^F \geq \sum_{l \in \mathcal{D}} (d_{l,t} + r_{j,t}), \quad \forall i, \forall t \in \mathcal{T}, \tag{4.10}$$

where  $d_{l,t}$  is the system total forecasted demand;  $r_{j,t}$  accounts for reserves; and  $\mathcal{G}_i$  is the set of generators that provides reserve (in the following, we assume  $\mathcal{G}_i \equiv \mathcal{G}$ ). For simplicity, the amount of reserve is assumed to be a percentage of the total demand. The reserve percentage value is lower for shorter scheduling timescales assuming that better forecast is available [67].

### Reference angle

Finally, as it is well-known, the voltage phase angle at some node of the network has to be assigned:

$$\theta_{n,t} = 0, \quad \forall t \in \mathcal{T}, \tag{4.11}$$

where  $n$  is the node chosen to be the reference angle.

### Remarks on the UC model

Equations (4.1)-(4.11) form a conventional model of d-UC. The aim, in fact, is not to propose a novel formulation of the UC but rather to show how the UC can be embedded into the dynamic model of power systems. In the following, the d-UC is modeled using different sub-hourly time periods, ranging from 15 to 3.75-minutes. Moreover, a rolling

(moving window) approach with a planning horizon of 24 hours is considered to account for better forecast. In other words, the d-UC problem (4.1)-(4.11) is solved at every time period  $t$  for the next 24 hours.

The average demand of each load is assumed to vary as a piece-wise linear function according to a predefined profile. To simulate uncertainty, the values  $d_{l,t}$  utilized to solve the d-UC problem at each period differ from the actual demand of the loads by a given percentage. A normal distribution function with different standard deviations per period, say,  $\sigma_t$ , is used to generate the forecast error. The value of the standard deviation increases linearly as a function of  $t$ . Specifically,  $\sigma_t$  is null for current loading condition, i.e.  $t = 0$ , and is maximum for the last period of the planning horizon  $\mathcal{T}$ .

#### 4.4 Interaction between d-UC and HDAEs

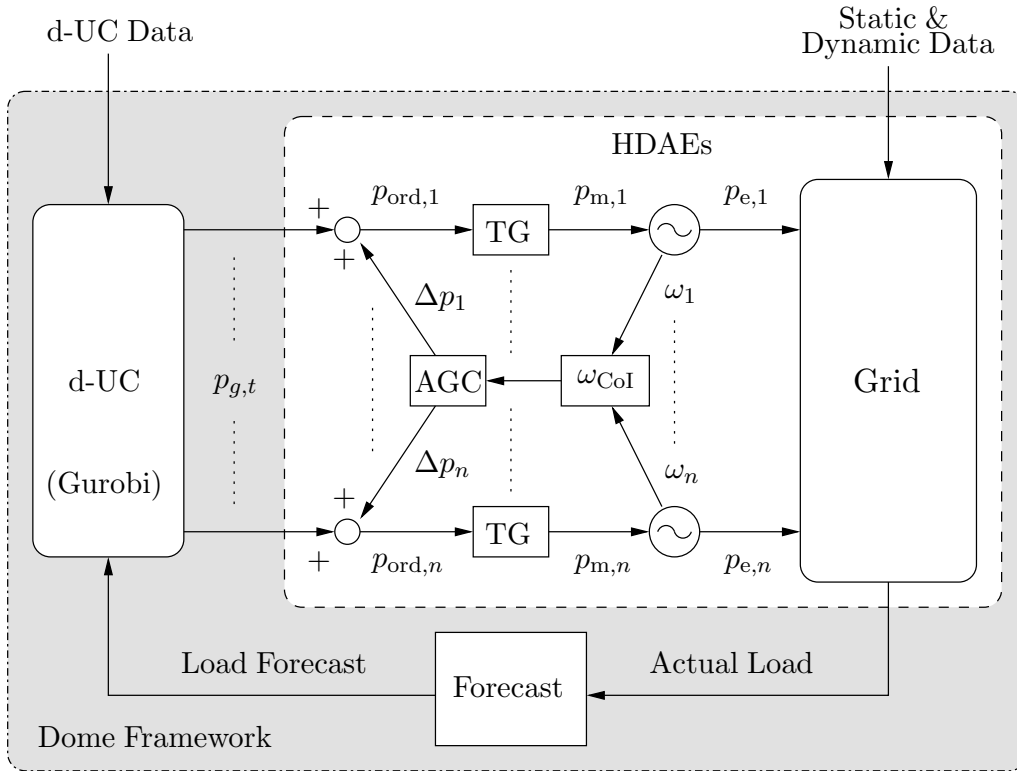


Figure 4.1: Interaction between the d-UC problem, AGC, TGs, synchronous machines and the grid.

It is time to embed the d-UC equations (4.1)-(4.11) into equations (2.1). One has two ways to do so: embed d-UC into an existing power system dynamic model (HDAEs), or

the other way round. This thesis proposes the former approach, i.e. embedding the d-UC problem (4.1)-(4.11) into the TDS routine of Dome [85].

Figure 4.1 shows the connection and the interactions between d-UC, TGs, AGC, generators, demands and the rest of the grid. In particular, the solutions of the d-UC ( $p_{g,t}, \forall g \in \mathcal{G}$ ) and the output of the AGC ( $\Delta p$ ), are utilized to change the power order set-point ( $p_{\text{ord}}$ ) of the TGs of the power plants which in turn changes the mechanical ( $p_m$ ) and electrical ( $p_e$ ) power of synchronous generators, respectively.

## 4.5 Case Study 1: Impact of Different Scheduling Time Periods of d-UC

This case study investigates the impact of different scheduling periods of the d-UC on the dynamics response of the power system based on a modified version of the IEEE 39-bus system [57]. While the rolling UC is solved for 24 hours at every period, in the discussions below, we show only the first hour of the planning horizon, which has a demand forecast of 700 MW [19].

Several scenarios are considered to study the impact of the uncertainty of the net-load, i.e. total load minus RES generation, on the dynamic behavior of the system. The first four scenarios compare the effects of the scheduling period of the UC problem on frequency variations. Periods of 15, 10, 7.5 and 3.75 minutes are considered. Then, the impact of net-load volatility (short-term noise) on the system's frequency is discussed. Finally, the combined effect of uncertainty and a large contingency on frequency deviations is shown.

The total number of state and algebraic variables of the system for the first four case studies is 131 and 223, respectively, while in the fifth scenario we have an increase in the number of state variables, from 131 to 169 (i.e. noise added to the 19 loads of the system). The total computing times to solve the TDS and the d-UC for the 15, 10, 7.5, 3.75-minute scheduling periods and the noise case are 1 min and 34 s, 1 min and 39 s, 1 min and 44 s, 2 min and 25 s and 4 min and 46 s, respectively.

## 15-minute Scheduling

In this scenario, d-UC is solved four times and a maximum of 30% of uncertainty is applied to the end of the first hour. Figure 4.2 shows the mechanical power of two relevant synchronous machines, whereas Fig. 4.3 shows the transient behavior of the frequency of the CoI of the system ( $\omega_{\text{CoI}}(t)$ ).

Electro-mechanical oscillations occur every 15-minutes due to a change in the operating points of the synchronous machines enforced by the d-UC. In the periods between two scheduling events of the d-UC, machine powers vary due to load ramps, but the frequency is almost steady-state thanks to the action of primary and secondary frequency regulations.

The average value of the objective function for these four periods is found to be \$553,346.4.

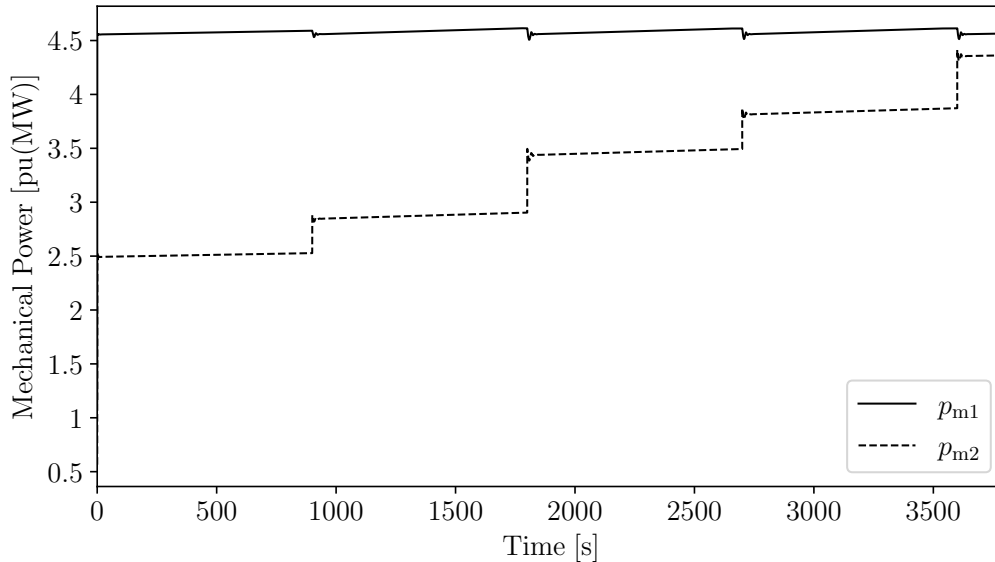


Figure 4.2: Mechanical power of two relevant machines for the 15 minute scheduling period.

## 10 Minute Scheduling

In this scenario, the hour is divided into six scheduling time intervals and uncertainty is added to the load, but it is proportionally lower compared to the 15-minute scenario as a more reliable forecast is assumed to be available. Figure 4.4 shows that the amplitude and duration of the oscillations of the  $\omega_{\text{CoI}}(t)$  decreases with respect to the 15-minute scenario. This is due to both lower uncertainty and lower load variations in the shorter period.

The average value of the objective function per period is \$551,575.1, hence lower than for the 15-minute scenario. The decrease of the objective function is a consequence of

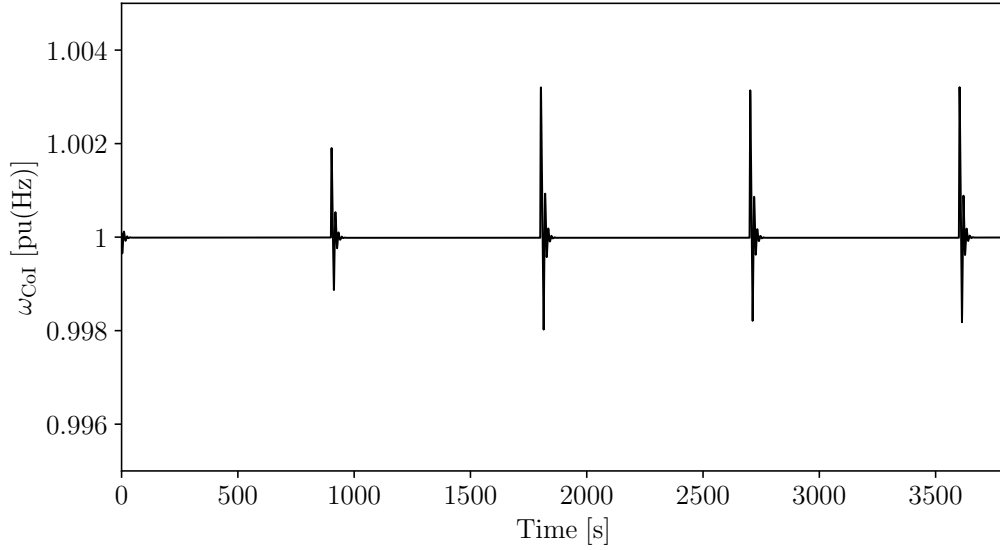


Figure 4.3: Frequency of the center of inertia for 15-minute scheduling period.

the lower reserves and uncertainty and, in turn, of the shorter time period. It has to be noted that the net-load consumption is assumed to vary linearly between two consecutive periods. If different paths are assumed, the solution of the sub-hourly d-UC problem can become more expensive [113]. A proper modelling of the transient behavior and the control of the system between consecutive solutions of the UC problem is thus crucial to avoid unnecessarily increasing the price of electricity.

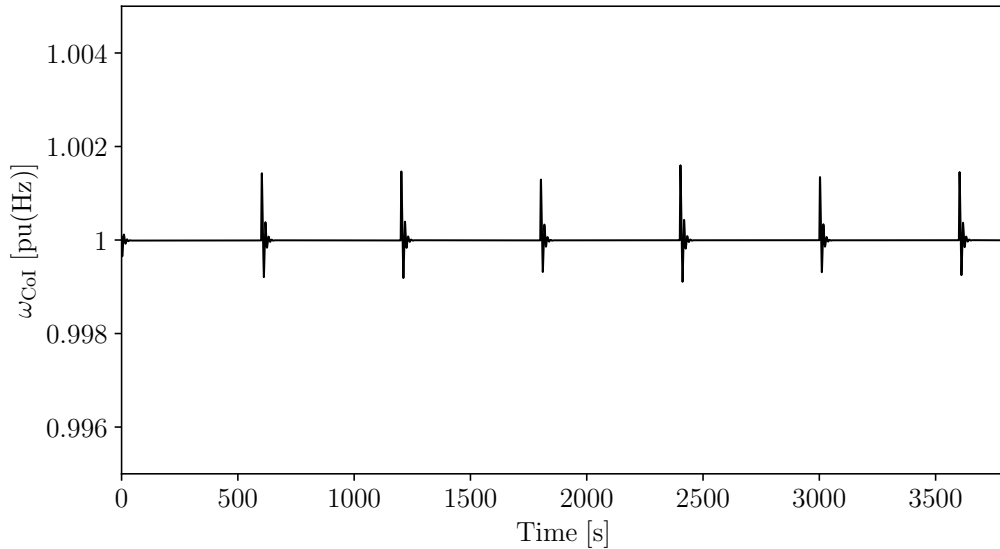


Figure 4.4: Frequency of the center of inertia for the 10 minute UC scheduling period.

## 7.5 and 3.75-Minute Schedulings

The results of these scenarios are shown in Figs. 4.5 and 4.6. The trend shown by the 10 minute scheduling is confirmed: shorter periods leads to lower frequency variations to the lower uncertainty. Also the cost of electricity decreases: the average values of the objective function for these two scenarios are \$550,938.35 and \$550,033.97, respectively. These results suggest that a smoother operation (e.g. more frequent solutions of the d-UC problem) is not just better from a dynamic point of view, but it is also more economical.

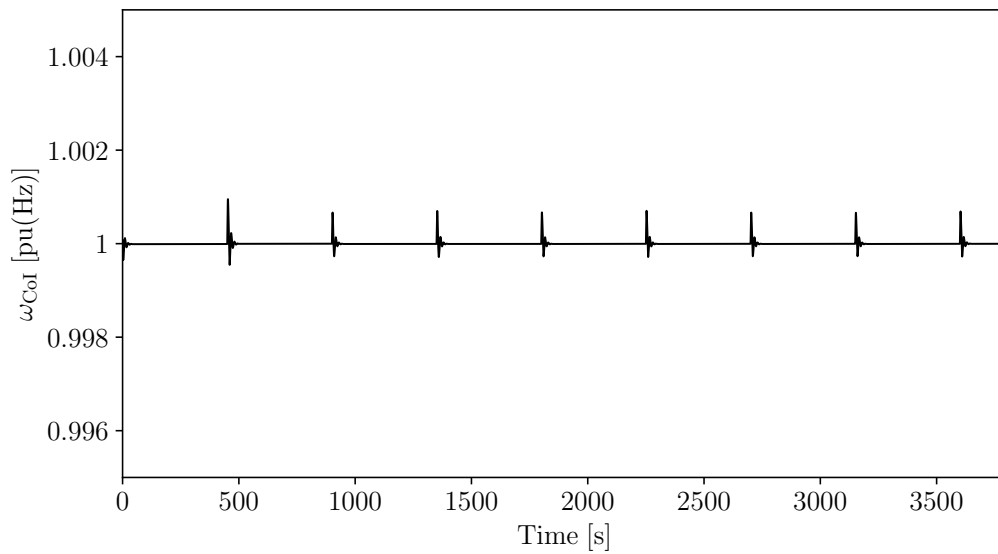


Figure 4.5: Frequency of the center of inertia for 7.5-minute d-UC scheduling period.

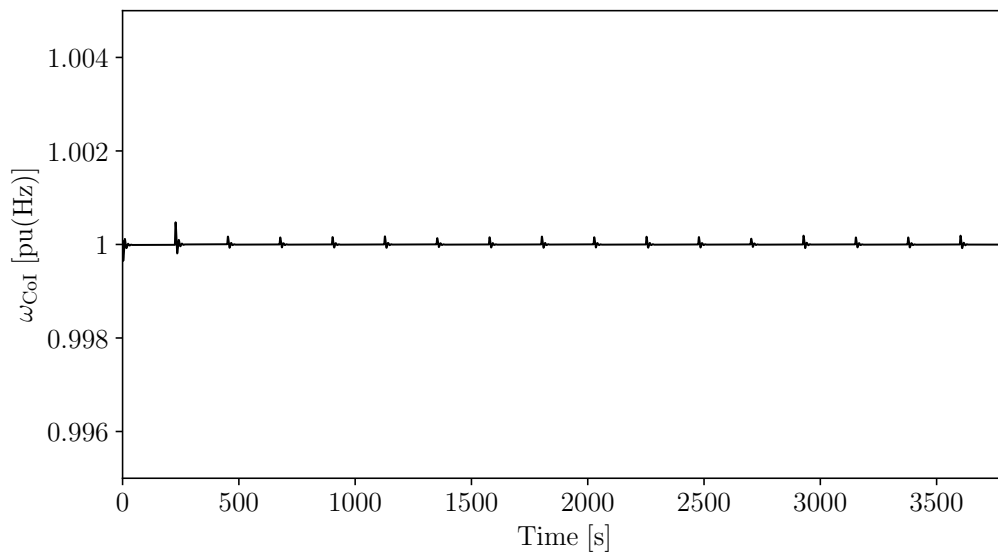


Figure 4.6: Frequency of the center of inertia for 3.75-minute scheduling period.

## Effect of Noise

In this scenario, volatility is added to the load net consumption as proposed in [87]. This noise models both load and DER short-term fluctuations. Simulation results indicate that noise can significantly increase frequency variations. Figures 4.7 and 4.8 show the worst case scenario, namely the 15 minute scheduling with noise. In addition, the average value of the objective function is \$556,689.32 and so slightly higher compared to the 15-minutes case without noise.

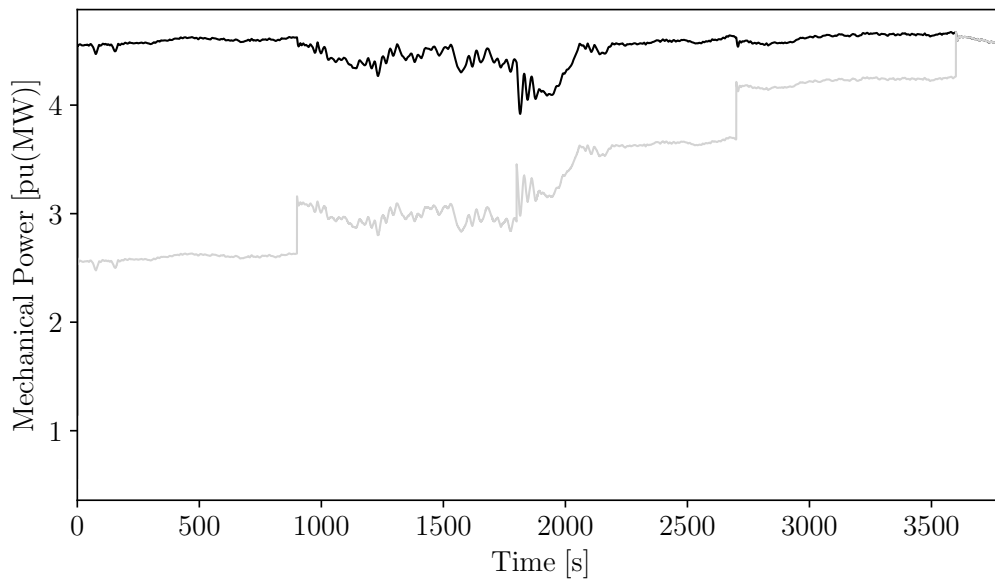


Figure 4.7: Mechanical power of the relevant machines for 15-minute scheduling and noise.

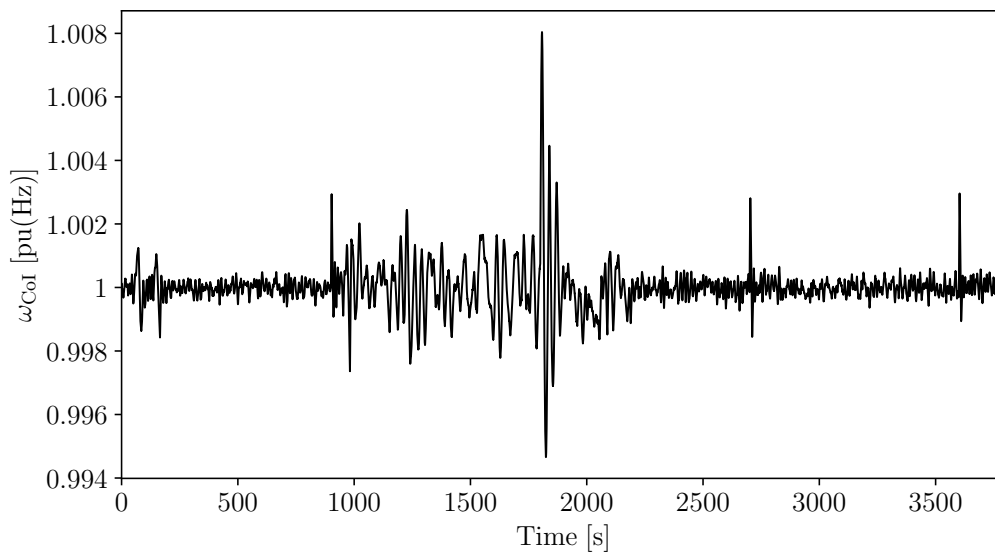


Figure 4.8: Frequency of the center of inertia for 15-minutes scheduling and noise.

## Effect of Contingencies

A contingency, i.e. the outage of line 1, occurring at 1,802 s and cleared after 200 ms for the scenarios of 15 and 3.75-minute scheduling scenarios illustrates the impact of the d-UC on the stability of the system. The time at which the contingency occurs is chosen on purpose to be in the seconds after the solution of the d-UC problem. Figures 4.9 and 4.10 show the rotor speeds of the machines following the d-UC scheduling and the contingency. As expected, the highest impact of the contingency on the frequency occurs if a 15-minute scheduling period is used.

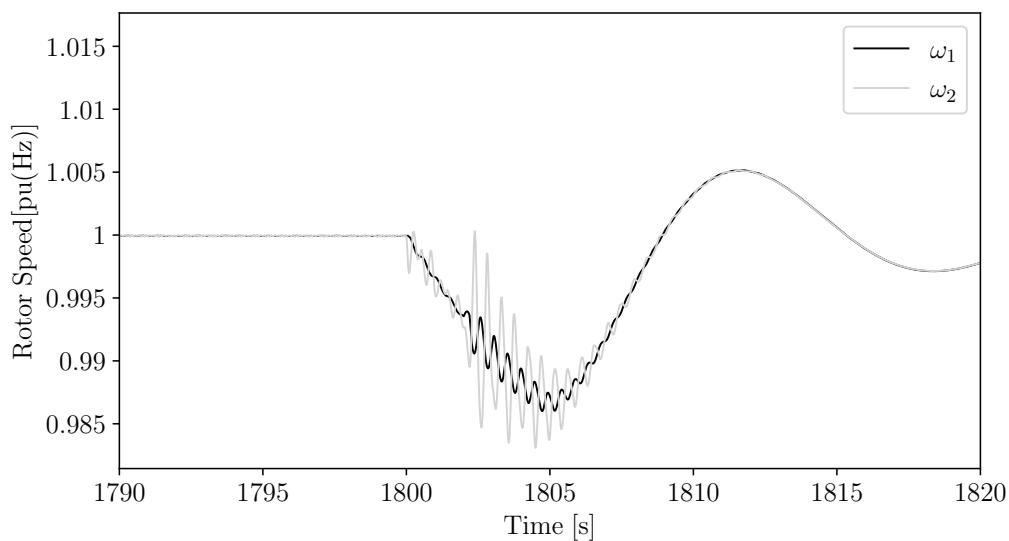


Figure 4.9: Frequency of two synchronous machines following a contingency for the 15-minute scheduling.

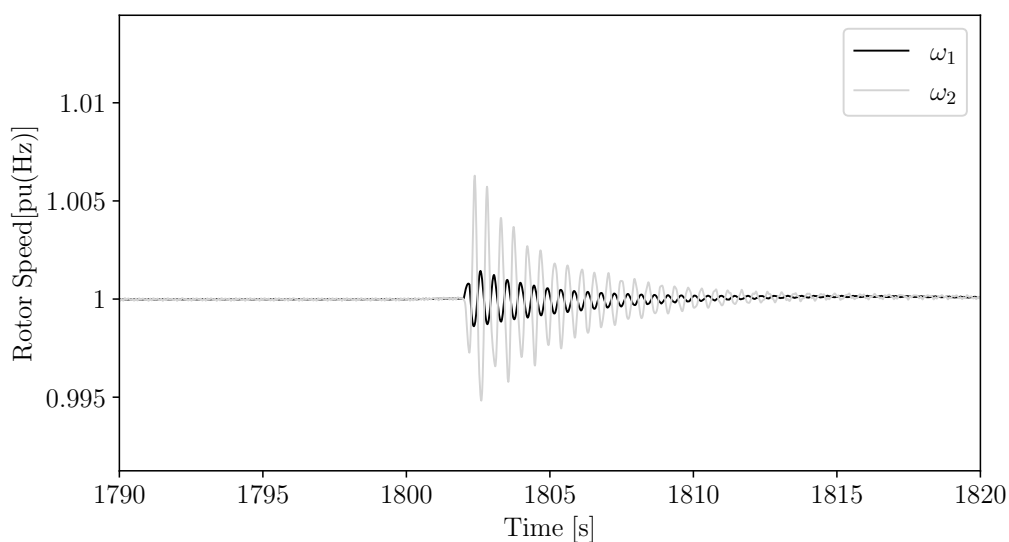


Figure 4.10: Frequency of two synchronous machines following a contingency for the 3.75-minute scheduling.

## 4.6 Case Study 2: Impact of Different Net-Load Volatility and Control/Machine parameters

This case study carries out a sensitivity analysis with respect to net-load volatility and control/machine parameters. Four case studies are considered on the modified IEEE 39-bus system. The first two scenarios use a 15-minute scheduling period while the last two use a 5-minute scheduling period. Each scenario is characterized by a different amount of load stochastic variations.

The base case (reference) machine/control parameters are set as follows: gain of the AGC is  $K_o = 50$ , droop of the TGs is  $\mathcal{R} = 0.05$ , and the inertia of the synchronous machines is taken equal to the original values, say  $M_o$ , used in [57]. When solving the sensitivity analysis, these parameters are varied, one at a time, and their impact on the standard deviation of the frequency of the system ( $\sigma$ ) is observed. Next, to simulate uncertainty, the load is assumed to differ from the forecast by a maximum of 30% in the first hour in all scenarios. In other words, the load in the last period of the first hour is chosen to be 30% higher than the forecast, and it is proportionally lower for other periods of this hour.

The total number of state and algebraic variables of the system for all scenarios are 169 and 223, respectively. The average computing time for each simulation is about 5-minutes.

### Scenario 1 – 15-Minute Scheduling with High Noise

The standard deviation of the white noise for this scenario is 1% of the base case load. During the first hour, the d-UC is solved four times (i.e. 4 periods of 15-minutes) and the average value of the objective function for these 4 periods is found to be \$561,784.79. It is relevant to note that this cost is lower compared to the one found in some other works [60], [18]. This is mainly due to the fact that since we are using a 15-minute scheduling interval, the value of the total reserve is taken 2.5% of the total demand and so proportionally lower compared to the above works that use a value of 10%.

Simulation results of this scenario are shown in Table 4.1. These indicate that, as the gain  $K_o$  of the AGC increases, the standard deviation of the frequency decreases. Also, as expected, if the droop of the TGs increases, the standard deviation of the frequency increases. Interestingly enough though, decreasing the inertia of the system leads to

Table 4.1: 15-minute scheduling with high noise – Standard deviation  $\sigma$  of the frequency for different control/machine parameters

$K_o$	$\sigma$ $10^{-4}$ pu	$\mathcal{R}$	$\sigma$ $10^{-4}$ pu	$M$	$\sigma$ $10^{-4}$ pu
25	9.73	0.02	4.39	$2M_o$	6.85
50	7.5	0.05	7.5	$M_o$	7.5
100	5.09	0.08	9.26	$0.5M_o$	7.43

slightly lower standard deviations of the frequency. This is due to the fact that the distribution of the frequency is not exactly a Gaussian distribution because of the jumps of the power imposed by the d-UC [83].

## Scenario 2 – 15-Minute Scheduling with Low Noise

The standard deviation of the load noise in this scenario is chosen to be five times lower compared to Scenario 1. The value of the objective function is found to be \$559,191.47 and hence lower than Scenario 1. This is because the net-load volatility is lower. The simulation results of the sensitivity analysis are shown in Table 4.2. As expected, increasing the gain  $K_o$  of the AGC decreases  $\sigma$ ; increasing the droop  $\mathcal{R}$  of TGs leads to higher values of  $\sigma$ ; and decreasing the inertia  $M$  of synchronous machines increases the standard deviation of the frequency.

Table 4.2: 15-minute scheduling with low noise – Standard deviations  $\sigma$  of the frequency for different control/machine parameters

$K_o$	$\sigma$ $10^{-4}$ pu	$\mathcal{R}$	$\sigma$ $10^{-4}$ pu	$M$	$\sigma$ $10^{-4}$ pu
25	3.74	0.02	1.57	$2M_o$	2.84
50	2.98	0.05	2.98	$M_o$	2.98
100	2.31	0.08	3.99	$0.5M_o$	3.01

## Scenario 3 – 5-Minute Scheduling with High Noise

In this scenario, load noise is proportionally lower to scenario one. The value of the objective function is found to be \$557,373.86 and hence lower than the other two scenarios. This is the result of lower reserves and lower noise and uncertainty of the net-load. Therefore, it can be said that shorter scheduling periods of the d-UC leads to lower operating costs. On the other hand, the sensitivity analysis with respect to different

parameters is shown in Table 4.3. Similar to scenario one, increasing the gain  $K_o$  of the AGC decreases  $\sigma$ ; increasing  $\mathcal{R}$  leads to higher values of  $\sigma$ ; and decreasing inertia  $M$  increases the value of  $\sigma$ .

Table 4.3: 5-minute scheduling with high noise – Standard deviations  $\sigma$  of the frequency for different control/machine parameters

$K_o$	$\sigma$ $10^{-4}$ pu	$\mathcal{R}$	$\sigma$ $10^{-4}$ pu	$M$	$\sigma$ $10^{-4}$ pu
25	6.68	0.02	3.71	$2M_o$	3.84
50	5.29	0.05	5.29	$M_o$	5.29
100	4.71	0.08	6.97	$0.5M_o$	6.33

## Scenario 4 – 5-Minute Scheduling with Low Noise

The white noise of the load is reduced 5 times with respect to Scenario 3. The objective function is found to be \$556,421.26 and, hence, lower than all other scenarios. It can be concluded that the shorter the scheduling period of the UC (i.e. lower uncertainty) the lower the total operating costs. Moreover, the sensitivity analysis is shown in Table 4.4. Again, similar to Scenario 1, increasing the inertia leads to a higher frequency standard deviation. Following the same rationale discussed in Scenario 1, a higher value of  $\sigma$  with high inertia is due to the fact that, after each d-UC scheduling, the frequency takes a longer time to recover to its nominal value.

Table 4.4: 5-minute scheduling with low noise – Standard deviations  $\sigma$  of the frequency for different control/machine parameters

$K_o$	$\sigma$ $10^{-4}$ pu	$\mathcal{R}$	$\sigma$ $10^{-4}$ pu	$M$	$\sigma$ $10^{-4}$ pu
25	3.8	0.02	1.73	$2M_o$	2.99
50	2.79	0.05	2.79	$M_o$	2.79
100	2.16	0.08	3.62	$0.5M_o$	2.87

## 4.7 Conclusions

This chapter presents a framework to embed the sub-hourly d-UC problem into TDS. The framework allows studying the impact of different scheduling periods of the d-UC and the effect of the net load variability and uncertainty on the system’s dynamic behaviour.

In the proposed approach, the d-UC problem is modelled as a slow “discrete controller” that responds to the time-varying loading condition of the grid by changing the power set-points of the TGs. In particular, a sub-hourly MILP d-UC is used to accommodate the variable net-load.

The results of the first case study indicate that reducing the time intervals at which the d-UC problem is solved help: (i) reduce frequency variations; (ii) reduce electricity price; and (iii) mitigate the impact of volatility and contingencies. These findings suggest that power system operators should switch to the utilization of the sub-hourly modelling instead of conventional hourly resolution. This is particularly important given the need for higher flexibility in modern power systems characterised by high shares of RESs.

On the other hand, the results of the second case study show that: (i) increasing the gain  $K_o$  of the AGC decreases  $\sigma$ ; (ii) increasing  $\mathcal{R}$  leads to higher values of  $\sigma$ ; and (iii) decreasing inertia  $M$  increases the value of  $\sigma$ . However, depending on the scheduling period used and the amount of noise in the system, increasing the inertia  $M$  may lead to a higher frequency standard deviation. As aforementioned, this is because the frequency takes a longer time to recover to its nominal value after each d-UC scheduling.

Given these findings, it can be concluded that the proposed software framework provides valuable information to TSOs and, as such, is a useful tool when operating power systems with growing volumes of RESs.

# Chapter 5

## Interaction between Stochastic Sub-Hourly Unit Commitment and Power System Dynamics

### 5.1 Introduction

Since large amounts of stochastic RESs can significantly impact the performance of the system [86, 126], stochastic programming has been introduced in recent years to properly account for uncertainty (e.g. wind) when scheduling the system [23]. For example, [114] shows that using a s-UC reduces operating costs and improves system performance. In the same vein, the authors in [17] show that a stochastic market-clearing procedure allows greater wind penetration than a deterministic approach. Moreover, in [120] the authors propose a stochastic real-time market with 15-min dispatch intervals and show that it outperforms the relevant deterministic approach. In [47], a stochastic economic dispatch (15-minute dispatch interval) is proposed where the authors conclude that the stochastic approach leads to lower operating costs compared to that of the deterministic approach. Nevertheless, they acknowledge the computational burden of the stochastic approach as the main limitation for practical applications.

The works above study the impact of the sub-hourly modelling in power systems from the economic and/or operational perspective. The focus of this chapter, on the other hand, is on the impact of the sub-hourly s-UC on power system dynamics. If sub-hourly scheduling timescales are used, say 15-minute or 5-minute, in fact, then these timescales

can overlap with long-term dynamics [69]. Therefore, it appears worthwhile and timely to embed the sub-hourly s-UC problem into a fully-fledged transient stability analysis software tool [62,63] and study the dynamic behaviour of power systems.

The remainder of the chapter is organized as follows. Section 5.2 presents the stochastic long-term power system model. Section 5.3, 5.4 and 5.5 describe the formulation of the complete, simplified and alternative s-UC problem, respectively. Section 5.6 provides a modified version of the proposed software framework able to embed the various s-UC formulations in the TDS routine of Dome. Section 5.7 discusses the impact of different scheduling periods of the complete s-UC problem on power system dynamics. Section 5.8 focuses on the effects of different s-UC and frequency controllers/machine parameters on the system's dynamic response. Finally, conclusions are drawn in Section 5.9.

## 5.2 Stochastic Long-Term Power System Model

The large-scale deployment of stochastic RESs, e.g. wind, significantly increases the random perturbations and inevitably affects power systems' safe and stable operation [127]. As a result, the adoption of Stochastic Differential Equations (SDEs) to model this randomness in power systems has gained significant interest in recent years. However, most of the literature focus on the impact of wind power variability (modelled as SDEs) on transient and small-signal stability, respectively [123]. On the other hand, stochastic long-term stability analysis of power systems has received little attention. This is of particular importance considering the expected trends regarding the integration of RES into modern power systems.

The stochastic long-term dynamic model of power systems can be represented as a set of hybrid nonlinear SDAEs [87], as follows:

$$\begin{aligned}
 \dot{\mathbf{x}} &= \mathbf{f}(\mathbf{x}, \mathbf{y}, \mathbf{u}, \mathbf{z}, \dot{\boldsymbol{\eta}}), \\
 \mathbf{0} &= \mathbf{g}(\mathbf{x}, \mathbf{y}, \mathbf{u}, \mathbf{z}, \boldsymbol{\eta}), \\
 \dot{\boldsymbol{\eta}} &= \mathbf{a}(\mathbf{x}, \mathbf{y}, \boldsymbol{\eta}) + \mathbf{b}(\mathbf{x}, \mathbf{y}, \boldsymbol{\eta}) \boldsymbol{\zeta},
 \end{aligned} \tag{5.1}$$

where  $\mathbf{f}$  and  $\mathbf{g}$  represent the differential and algebraic equations, respectively;  $\mathbf{x}$  and  $\mathbf{y}$  represent the state and algebraic variables, such as generator rotor speeds and bus voltage angles, respectively;  $\mathbf{u}$  represents the inputs, such as the schedules of synchronous

generators;  $\mathbf{z}$  represents discrete variables;  $\boldsymbol{\eta}$  represents the stochastic characterization of wind speed;  $\mathbf{a}$  and  $\mathbf{b}$  are the *drift* and *diffusion* of the SDEs, respectively; and  $\boldsymbol{\zeta}$  is the white noise. It is worth mentioning that (5.1) is solved using numerical integration techniques. This is possible as the algebraic equations  $\mathbf{g}$ , in (5.1), do not explicitly depend on white noises  $\boldsymbol{\zeta}$ , or on  $\dot{\boldsymbol{\eta}}$  [87]. In this chapter, an implicit trapezoidal integration method is used for functions,  $\mathbf{f}$  and  $\mathbf{a}$ , while the Euler-Maruyama method is used to integrate the stochastic term  $\mathbf{b}$ . Further details related to the numerical integration of the SDAEs can be found in [87].

It is necessary to consider both electromechanical and long-term dynamic models, when one performs stochastic long-term dynamic simulations [68]. With this regard, (5.1) includes the dynamic models of conventional machines (4th order models) and their primary controllers; AGC; wind power plants ( 5th order Doubly-Fed Induction Generator) [84]; and the model of sub-hourly s-UC. [It is worth noting that we have not included in the system a fast frequency control in wind power plants. This controller, in fact, while can help improve the dynamic response of the system does not alter the conclusions that are drawn in this chapter.](#)

### 5.2.1 Modelling of stochastic processes

Modelling the stochastic nature of wind power is critical in power system dynamic studies [56]. In this context, (5.1) includes only wind power variations with respect to the forecast wind generation as a stochastic perturbations. An Ornstein-Uhlenbeck Process (OUP) is used to model the stochastic nature of the wind speed  $v_s$  that enters into the wind turbine, as follows:

$$\begin{aligned} v_s(t) &= v_{s0} + \eta_v(t) \\ \dot{\eta}_v(t) &= \iota_v(\epsilon_v - \eta_v(t)) + b_v \zeta_v \end{aligned} \tag{5.2}$$

where  $v_{s0}$  is the wind speed initial value;  $\eta_v$  is the stochastic variable that is dependent on the drift  $\iota_v(\epsilon_v - \eta_v)$ , and diffusion term  $b_v$  of the SDEs;  $\iota$  is the mean reversion speed that indicates the rate at which  $\eta_v$  tends to the mean value  $\epsilon_v$ ; and  $\zeta_v$  represents the white noise.

### 5.3 Complete Stochastic Unit Commitment Formulation

As the penetration of highly variable RES increases, so does the uncertainty in power systems. This complicates the real-time balance between generation and demand. Therefore it is of particular importance to model the uncertainty when scheduling the system. There are different methodologies and techniques proposed for optimization under uncertainty, with one of the most popular being the two-stage stochastic programming. In the context of UC, the two-stage s-UC makes use of a probabilistic model for the uncertain input parameters, e.g. wind generation, and is usually approximated by a set of scenarios representing the plausible realizations of these random parameters [23].

In this chapter, a standard MILP s-UC problem is implemented based on [16], in which wind power production is considered as an uncertain parameter of the system, as follows:

$$\begin{aligned} & \min_{\mathcal{H}, \mathcal{W}} \sum_{t \in \mathcal{T}} \sum_{g \in \mathcal{G}} (C_g^F z_{g,t}^F + C_g^{SU} z_{g,t}^{SU} + C_g^{SD} z_{g,t}^{SD}) \\ & + \sum_{\xi \in \mathcal{S}} \pi_\xi \left[ \sum_{t \in \mathcal{T}} \sum_{g \in \mathcal{G}} C_g^V p_{g,t,\xi} + \sum_{t \in \mathcal{T}} \sum_{l \in \mathcal{D}} C^L d_{l,t,\xi}^{SH} \right] \end{aligned} \quad (5.3)$$

such that

$$z_{g,t}^{SU} - z_{g,t}^{SD} = z_{g,t}^F - z_{g,t-1}^F \quad (5.4)$$

$$(\forall g \in \mathcal{G}, \forall t \in \{2, \dots, T\})$$

$$z_{g,t}^{SU} - z_{g,t}^{SD} = z_{g,t}^F - IS_g \quad (5.5)$$

$$(\forall g, \forall t \in \{1\})$$

$$z_{g,t}^{SU} + z_{g,t}^{SD} \leq 1 \quad (5.6)$$

$$(\forall g, \forall t \in \{1, \dots, T\})$$

$$z_{g,t}^F = IS_g \quad (5.7)$$

$$(L_g^{UP} + L_g^{DW} > 0, \forall g, \forall t \leq L_g^{UP} + L_g^{DW})$$

$$\sum_{\tau=t-UT_g+1}^t z_{g,\tau}^{SU} \leq z_{g,t}^F \quad (5.8)$$

$$(\forall g, \forall t > L_g^{UP} + L_g^{DW})$$

$$\sum_{\tau=t-DT_g+1}^t z_{g,\tau}^{SD} \leq 1 - z_{g,t}^F \quad (5.9)$$

$$(\forall g, \forall t > L_g^{UP} + L_g^{DW})$$

$$\begin{aligned} \sum_{g \in \mathcal{G}_n} p_{g,t,\xi} - \sum_{l \in \mathcal{D}_n} d_{l,t} + \sum_{l \in \mathcal{D}_n} d_{l,t,\xi}^{SH} + \sum_{k \in \mathcal{K}_n} W_{k,t,\xi} \\ - \sum_{k \in \mathcal{K}_n} W_{k,t,\xi}^{SP} = \sum_{m \in \mathcal{M}_n} \frac{(\theta_{n,t,\xi} - \theta_{m,t,\xi})}{X_{n,m}} \end{aligned} \quad (5.10)$$

$$(\forall n, \forall t, \forall \xi \in \mathcal{S})$$

$$p_{g,t,\xi} \leq P_g^{\max} z_{g,t}^F \quad (5.11)$$

$$(\forall g, \forall t, \forall \xi \in \mathcal{S})$$

$$p_{g,t,\xi} \geq P_g^{\min} z_{g,t}^F \quad (5.12)$$

$$(\forall g, \forall t, \forall \xi \in \mathcal{S})$$

$$p_{g,t,\xi} \leq (P_g^{IS} + RU_g) z_{g,t}^F \quad (5.13)$$

$$(\forall g, \forall t \in \{1\}, \forall \xi \in \mathcal{S})$$

$$p_{g,t,\xi} \geq (P_g^{IS} - RD_g) z_{g,t}^F \quad (5.14)$$

$$(\forall g, \forall t \in \{1\}, \forall \xi \in \mathcal{S})$$

$$p_{g,t,\xi} - p_{g,t-1,\xi} \leq (2 - z_{g,t-1}^F - z_{g,t}^F) P_g^{SU} \quad (5.15)$$

$$+ (1 + z_{g,t-1}^F - z_{g,t}^F) RU_g$$

$$(\forall g, \forall t \in \{2, \dots, T\}, \forall \xi \in \mathcal{S})$$

$$p_{g,t-1,\xi} - p_{g,t,\xi} \leq (2 - z_{g,t-1}^F - z_{g,t}^F) P_g^{SD} \quad (5.16)$$

$$+ (1 - z_{g,t-1}^F + z_{g,t}^F) RD_g$$

$$(\forall g, \forall t \in \{2, \dots, T\}, \forall \xi \in \mathcal{S})$$

$$d_{l,t,\xi}^{SH} \leq d_{l,t} \quad (5.17)$$

$$(\forall l, \forall t, \forall \xi \in \mathcal{S})$$

$$W_{k,t,\xi}^{SP} \leq W_{k,t,\xi} \quad (5.18)$$

$$(\forall k, \forall t, \forall \xi \in \mathcal{S})$$

$$-P_{n,m}^{\max} \leq \frac{(\theta_{n,t,\xi} - \theta_{m,t,\xi})}{X_{n,m}} \leq P_{n,m}^{\max} \quad (5.19)$$

$$(\forall n, m \in \mathcal{M}_n, \forall t, \forall \xi \in \mathcal{S})$$

$$p_{g,t,\xi}, d_{l,t,\xi}^{SH}, W_{k,t,\xi}^{SP} \geq 0 \quad (5.20)$$

$$(\forall g, \forall l, \forall k, \forall t, \forall \xi \in \mathcal{S})$$

$$z_{g,t}^F, z_{g,t}^{SU}, z_{g,t}^{SD} \in \{0, 1\} \quad (5.21)$$

$$(\forall g, \forall t)$$

where  $\mathcal{H} = \{z_{g,t}^F, z_{g,t}^{SU}, z_{g,t}^{SD}\}$  and  $\mathcal{W} = \{p_{g,t,\xi}, d_{l,t,\xi}^{SH}, W_{k,t,\xi}^{SP}\}$ ; and the initial state conditions are as follows:

$$IS_g = \begin{cases} 1 & \text{if } ON_g > 0 \\ 0 & \text{if } ON_g = 0 \end{cases}$$

$$L_g^{UP} = \min\{T, (UT_g - ON_g)IS_g\}$$

$$L_g^{DW} = \min\{T, (DT_g - OFF_g)(1 - IS_g)\}$$

Equations (5.3) represent the total cost to be minimized which includes the fixed, start-up, shut-down and variable cost of the generating units, as well as the cost of involuntarily demand curtailment. Equations (5.4)-(5.6) model the logical expression between the binary variables (i.e. start-up and shut-down of generating units). Equations (5.7)-(5.9) model the minimum and maximum up- and down-time constraints. The power balance constraint is modeled through equations (5.10). While the capacity limits of generating units are modeled through equations (5.11)-(5.12) and their respective ramping limits through (5.13)-(5.16). Equations (5.17)-(5.18) model the limits of the involuntary demand curtailment and wind power spillage, respectively. Transmission capacity limits are enforced by equations (5.19). Finally, equations (5.20)-(5.21) refer to the variable declarations.

The model shown in (5.3)-(5.21) is the deterministic equivalent of the original two-stage stochastic programming problem. It is called a two-stage problem since there are first-stage and second-stage variables, also known as here-and-now and wait-and-see variables, respectively [23]. In particular,  $z_{g,t}^F, z_{g,t}^{SU}, z_{g,t}^{SD}$  are first-stage decision variables that represent the status of generating unit  $g$  in time period  $t$  (i.e. ON/OFF status,

start-up and shut-down). These decisions do not depend on uncertainty realization  $\xi$ , and are generally made one day in advance. Similarly,  $p_{g,t,\xi}$ ,  $d_{l,t,\xi}^{SH}$ ,  $W_{k,t,\xi}^{SP}$ ,  $\theta_{n,t,\xi}$  are second-stage decision variables that represent the active power dispatch of generating units  $g$  in time period  $t$  and scenario  $\xi$ , the involuntary power curtailment from load  $l$  in time period  $t$  and scenario  $\xi$ , wind power spillage from wind production unit  $k$  in time period  $t$  and scenario  $\xi$ , and voltage angle at node  $n$  in time period  $t$  and scenario  $\xi$ , respectively. All second-stage decision variables depend on uncertainty realization  $\xi$ . Further details of the s-UC can be found in [16] and references therein.

### Scenarios and Rolling Horizon within the s-UC

To illustrate the modelling of s-UC wind uncertainty and volatility, and rolling planning horizon used in this chapter, we show below the power balance equations of the complete s-UC, as follows:

$$\begin{aligned} & \sum_{g \in \mathcal{G}_n} p_{g,t,\xi} - \sum_{l \in \mathcal{D}_n} d_{l,t} + \sum_{l \in \mathcal{D}_n} d_{l,t,\xi}^{SH} + \sum_{k \in \mathcal{K}_n} W_{k,t,\xi} \\ & - \sum_{k \in \mathcal{K}_n} W_{k,t,\xi}^{SP} = \sum_{m \in \mathcal{M}_n} \frac{(\theta_{n,t,\xi} - \theta_{m,t,\xi})}{X_{n,m}}, (\forall n, \forall t, \forall \xi \in \mathcal{S}) \end{aligned} \quad (5.22)$$

where  $p_{g,t,\xi}$  is the active power of conventional generating units  $g$ , at time period  $t$ , and scenario  $\xi$  (i.e. equivalent of the second-stage variable  $u_{f,t,\xi}$  in section 5.3);  $d_{l,t}$  is the demand for load  $l$  at time period  $t$ ;  $d_{l,t,\xi}^{SH}$  is the power curtailment from load  $l$ , at time period  $t$ , and in scenario  $\xi$ ;  $W_{k,t,\xi}$  and  $W_{k,t,\xi}^{SP}$  represent the power generation and curtailment, respectively, from wind unit  $k$ , in time period  $t$ , and scenario  $\xi$ ;  $X_{n,m}$  is the reactance of line  $n - m$ ;  $\theta_{n,t,\xi}$  represent the voltage angle at node  $n$ , time period  $t$ , and scenario  $\xi$ ; and  $\mathcal{K}_n$ ,  $\mathcal{M}_n$  are the sets of stochastic power generation (i.e. wind) located at node  $n$ , and nodes  $m \in \mathcal{N}$  connected to node  $n$  by transmission line, respectively.

### Modelling wind uncertainty

Similar to [90], a wind power penetration level  $W_{k,t,\xi}$  is defined as a percentage of the demand  $d_{l,t}$ , and named the medium scenario,  $W_{k,t,\xi}^m$ . Then, high and low wind power scenarios ( $W_{k,t,\xi}^h$ ,  $W_{k,t,\xi}^l$ ) are built as percentages of the medium scenario, as follows:

$$\begin{aligned}
W_{k,t,\xi}^l &= W_{k,t,\xi}^m \times (1 - j/100) \\
W_{k,t,\xi}^h &= W_{k,t,\xi}^m \times (1 + j/100)
\end{aligned}
\tag{5.23}$$

where  $j$  is the percentage of deviation of the the high and low scenarios with respect to the medium one.

The consistency of the wind power scenarios with real-world information is compared using wind power data of the Irish system [35]. Specifically, the 15-minute rate of change of wind power is determined based on one typical day per month of 2018 (see Fig. 5.1). Based on these data, wind power does not appear to change more than 10% in 15 minutes. For this reason, in the case study,  $j = 10\%$  is assumed.

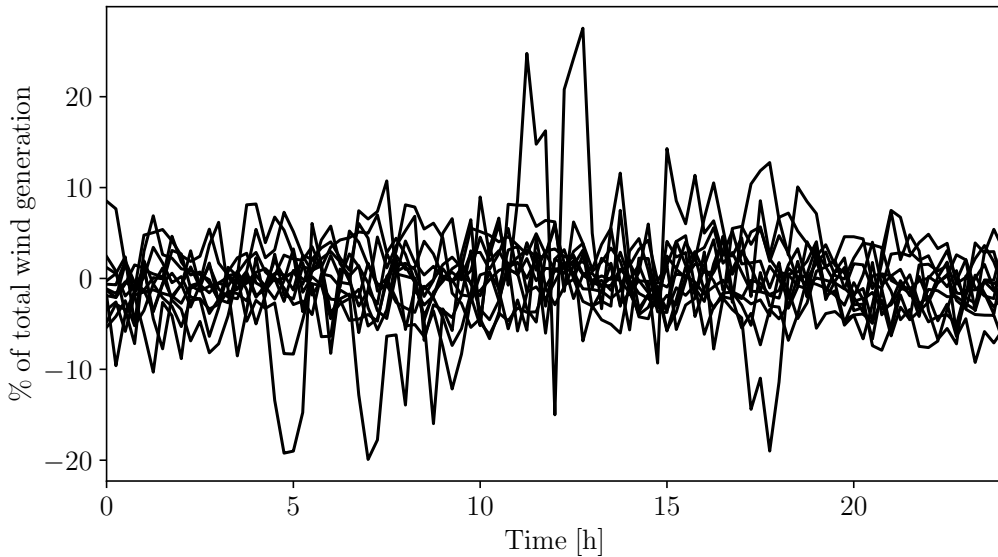


Figure 5.1: Wind power 15min rate of change for 12 typical day in the Irish system in 2018.

### Modelling wind volatility

Wind power volatility is modelled as small fluctuations with respect to the average value for a given period. Hence, uncertainty is related to wind power forecast, e.g. wind scenarios, while volatility is considered as a percentage, e.g. standard deviation, on top of the wind power forecast [121]. A normal distribution  $N(0, \sigma^2)$  with zero mean and given standard

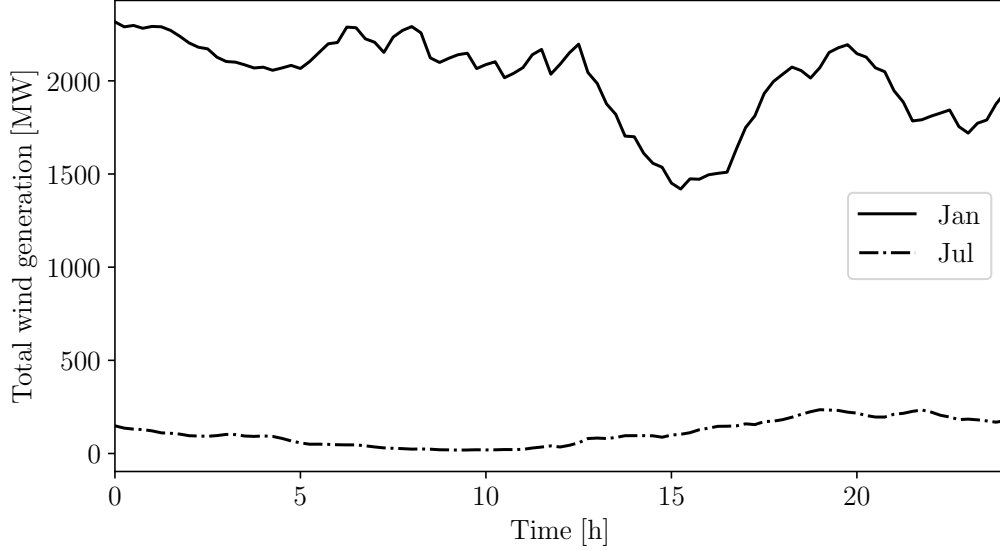


Figure 5.2: Wind power profile for two typical days (Jan, Jul) in the Irish system in 2018.

deviation is attached to each wind power scenario, as follows:

$$\begin{aligned}
 W_{k,t,\xi}^{l1} &= W_{k,t,\xi}^l + N(0, \sigma^2) \\
 W_{k,t,\xi}^{m1} &= W_{k,t,\xi}^m + N(0, \sigma^2) \\
 W_{k,t,\xi}^{h1} &= W_{k,t,\xi}^h + N(0, \sigma^2)
 \end{aligned} \tag{5.24}$$

where  $W_{k,t,\xi}^{l1}$ ,  $W_{k,t,\xi}^{m1}$ ,  $W_{k,t,\xi}^{h1}$  are the new low, medium and high wind power scenarios, respectively, after adding the volatility.

An important aspect to keep in mind when building the scenarios is the relationship between the wind power level and its standard deviation  $\sigma$ . With this aim, two typical days are analysed for two months, namely January (high wind) and July (low wind). The wind power profile for these typical days is shown in Fig. 5.2. It appears that wind varies more in January than in July. More specifically, the standard deviation of wind power generation is found to be 234.78 MW and 68.46 MW, for January and July, respectively, and that high wind leads to higher  $\sigma$ .

Note that the goal is not to propose new s-UC models to deal with wind power uncertainty and volatility but rather to study the impact of a well assessed s-UC formulation on power system dynamics. For this reason, it is not necessary to consider more sophisticated s-UC models. As a matter of fact, the first case study shows that,

depending on the wind penetration and planning horizon, a s-UC might not be needed at all.

### Modelling the rolling planning horizon

Scheduling the system frequently (i.e. more than once a day) allows having better wind and load forecasts. As a result, fewer reserves are required [114]. This chapter uses a rolling planning approach for updating the wind power forecast ( $W_{k,t,\xi}$ ) with a planning horizon of 24 h. During the first hour of the planning horizon, the high/low wind scenarios increase/decrease as a linear function from the medium scenario and after that, they have a fixed error, e.g.  $j = 10\%$ . The s-UC model is solved at every period  $t$  during the first 12 h with a planning horizon of 24 h.

When rolling forward, the status of the units of the previous horizon serves as an initial status for the next horizon. Between two scheduling events of the s-UC, e.g. 15 or 5-minutes, wind and load profiles are modelled as linear ramps.

## 5.4 Simplified Stochastic Unit Commitment Formulation

The level of complexity of s-UC formulations proposed so far in the literature varies significantly [54]. For example, a well-assessed MILP s-UC formulation is provided in [16]. Such a model considers several technical constraints, e.g. ramping limits of generators and capacity limits of transmission lines, to name a few. These constraints improve the performance of the schedules but are not crucial in this chapter, which focuses on the impact on long-term power system dynamics. Hence, a simplified model of s-UC is considered, as follows:

$$\underset{z_{g,t}^F, p_{g,t,\xi}}{\text{minimize}} \sum_{t \in \mathcal{T}} \sum_{g \in \mathcal{G}} C_g^F z_{g,t}^F + \sum_{\xi \in \mathcal{S}} \pi_{\xi} \left[ \sum_{t \in \mathcal{T}} \sum_{g \in \mathcal{G}} C_g^V p_{g,t,\xi} \right] \quad (5.25)$$

such that

$$p_{g,t,\xi} \leq P_g^{\max} z_{g,t}^F \quad \forall g, \forall t, \forall \xi \in \mathcal{S} \quad (5.26)$$

$$p_{g,t,\xi} \geq P_g^{\min} z_{g,t}^F \quad \forall g, \forall t, \forall \xi \in \mathcal{S} \quad (5.27)$$

$$\sum_{g \in \mathcal{G}} p_{g,t,\xi} - \sum_{l \in \mathcal{D}_n} d_{l,t} + \sum_{k \in \mathcal{K}_n} W_{k,t,\xi} = \sum_{m \in \mathcal{M}_n} \frac{(\theta_{n,t,\xi} - \theta_{m,t,\xi})}{X_{n,m}}, \quad \forall n, \forall t, \forall \xi \in \mathcal{S} \quad (5.28)$$

$$z_{g,t}^F \in \{0, 1\}, \quad \forall g \in \mathcal{G}, \forall t \in \mathcal{T} \quad (5.29)$$

where  $z_{g,t}^F$  is a first-stage decision variable that models the status (ON/OFF) of the conventional machines in time period  $t$ ;  $C_g^F$  and  $C_g^V$  represents the fixed and variable production cost of generation unit  $g$ , respectively;  $\pi_\xi$  is the probability of wind power scenario  $\xi$ ;  $p_{g,t,\xi}$  is a variable that represents the active power of the machine  $g$  in scenario  $\xi$  and time period  $t$ ;  $P_g^{\max}$  and  $P_g^{\min}$  represents the maximum and minimum active power limits of generation unit  $g$ , respectively;  $d_{l,t}$  represents the demand for load  $l$  at time period  $t$ ;  $W_{k,t,\xi}$  is the wind power production of wind generation unit  $k$ ,  $\theta_{n,t,\xi}$  are the voltage angles at node  $n$  and at time period  $t$  in scenario  $\xi$ , respectively;  $X_{n,m}$  is the reactance of the transmission line  $n - m$ ; and  $\mathcal{K}_n$ ,  $\mathcal{M}_n$  represents the sets of wind power generation connected at node  $n$ , and nodes  $m \in \mathcal{N}$  connected to node  $n$  through a line, respectively. Finally, constraints (5.25) to (5.29) model the objective function, maximum and minimum power output of generators, nodal power balance equation (DC power flow), and variable declarations, respectively.

## 5.5 Alternative Stochastic Unit Commitment Formulation

The literature provides several different formulations of the s-UC problem [129]. Therefore it is relevant to compare and study the impact that these models have on the power system dynamic behaviour. In this context, an alternative sub-hourly s-UC model with respect to the one discussed in the previous section has been adapted based on [46], as follows:

$$\begin{aligned} & \underset{z_{g,t}^F, p_{g,t}, r_{g,t,\xi}^U, r_{g,t,\xi}^D, W_{k,t}}{\text{minimize}} \sum_{t \in \mathcal{T}} \sum_{g \in \mathcal{G}} C_{g,t}^{SU} + C_g^V p_{g,t} \\ & + \sum_{\xi \in \mathcal{S}} \pi_\xi \left[ \sum_{t \in \mathcal{T}} \sum_{g \in \mathcal{G}} C_g^V (r_{g,t,\xi}^U - r_{g,t,\xi}^D) \right] \end{aligned} \quad (5.30)$$

such that

$$C_{g,t}^{SU} \geq C_g^{SU} (z_{g,t}^F - z_{g,t-1}^F), \quad \forall g, \forall t \quad (5.31)$$

$$C_{g,t}^{SU} \geq 0, \quad \forall g, \forall t \quad (5.32)$$

$$z_{g,t}^F P_g^{\min} \leq p_{g,t} \leq z_{g,t}^F P_g^{\max}, \quad \forall g, \forall t \quad (5.33)$$

$$\sum_{g \in \mathcal{G}} p_{g,t} + \sum_{k \in \mathcal{K}} W_{k,t} = l_t, \quad \forall t \quad (5.34)$$

$$z_{g,t}^F P_g^{\min} \leq (p_{g,t} + r_{g,t,\xi}^U - r_{g,t,\xi}^D) \leq z_{g,t}^F P_g^{\max}, \quad \forall g, \forall t, \forall \xi \quad (5.35)$$

$$\sum_{g \in \mathcal{G}} (p_{g,t} + r_{g,t,\xi}^U - r_{g,t,\xi}^D) + \sum_{k \in \mathcal{K}} W_{k,t,w} = l_t, \quad \forall t, \forall \xi \quad (5.36)$$

$$0 \leq r_{g,t,\xi}^U \leq R_{g,t}^{U\max}, \quad \forall g, \forall t, \forall \xi \quad (5.37)$$

$$0 \leq r_{g,t,\xi}^D \leq R_{g,t}^{D\max}, \quad \forall g, \forall t, \forall \xi \quad (5.38)$$

$$z_{g,t}^F \in \{0, 1\}, \quad \forall g, \forall t \quad (5.39)$$

where, apart from the variables and parameters already defined above,  $C_{g,t}^{SU}$  models the start-up cost of generation unit  $g$  incurred at the beginning of time period  $t$ ;  $r_{g,t,\xi}^U$  and  $r_{g,t,\xi}^D$  are decision variables and represents the increase and decrease in the active power output of generation unit  $g$  at time period  $t$ , respectively, say, during real-time operation (e.g. to compensate wind power fluctuations); while all other parameters and variables have analogous meanings as in the previous s-UC formulation.

The main difference between problem (5.30)-(5.39) and problem (5.25)-(5.29) is that in the former the active power of generation units,  $p_{g,t}$ , is a first-stage variable and does not adapt to the uncertainty realization. Also, note that model (5.25)-(5.29) has a slightly different objective function, namely it does not include the start-up cost ( $C_{g,t}^{SU}$ ) as compared to that of model (5.30)-(5.39).

## 5.6 Interaction between s-UC and SDAEs

It is time to merge all of the above in a single framework. Generally speaking, the goal is to embed s-UC equations (5.3)-(5.21), (5.23)-(5.24), (5.25)-(5.29), and (5.30)-(5.39) into equations (5.1).

Figure 5.3 shows the overall structure of the recently proposed co-simulation framework. The tool is composed of two parts, namely the dynamic model of power systems (SDAEs) and the discrete model of s-UC. Dome coordinates the co-simulation, i.e. the exchange

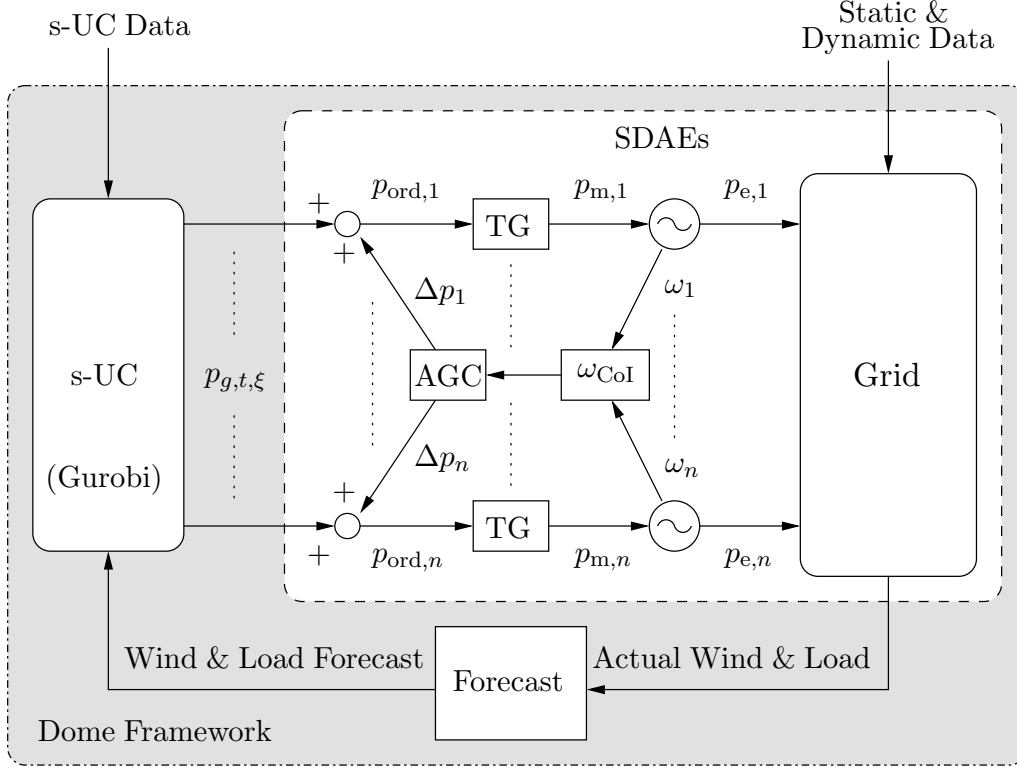


Figure 5.3: Interaction between the s-UC problem, AGC, TGs, synchronous machines and the grid.

of information between the s-UC and the SDAEs. In particular, the output of the s-UC models, namely the active power of generating units ( $p_{g,t,\xi}$ ), serves as an input to the SDAEs, i.e. change the power set-point of the TGs of the power plants. Finally, a Monte Carlo Method (MC) is utilized to simulate large sets of realizations of the stochastic processes of wind and loads. Each realization defines the “reality” that needs to be updated to solve the next s-UC problem. Such feedback is required to update the forecast of wind ( $W_{k,t,\xi}$ ) and loads as utilized in the s-UC problem.

The s-UC model (5.3)-(5.21) uses the active power of the generators, namely  $p_{g,t,\xi}$ , as a second-stage decision variable. In other words,  $p_{g,t,\xi}$  adapts to the uncertainty realization  $\xi$ . Since we are interested in having a single power dispatch for each generator and for each time period, a reasonable trade-off consists in taking a weighted-sum of the scenarios  $\xi$ . In the literature, one may find different formulations of s-UC for the active power of generators. For example, in [46], the authors use the active power as a first-stage decision variable ( $p_{g,t}$ , set-points) and then use up/down reserve deployment (production changes) as a second-stage decision variable to accommodate wind variability (real-time).

## 5.7 Case Study 1: Impact of Different Scheduling Time Periods

From a system operator point of view, it is useful to study the impact that different levels of uncertainty and volatility, e.g. wind forecast errors, within the s-UC model have on power system dynamic performance. At the time of this writing, TSOs still rely on d-UC formulations. Therefore, a comparison between d-UC and s-UC approaches is relevant. Also, since different TSOs use different scheduling timescales and/or different rolling approaches, e.g. every 15-minute [24], or every 5-minute [78], a comparison of the effect of these strategies is also carried out in this section. Moreover, the impact of contingency and renewable penetration on the transient response of the system and long-term frequency deviations, respectively, using different s-UC strategies is shown as well. Finally, the impact of different wind power scenarios of the s-UC on the system's dynamic response is discussed.

All simulations are based on a modified version of the IEEE 39-bus system [57]. The data of the s-UC can be found in Table A.3.

The focus is on the first 12 hours of the planning horizon. During these hours the demand increases from 700 MW in the first hour to 1500 MW in the 12 hour. For simplicity, a wind profile that follows the demand is modelled. In other words, we assume the same wind penetration level for the medium scenario during these hours, namely 25%, and based on this we build the low and high scenario accordingly. Such a relationship between demand and wind power corresponds to a typical day in 2018 in the Irish system. It should be noted here that one may choose any other profile for the demand and wind but according to our studies that does not change the relevant conclusions. Wind generation is given by three wind power plants connected at bus 20, 21 and 23, respectively, with a nominal capacity of 300 MW each.

The total number of state and algebraic variables of the SDAE model for all scenarios are 173 and 277, respectively. Regarding the s-UC variables, the model includes three first-stage variables, namely the ON/OFF, start-up and shut-down status of generating units, and four second-stage variables, namely the active power of conventional units (set-points), the demand and wind power curtailment, and the bus voltage angle, respectively. The total numbers of the first-stage and second-stage variables for the 15-minute model

are 2,880 and 20,448, respectively. While the total numbers of these variables for the 5-minute model are 8,640 and 61,344, respectively. Therefore even considering only three wind power scenarios, shortening the time period of s-UC, lead to a huge increase in the size of the s-UC model. In fact, this is one of the main limitations of s-UC approaches, especially when considering their use for real-time operations of power systems.

Finally, a MC is used in all scenarios (100 simulations are solved for each scenario). The standard deviation of the frequency of the COI,  $\sigma_{\text{COI}}$ , (computed as the average of the standard deviation obtained for each trajectory) is utilized as an index to evaluate the impact of s-UC on the dynamic response of the system. The software tool Dome used in the simulations includes a set of dynamic models similar to the ones provided by commercial software tools but with the additional feature of being able to model and properly integrate stochastic processes. Note that EMT models are not considered because they are not suitable for the simulation of several minutes of an interconnected power system due to their computational burden.

## 15-Minute Scheduling

In this section, a 15-minute scheduling time period is used. The average value of the objective function is found to be approximately \$412,000, hence, lower than the value found in, for example, [18]. This is due to the fact that wind generation is explicitly accounted in the objective function, and since its marginal production cost is considered zero, it leads to lower operational costs. Each scenario is characterized by an appropriate amount of wind stochastic variations. When solving the sensitivity analysis, the s-UC probabilities are varied, and their impact on the standard deviation of the frequency of the system ( $\sigma_{\text{COI}}$ ) is observed.

In order to compare results, a base-case scenario is considered with the following properties: s-UC probabilities for the low, medium and high wind power scenarios are set to 20%, 60%, 20%, respectively. Similarly, when we run the MC-TDS, the system is assumed to be with the following probabilities: 20%, 60%, 20% for the low, medium and high wind power scenario, respectively. As mentioned in the rolling planning section, the low and high scenario differs from the medium scenario by 10%. This base case is shown in Fig. 5.4, 5.5, while Fig. 5.4 shows the trajectories of  $\omega_{\text{COI}}(t)$ , and Fig. 5.5 shows the trajectories of the wind speed scenarios.

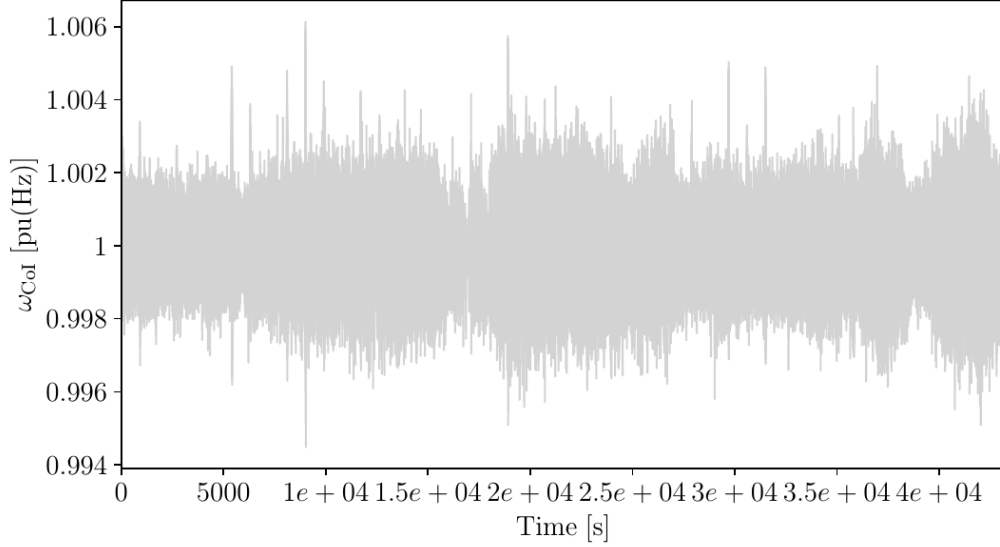


Figure 5.4: 15-minute scheduling – Trajectories of  $\omega_{CoI}(t)$  for 12h.

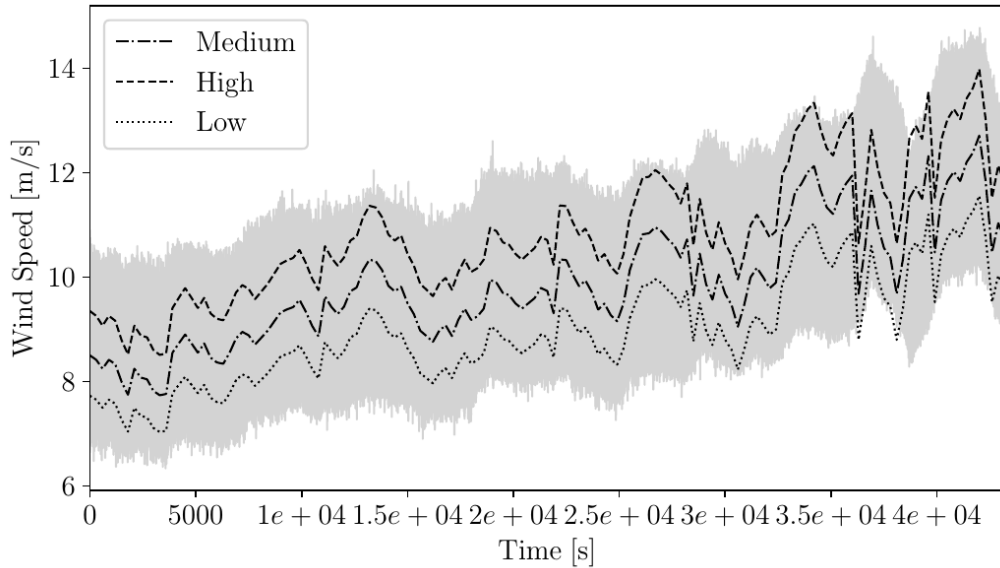


Figure 5.5: 15-minute scheduling – Trajectories of wind speeds for 12h. Dashed lines indicate the high, medium and low scenarios, respectively, while black line indicate the same scenarios with inclusion of volatility.

It is interesting to note that, in Fig. 5.4, the frequency jumps due to a change in the operating point of the machines forced by the s-UC, i.e. new schedules. These jumps are very similar to real-world power systems behaviour observed in, for example, the continental European grid [38, 102]. Finally, it is worth mentioning that the wind speed profile in Fig. 5.5 is obtained by adding some stochastic noise on each of the three wind scenarios.

Table 5.1: 15-minute scheduling –  $\sigma_{\text{CoI}}$  for different s-UC probabilities with  $j = 10\%$ .

Scenario	s-UC			MC – TDS			$\sigma_{\text{CoI}} (10^{-4})$
1	20%	60%	20%	20%	60%	20%	8.47
2	40%	50%	10%	20%	60%	20%	8.59
3	100%	0%	0%	20%	60%	20%	8.67
4	0%	100%	0%	20%	60%	20%	8.72
5	0%	0%	100%	20%	60%	20%	8.02
6	0%	20%	80%	20%	60%	20%	8.17
7	0%	40%	60%	20%	60%	20%	8.32
8	0%	60%	40%	20%	60%	20%	8.41
9	0%	80%	20%	20%	60%	20%	8.52

### Impact of different s-UC strategies

Table 5.1 shows some of the most relevant results of the sensitivity analysis. Specifically, scenario 1 assumes a s-UC with wind probabilities 20%, 60%, 20% and a MC-TDS with the same probabilities. Thus, it is assumed that what was forecast by the s-UC will actually happen in reality.  $\sigma_{\text{CoI}}$  for this scenario is  $8.47 \cdot 10^{-4}$ . In Scenario 2 the probabilities of the s-UC differ from that of the system by a relevant value. The value of  $\sigma_{\text{CoI}}$  is  $8.59 \cdot 10^{-4}$ , and thus higher than scenario 1 due to the error in the s-UC probabilities.

Scenario 3 assumes a s-UC with 100% low wind (one scenario, equivalent to d-UC). The value of  $\sigma_{\text{CoI}}$  for this scenario is  $8.67 \cdot 10^{-4}$  and so higher than scenario 1 for the same reason above. Similarly, Scenario 4 assumes a s-UC with 100% medium wind. This leads to higher frequency variations compared to scenario 1, with  $\sigma_{\text{CoI}} = 8.72 \cdot 10^{-4}$ . Next, Scenario 5 assumes a s-UC with 100% high wind. Quite surprisingly, this scenario appears to be the best from the dynamic point of view with  $\sigma_{\text{CoI}} = 8.02 \cdot 10^{-4}$ .

To analyse this relevant case, more scenarios are considered. In Scenarios 6 to 9 in Table 5.1, the probabilities of s-UC are varied from a s-UC with 100% high wind to a s-UC with 100% medium, and it can be seen that  $\sigma_{\text{CoI}}$  increases almost linearly. Therefore, even though Scenario 5 assumes an error in the s-UC probabilities, synchronous machines and the respective controls (primary and secondary) can regulate it very fast.

To further analyse this, in Table 5.2 the wind power uncertainty level is increased from  $j = 10\%$  to  $j = 30\%$  with a step of 10% for both, Scenario 1 and Scenario 5, respectively. For  $j \geq 30\%$ , Scenario 1 gives the better dynamic behaviour. It appears that, if the wind forecast error is small, then from the dynamic performance viewpoint of the system, it is better to solve a d-UC with high wind power.

Table 5.2: 15-minute scheduling –  $\sigma_{\text{CoI}}$  for different s-UC probabilities and different  $j$ .

Scenario	$j$	s-UC			MC – TDS			$\sigma_{\text{CoI}} (10^{-4})$
1	10%	20%	60%	20%	20%	60%	20%	8.47
1	20%	20%	60%	20%	20%	60%	20%	12.58
1	30%	20%	60%	20%	20%	60%	20%	17.20
5	10%	0%	0%	100%	20%	60%	20%	8.02
5	20%	0%	0%	100%	20%	60%	20%	12.41
5	30%	0%	0%	100%	20%	60%	20%	17.37

Table 5.3: 15-minute scheduling –  $\sigma_{\text{CoI}}$  for different stochastic unit commitment probabilities with  $j = 10\%$ .

Scenario	s-UC			MC – TDS			$\sigma_{\text{CoI}} (10^{-4})$
1	0%	0%	100%	0%	0%	100%	8.01
2	0%	100%	0%	0%	100%	0%	2.90
3	100%	0%	0%	100%	0%	0%	1.46

It is worth observing that the differences in the system’s long-term frequency deviations between scenarios are marginal (maximum of 3.5 mHz). This is mainly because, since the scheduling is repeated with a short period, it reduces the forecast error, which leads different s-UC strategies to produce similar schedules for the generators. This indicates that system operators may prefer to use deterministic approaches when scheduling the system as the complexity of the stochastic one does not provide a solution with a significant added value for the operation of the system.

Finally, Table 5.3 compares three deterministic cases, namely low, medium and high s-UC wind power scenarios. The deterministic low wind power scenario leads to better dynamic behaviour (lower  $\sigma_{\text{CoI}}$ ).

### Impact of s-UC wind uncertainty

To simulate the impact of the s-UC wind power uncertainty, the uncertainty level is increased from  $j = 10\%$  to  $j = 40\%$  with a step of 10% (volatility is kept constant). Four  $\sigma_{\text{CoI}}$  are calculated and Fig. 5.6 shows  $\sigma_{\text{CoI}}$  as a function of wind power uncertainty. The higher wind uncertainty, the higher  $\sigma_{\text{CoI}}$ . This relationship is almost linear within the used range. This suggests that as power systems accommodate more RES, i.e. higher uncertainty, TSOs will have to ensure they have the necessary sources (power reserves) to cope with this uncertainty.

Figure 5.7 shows the total cost as a function of wind uncertainty. The higher the wind uncertainty, the higher the cost due to more ramp-up and ramp-down of generators. Hence, despite RES being a cheap source of energy, their intermittent nature, requires more reserves to cope and so there will be an increase of the cost of ancillary service. These results confirm the conclusions of previous works, e.g. [90].

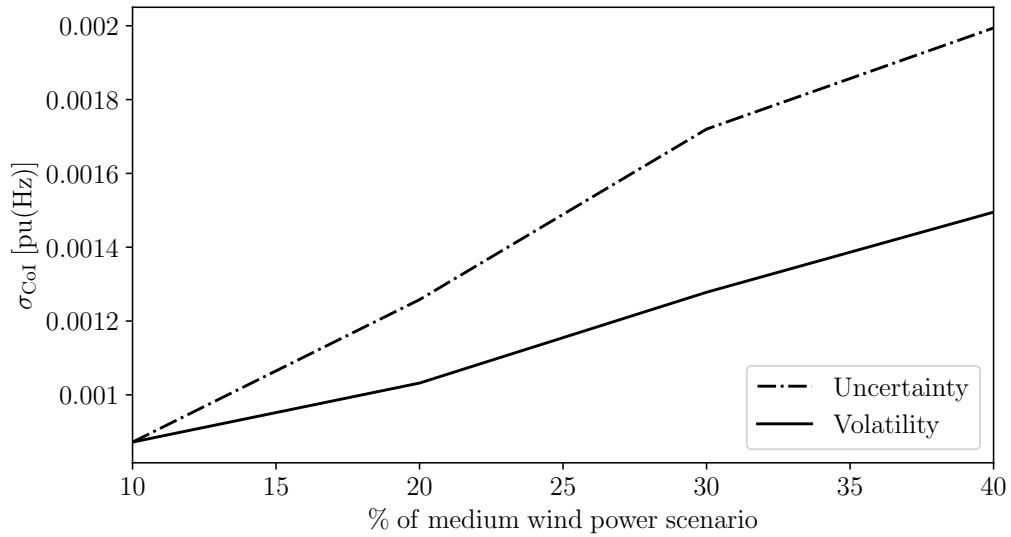


Figure 5.6: 15-minute scheduling –  $\sigma_{CoI}$  as a function of wind uncertainty and volatility.

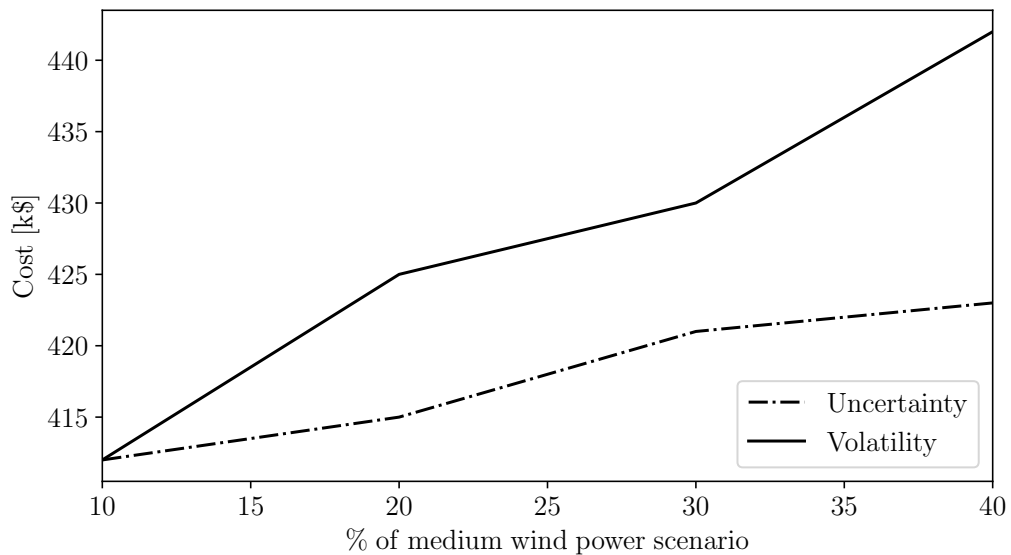


Figure 5.7: 15-minute scheduling – Expected cost as a function of wind uncertainty and volatility.

### **Impact of s-UC wind volatility**

To study the impact of s-UC wind power volatility on power system dynamics, different volatility levels are considered, i.e. higher standard deviations means high wind volatility. The standard deviation of wind scenarios is increased from 10% to 40% with a step of 10% while uncertainty is kept constant.

Figure 5.6 shows  $\sigma_{CoI}$  as a function of wind power standard deviation. The higher the wind power volatility, the higher the frequency variations. Similarly to the results shown in Fig. 5.6, this relationship appears to be almost linear within the considered range. As mentioned above, this supports the idea for increased ancillary services by TSOs in the future.

Figure 5.7 shows the total cost as a function of wind volatility. It can be seen that higher wind power volatility leads to higher costs due to higher ramping of generating units. Wind power volatility has thus a more significant effect than uncertainty on costs.

### **5-Minute Scheduling**

In this scenario, the wind power uncertainty level is assumed proportional lower compared to the 15-minute scheduling period ( $j = 3.33\%$ ). This assumption is made based on the 15-minute rate of change of wind power shown above (Fig. 5.1). Next, the base case scenario is depicted in Figs. 5.8, 5.9. Compared to the base-case scenario in the 15-minute case study (Fig. 5.4), frequency variations are lower (Fig. 5.8). Also, it is interesting to note that high frequency variations correspond to the wind ramp-up. Regarding the total operating cost, its average value is approximately \$408,000, and hence, lower than in the 15-minute case study due to lower uncertainty.

### **Impact of different s-UC strategies**

Furthermore, a sensitivity analysis similar to the 15-minute scheduling is carried out and Table 5.4 shows the relevant results. A reduction of the value of  $\sigma_{CoI}$  is observed for all scenarios. This is due to the lower level of wind power uncertainty. In particular, if we compare scenarios 1, 3 and 5, respectively, we can see that the differences are less significant. It appears that, if the uncertainty level is low and the system is scheduled more frequently, then differences between d-UC and s-UC becomes less evident. This result

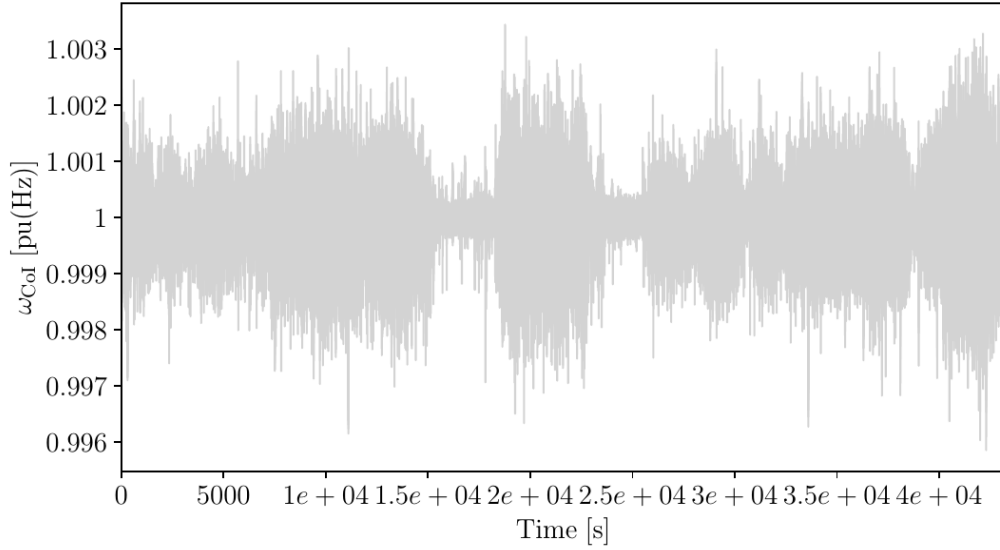


Figure 5.8: 5-minute scheduling – Trajectories of  $\omega_{CoI}(t)$  for 12h.

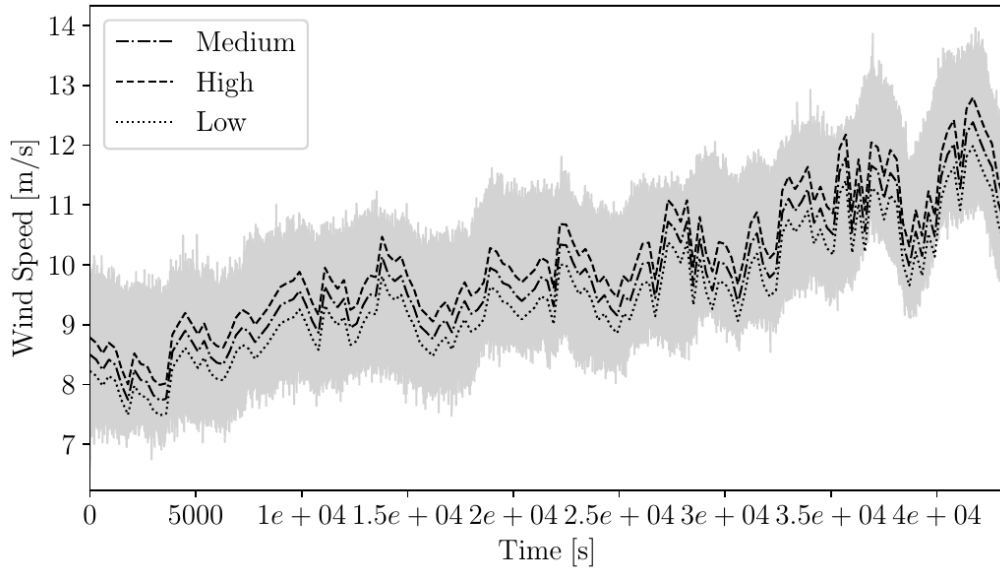


Figure 5.9: 5-minute scheduling – Trajectories of wind speeds for 12h. Dashed lines indicate the high, medium and low scenarios, respectively, while black line indicate the same scenarios with inclusion of volatility.

can be explained by the fact that, even if there is an error in the forecast, the machines and the relevant controls will easily account for it. Therefore, if shorter interval of s-UC are used and the system is scheduled more frequently, like, for example, in Australia [78], then system operators can still rely on deterministic approaches without compromising the dynamic performance of the system.

Table 5.4: 5-minute scheduling –  $\sigma_{\text{CoI}}$  for different s-UC probabilities with  $j = 3.333\%$ .

Scenario	s-UC			MC – TDS			$\sigma_{\text{CoI}} (10^{-4})$
1	20%	60%	20%	20%	60%	20%	5.45
2	40%	50%	10%	20%	60%	20%	5.51
3	100%	0%	0%	20%	60%	20%	5.44
4	0%	100%	0%	20%	60%	20%	5.70
5	0%	0%	100%	20%	60%	20%	5.48
6	0%	20%	80%	20%	60%	20%	5.53
7	0%	40%	60%	20%	60%	20%	5.55
8	0%	60%	40%	20%	60%	20%	5.55
9	0%	80%	20%	20%	60%	20%	5.59

Table 5.5: 5-minute scheduling –  $\sigma_{\text{CoI}}$  for different s-UC probabilities with  $j = 3.333\%$ .

Scenario	s-UC			MC – TDS			$\sigma_{\text{CoI}} (10^{-4})$
1	0%	0%	100%	0%	0%	100%	5.46
2	0%	100%	0%	0%	100%	0%	3.38
3	100%	0%	0%	100%	0%	0%	2.43

While the sensitivity analysis in the case of the perfect forecast is shown in Table 5.5. The deterministic case with low wind gives better dynamic behaviour, thus confirming the conclusions drawn for the 15-minute s-UC.

### Impact of s-UC wind uncertainty

Moreover, similar to the 15-minute case, the effect of wind power uncertainty on power system dynamics using 5-minute scheduling is discussed. With this aim, the wind power uncertainty level is increased from  $j = 10\%$  to  $j = 40\%$  with a step of 10%.

Figure 5.10 shows  $\sigma_{\text{CoI}}$  as a function of wind power uncertainty. Again, we can see that such a relationship is almost linear within the used range. This suggests that, even using shorter s-UC timescales, e.g. 5 minutes, higher shares of RES will likely affect the system’s dynamic performance.

### Impact of s-UC wind volatility

Following the same procedure as in the 15-minute case study, the standard deviation of wind power scenarios is increased from 10% to 40% with a step of 10%. Then, Fig. 5.10 shows  $\sigma_{\text{CoI}}$  as a function of wind power volatility. This relationship is almost linear within the considered range, and these findings support the conclusions made above.

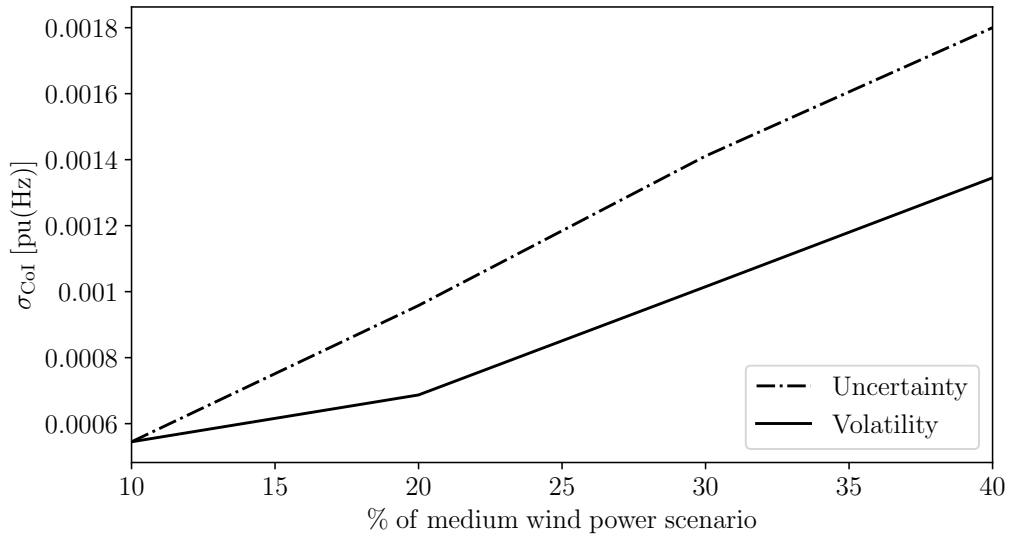


Figure 5.10: 5-minute scheduling –  $\sigma_{CoI}$  as a function of wind uncertainty and volatility.

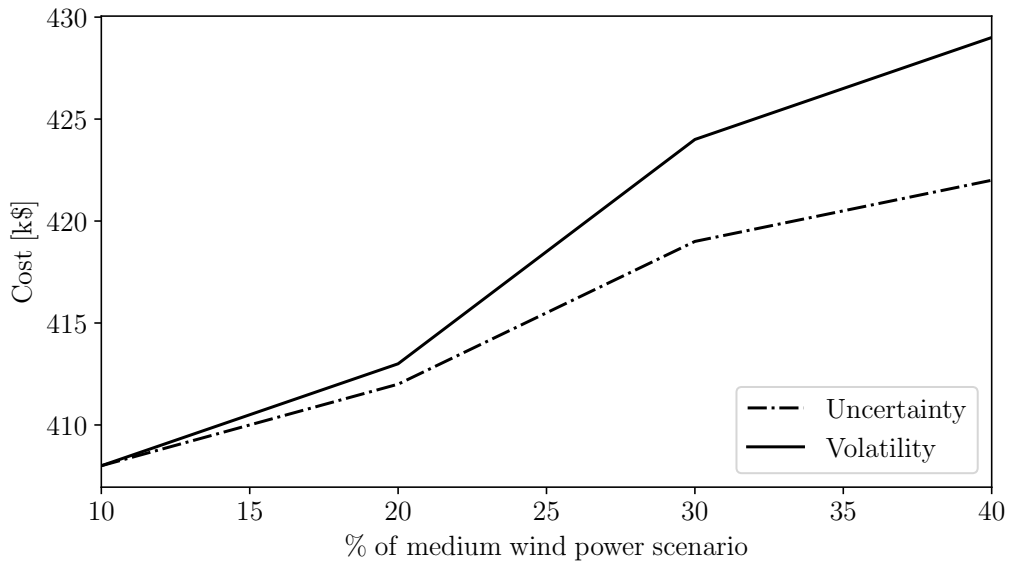


Figure 5.11: 5-min scheduling – Expected cost as a function of wind uncertainty and volatility.

Finally, the impact of wind power volatility on costs is shown in Fig. 5.11. Results indicate that the higher the wind power volatility, the higher the cost due to more ramping of generating units.

## Impact of contingency on the transient response of the system using s-UC and d-UC

This section discusses whether a contingency leads to different dynamic behaviour of the system if using a s-UC or d-UC. With this aim, the comparison is performed using scenario 1 (stochastic) and scenario 5 (deterministic) from Table 4.1.

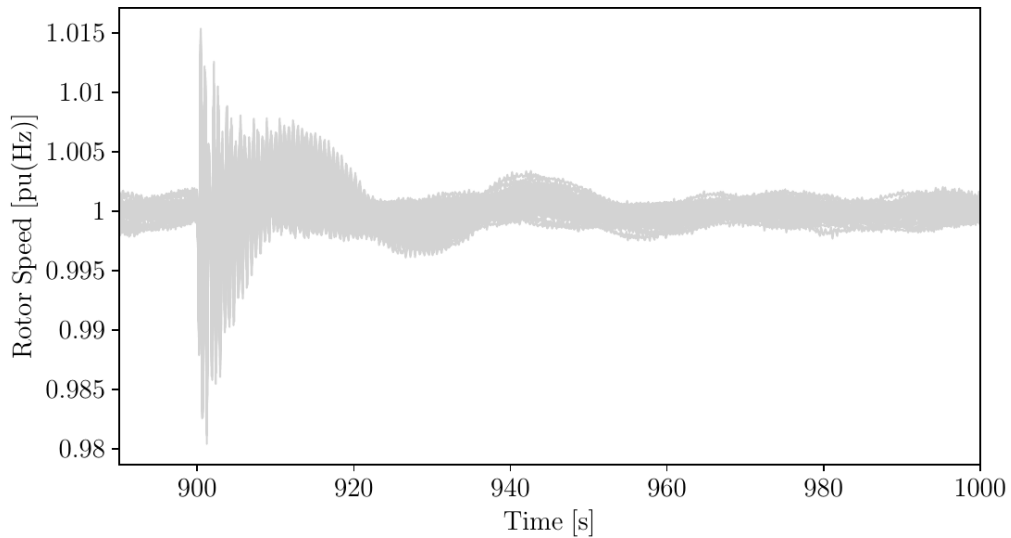


Figure 5.12: s-UC and 25% wind penetration – Trajectories of the rotor speed of relevant machines following a contingency.

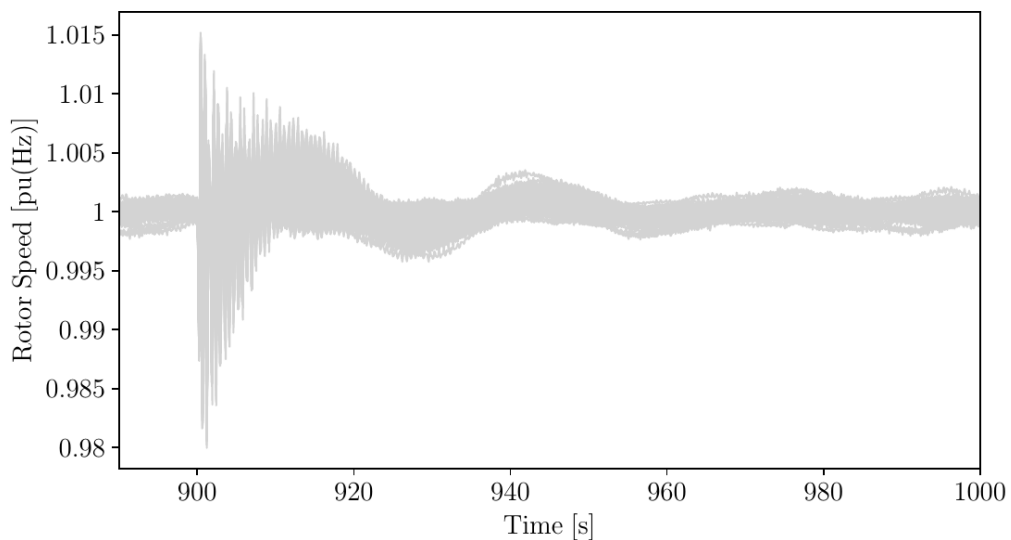


Figure 5.13: d-UC and 25% wind penetration – Trajectories of the rotor speed of relevant machines following a contingency.

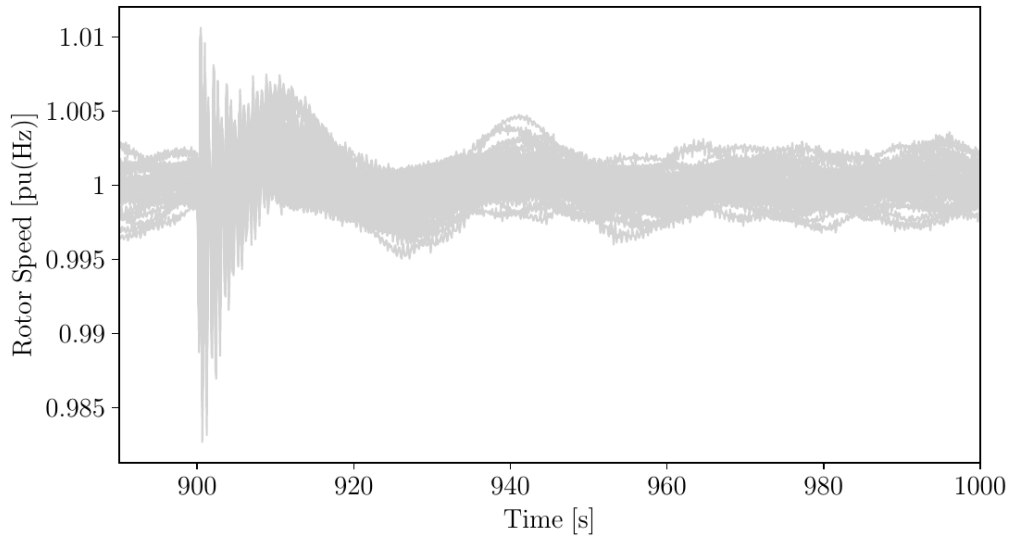


Figure 5.14: s-UC and 50% wind penetration – Trajectories of the rotor speed of relevant machines following a contingency.

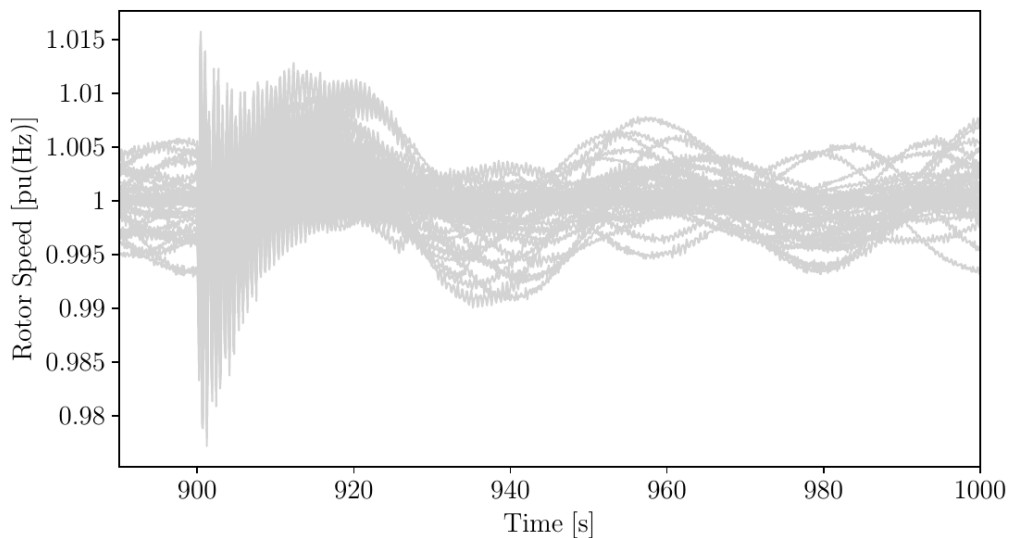


Figure 5.15: d-UC and 50% wind penetration – Trajectories of the rotor speed of relevant machines following a contingency.

A three-phase fault is applied at  $t = 900$  s and cleared after 200 ms by disconnecting line 1. The impact of the contingency is shown in Figs. 5.12 and 5.13. Specifically, Fig. 5.12 depicts the trajectories of the rotor speed of the relevant machines during the contingency when using a s-UC. Similarly, Fig. 5.13 depicts the trajectories of the rotor speed of the relevant machines during the contingency when using a d-UC. Results indicate that for the considered case study the impact of contingency is almost identical. This is because the generator schedules obtained with the s-UC and d-UC do not differ significantly.

The same contingency is applied for the case of 50% wind penetration. Figures 5.14 and 5.15 show the trajectories of the rotor speed of the relevant machines during the contingency when using a s-UC and d-UC, respectively. In this case, the s-UC leads to a better transient response of the system following a contingency. It appears that one cannot know *a priori* which strategies of s-UC are better from the dynamic viewpoint of the system before solving both s-UC and d-UC problems.

## Impact of renewable penetration on long-term frequency deviations using different s-UC strategies

Increasing the penetration levels of RESs changes the system's stability and dynamic performance and makes real-time system operation more difficult for TSOs [126]. In this context, this section focuses on the impact of high penetration levels of RESs, namely 50%, on the long-term frequency deviations using different s-UC strategies. A sensitivity analysis with respect to different s-UC probabilities for the low, medium and high wind power scenario is carried out with this aim.

Table 5.6 shows some relevant results of the analysis. There is a significant increase in the value of  $\sigma_{\text{CoI}}$  in all scenarios compared to 25% of wind penetration. This is to be expected as fewer synchronous generators that provide frequency regulation (primary and secondary) are now scheduled to be online and more power is being produced by stochastic sources.

Interestingly, the deterministic scenario with high wind power (scenario 5) is the worst with  $\sigma_{\text{CoI}} = 2.61 \cdot 10^{-3}$ . Scenario 5, in fact, schedules fewer synchronous generators to be online compared to the same scenario in the previous Section. In other words, there is less frequency regulation available online to cope with wind power uncertainty. Therefore, depending on the level of wind power uncertainty and wind penetration level, TSOs can solve a s-UC or d-UC with high wind. Specifically, according to our results, it is better to solve a d-UC with high wind power for low wind power uncertainty ( $j < 30\%$ ) and 25% wind penetration level. On the other hand, if the wind penetration level is 50%, TSOs can solve a s-UC and/or d-UC with medium and low wind power.

Table 5.6: 15-minute scheduling –  $\sigma_{\text{CoI}}$  for different s-UC probabilities with  $j = 10\%$  and  $50\%$  wind penetration.

Scenario	s-UC			MC – TDS			$\sigma_{\text{CoI}} (10^{-4})$
1	20%	60%	20%	20%	60%	20%	19.03
2	40%	50%	10%	20%	60%	20%	18.95
3	100%	0%	0%	20%	60%	20%	19.09
4	0%	100%	0%	20%	60%	20%	19.09
5	0%	0%	100%	20%	60%	20%	26.18

## Impact of the number of s-UC wind scenarios on the dynamic response of the system

In this section, we compare the impact of the number of s-UC wind scenarios on the dynamic behaviour of the power system. The comparison is performed using a 15-minute scheduling time period and 25% wind penetration. With this aim, we consider 10 wind power scenarios and perform a sensitivity analysis. Wind power scenarios are built according to the wind maximum variation width  $j$  (see Fig. 5.1). In order to compare the results, a base-case scenario is considered with the following properties: s-UC probabilities for the 10 scenarios (starting from low to high wind) are set as follows: 5%, 5%, 10%, 10%, 30%, 10%, 10%, 10%, 5%, 5%. Similarly, when we run the MC-TDS, the system is assumed to be with the following probabilities: 5%, 5%, 10%, 10%, 30%, 10%, 10%, 10%, 5%, 5%, starting from low to high wind scenario, respectively.

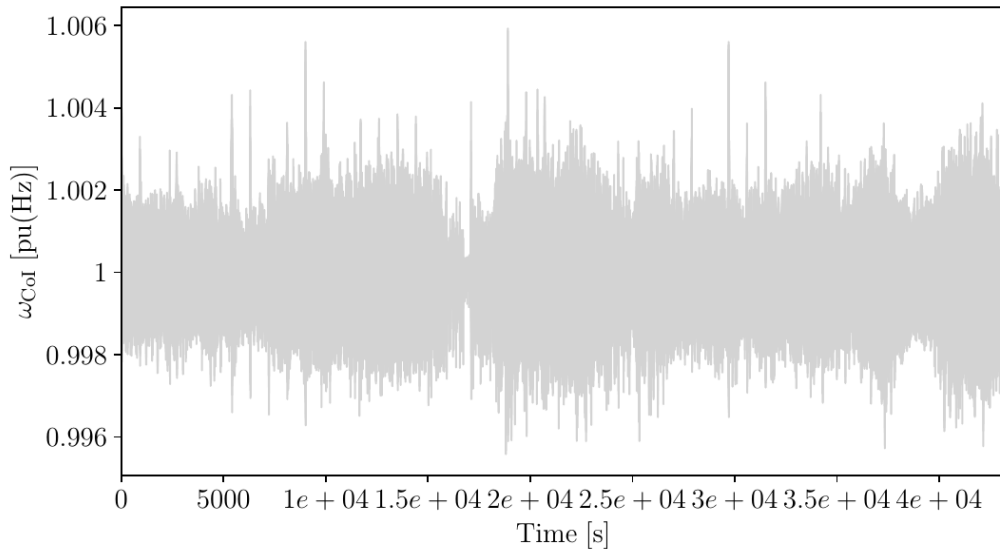


Figure 5.16: 15-minute scheduling – Trajectories of  $\omega_{\text{CoI}}(t)$  for 10 s-UC wind power scenarios.

Table 5.7: 15-minute scheduling – Different s-UC probabilities with  $j = 10\%$  and 10 wind power scenarios.

Scenario	s-UC
1	5%, 5%, 10%, 10%, 30%, 10%, 10%, 10%, 5%, 5%
2	20%, 5%, 5%, 10%, 10%, 5%, 10%, 10%, 5%, 20%
3	100%, 0%, 0%, 0%, 0%, 0%, 0%, 0%, 0%, 0%
4	0%, 0%, 0%, 0%, 100%, 0%, 0%, 0%, 0%, 0%
5	0%, 0%, 0%, 0%, 0%, 0%, 0%, 0%, 0%, 100%

Table 5.8: 15-minute scheduling –  $\sigma_{\text{CoI}}$  for different s-UC probabilities with  $j = 10\%$  and 10 wind power scenarios.

Scenario	MC – TDS	$\sigma_{\text{CoI}} (10^{-4})$
1	5%, 5%, 10%, 10%, 30%, 10%, 10%, 10%, 5%, 5%	8.74
2	5%, 5%, 10%, 10%, 30%, 10%, 10%, 10%, 5%, 5%	8.77
3	5%, 5%, 10%, 10%, 30%, 10%, 10%, 10%, 5%, 5%	8.82
4	5%, 5%, 10%, 10%, 30%, 10%, 10%, 10%, 5%, 5%	8.99
5	5%, 5%, 10%, 10%, 30%, 10%, 10%, 10%, 5%, 5%	8.90

Figure 5.16 shows the trajectories of  $\omega_{\text{CoI}}(t)$  for this base case scenario. Compared to Fig. 5.4 (3 s-UC wind power scenarios), there is no significant difference in the system’s dynamic behaviour. To further support this, Tables 5.7 and 5.8 show some of the relevant results of the sensitivity analysis. As it can be seen, the long-term frequency deviations are similar to those in Table 4.1 and do not differ significantly between scenarios. It appears that, for the considered case, increasing the number of s-UC wind power scenarios from 3 to 10 does not have a significant impact on the dynamic response of the system. Furthermore, these results support the above conclusion that a highly sophisticated s-UC might not be necessary if the scheduling is repeated with a short period.

## 5.8 Case Study 2: Impact of Different s-UC and Frequency Controllers/Machine Parameters

This case study provides a sensitivity analysis of the impact of different frequency controllers/machine parameters using a s-UC, a d-UC and different scheduling time periods [70]. This analysis allows comparing and drawing conclusions on the effect of these parameters on the dynamic performance of the system. The case study also compares the impact that different formulations of s-UC have on the dynamic performance of power systems.

The focus of this case study is on the first 4 hours of the planning horizon. Wind power uncertainty, volatility and rolling planning horizon within the s-UC are modeled as in [66]. All other data are the same as in case study 1. The case study results are based on a MC, where 50 simulations are considered for each scenario.

## Sensitivity Analysis with Respect to Different Frequency Controllers/Machine Parameters

In this section, we vary (one at a time) three relevant frequency control/machine parameters and observe their impact on the standard deviation of the frequency.

The following base-case scenario is considered: the value of the gain of the AGC is taken equal to  $K_o = 50$ , the value of the droop of the TGs is taken equal to  $\mathcal{R} = 0.05$ , and the value of inertia of the machines is taken equal to the original values. In the scenarios below, the total inertia of the system and the gain of AGC is decreased up to 45% from the base case. Similarly, the aggregated system droop is increased up to 45% from the base case. Finally, since system operators still rely on d-UC and different sub-hourly scheduling periods [24], this sensitivity is performed using 15- and 5-minute periods and different s-UC formulations.

In the following, the sub-indexes  $S$  and  $D$  indicate control parameters for stochastic and deterministic scenarios, respectively.

### s-UC with 15-minute time period

In this scenario, we use a 15-minute scheduling time period and set the s-UC probabilities for the low, medium and high wind power scenario equal to 20%, 60%, 20%, respectively. Same probabilities are used when solving the MC-TDS. Next, the relevant frequency control/machine parameters are varied accordingly up to 45% of their base case value.

Figure 5.17 shows the effect of the variation of these parameters on  $\sigma_{\text{CoI}}$ . The gain of AGC,  $K_S$ , has the highest impact on  $\sigma_{\text{CoI}}$ . The relationship between the gain  $K_S$ , the droop  $\mathcal{R}_S$ , and  $\sigma_{\text{CoI}}$  is almost linear within the used range. This indicates larger frequency deviations as synchronous generators are replaced with RES (assuming that RES will not provide frequency regulation). On the other hand, the inertia  $M_S$  appears to have a small impact on long-term frequency deviation. This result indicates that while the

inertia is the main parameter impacting on the frequency dynamics following a major contingency, this is not the case on its impact on the  $\sigma_{\text{CoI}}$  (see also [118], which draws a similar conclusion).

## d-UC with 15-minute time period

As discussed above, system operators still rely on a d-UC formulation when scheduling the system. Therefore, it is essential to compare the impact of the variation of the relevant control/machine parameters on  $\sigma_{\text{CoI}}$ , using a s-UC and a d-UC. With this aim, we set the d-UC probabilities for the low, medium and high wind power scenarios equal to 0%, 100%, 0%, respectively. Thus, perfect forecast, which corresponds to the medium scenario, is assumed. However, when solving the MC-TDS, 20%, 60%, 20% probabilities are used to generate the three wind power scenarios. This creates a mismatch between forecast and actual wind variations and allows evaluating the robustness of the s-UC and d-UC formulations. Figure 5.17 shows the impact on  $\sigma_{\text{CoI}}$  of varying control/machine parameters.

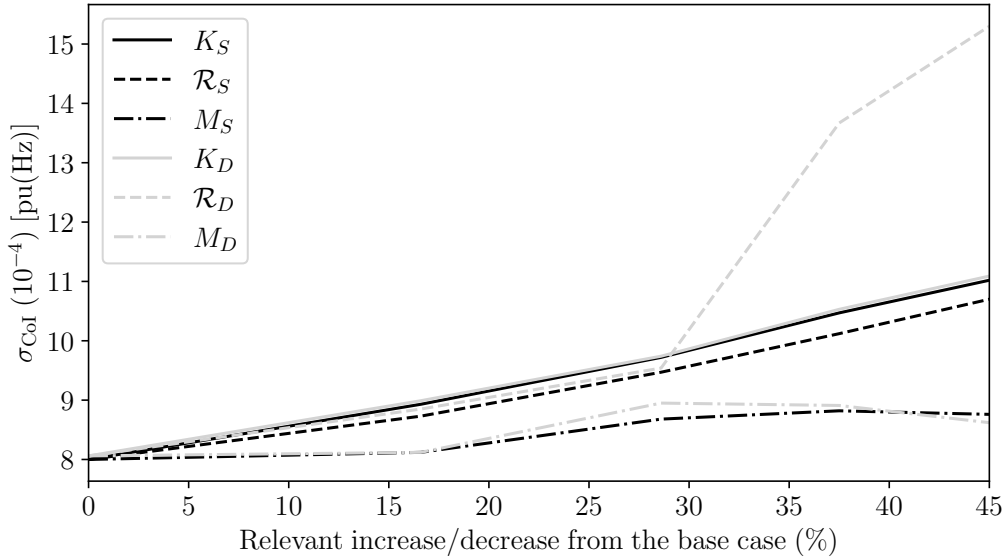


Figure 5.17: 15-minute time period –  $\sigma_{\text{CoI}}$  as a function of different frequency controllers/machine parameters using the complete s-UC and d-UC models.

A relevant difference concerning the scenario above is that the droop  $\mathcal{R}_D$  has the highest impact on  $\sigma_{\text{CoI}}$  when its value is  $\geq 30\%$  with respect to the base case. On the other hand, the gain of the AGC,  $K_D$  and the inertia  $M_D$  have similar impact on  $\sigma_{\text{CoI}}$  as in the previous scenario. It appears that, the impact of different control parameters on  $\sigma_{\text{CoI}}$  depends on the UC formulation (deterministic or stochastic). Thus, it is not obvious

which one (i.e.  $\mathcal{R}$  or  $K$ ) has the highest impact on  $\sigma_{\text{CoI}}$ . Fig. 5.17 compares the results of scenarios 1 and 2 and shows that using a s-UC leads to lower frequency variations. Furthermore, it should be noted that the differences between scenarios in Fig. 5.17, for example,  $\mathcal{R}_S$  and  $\mathcal{R}_D$  after 28%, are due to the fact that both models, namely s-UC and d-UC, produce different schedules for generators.

## **Sensitivity analysis using the simplified and alternative s-UC, and 15-minute time period**

Here, we perform the same sensitivity analysis as above, but this time using the simplified and alternative s-UC models, respectively. Such an analysis allows comparing and drawing conclusions on the impact of different frequency control/machine parameters on  $\sigma_{\text{CoI}}$ , using different sub-hourly s-UC models. With this aim, Fig. 5.18 shows the relevant results of the sensitivity analysis. Note that the sub-indexes Sim and Alt indicate control parameters for simplified and alternative s-UC scenarios, respectively. As expected, results are, in general, very similar to the ones discussed in previous sections. The gain of the AGC, in this case,  $K_{\text{Sim}}$  and  $K_{\text{Alt}}$ , has most of the time the highest impact on  $\sigma_{\text{CoI}}$ , as well as the inertia of the machines appears to have a small impact. Moreover, using an alternative s-UC model and varying its relevant parameters leads to lower frequency variations. This is because the alternative s-UC model schedules more generators to be online compared to the other three UC models. Thus, depending on the s-UC model, different control parameters (e.g.  $K$  or  $\mathcal{R}$ ) can have a different impact on  $\sigma_{\text{CoI}}$ .

## **s-UC with 5-minute time period**

This scenario investigates whether a shorter scheduling time period of s-UC, namely 5-minute, changes the results and conclusions drawn for the 15-minute time period. Due to the shorter time period, the wind power uncertainty level within s-UC is lower compared to the previous section. Both s-UC and MC-TDS probabilities for the low, medium and high scenarios are set equal to 20%, 60% and 20%, respectively.

Figure 5.19 shows the effect of the variation of the relevant control parameters on  $\sigma_{\text{CoI}}$ . The most visible effect of reducing the time period to 5-minutes is that the value of  $\sigma_{\text{CoI}}$  decreases in all scenarios due to a lower wind power uncertainty. Also in this case, the

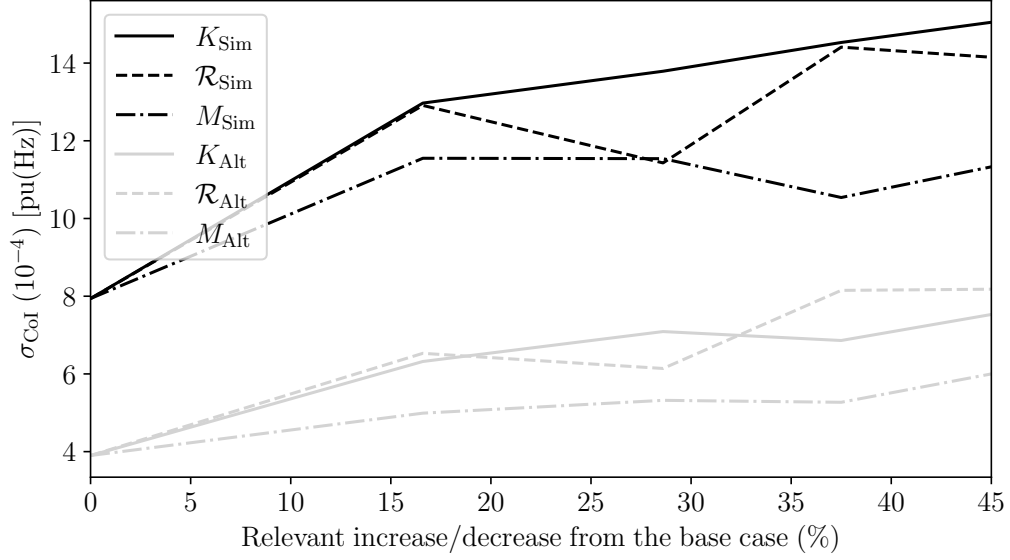


Figure 5.18: 15-minute time period –  $\sigma_{CoI}$  as a function of different frequency controllers/machine parameters using the simplified and alternative s-UC models.

gain of the AGC,  $K_S$ , has the highest impact on  $\sigma_{CoI}$ . The relationship is linear in the considered range, which indicates the need to increase the frequency regulation to keep long-term frequency deviations within certain limits. Finally, the inertia has little effect on  $\sigma_{CoI}$ , supporting the conclusions above.

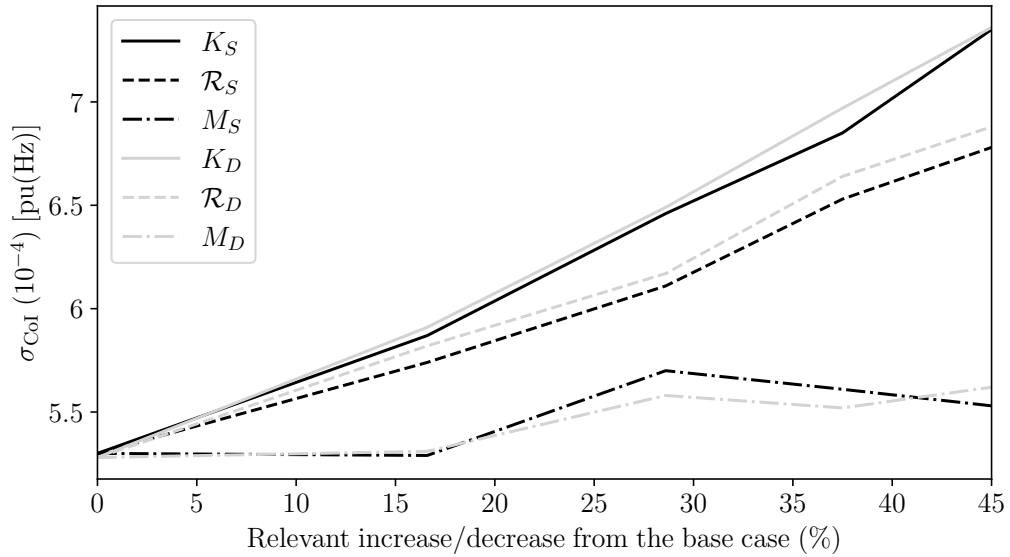


Figure 5.19: 5-minute time period –  $\sigma_{CoI}$  as a function of different frequency controllers/machine parameters.

## d-UC with 5-minute time period

Figure 5.19 shows the effect of the variation of control/machine parameters using a 5-minute scheduling and d-UC. Results are very similar to the 5-minute scheduling s-UC. To better show the differences, Fig. 5.19 compares the results of both scenarios, where it can be observed that the s-UC leads, in general, to lower frequency variations. Also, in both scenarios, the gain of the AGC has the highest impact on  $\sigma_{CoI}$ , whereas the inertia has a small impact.

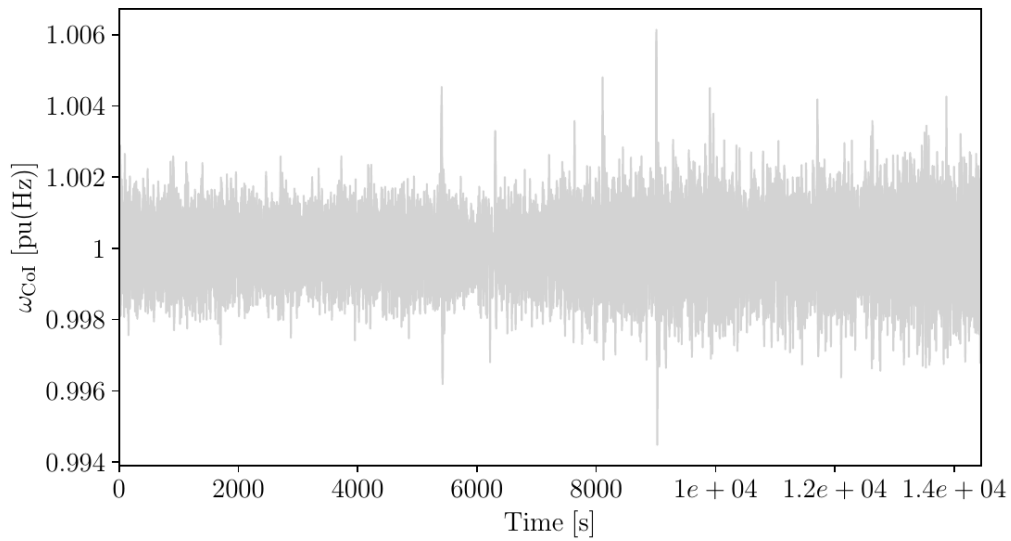


Figure 5.20: Trajectories of  $\omega_{CoI}(t)$  for 15-minute time period and complete s-UC.

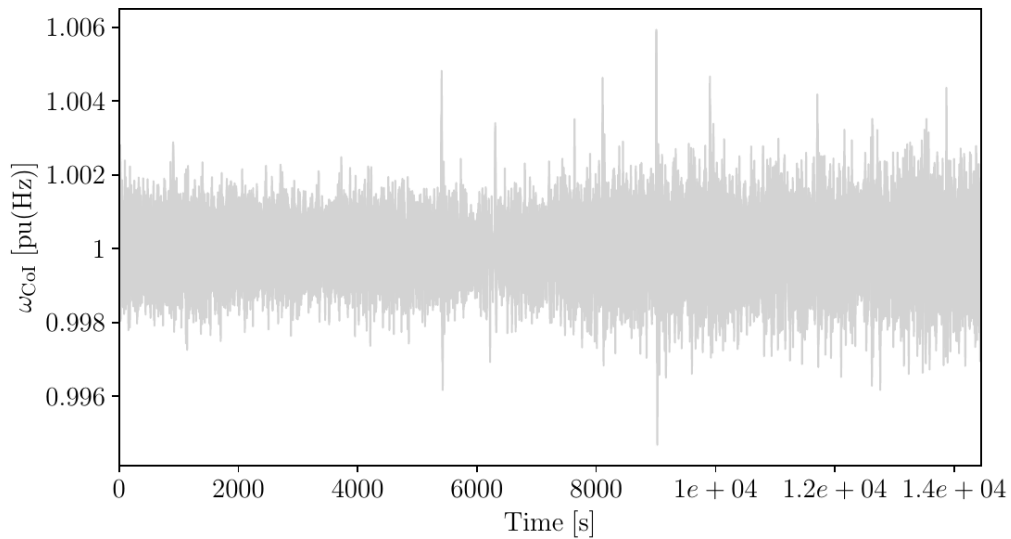


Figure 5.21: Trajectories of  $\omega_{CoI}(t)$  for 15-minute time period and simplified s-UC.

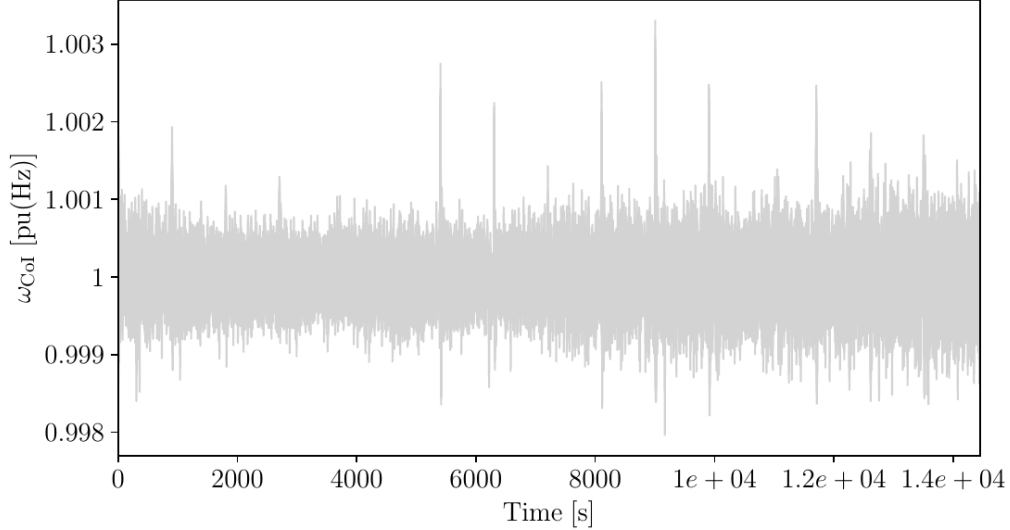


Figure 5.22: Trajectories of  $\omega_{CoI}(t)$  for 15-minute time period and alternative s-UC model.

## Comparison of Different s-UC Models

Even though system operators are skeptical regarding s-UC approaches due to their complexity, they acknowledge the need to better represent uncertainty when scheduling the system [129].

For this reason, the objective of this section is to compare the impact that these models have on long-term power system dynamics. Such a comparison is made using a 15-minute time period.

We first compare the impact on the dynamic response of the power system of the s-UC formulations (5.3)-(5.21) (complete s-UC) and (5.25)-(5.29) (simplified s-UC).

Figures 5.20 and 5.21 show the  $\omega_{CoI}(t)$ , of the complete and simplified s-UC models. The two formulations returns an almost identical  $\omega_{CoI}(t)$ , namely  $\sigma_{CoI} = 8.00 \cdot 10^{-4}$  pu(Hz) for the complete s-UC and, while that of the simplified s-UC is  $\sigma_{CoI} = 7.94 \cdot 10^{-4}$ . Specifically, the difference is about 1%. Figures 5.23 and 5.24 show the mechanical power of the conventional synchronous generators 1, 2 and 4, of the complete and simplified s-UC model. The two models produce similar schedules. In fact, at the beginning of the planning horizon, the simplified s-UC model alternates the schedules for generators 2 and 4, and after some time (i.e. after 6000 s) it produces the same schedules as the complete s-UC model. It appears, thus, that for this particular system and for normal operation conditions, the differences between using a complete s-UC model and a simplified one are

negligible. These results suggest that an involved UC formulation is not necessarily the best in normal operating conditions of the system.

Next, we compare the impact on system dynamics of the problem (5.3)-(5.21) (complete s-UC) and the problem (5.30)-(5.39) (alternative s-UC). With this aim, a MC-TDS per each s-UC formulation is carried out.

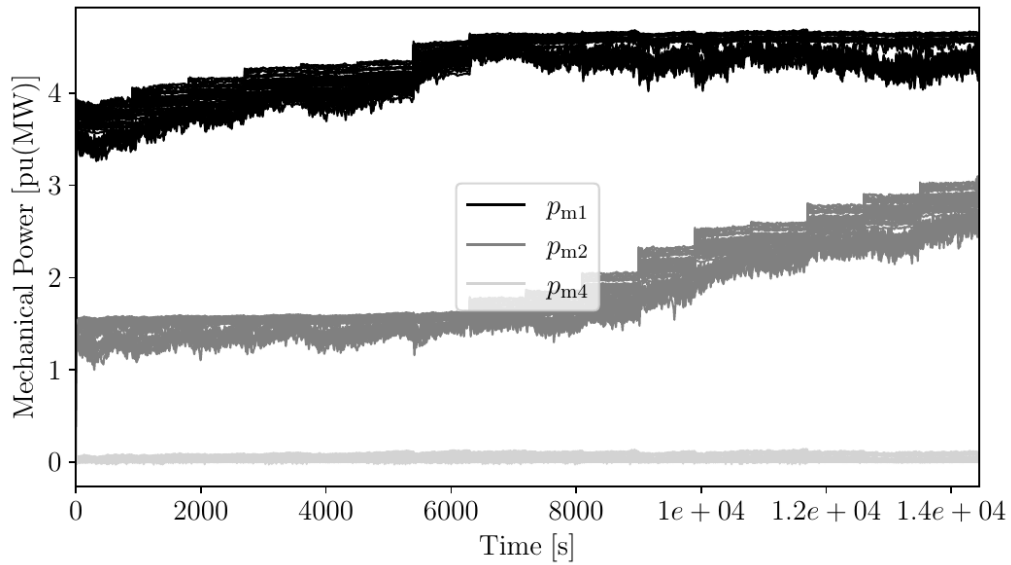


Figure 5.23: Mechanical power of synchronous generators 1, 2 and 4, for 15-minute time period and complete s-UC model.

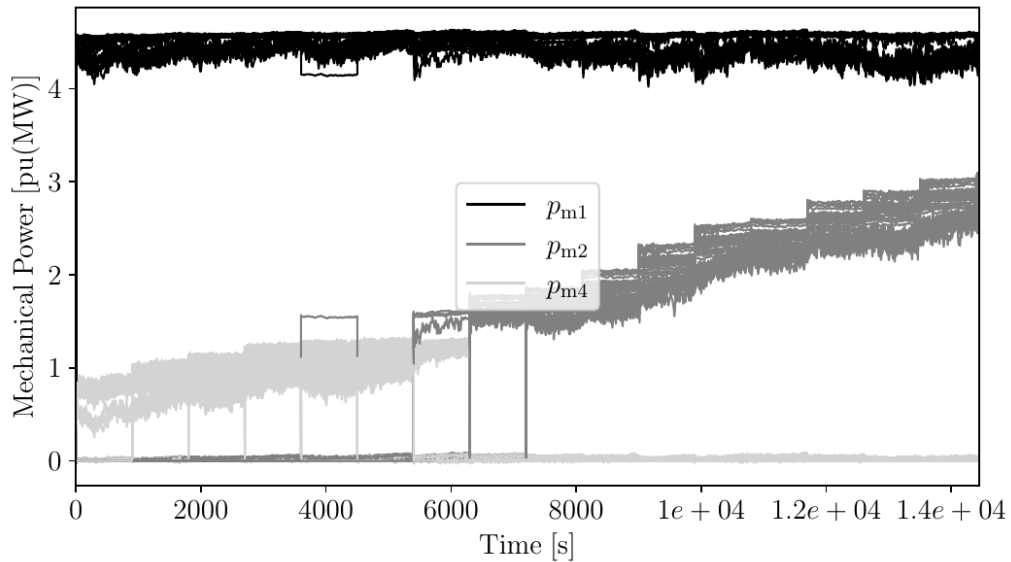


Figure 5.24: Mechanical power of synchronous generators 1, 2 and 4, for 15-minute time period and simplified s-UC model.

Figure 5.22 shows  $\omega_{coI}(t)$  for the alternative s-UC model. Compared to the complete s-UC model (see Fig. 5.20), the alternative formulation leads to lower frequency variations,

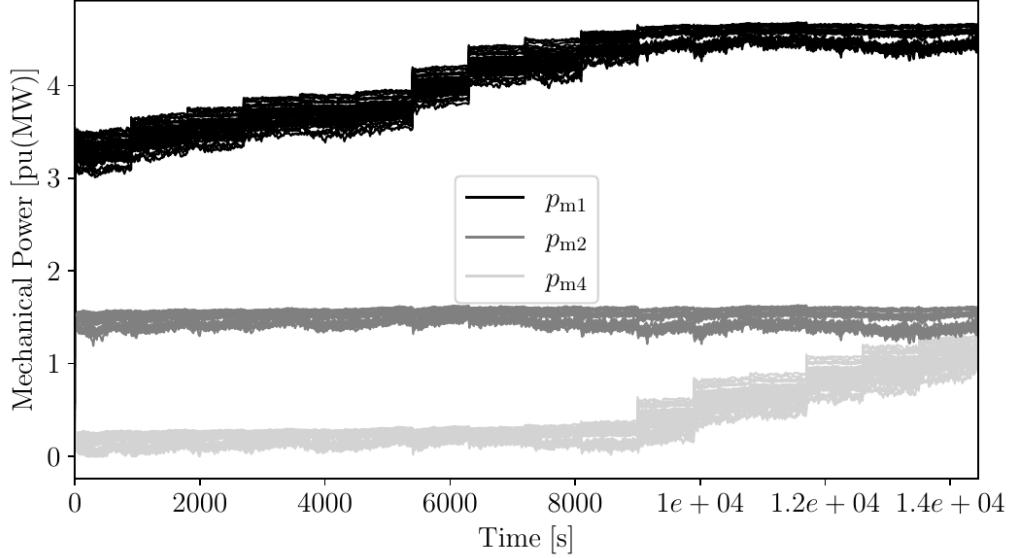


Figure 5.25: Mechanical power synchronous generators 1, 2 and 4, for 15-minute time period and alternative s-UC model.

i.e.  $\sigma_{\text{CoI}} = 3.90 \cdot 10^{-4}$ . In other words, the differences between the models is about 48%. This is due to fact that the two s-UC formulations produce slightly different schedule for generators. Specifically, the alternative s-UC model schedules a few more generators (Fig. 5.25) compared to the complete s-UC model (Fig. 5.23). This, in turn, implies more regulation, which helps better manage wind uncertainty. This can be observed in Fig. 5.22 where, in the time between two scheduling events – i.e. 15-minutes – frequency variations are lower due to the increased frequency regulation available in the system.

This result had to be expected. From the dynamic point of view, in fact, it is better to schedule more conventional synchronous generators, which provide both primary and secondary frequency regulations, rather than wind generation.

## 5.9 Conclusions

This chapter analyses the impact of the sub-hourly s-UC problem on the dynamic response of the power system. More specifically, the chapter focuses on the effect of different s-UC strategies and different wind uncertainty and volatility scenarios included in the s-UC on frequency variations. Also, the chapter performs a thorough sensitivity analysis to assess the impact on long-term power system dynamics of different frequency control/machine parameters and different sub-hourly s-UC formulations. With this aim, various standard and sophisticated s-UC are used to capture wind uncertainty, while the variability is

captured through a sub-hourly UC. Then, the sub-hourly s-UC are embedded into a TDS, and a rolling approach is used to account for wind and load forecast updates.

Simulation results of the first case study based on MC-TDS show no significant difference on long-term frequency deviations of the system when using different s-UC strategies. Results also suggest that for low wind uncertainty and 25% wind penetration level, system operators may want to solve a d-UC with high wind. However, as the s-UC wind uncertainty increases, then a s-UC approach is to be preferred. In addition, if the system is scheduled more frequently, then differences between stochastic and deterministic approaches become less evident. From the dynamic performance point of view, thus, the computational complexity of the stochastic methods does not provide an added value compared to that of deterministic ones.

Furthermore, results show that s-UC wind power uncertainty has a more substantial impact than volatility on the system's dynamic behaviour. They also indicate an almost linear relationship between s-UC wind uncertainty and volatility and frequency variations. This means that as the share of RESs deepen into modern power systems, i.e., higher wind uncertainty and volatility, it will be difficult for TSOs to manage the real-time balance between generation and demand. Therefore, there is a clear need for a linear increase of the spinning reserves.

Regarding the impact of s-UC wind scenarios, the case study shows that increasing the number of scenarios does not lead to any significant difference in the long-term frequency deviations. This result supports the conclusion that a highly sophisticated s-UC might not be needed if the scheduling is repeated frequently and with a short time period.

Moreover, results demonstrate that s-UC and d-UC for 25% wind penetration lead to an almost identical transient response of the system following a contingency. On the one hand, s-UC leads to a better transient response of the system in case of 50% wind penetration. On the other hand, when the wind penetration level reaches 50%, solving a s-UC and/or d-UC with medium and low wind power leads to lower long-term frequency deviations.

Simulation results of the second case study reveal that the gain of the AGC is the main parameter impacting the long-term frequency deviation. On the other hand, synchronous machine inertia has a negligible effect on the standard deviation of the frequency. The results also highlight that the power system's dynamic behaviour differences are marginal

when using a complete or a simplified s-UC model. Furthermore, a s-UC leads to lower variations of the frequency compared to a d-UC. An interesting result is that different formulations of the s-UC problem can schedule conventional power plants in different locations and/or numbers. These differences can significantly impact long-term power system dynamics, and hence the formulation of the s-UC has to be carefully chosen.

Given the above findings, we can conclude that: (i) TSOs can still rely on deterministic approaches when scheduling the system for wind power penetration levels below 25%; (ii) for higher wind power penetration levels, stochastic approaches should be employed and preferred by TSOs; (iii) there is a need for a linear increase of spinning reserves as the share of RESs increases; and (iv) the gain of the AGC and the formulation of the s-UC have to be carefully chosen as they may greatly impact the standard deviation of the frequency.

# Chapter 6

## A Dynamic Behavioral Model of the Long-Term Development of Solar Photovoltaic Generation driven by Feed-in Tariffs

### 6.1 Introduction

This chapter focuses on the modelling and simulation of the very long-term dynamics in power systems, namely the dynamics of incentive policies such as that FiT for PVs development. While FiT has provided a good platform for increasing the number of PV installations, it has also put a massive burden on the national budgets. This is because governments put in place extremely favorable and generous FiT schemes. However, generous FiT prices may lead to economic instability and eventually to the collapse of the scheme. Hence, defining appropriate policies is of utmost importance [55].

In this context, the objective of the chapter is to introduce a novel dynamic model based on nonlinear delay DAEs to simulate the evolution of the PV capacity and its commitment in the power grid. The model assumes the FiT budget, the PV cost and the public's willingness to install PVs as the main drivers for solar PV installations. The model's accuracy is validated against historical data of two of the biggest PV markets in the world driven by FiT, namely Italy during 2008-2014, and Germany during 2000-2014.

A sensitivity analysis based on the Italian PV market is also carried out to identify the impact of the parameters of the proposed model.

The remainder of the chapter is organized as follows. Section 6.2 presents the background of FiT schemes in Italy and Germany. Section 6.3 introduces the proposed dynamic model. The model validation test and the sensitivity analysis are presented in Section 6.4 and Section 6.5, respectively. Finally, Section 6.6 states the main conclusions of the chapter and discusses relevant policy implications.

## 6.2 FiT Evolution in Italy and Germany

### Italy

The solar PV capacity in Italy experienced an unexpected and exponential growth between 2008 and 2012 [8]. The main driver of the increase was the favorable and generous FiT applied by the Italian government through the so-called energy bill [72, 101]. The first energy bill was introduced in 2005 and lasted until 2007. While it included a very high FiT price, namely 490 EUR/MWh, this energy bill also had a cap of 100 MW. The capacity cap and the excessive bureaucratization regarding the procedures for the installations were a huge barrier to incentivize the investors [101].

In 2008, the Italian government introduced the second energy bill. This bill remained in place until 2010. It foresaw a 2% decrease of the FiT price and removed the administrative procedure and the cap on the overall PV capacity. Despite reducing the FiT price, the bill had a positive impact with 432 MW additions in 2008. This deployment led to an aggregate cost of 110 MEUR.

The solar PV capacity tripled in 2009 with a capacity of 1,114.4 MW and an annual cost of 303 MEUR [101]. At this point, the Italian government realized that the incentive cost was creating a considerable burden on the national budget. Thus, the government introduced the third energy bill, which foresaw a cut of the FiT price. Despite the new changes, the rush in the PV investment continued, and 3.74 GW were added. In terms of costs, 800 MEUR were paid in 2009 [101]. Furthermore, it is relevant to mention that this bill set an aggregate cap of 23 GW and 6,700 MEUR for the installed capacity and incentive cost, respectively.

In 2012, the Italian government revised the energy bill again and significantly decreased the FiT price. Finally, on the 7th of July 2013, the assigned annual incentive budget of 6,700 MEUR was reached thus leading to the removal the FiT [32].

## Germany

In 2010, Germany was the world's largest market for PVs with approximately 17.3 GW of installed capacity [119]. The growth was directly related to the so called renewable energy sources act in 2000 that introduced the FiT mechanism [74]. The act restored a secure climate for investment as it guaranteed a fixed price for PV-generated electricity for a period of 20 years. In other words, it provided long-term financial security for investors and made the PV technology economically viable [104].

The German FiT mechanism for solar PV power is regarded by many as a highly effective and widely copied policy instrument that led to a significant diffusion and development of PV technology [52]. Since its implementation in 2000, the installed capacities of renewable energy technologies increased remarkably, by more than eightfold between 2000 and 2015 [7].

The initial plan was to review the FiT scheme every year to take into account technological and price developments [50]. For example, the amending law of 2004 stated that the FiT price for PV and other renewable technologies should be increased to reflect the cost situation of the technologies [98]. Then the modification of the renewable act in 2009 established an increase in the reduction of FiT from 5% to 10% [104].

The renewable act was further amended in 2012 and decided to reduce FiT by 1% per month, and set a 52 GW PV capacity threshold [74]. Finally, the German government moved away from the FiT approach in 2014, and introduced pilot auctions for solar energy [75].

## 6.3 Proposed Model

This section presents the proposed dynamic model. The objective of the model is to simulate and [match](#) long-term variation of indices such as the number of solar PV installations and solar PV generation capacity. This model properly accounts for the

dynamic coupling between different variables of the system, for example, between the FIT price and the number of PV installations.

The remainder of this section describes the mathematical formulation of the proposed solar PV energy policy model. For clarity, the description of all variables is given in Table A.4 of Appendix A.3.

## PV Installation Costs

In this chapter, we use the *learning-by-doing* concept to model solar PV system costs [125]. It is well-known that as the cumulative output of a product increases, its cost decreases due to gained experience. For example, the learnings earned from the solar PV panel unit production process accumulate and, over time, lead to a cheaper production of future units.

In mathematical terms, this can be expressed as follows [79]:

$$\vartheta(t) = \vartheta_o \cdot \left( \frac{\Phi(t)}{\Phi_o} \right)^{-\beta}, \quad (6.1)$$

where  $\vartheta(t)$  is the cost of installing a MW unit (EUR/MW);  $\vartheta_o$  is the initial cost at  $t = 0$ ;  $\Phi_o$  and  $\Phi(t)$  are the initial and cumulative MW installed to the system, respectively; and  $\beta$  is the learning parameter. Equation (6.1) means that production costs will decrease exponentially and tend to zero in the long run [119].

The rate of the cost reduction can be quantified by referring to the learning rate (expressed as a percentage), which is calculated as follows:

$$L_R = 1 - 2^{-\beta}. \quad (6.2)$$

For example, a value of  $\beta = 0.322$  means that doubling solar PV installations will lead to approximately a 20% reduction to the PV panel production cost.

## Cumulative PV Installations

This study assumes that three main factors decide the number of PV installations, namely FIT budget, PV cost and willingness of the people to install PVs. The factors represent economic indicators that motivate people to install solar PVs. Note that these are common

assumptions made in the literature as it is shown in practice that *the national or regional installation of solar PV systems depends on factors such as solar PV cost, FIT price, and the installation subsidies provided* [53].

In this context, the cumulative PV installations are calculated through the following differential equation:

$$T_{\Phi} \cdot \dot{\Phi}(t) = \frac{w(t) \cdot \varepsilon(t)}{\vartheta(t)}, \quad (6.3)$$

$\varepsilon$  represents the cumulative revenue of the FIT scheme (EUR) (see Eq. (6.10) below); and  $w(t)$  represents the willingness of people to install PVs (see Eq. (6.6)). It is worth noticing that Eq. (6.3) allows relating FIT policy parameters (e.g., FIT price through  $w(t)$ , see Eq. (6.6) below) to actual PV deployment (i.e.,  $\Phi(t)$ ).

## Feed-in Tariff Price Dynamics

The evolution of the FIT price is described by the following equation:

$$\Theta(t) = \phi(t - \tau), \quad (6.4)$$

where  $\Theta(t)$  represents the FIT price (equal to the delayed value of  $\phi(t)$ );  $\tau$  is a time delay that models the time that has elapsed when the FIT starts decreasing; and  $\phi(t)$  is a proper decreasing function, defined as follows:

$$T_{\phi} \cdot \dot{\phi}(t) = \phi(t - \tau) - \phi_o, \quad (6.5)$$

with  $T_{\phi}$  being its time constant and  $\phi_o$  representing an input disturbance. To model the decrease of the FIT price by the governments over time, we assume that the value of  $\phi_o$  is 20% greater than the initial value of  $\phi(t)$ , say  $\phi(t_0)$ . Therefore, there will be a negative balance in Eq. (6.5) which means that  $\phi(t)$  will start decreasing after a time that is equal to the delay  $\tau$ . Note that in practice, the governments cannot decrease the FIT price indefinitely. Hence, in order to prevent that Eq. (6.5) becomes lower than a certain minimum value, we implement a limit on the value of  $\Theta(t)$  and  $\phi(t)$ , respectively (see Eqs. (A.4)-(A.5) in Appendix A.3).

## Willingness of People to Install PVs

People's willingness is a crucial factor to increase the solar PV capacity [53, 81]. It is well-known that people are more willing to do something if the incentive is high. For this reason, in this chapter, we assume that the willingness of people to install PVs is proportional to the FiT price, as follows:

$$w(t) = \frac{\Theta(t)}{\Theta_o}, \quad (6.6)$$

where  $\Theta_o$  is the initial FiT price. Thus, the model assumes that people's behavior to install PVs follows a strategy that is based on pure economic return [53]. Furthermore, it is assumed that when  $\Theta$  hits the lower limit, say  $\Theta^{\min}$ ,  $w(t)$  will still decrease. This implies that even though the FiT price is constant, people's willingness will continue to decrease since the FiT price is too low.

The assumption that the willingness of people to install PVs is proportional to the FiT price (Eq. (6.6)) is widely accepted in the literature [53].

## Contribution of Solar PV in the Energy Mix

The contribution of solar PVs in the energy mix is modeled through the following algebraic equation [104]:

$$\varphi_{pv}(t) = \Phi(t) \cdot I \cdot P_R, \quad (6.7)$$

where  $\varphi_{pv}(t)$  represents the energy produced by PV generation (MWh);  $\Phi$  represents the number of PV plants/MW installed in the system (in this chapter, we assume 1 PV plant = 1 MW);  $I$  is the reference PV yield (MWh/MW) e.g. in a year;  $P_R$  is the performance ratio (e.g. 85%).

In general, it is useful to estimate the cumulative solar PV generation. With this aim, the following differential equation is introduced:

$$T_v \cdot \dot{v}_{pv}(t) = \Phi(t) \cdot I \cdot P_R, \quad (6.8)$$

where  $v_{pv}$  represents the cumulative PV generation and  $T_v$  represents its time constant.

## Cumulative Expenses to Support Solar PV Generation

As mentioned above, under the FiT program, investors are paid using a fixed price ( $\Theta$ ) for the electricity generated and fed into the grid from the solar power plant. The cumulative expenses to support solar PV generation can be [calculated](#) using the following differential equation [98]:

$$T_\chi \cdot \dot{\chi}(t) = \Theta(t) \cdot \varphi_{pv}(t), \quad (6.9)$$

where  $\chi$  represents the cumulative expenses to support the solar PV production and  $T_\chi$  represents its time constant.

## Cumulative Revenue of the FiT Fund

Incentives such as FiT are generally paid by the consumers through a surcharge on the electricity bill [7]. In this context, the cumulative revenue of the FiT fund can be modeled through the following differential equation [98]:

$$T_\varepsilon \cdot \dot{\varepsilon}(t) = \rho \cdot L_P \cdot E_C \cdot u, \quad (6.10)$$

where  $T_\varepsilon$  represents the time constant of  $\varepsilon(t)$ ;  $\rho$  represents the electricity price;  $L_P$  is the constant levy given as a percentage of the electricity price;  $E_C$  is the total energy consumption (assumed constant in this chapter unless stated otherwise); and  $u = 1$  if:

$$\varepsilon(t) > \chi(t), \forall t, \quad (6.11)$$

holds. Otherwise  $u = 0$ . Equation (6.11) represents the viability condition of the FiT scheme [98]. In other words, the condition for the FiT viability is that the cumulative revenue of the FiT fund ( $\varepsilon(t)$ ) should be greater at any time than the cumulative expenses ( $\chi(t)$ ).

## Variable Limits

In practice, there are limits on certain variables of the system. For example, the FiT budget is not infinite, or the FiT price cannot decrease indefinitely. Appendix A.3 presents the implementation of the limiters for the variables of the proposed model.

## 6.4 Model Validation

The accuracy of the model is validated based on two of the most important PV markets in Europe and globally, namely Italy for the period 2008-2014 and Germany for the period 2000-2014. With this aim, simulation results produced with the proposed model are compared against historical data. Six key and highly uncertain variables of the model are selected for illustration. These are: (1) cumulative PV capacity; (2) cumulative PV generation; (3) PV cost; (4) cumulative FiT budget; (5) FiT price; and (6) people's willingness.

For completeness and reproducibility of the results, the input data of the model are given in Appendix A. In particular, the parameter values and historical data are given in Tables A.5-A.6 for Italy, and in Tables A.7-A.8 for Germany. It is relevant to note that some of the parameters can be obtained by conducting surveys [15].

### Solar PV Development in Italy 2008-2014

Figures 6.1-6.5 compare the historical PV installed capacity, generation, fund, costs, and FiT price values with their respective simulated values, while Fig. 6.6 shows the evolution of the willingness of the people.

Results indicate that, if the parameters are properly chosen, the model can accurately reproduce the historical data. In particular, the model is able to **match** the relatively slow response of the installed PV capacity to the policy during the first years (see Fig. 6.1). This slow response implies that during the first years there is a high inertia mainly due to high initial PV costs (Fig. 6.4), even though the willingness of the people to install PV is high (Fig. 6.6). Note that the current model does not account for other factors that may impact the PV installation in the first years, e.g. such as large development times and/or administrative procedures.

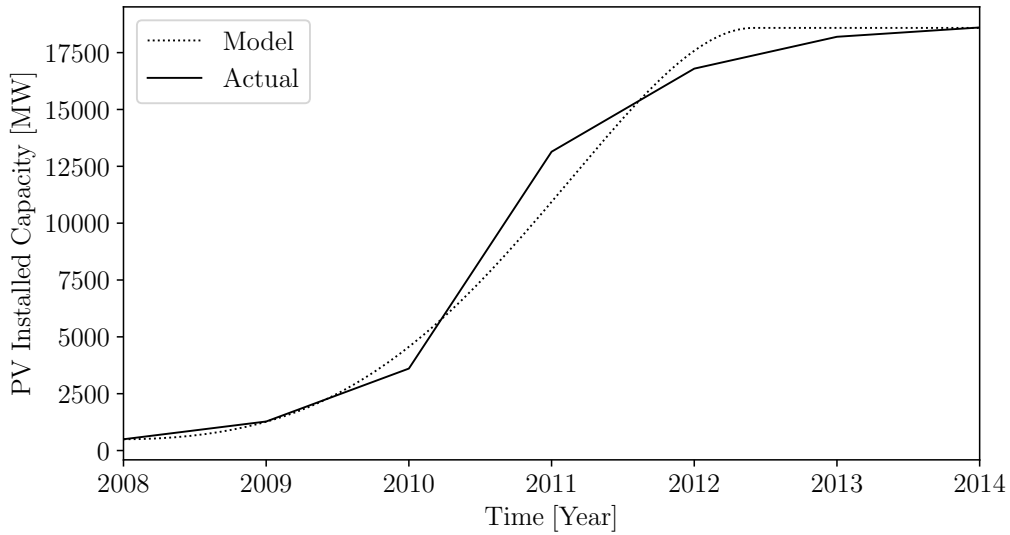


Figure 6.1: Italian case: Cumulative solar PV installations.

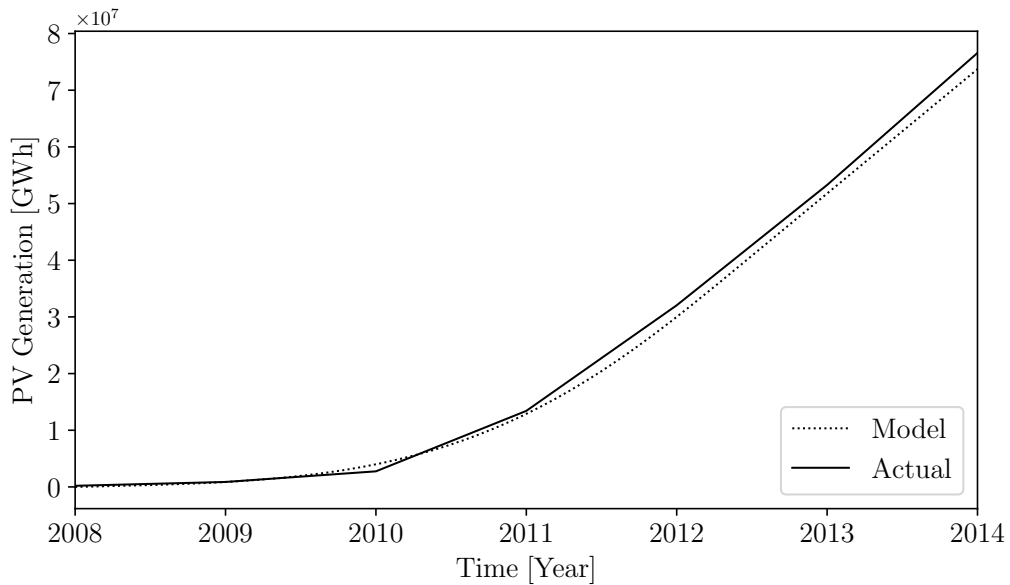


Figure 6.2: Italian case: Cumulative solar PV generation.

It is also worth observing that the model almost perfectly matches the cumulative solar PV generation over the years (Fig. 6.2) and forecasts reasonably well the FIT fund (Fig. 6.3). Furthermore, the validation of the learning-by-doing model against real data from the Italian market (Eq. (6.1)) is shown in Fig. 6.4. In particular, it can be observed that in the first few years the model underestimates the cost reductions, while in the last two years the model overestimates the PV costs (Fig. 6.4). However, it appears that these differences in the cost do not significantly impact the PV installed capacity (Fig. 6.1).

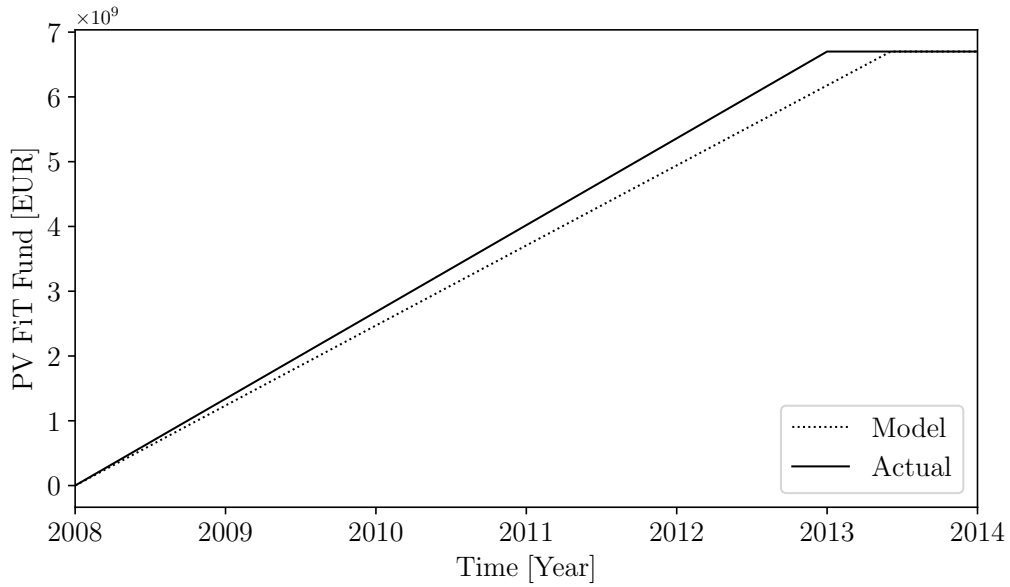


Figure 6.3: Italian case: Cumulative FiT fund.

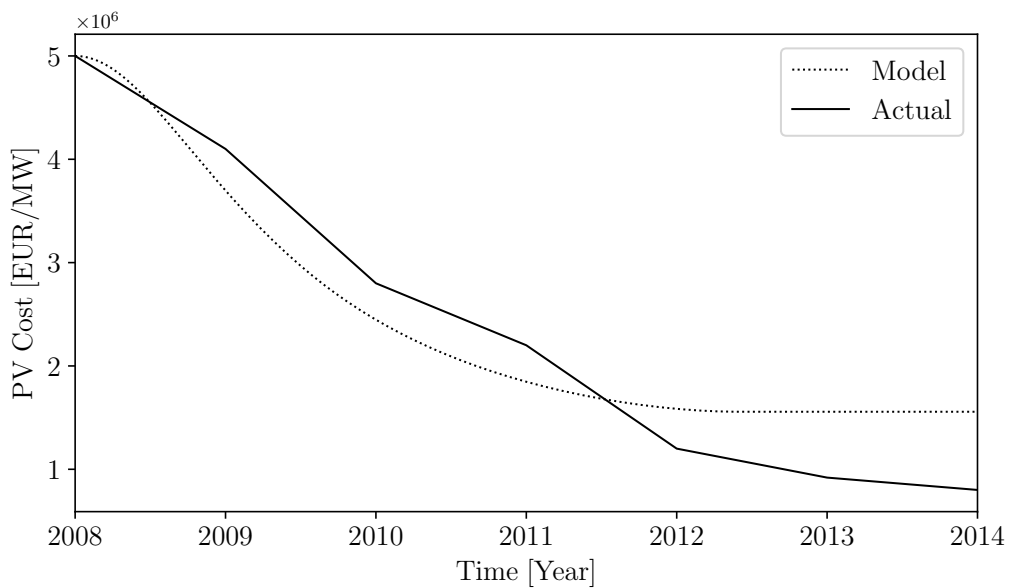


Figure 6.4: Italian case: Solar PV cost.

With regard to the FiT price, Fig. 6.5 shows that the model forecasts very well its evolution in the considered period of analysis. Therefore, the use of Eq. (6.4) appears to be useful in [reproducing](#) the change of FiT price over time. The willingness of the people to install solar PVs is shown in Fig. 6.6. As expected, evolution of the willingness is proportional to the FiT price (Fig. 6.5). However, it is interesting to note that people's willingness reaches the limit ( $210^{-5}$  considered in this chapter) at around 2012 when the

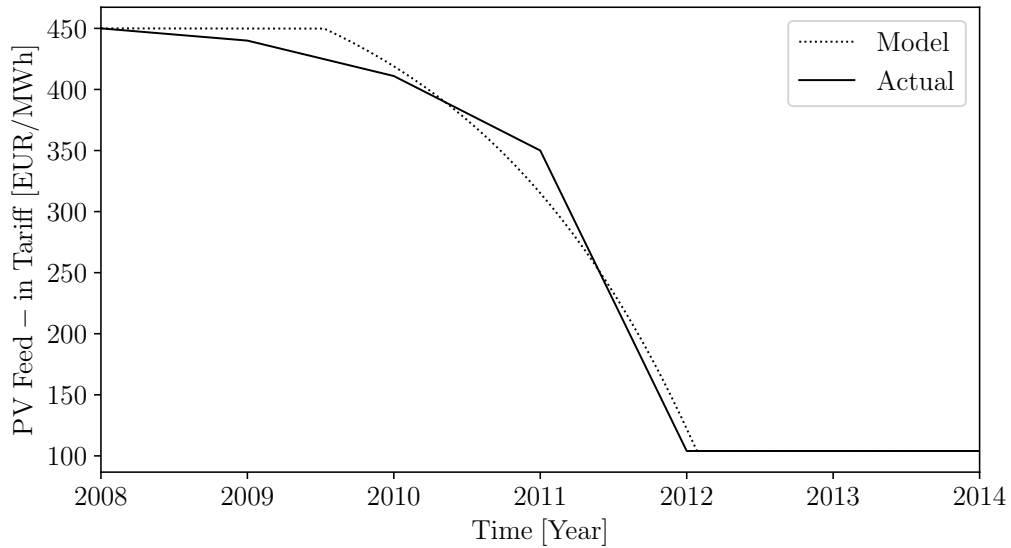


Figure 6.5: Italian case: Solar PV FiT price.

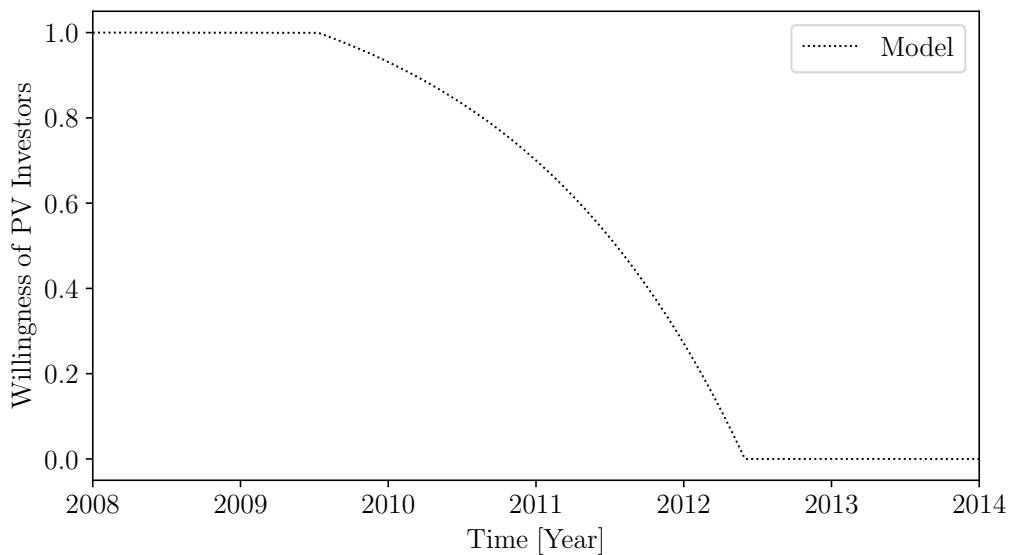


Figure 6.6: Italian case: Willingness of people to install solar PVs.

FiT price was fixed and the lowest of the policy. These results explain the small increase of the solar PV installations after 2013 (see Fig. 6.1). Thus, keeping high FiT prices is crucial to increase the willingness of people to install PVs.

## Solar PV Development in Germany 2000-2014

This second example validates the model against historical data of the solar PV systems in Germany in the period 2000-2014. This is needed to check if the model is general

enough to [match](#) different PV markets. With this aim, and similar to the Italian case, Figs. 6.7-6.11 show the comparison between historical values and simulated ones. Moreover, Fig. 6.12 shows the evolution of the willingness of the people to install PVs. In general,

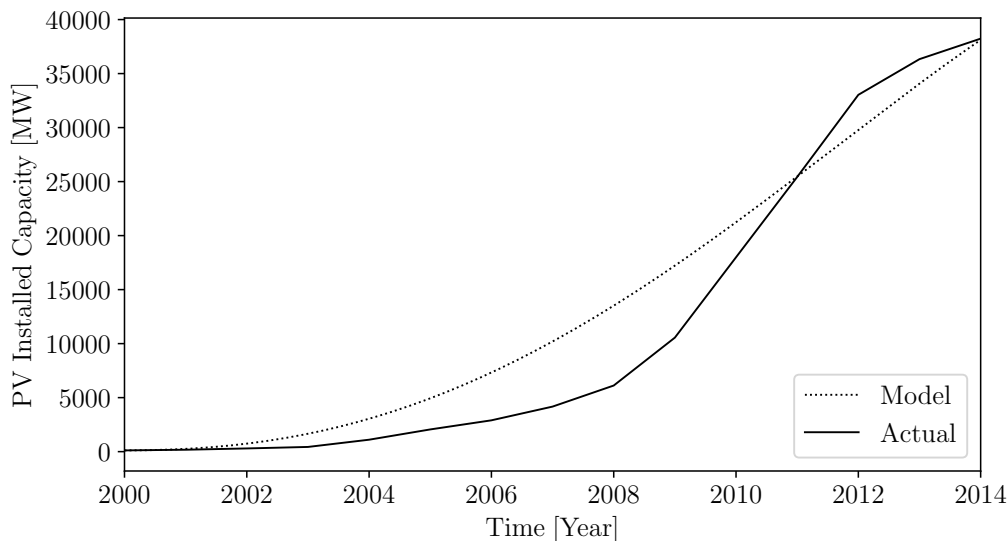


Figure 6.7: German case: Cumulative solar PV installed.

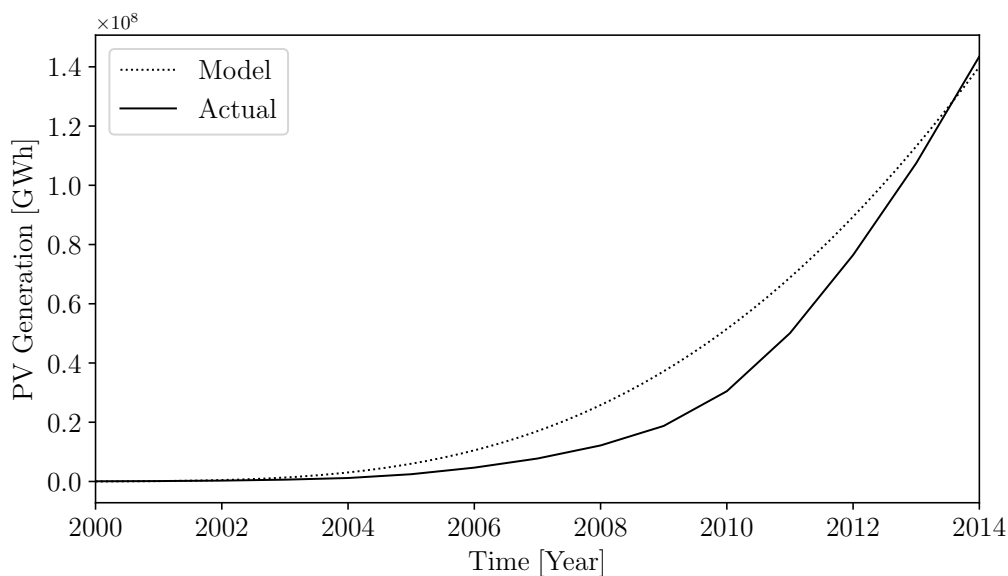


Figure 6.8: German case: Cumulative solar PV generation.

the proposed model is able to [match](#) the development of the PV market in Germany between 2000-2014. However, compared to the Italian case, the differences between historical and simulated values are slightly more evident. Specifically, while the model is able to accurately reproduce the historical data of the PV installations (Fig. 6.7) and

generation (Fig. 6.8), PV costs (Fig. 6.9), FiT budget (Fig. 6.10) and FiT price (Fig. 6.11) are [calculated](#) with less accuracy. The main reason for these deviations is that several

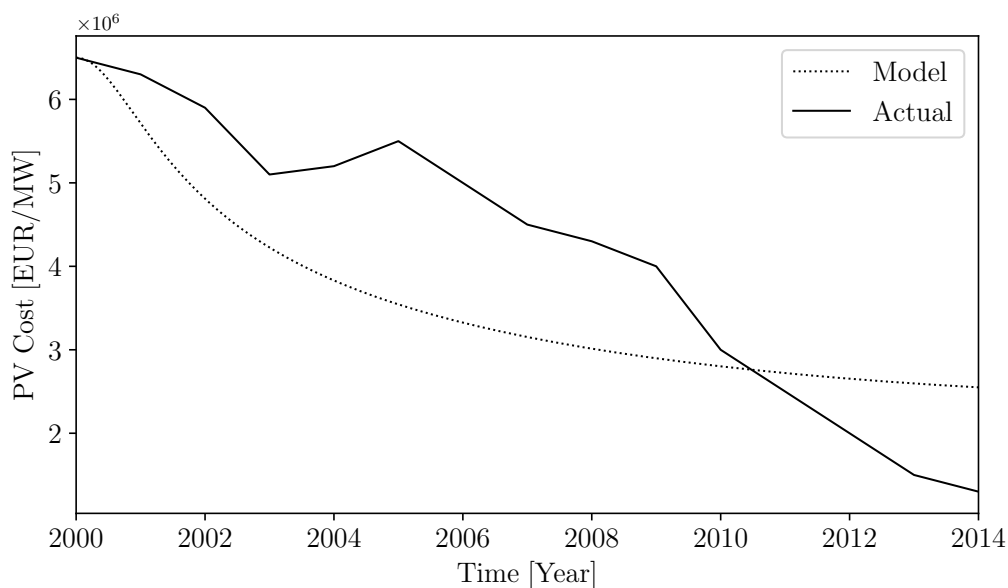


Figure 6.9: German case: Solar PV cost.

parameters, e.g. the electricity price  $\rho$  and the levy constant  $LP$ , are time-dependent and change significantly over the years. This is however unpredictable and cannot be properly modelled *a priori*. For example, at the beginning, the electricity price  $\rho$  and the levy constant were small [7]. The government then realised that to incentivize the PV market further, they needed to increase the burden on the consumer electricity bill. As a result, the FiT budget does not increase linearly, as [calculated](#) by the proposed model (see Fig. 6.10). It is relevant to note, however, that while the proposed model cannot anticipate the changes in the policy, it provides a tool to estimate what happens if some of the parameters are varied. This feature is discussed in detail in Section 6.5. Fig. 6.12 shows the evolution of the willingness of the public to install PV panels. While the willingness has generally the same trend as the FiT price (Fig. 6.11), its behavior changes when it reaches its lowest value. Specifically, Fig. 6.12 shows that at the end of the period of analysis (i.e. the year 2014), the willingness has a value of more than 0.4. This value is significantly higher compared to that obtained in Italy ( $210^{-5}$ ). This means that, compared to Italy, the willingness of people in Germany was relatively high. These results can explain the development of solar PV installations in Germany, where there is

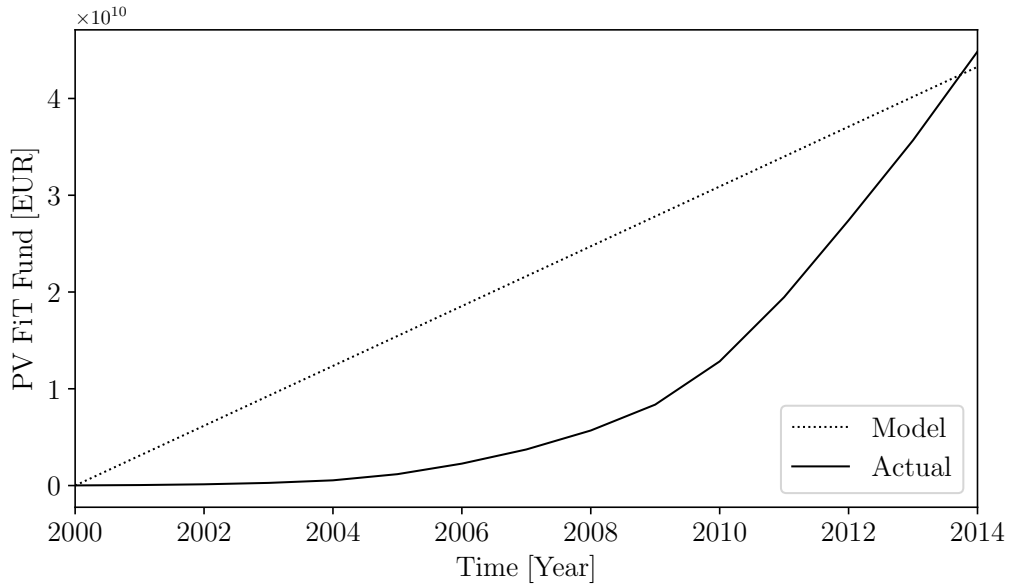


Figure 6.10: German case: Cumulative FiT fund.

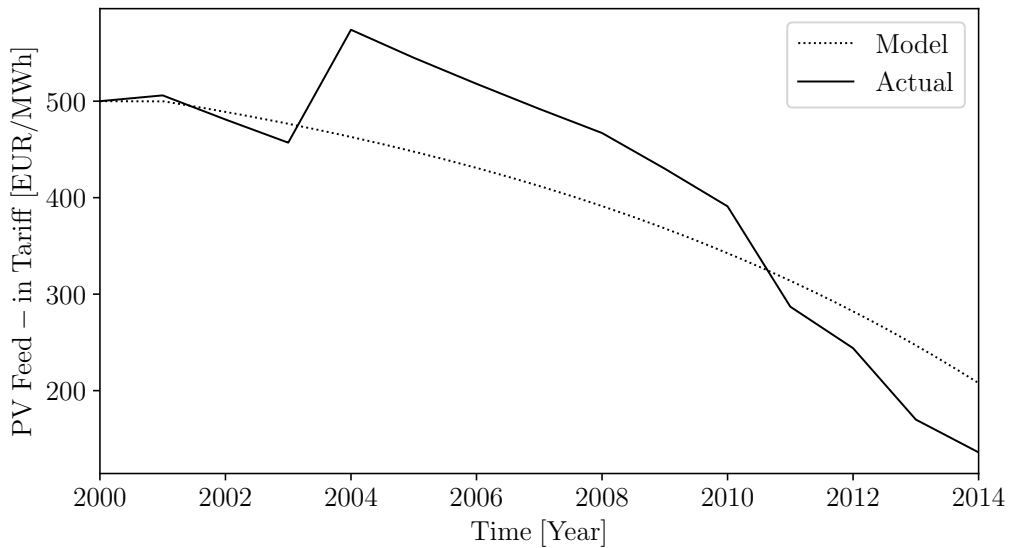


Figure 6.11: German case: Solar PV feed-in tariff price.

still a strong increase in the number of PVs installed [41]. In contrast, Italy's PV market has seen a prolonged rise in the number of PVs after 2014 [112].

While the German case has idiosyncrasies that cannot be fully captured, the proposed model is still able to give the correct trend in all cases. Therefore, it is fair to say that, overall, the proposed model passes the validation test.

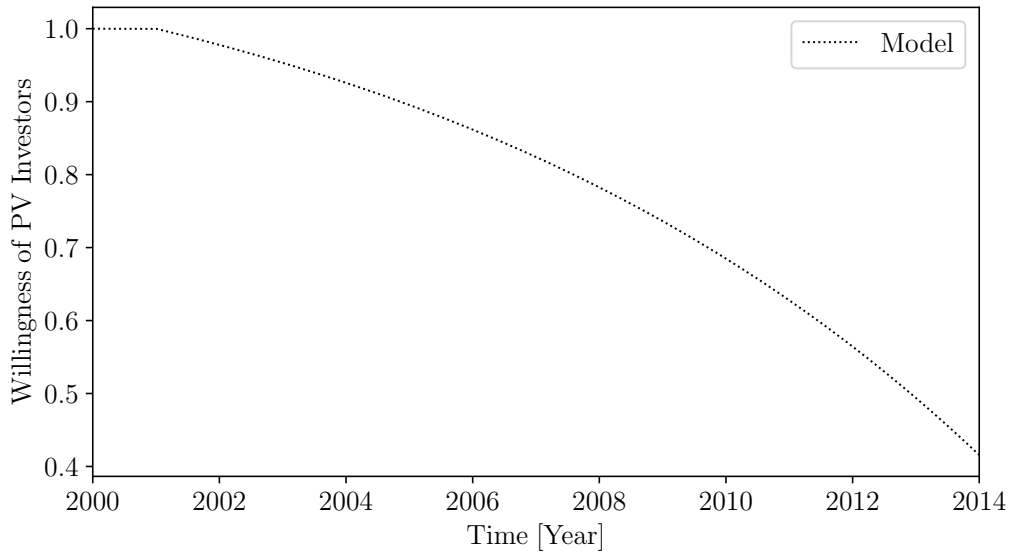


Figure 6.12: German case: Willingness of people to install solar PVs.

## 6.5 Sensitivity Analysis

This section presents a sensitivity analysis of the model using the Italian case for the period 2008-2014. [Using adequate parameters is, in fact, crucial to accurately reproduce the historical PV data \[98\].](#) Unless stated otherwise, for all scenarios, we show two variables of the system, namely the cumulative solar PV capacity and generation.

### Effect of Different Cost Modelling

This section compares different PV cost modelling and their impact on the PV capacity and generation. As discussed in Section 6.3, we have proposed the utilization of the learning-by-doing model, which is based on Eq. (6.1). While this model is heuristic, we show in this section that it is actually quite accurate. For illustration, we compare the proposed learning-by-doing and a simple linear cost modelling and show their effect on the evolution of the PV capacity and generation.

Figures 6.13-6.14 show the evolution of the PV capacity and generation during the period 2008-2014 for different PV cost modelling. The learning-by-doing approach leads to a better forecast compared to the linear one, i.e. the linear cost modelling leads to an underestimate of the PV capacity. These results support the utilization of Eq. (6.1).

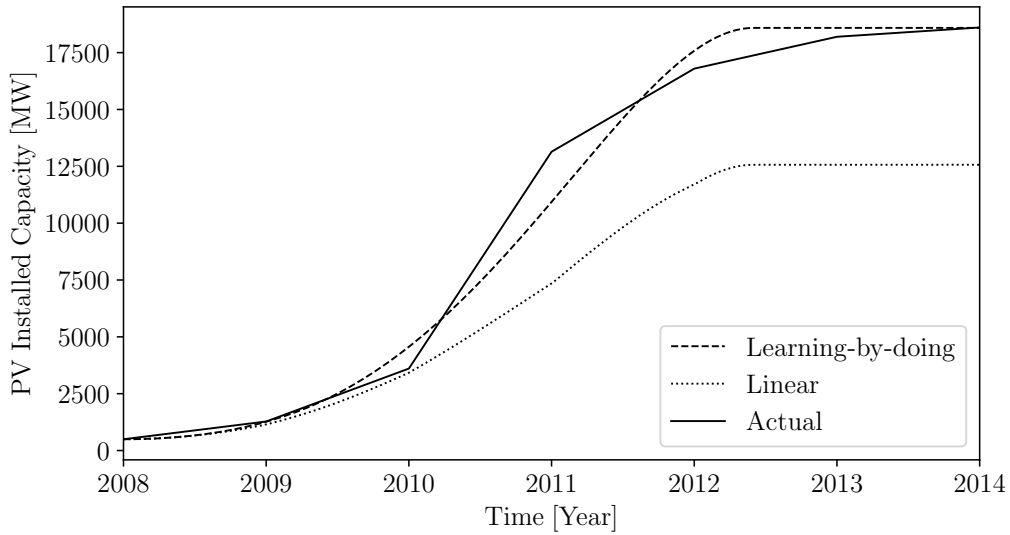


Figure 6.13: Italian case: Cumulative solar PV installed.

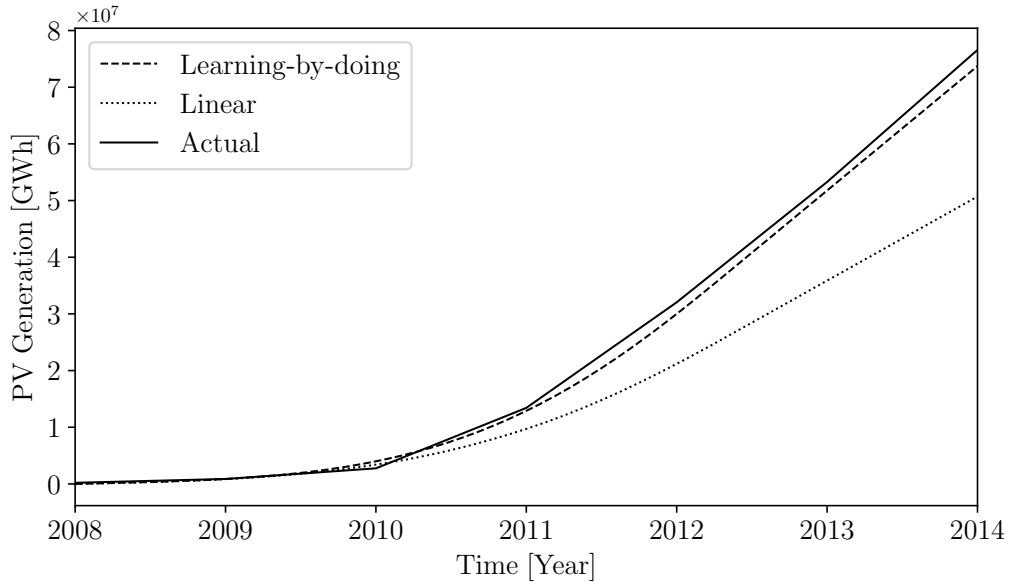


Figure 6.14: Italian case: Cumulative solar PV generation.

### Effect of $\beta$

In this section, we compare the effect of different learning coefficients  $\beta$  in the evolution of the PV technology. Such analysis is relevant because the value of the parameter  $\beta$  is not always obvious [36]. For example, different values of  $\beta$  are indicated for Germany in [53] and [104]. For this reason, the sensitivity analysis is carried out using three values of  $\beta$ , namely, 0.2, 0.322, and 0.4 [104].

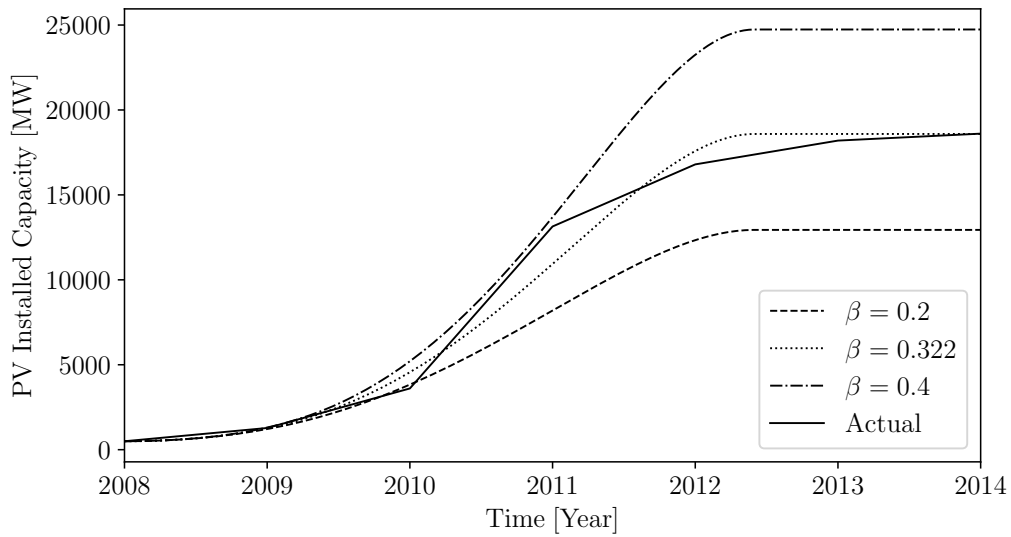


Figure 6.15: Italian case: Cumulative solar PV installed.

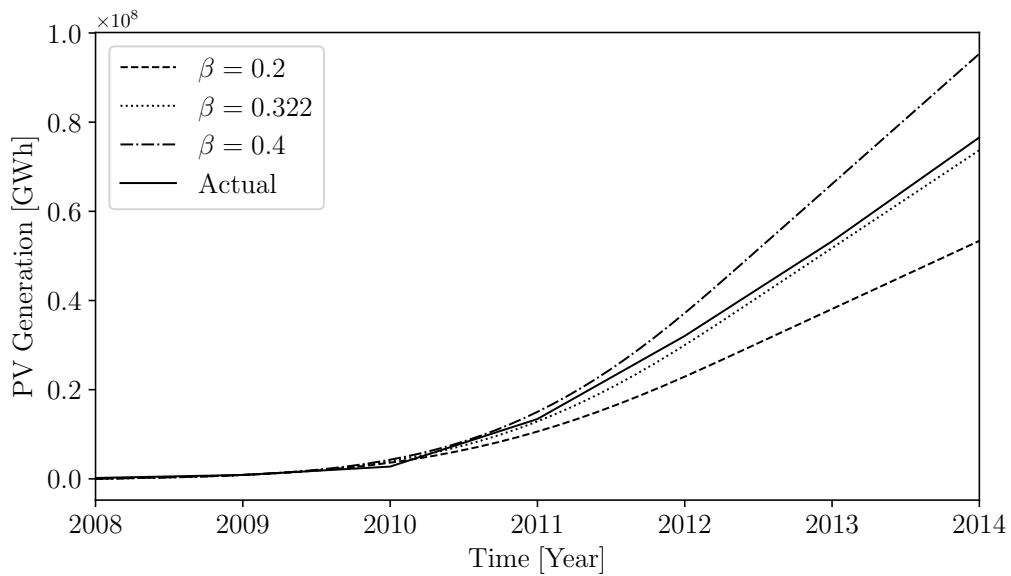


Figure 6.16: Italian case: Cumulative solar PV generation.

Figures 6.15-6.16 show that results are sensitive to the value of the learning parameter  $\beta$ . Moreover, it can be seen that larger values of  $\beta$  lead to higher PV installed capacity and generation. This was to be expected. Larger values of  $\beta$  mean a higher accumulation of experience as well as a faster decrease of the PV system costs.

## Effect of Load Consumption

Another relevant but uncertain parameter of the model is the load power consumption. Three scenarios are assumed namely 1% consumption increase per year, constant load consumption, and 1% decrease per year. The results of the sensitivity analysis are shown in Figs. 6.17-6.18. These figures show that different levels of load power consumption

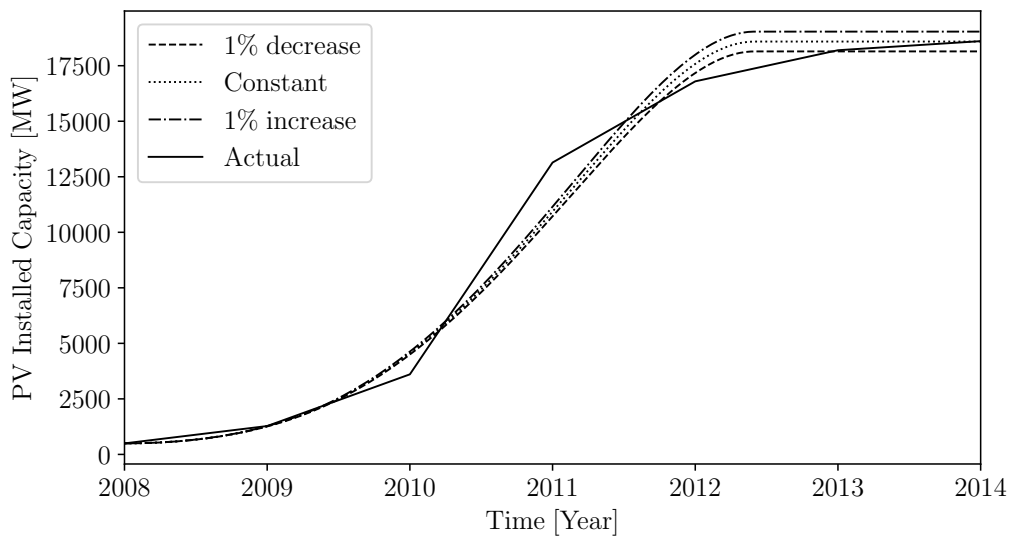


Figure 6.17: Italian case: Cumulative solar PV installed.

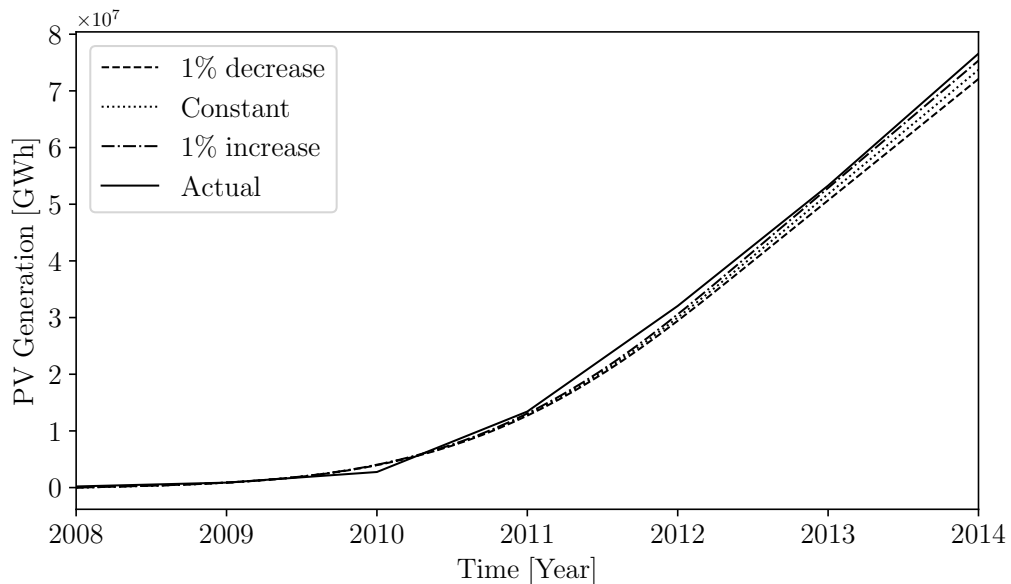


Figure 6.18: Italian case: Cumulative solar PV generation.

lead to similar trends in the evolution of PV capacity. It appears, thus, that the load

power consumption is not a highly sensitive parameter of the model. However, it is worth observing that the higher the load consumption, the bigger the increase of the PV capacity and generation. In other words, the increase of  $E_C$  impacts positively on the development of the PV market.

## Effect of Levy

In this section, we perform a sensitivity analysis with respect to different levy constant values  $LP$ . This parameter defines the level of financial support from the governments to support the development of different energy technologies (see Eq. (6.10)). It has been observed that over time this parameter changes significantly (i.e. very uncertain) [7]. With this aim, three scenarios are considered, namely  $LP = 10\%$ ,  $LP = 15\%$ , and  $LP = 20\%$ , respectively. These values are realistic and are consistent with what happened in Italy [101].

Figures 6.19-6.20 show that the levy constant is a highly sensitive parameter. This was to

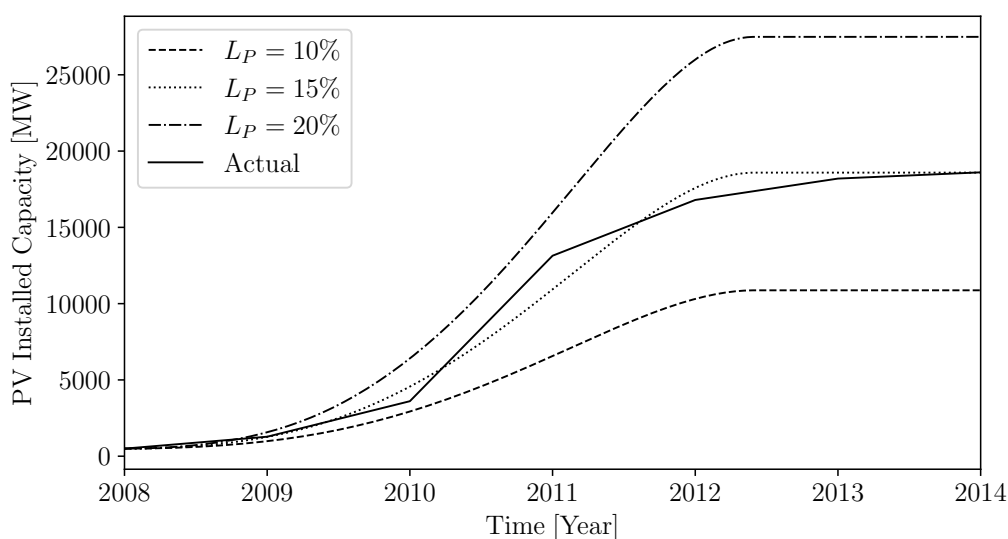


Figure 6.19: Italian case: Cumulative solar PV installed.

be expected as this parameter defines the amount of money (budget) that the government puts in place to support the PV technology. These results confirm the previous conclusion that government financial support is crucial for successfully integrating and fostering the solar PV market.

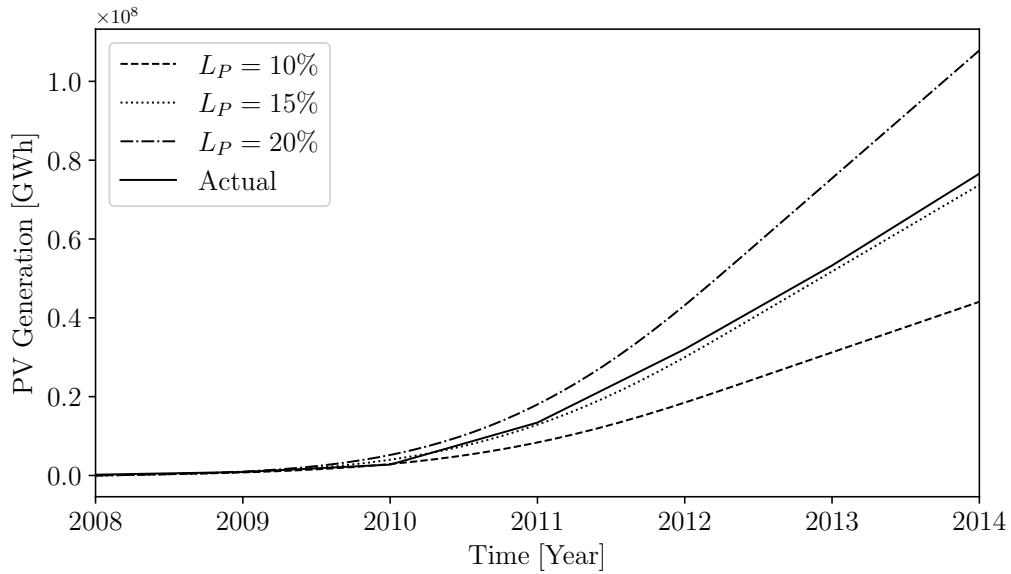


Figure 6.20: Italian case: Cumulative solar PV generation.

### Effect of the Electricity Price

This section discusses the impact of the electricity price  $\rho$  on the evolution of the PV market. Similar to the previous sections, a sensitivity analysis is carried out considering three values of  $\rho$ , namely 100, 200, and 300 EUR/MWh, respectively. Figures 6.19-6.20

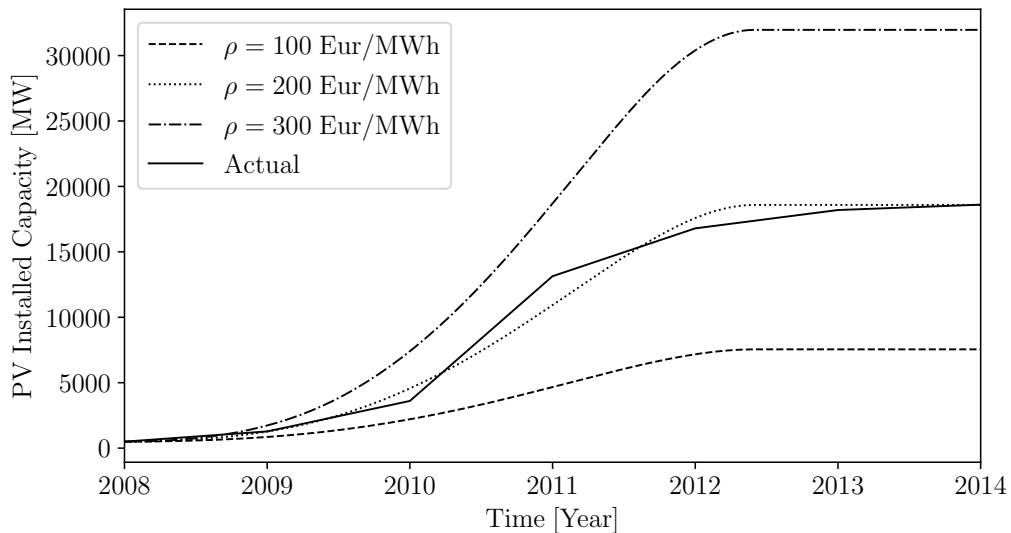


Figure 6.21: Italian case: Cumulative solar PV installed.

show that with the increase of  $\rho$  there is an increase in the solar PV installations and generation. This has also to be expected because increasing  $\rho$  means that there is more

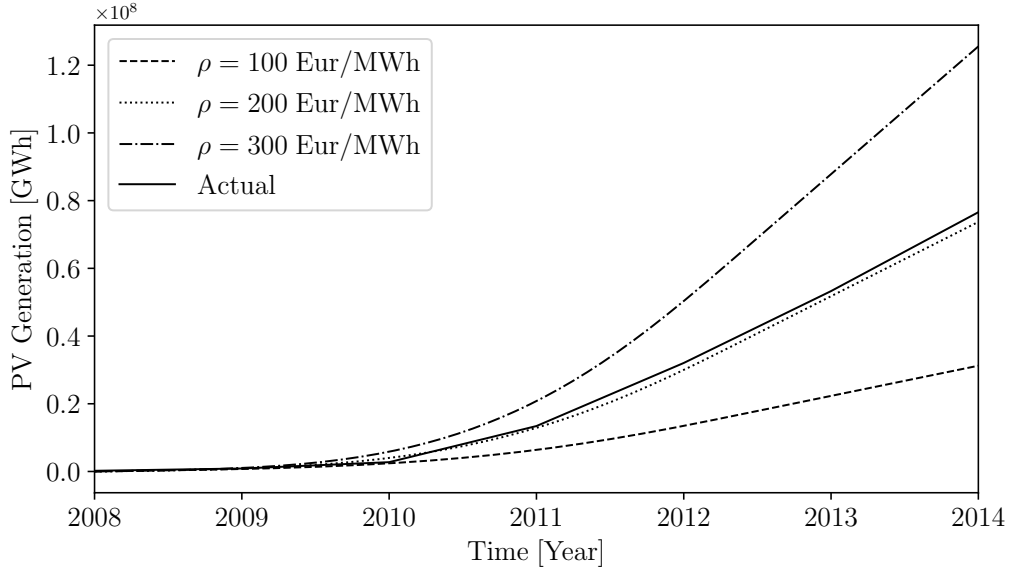


Figure 6.22: Italian case: Cumulative solar PV generation.

money to support the development of the PV market (Eq. (6.10)). It can be concluded that the electricity price  $\rho$  is a highly sensitive parameter of the model.

### Effect of $\varepsilon^{\max}$

The Italian government closed the FiT program in July 2013 when the budget limit was reached (i.e. 6,700 MEUR) [72]. It is relevant to study the impact of such a cap on the evolution of the PV market. In the proposed model, this information is given by  $\varepsilon^{\max}$ . With this aim, we vary the value of  $\varepsilon^{\max}$  and observe its impact on the PV capacity and generation. Three values are used, namely 4,700, 6,700, and 8,700 MEUR, respectively.

Figures 6.23-6.26 show the relevant results of the sensitivity analysis. Interestingly, there are no significant differences with respect to the PV installed capacity and generation. This can be explained by the fact that in 2012 the FiT price is too low (104 EUR/MWh) to incentivize people to install solar PVs (see Fig. 6.26). This negatively affects the people's willingness, which hits the lower limit considered in this work, i.e.  $210^{-5}$ , as shown in Fig. 6.6. It descends that keeping high FiT prices is vital if an energy policy is to be successful. By doing that, governments can increase the willingness of people to install solar PVs. However, high FiT rates may lead to economic instability [21]. Therefore governments should find a trade-off between compensation for investors and a reasonable burden for the energy consumers [98].

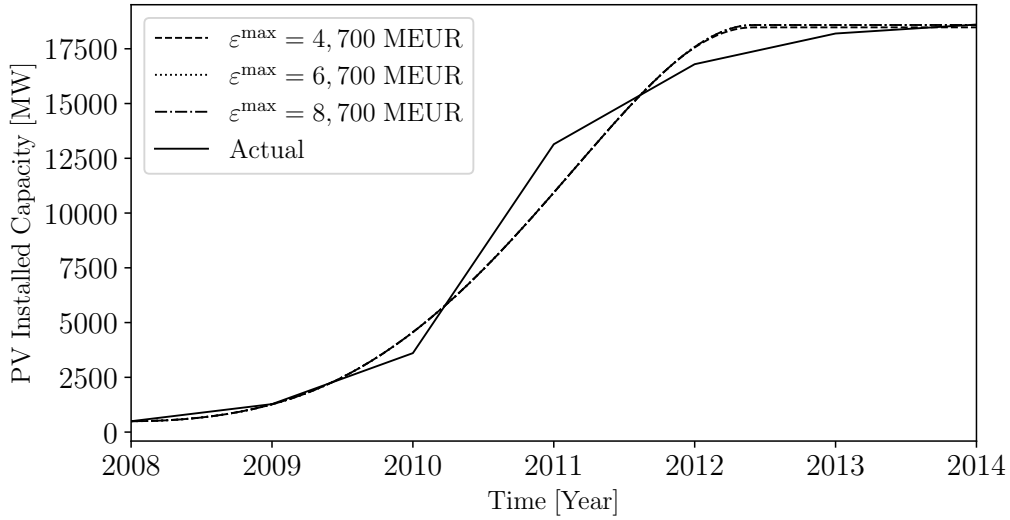


Figure 6.23: Italian case: Cumulative solar PV installed.

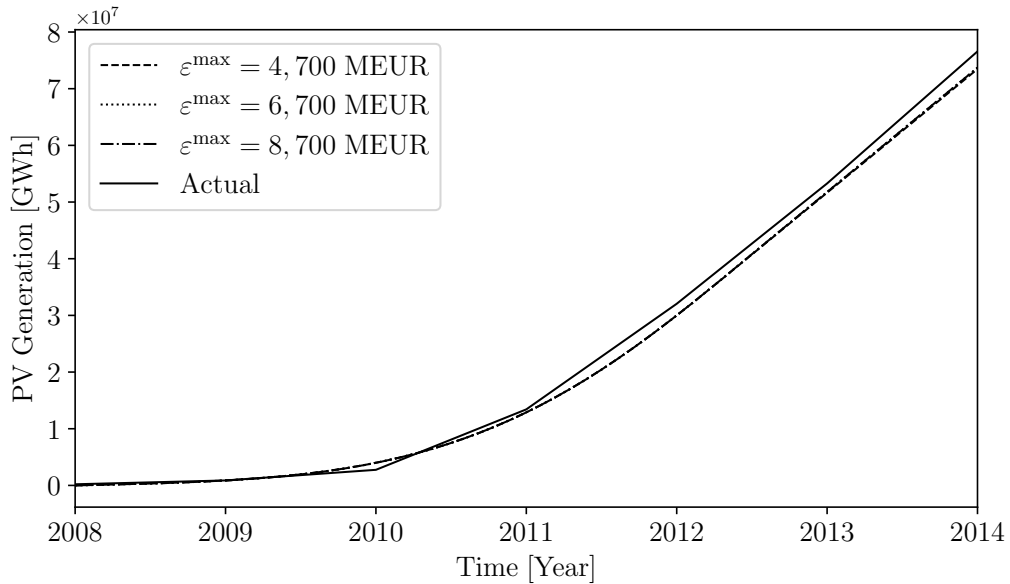


Figure 6.24: Italian case: Cumulative solar PV generation.

### Effect of $T_{\Phi}$

Since we are using a dynamic model based on differential equations, it is relevant to perform a sensitivity analysis with respect to the time constants of the main state variables of the system, namely  $T_{\Phi}$ ,  $T_{\phi}$  and  $T_{\epsilon}$ . In this first scenario, we discuss the effect of the time constant of the cumulative solar PV capacity,  $T_{\Phi}$ . Figures 6.27-6.28 plot the relevant results. It can be seen that  $T_{\Phi}$  is a highly sensitive parameter of the system and greatly impacts the number of PV installations and the cumulative PV generation. For example,

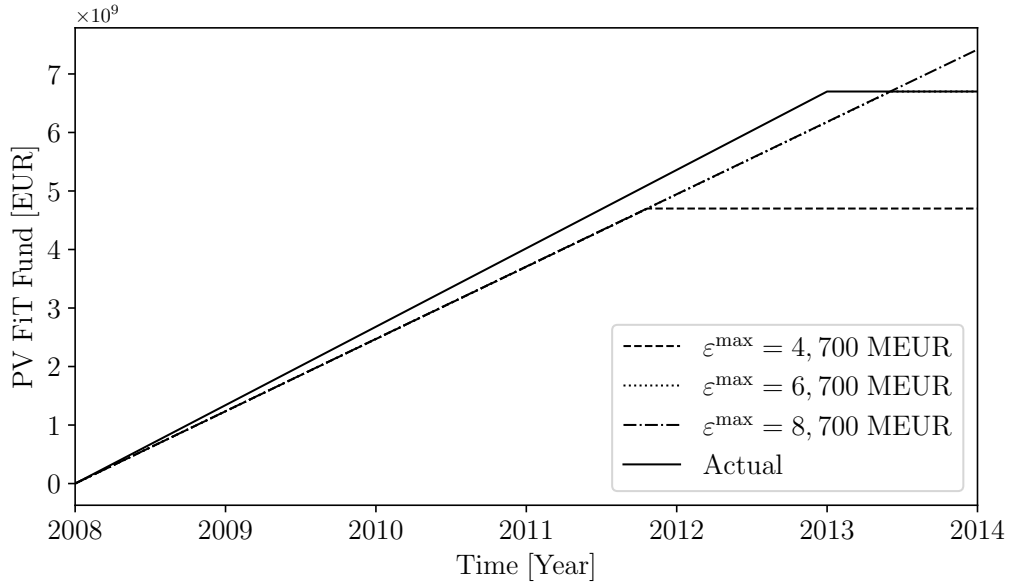


Figure 6.25: Italian case: Cumulative FiT fund.

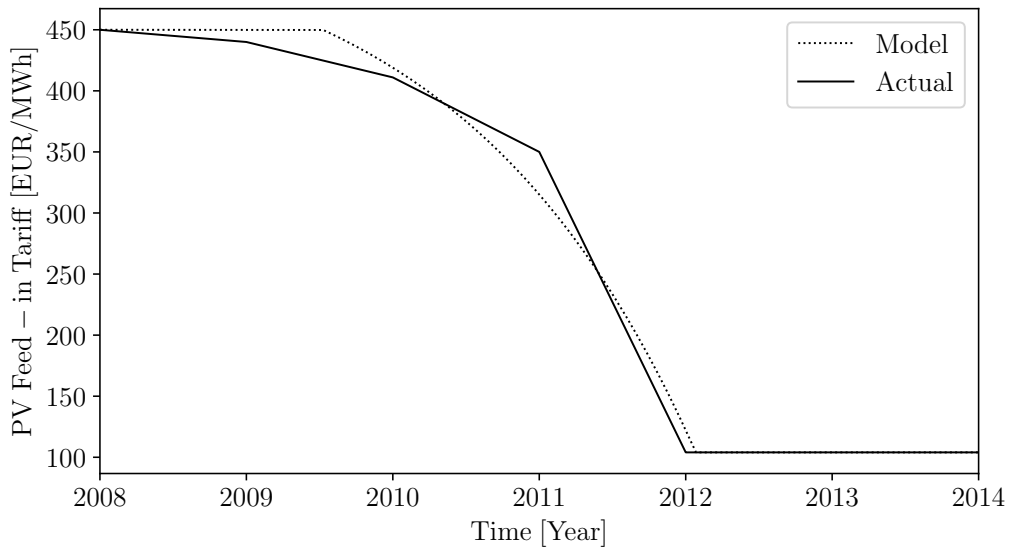


Figure 6.26: Italian case: Solar PV FiT.

decreasing  $T_\Phi$  from 70 days (which is the base case) to 46 days leads to an increase of more than 1 GW installed capacity.

### Effect of $T_\phi$

Another relevant time constant of the model is  $T_\phi$ , which defines the dynamics of the FiT price and willingness of the people (Eq. (6.5)). In this context, and similar to the previous scenario, a sensitivity analysis is performed and the relevant results are shown

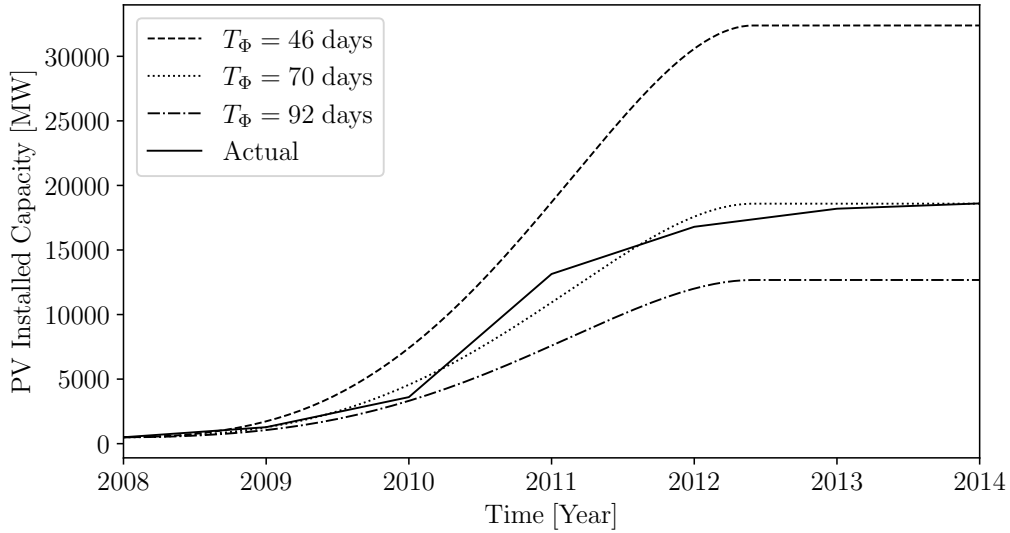


Figure 6.27: Italian case: Cumulative solar PV installed.

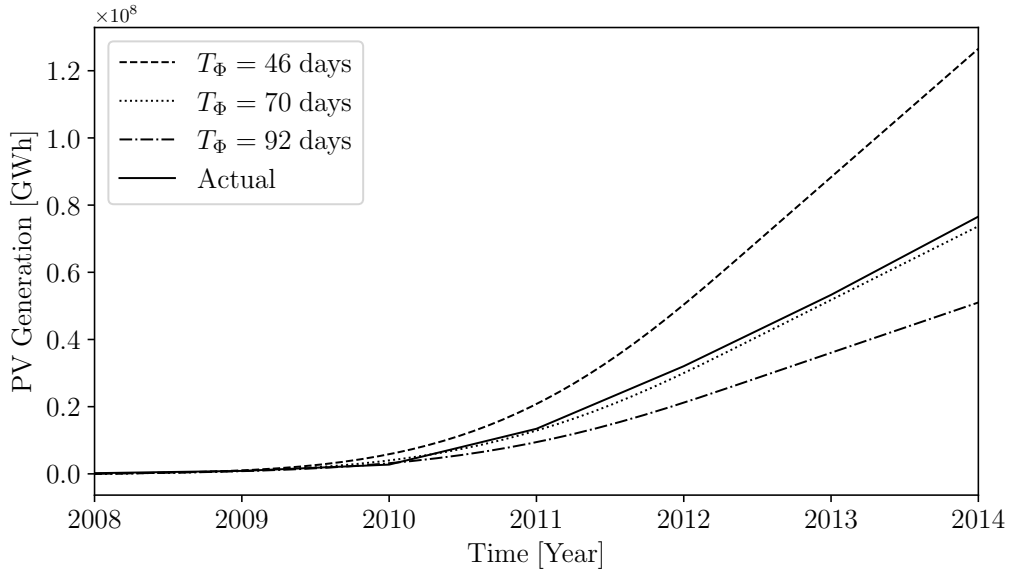


Figure 6.28: Italian case: Cumulative solar PV generation.

in Figs. 6.29-6.30. Both figures indicate that the evolution of the PV capacity and generation over the years is highly sensitive to  $T_\phi$ .

### Effect of $T_\varepsilon$

This scenario discusses the sensitivity analysis with respect to the time constant of the FiT budget,  $T_\varepsilon$  (Eq. (6.10)). Figures 6.31-6.32 show relevant results.

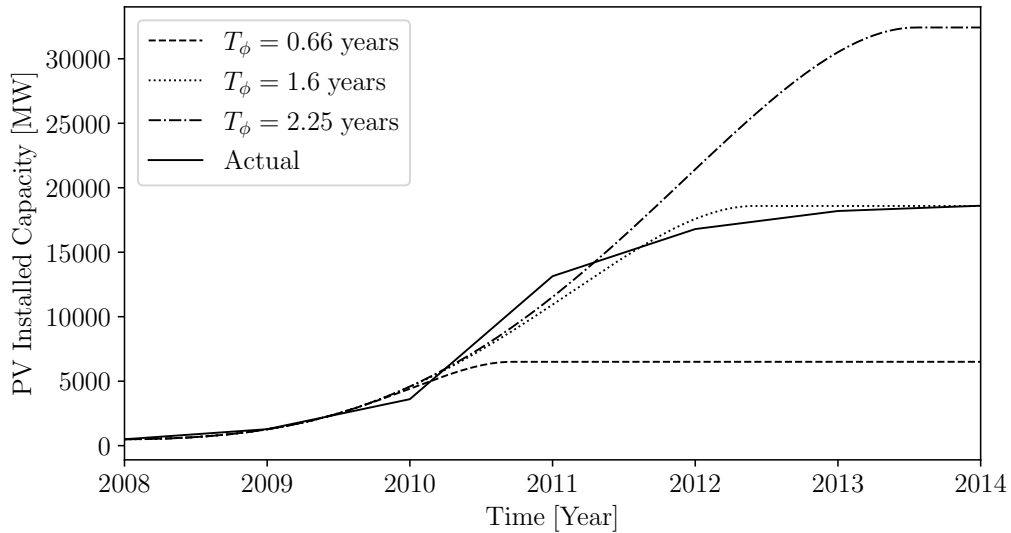


Figure 6.29: Italian case: Cumulative solar PV installed.

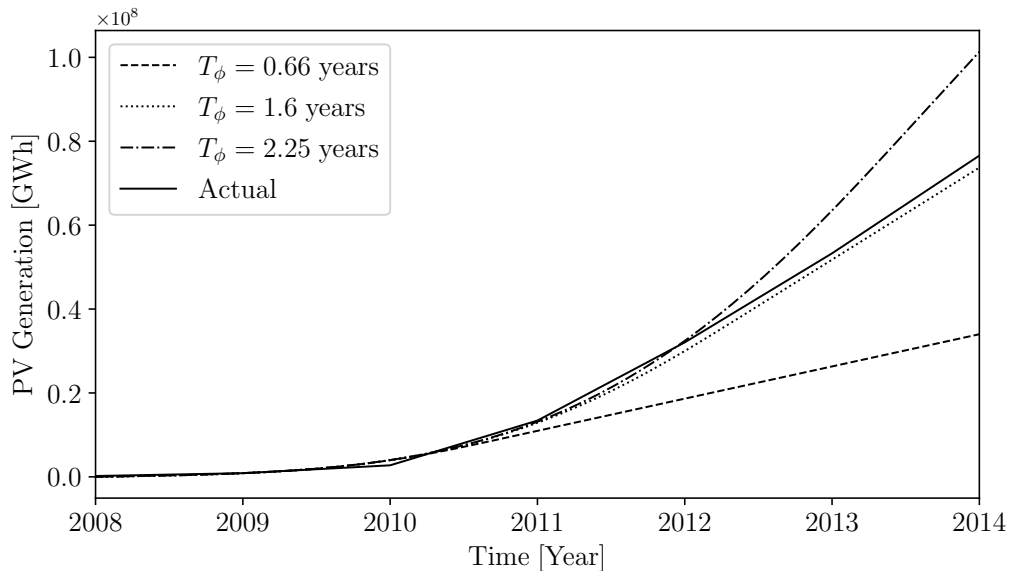


Figure 6.30: Italian case: Cumulative solar PV generation.

Decreasing the time constant  $T_\varepsilon$  from 8 hours (base case) to 3 hours leads to an increase with more than 3 GW of PV installed capacity (see Fig. 6.31).

## 6.6 Conclusions and Policy Implications

This chapter presents the last contribution of this thesis, namely a long-term dynamic model to assess energy policies promoting solar PV through FiT schemes. The proposed model appears to be general enough to reproduce with good accuracy the long-term

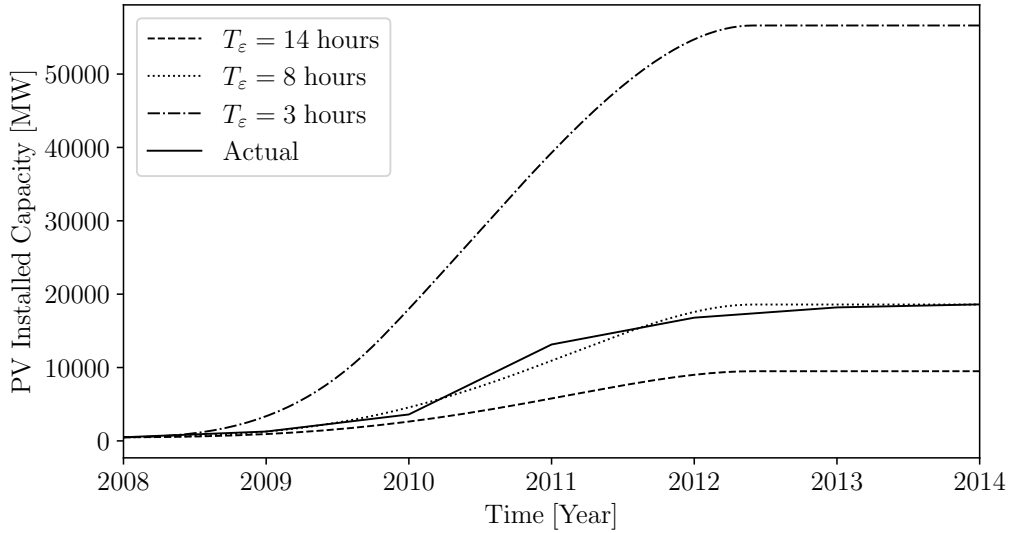


Figure 6.31: Italian case: Cumulative solar PV installed.

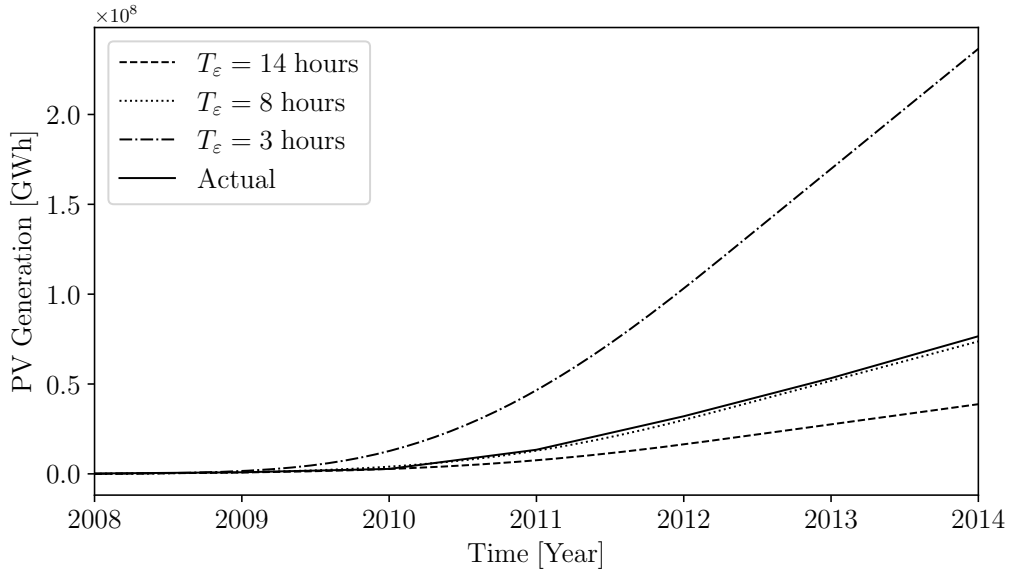


Figure 6.32: Italian case: Cumulative solar PV generation.

development of the solar PV market in both countries (see Figs. 6.1-6.12). We believe that the model is a useful tool for policy-making institutions to [study](#) the long-term behavior of an energy technology such as that of PV. The [study](#) is facilitated by the fact that one can easily implement the proposed model and reproduce the results in any of the many software packages designed to integrate a set of differential equations. This is an advantage compared to other complex methods presented in the literature that require specific software tools [48, 53, 55]. The model provides valuable information to

policymakers by relating, for example, FiT policy parameters (e.g., FiT price) to actual PV deployment.

The development of the PV markets in Italy and Germany is directly related to FiT levels. For example, low tariffs in Italy contributed to discouraging people from installing solar PVs (i.e. very low willingness). When comparing the two countries considered in this work, the model validation test showed that people in Germany had a much higher willingness (18,000 times higher than people in Italy according to this work) at the end of the period of analysis. These results support the idea that despite declining investment costs, incentive policies are still required to increase the share of alternative technologies such as solar PV [55]. This is especially the case of Italy, where the FiT scheme was replaced with other policy mechanisms [72].

The parametric sensitivity analysis of the model in Section 6.5 for the solar PV market in Italy revealed that the learning-by-doing approach is accurate enough to [match](#) the PV cost and capacity evolution. Furthermore, it is shown that the learning parameter  $\beta$ , the levy constant  $LP$ , the electricity price  $\rho$  as well as the time constants of the state variables of the system are highly sensitive parameters of the model, and as such, they have to be carefully chosen in order to obtain a realistic forecast of the PV capacity. In particular, while the first three parameters can be predicted reasonably well, that is not the case with the time constants. Specifically, one of the most critical time constant to predict is  $T_\Phi$  and subsequently, the most difficult data to fit is the cumulative solar PV capacity. Indeed, most of the time constants have to be first guessed and then tuned by trial-and-error by the user and thus can be considered a current limitation of the model. Finally, the sensitivity of the parameters of the load consumption and the system total budget do not change the effect of the incentives significantly.

# Chapter 7

## Conclusions and Future Work

The research presented in this thesis addresses the modelling and simulation of long and very long-term dynamics in modern power systems. The thesis proposes various tools to evaluate the impact of different short-term electricity markets formulations on power system stability, and the evolution of solar PVs driven by FIT policy. The aim of this chapter is to summarize the main conclusions of the thesis and outline future work directions.

- *Automatic Generation Control*: Chapters 2 and 3 investigate the effect of discrete secondary controllers on the dynamic response of the system. The research highlights that increasing too much the time interval at which the AGC updates the power set-points of TGs leads to a limit cycle. The only effective solution to remove this issue is to keep as short as possible the AGC time interval. This is not a major constraint as, in practice, the AGC installed in the control centers of TSOs uses execution cycles that vary in the range of 2 to 6 s, which do not create instability issues. However, Chapter 2 shows that if real-time electricity markets or MAGC use the power imbalance to update the electricity price and use dispatch periods that range from some tens of seconds up to a few minutes, these markets might lead to some sort of limit-cycles. There are two ways to avoid the limit cycle. One is to use “short” MAGC time periods, for example, 5 s and the other one is to use “long” MAGC time periods, for example, 10 minutes.

Furthermore, the first case study highlights that ESSs can successfully remove the long-term frequency deviations caused by the MAGC. However, the capacities of

the ESSs as well as the deadband and droop coefficient of the ESS controllers have to be carefully designed to avoid the outbreak of unexpected dynamic behaviors.

The second case study shows that an AGC-based approach yields better dynamic performance than a MILP-based VPP approach. However, despite this advantage, TSOs should consider possible dynamic couplings between the conventional AGC and the AGC-based VPP. Moreover, Chapter 3 demonstrates that accounting for the memory effect of suppliers make the latter adopt a conservative behavior. Therefore, power system operators should consider taking into account such an aspect of market participants in current and future electricity markets. In contrast, the second example shows that the memory of market participants has a negligible impact on power system dynamics due to its intrinsic long timescale.

Future work on this topic can expand in many directions. For example, it would be interesting to study the impact of other relevant discrete secondary controllers of power systems, e.g. the secondary voltage control and hierarchical controllers of microgrids. It is also interesting to further investigate long-term dynamics driven by ESS controllers, e.g. load levelling and shifting and applying the proposed VPP methods to microgrids with a high penetration of DERs. We also aim to study the stability of the equilibriums of the short-term electricity market model with memory, and construct optimization techniques to obtain optimal solutions for the case of existence but not uniqueness of solutions for this system.

- *Unit Commitment*: Chapters 4 and 5 focus on the impact interactions between the sub-hourly d-UC and s-UC and the actual response of the grid. TDSs on the IEEE 39-bus system indicate that shorter scheduling periods of the d-UC and s-UC are to be preferred from the system's dynamic behaviour. This is because they help reduce frequency variations and the electricity price and mitigate the impact of volatility and contingencies. The results of Chapter 5 also show that different s-UC strategies lead to very similar long-term frequency deviations of the system. Then, if the system is scheduled frequently, there are no significant differences between d-UC and s-UC formulations. This is an important information for system operators since they currently mostly rely on deterministic approaches. Moreover, it is demonstrated that in the case of 50% wind penetration, the sub-hourly s-UC leads to a better transient

response of the system compared to the sub-hourly d-UC. Another interesting result is that different formulations of the s-UC can have different impact on long-term power system dynamics. Hence, the formulation of the s-UC has to be carefully chosen. The sensitivity analysis concerning different frequency controllers/machine parameters revealed that the gain of the AGC is the main parameter impacting the long-term frequency deviation. For this reason, such a parameter has to be carefully chosen by TSOs. In contrast, the synchronous machine inertia has a negligible effect on the standard deviation of the frequency.

Future work envisages the design of a feedback control that will take a signal from the system and send it to the UC. Other works will also consider the interaction between UC, microgrids and DAEs. Also, a study on the impact of sub-hourly UC with inclusion of voltage constraints on long-term dynamic behaviour of the system will be considered.

- *PV Energy Policy*: Chapter 6 proposes a dynamic model based on nonlinear delay DAEs to predict the evolution of the solar PVs. The accuracy of the model is validated against historical data of two of the biggest PV markets in the world driven by FIT, namely Italy and Germany. It is shown that the model is able to reproduce with good accuracy the PV data of both countries. In particular, the validation test and the sensitivity analysis shows that the development of the PV markets in Italy and Germany is directly related to FIT levels. Further, it is found that people in Germany had a much higher willingness to install PVs than people in Italy. These results, in fact, support the idea that despite declining investment costs, incentive policies are still required to increase the share of alternative technologies such as solar PV.

A promising direction for future work is validating the model against other energy technologies, such as wind power and electric vehicles. This is particularly relevant considering the uptake of both technologies in recent years. It is also worth comparing the proposed model with the Volterra equations which are well-known to describe the evolution of different system variables such as energy production and consumption [116]. In fact, these equations define S shaped curves similar to the one shown in Fig. 6.1.

# Appendices

# Appendix A

## Data

### A.1 Chapters 2 and 3

This section provides chapters 2 and 3 data. Specifically, DERs data for the MILP-based VPP are given in Tab. A.1. While other relevant data are given in Tab. A.2. In particular,

Table A.1: DERs data for the MILP-based VPP. Based on [14].

Generator	Capacity MW	Response time minute	Ramping time minute
1	0.68	2.73	13.17
2	3.16	6.13	49.61
3	3.74	10.71	39.00
4	1.68	6.91	34.51
5	4.32	1.78	35.49
6	3.89	11.34	28.52
7	1.74	11.23	43.04
8	4.92	9.00	15.14
9	1.02	1.51	4.17
10	4.80	9.48	33.20

the value of initial electricity price  $\rho_o$  is assumed equal to 40 \$/MWh. Moreover, the gain of the AGC and the TG droop parameters are assumed equal to 2 and 0.05 pu(MW), respectively.

Table A.2: Parameters for AGC and MAGC. Based on [6].

Parameter	Description	Unit	Value
$\rho_o$	Initial electricity price	\$/MWh	40
$T_\rho$	Time constant of $\rho(t)$	s	50
$\mathcal{R}$	TG droops	pu(MW)	0.05
$K_o$	AGC feedback gain	-	2
$K_E$	MAGC feedback gain	-	15
$T_{g1}$	Time constant of $\Delta p_{g1}(t)$	s	35
$T_{g2}$	Time constant of $\Delta p_{g2}(t)$	s	30
$T_{g3}$	Time constant of $\Delta p_{g3}(t)$	s	25
$\mathcal{R}_d$	Deviation with respect to a perfect tracking integrator	-	0
$b_{g1}$	Parameter of the marginal cost of the 1 generator	\$/MWh	34
$b_{g2}$	Parameter of the marginal cost of the 2 generator	\$/MWh	35.99
$b_{g3}$	Parameter of the marginal cost of the 3 generator	\$/MWh	35.45
$c_{g1}$	Parameter of the marginal cost of the 1 generator	\$/MW <sup>2</sup> h	0.6
$c_{g2}$	Parameter of the marginal cost of the 2 generator	\$/MW <sup>2</sup> h	0.7
$c_{g3}$	Parameter of the marginal cost of the 3 generator	\$/MW <sup>2</sup> h	0.7

## A.2 Chapters 4 and 5

This section provides d-UC and s-UC data in Tab. A.3 [19]. Since these data do not correspond with that of the dynamic IEEE 39-bus system [57] (e.g. different loading levels), we adapted (scaled) the relevant dynamic data to that of 10-machine UC. Further, the value of load curtailment (present in the reference model of s-UC) is taken equal to \$1000/MWh [23]; the cost of wind is assumed zero; and the value of the fixed ( $C_g^F$ ) and variable ( $C_g^V$ ) cost coefficients is taken equal to the fixed and proportional cost coefficients  $a$  (\$/h) and  $b$  (\$/MWh), respectively, in [18].

Table A.3: d-UC and s-UC parameters. Based on [18,19].

Unit	$P_g^{\max}$ MW	$P_g^{\min}$ MW	$C_g^F$ \$/h	$C_g^V$ \$/MWh	$C_g^{SU}$ \$	$C_g^{SD}$ \$
1	455	150	1,000	16.19	9,000	9,000
2	455	150	970	17.26	10,000	10,000
3	130	20	700	16.60	1,100	1,100
4	130	20	680	16.50	1,120	1,120
5	162	25	450	19.70	1,800	1,800
6	80	20	370	22.26	349	349
7	85	25	480	22.74	520	520
8	55	10	660	25.92	60	60
9	55	10	665	27.27	60	60
10	55	10	670	27.79	60	60

## A.3 Chapter 6

This section provides the information concerning the variables, parameters and data of the model used in the simulation for two countries, namely Italy and Germany in Tables A.4-A.8.

Table A.4: Variables

Variable	Description	Unit	Reference
$\varphi(t)$	PV production	MWh	[104]
$\nu(t)$	Cumulative solar PV production	MWh	[104]
$\vartheta(t)$	PV cost	EUR/MW	[79]
$\Phi(t)$	Cumulative PV installations	MW	This work
$\Theta(t)$	FiT price	EUR/MWh	This work
$w(t)$	Willingness of people to install PVs	-	This work
$\phi(t)$	Function that models FiT price evolution	EUR/MWh	This work
$\chi(t)$	Cumulative expenses to support PV production	EUR	[98]
$\varepsilon(t)$	Cumulative revenue of the FiT fund	EUR	[98]

### Variable Limits

This section presents the limits of the relevant variables of the model.

$$\varphi_{pv}(t) \leq E_G \quad , \quad (\text{A.1})$$

where  $E_G$  represents the total energy generation (assumed to be constant in this work).

$$\begin{aligned} \text{if } \varepsilon(t) &\geq \varepsilon^{\max} & : \varepsilon(t) &= \varepsilon^{\max} \\ \text{if } \varepsilon(t) &\leq \varepsilon^{\min} & : \varepsilon(t) &= \varepsilon^{\min} \\ \text{otherwise} & & : &\text{Eq. (6.3)} \end{aligned} \quad (\text{A.2})$$

where  $\varepsilon^{\min}$  and  $\varepsilon^{\max}$  represent the minimum and maximum FiT fund, respectively.

$$\begin{aligned} \text{if } \Phi(t) &\geq \Phi^{\max} & : \Phi(t) &= \Phi^{\max} \\ \text{if } \Phi(t) &\leq \Phi^{\min} & : \Phi(t) &= \Phi^{\min} \\ \text{otherwise} & & : &\text{Eq. (6.3)} \end{aligned} \quad (\text{A.3})$$

where  $\Phi^{\min}$  and  $\Phi^{\max}$  represent the minimum and maximum PV installed capacity, respectively.

Table A.5: Parameter values, Italy. Based on this work and [1, 104, 112].

Parameter	Description	Unit	Value
Period of analysis	2008-2014	Year	6
$E_G$	Total energy generation	MWh	40,000
$E_C$	Total energy consumption	MWh	39,200
$I$	Reference PV yield	MWh/MW	1,250,000
$P_R$	Performance ratio	%	85
$\beta$	Learning coefficient		0.322
$\vartheta_o$	PV initial cost	MEUR/MW	5
$\Phi_o$	Initial PV MW installed	MW	496
$\Phi^{\max}$	Maximum cumulative PV installations	MW	103,000
$\Phi^{\min}$	Minimum cumulative PV installations	MW	496
$\varepsilon^{\max}$	Maximum PV fund	MEUR	6,700
$\varepsilon^{\min}$	Minimum PV fund	MEUR	0
$\phi^{\max}$	Maximum value of $\phi(t)$	EUR/MWh	450
$\phi^{\min}$	Minimum value of $\phi(t)$	EUR/MWh	0.01
$\phi(t_0)$	Initial value of $\phi(t)$	EUR/MWh	450
$\phi_o$	Disturbance of $\phi(t)$	EUR/MWh	$1.2\phi(t_0)$
$w^{\max}$	Maximum value of $w(t)$		1
$w^{\min}$	Minimum value of $w(t)$		$2 \cdot 10^{-5}$
$T_v$	Time constant of Eq. (6.8)	h	0.25
$T_\Phi$	Time constant of Eq. (6.3)	h	1,667
$T_\phi$	Time constant of Eq. (6.5)	h	14,139
$T_\chi$	Time constant of Eq. (6.9)	h	8
$T_\varepsilon$	Time constant of Eq. (6.10)	h	8
$\rho$	Electricity price	EUR/MWh	200
$L_P$	Levy constant	%	15
$\Theta_o$	Initial FiT price	EUR/MWh	450
$\tau$	Time delay of variable $\phi(t)$	h	13,333

$$\begin{aligned}
 &\text{if } \Theta(t) \geq \Theta^{\max} && : \Theta(t) = \Theta^{\max} \\
 &\text{if } \Theta(t) \leq \Theta^{\min} && : \Theta(t) = \Theta^{\min} \\
 &\text{otherwise} && : \text{Eq. (6.4)},
 \end{aligned} \tag{A.4}$$

where  $\Theta^{\min}$  and  $\Theta^{\max}$  represent the minimum and maximum FiT price, respectively.

$$\begin{aligned}
 &\text{if } \phi(t) \geq \phi^{\max} && : \phi(t) = \phi^{\max} \\
 &\text{if } \phi(t) \leq \phi^{\min} && : \phi(t) = \phi^{\min} \\
 &\text{otherwise} && : \text{Eq. (6.5)},
 \end{aligned} \tag{A.5}$$

where  $\phi^{\min}$  and  $\phi^{\max}$  represent the minimum and maximum value of  $\phi(t)$ , respectively.

Table A.6: PV historical data, Italy. Based on this work and [59, 80, 112].

Year	Capacity MW	Generation GWh	Cost MEUR/MW	Fund MEUR	FiT price EUR/MWh
2008	496	200	5	0	450
2009	1,277	877	4.1	1,340	440
2010	3,605	2,751	2.8	2,680	411
2011	13,141	13,419	2.2	4,020	350
2012	16,796	32,050	1.2	5,360	250
2013	18,197	53,279	0.920	6,700	104
2014	18,606	76,578	0.8	6,700	104

$$\begin{aligned}
 \text{if } w(t) \geq w^{\max} & : w(t) = w^{\max} \\
 \text{if } w(t) \leq w^{\min} & : w(t) = w^{\min} \\
 \text{otherwise} & : \text{Eq. (6.6)},
 \end{aligned} \tag{A.6}$$

where  $w^{\min}$  and  $w^{\max}$  represent the minimum and maximum value of  $w(t)$ , respectively.

Table A.7: Parameter values, Germany. Based on this work and [41, 53, 103].

Parameter	Description	Unit	Value
Period of analysis	2000-2014	Year	14
$E_G$	Total energy generation	MWh	60,000
$E_C$	Total energy consumption	MWh	58,800
$I$	Reference PV yield	MWh/MW	875,000
$P_R$	Performance ratio	%	85
$\beta$	Learning coefficient		0.322
$\vartheta_o$	PV initial cost	MEUR/MW	6.5
$\Phi_o$	Initial PV MW installed	MW	114
$\Phi^{\max}$	Maximum cumulative PV installations	MW	200,000
$\Phi^{\min}$	Minimum cumulative PV installations	MW	114
$\varepsilon^{\max}$	Maximum PV fund	MEUR	-
$\varepsilon^{\min}$	Minimum PV fund	MEUR	0
$\phi^{\max}$	Maximum value of $\phi(t)$	EUR/MWh	500
$\phi^{\min}$	Minimum value of $\phi(t)$	EUR/MWh	0.01
$\phi(t_0)$	Initial value of $\phi(t)$	EUR/MWh	500
$\phi_o$	Disturbance of $\phi(t)$	EUR/MWh	$1.2\phi(t_0)$
$w^{\max}$	Maximum value of $w(t)$		1
$w^{\min}$	Minimum value of $w(t)$		$2 \cdot 10^{-5}$
$T_v$	Time constant of Eq. (6.8)	h	0.28
$T_\Phi$	Time constant of Eq. (6.3)	h	15,972
$T_\phi$	Time constant of Eq. (6.5)	h	83,333
$T_\chi$	Time constant of Eq. (6.9)	h	8
$T_\varepsilon$	Time constant of Eq. (6.10)	h	5
$\rho$	Electricity price	EUR/MWh	150
$L_P$	Levy constant	%	5
$\Theta_o$	Initial FiT price	EUR/MWh	500
$\tau$	Time delay of variable $\phi(t)$	h	8,760

Table A.8: PV historical data, Germany. Based on this work and [7, 10, 103].

Year	Capacity MW	Generation GWh	Cost MEUR/MW	Fund MEUR	FiT price EUR/MWh
2000	114	60	6.5	14	500
2001	176	136	5.0	51	506
2002	296	292	5.0	129	481
2003	435	611	5.0	274	457
2004	1,105	1,168	5.0	540	574
2005	2,056	2,450	5.0	1,176	545
2006	2,899	4,670	5.0	2,266	518
2007	4,170	7,745	5.0	3,729	492
2008	6,120	12,165	5.0	5,689	467
2009	10,556	18,748	4.1	8,365	430
2010	17,994	30,477	2.8	12,830	391
2011	25,429	50,076	2.2	19,468	287
2012	33,033	76,456	1.2	27,407	244
2013	36,337	107,466	0.92	35,683	170
2014	38,236	143,522	0.8	44,849	136

# Bibliography

- [1] a2a, “Italian energy market overview,” 2017. [Online]. Available: <https://s3-eu-west-1.amazonaws.com/a2a-be/a2a/2017-03/Overview-Italian-Energy-Market-2015-2016.pdf> xvi, 153
- [2] AEMO, “AEMO annual report 2018—leading the transformation.” 2018. [Online]. Available: [https://www.aemo.com.au/-/media/files/about\\_aemo/annual-report/aemo-annual-report-2018.pdf](https://www.aemo.com.au/-/media/files/about_aemo/annual-report/aemo-annual-report-2018.pdf) 22
- [3] AEMO, “Australian energy market operator.” 2021. [Online]. Available: <https://www.aemo.com.au/> 3
- [4] H. Ahmadi and H. Ghasemi, “Security-constrained unit commitment with linearized system frequency limit constraints,” *IEEE Trans. on Power Systems*, vol. 29, no. 4, pp. 1536–1545, July 2014. 66
- [5] F. L. Alvarado, “The dynamics of power system markets,” *University of Wisconsin-Madison, Pserc Research Report*, pp. 97–01, 1997. 3, 22, 44
- [6] F. L. Alvarado, J. Meng, C. L. DeMarco, and W. S. Mota, “Stability analysis of interconnected power systems coupled with market dynamics,” *IEEE Transactions on Power Systems*, vol. 16, no. 4, pp. 695–701, Nov 2001. xv, 22, 23, 24, 29, 47, 151
- [7] M. A. Andor, M. Frondel, and C. Vance, “Germany’s energiewende: a tale of increasing costs and decreasing willingness-to-pay,” *The Energy Journal*, vol. 38, no. KAPSARC Special Issue, 2017. xvi, 121, 125, 131, 137, 156
- [8] M. Antonelli and U. Desideri, “Do feed-in tariffs drive PV cost or viceversa?” *Applied Energy*, vol. 135, pp. 721–729, 2014. 120

- [9] D. Apostolopoulou, P. W. Sauer, and A. D. Domínguez-García, “Automatic generation control and its implementation in real time,” in *2014 47th Hawaii International Conference on System Sciences*, 2014, pp. 2444–2452. 14
- [10] J. P. Baginski and C. Weber, “Coherent estimations for residential photovoltaic uptake in Germany including spatial spillover effects,” 2019. [Online]. Available: [https://papers.ssrn.com/sol3/papers.cfm?abstract\\_id=3357359](https://papers.ssrn.com/sol3/papers.cfm?abstract_id=3357359) xvi, 156
- [11] D. Baleanu, J. A. T. Machado, and A. C. Luo, *Fractional Dynamics and Control*. Springer Science & Business Media, 2011. 45
- [12] J. Barquín, “The new Spanish electricity market design,” in *Enerday 2014 – 9th Conference on Energy Economics and Technology*, 2014, pp. 1–10. 31
- [13] I. M. Batiha, R. El-Khazali, A. AlSaedi, and S. Momani, “The general solution of singular fractional-order linear time-invariant continuous systems with regular pencils,” *Entropy*, vol. 20, no. 6, 2018. 49
- [14] P. Beagon, M. D. Bustamante, M. T. Devine, S. Fennell, J. Grant-Peters, C. Hall, R. Hill, T. Kërçi, and G. O’Keefe, “Optimal scheduling of distributed generation to achieve linear aggregate response,” in *Proceedings from the 141st European Study Group with Industry*, June 2018, pp. 1–61. xv, 39, 40, 150
- [15] S. Bigerna and P. Polinori, “Assessing the determinants of renewable electricity acceptance integrating meta-analysis regression and a local comprehensive survey,” *Sustainability*, vol. 7, no. 9, pp. 11 909–11 932, 2015. 126
- [16] I. Blanco and J. M. Morales, “An efficient robust solution to the two-stage stochastic unit commitment problem,” *IEEE Transactions on Power Systems*, vol. 32, no. 6, pp. 4477–4488, Nov 2017. 84, 87, 90
- [17] F. Bouffard and F. D. Galiana, “Stochastic security for operations planning with significant wind power generation,” *IEEE Transactions on Power Systems*, vol. 23, no. 2, pp. 306–316, May 2008. 81
- [18] M. Carrión and J. M. Arroyo, “A computationally efficient mixed-integer linear formulation for the thermal unit commitment problem,” *IEEE Transactions on Power Systems*, vol. 21, no. 3, pp. 1371–1378, Aug 2006. xv, 66, 77, 95, 151

- [19] Y. Chen, F. Liu, W. Wei, S. Mei, and N. Chang, “Robust unit commitment for large-scale wind generation and run-off-river hydropower,” *CSEE Journal of Power and Energy Systems*, vol. 2, no. 4, pp. 66–75, Dec. 2016. xv, 71, 151
- [20] W. Chiu, H. Sun, and H. V. Poor, “Energy imbalance management using a robust pricing scheme,” *IEEE Transactions on Smart Grid*, vol. 4, no. 2, pp. 896–904, 2013. 3
- [21] A. Ciarreta, M. P. Espinosa, and C. Pizarro-Irizar, “Is green energy expensive? empirical evidence from the Spanish electricity market,” *Energy Policy*, vol. 69, pp. 205–215, 2014. 139
- [22] A. Conejo and L. Baringo, *Power System Operations*. Springer International Publishing, 2017. 66
- [23] A. Conejo, M. Carrión, and J. Morales, *Decision Making Under Uncertainty in Electricity Markets*. Springer, 2010. 81, 84, 86, 151
- [24] M. Costley, M. J. Feizollahi, S. Ahmed, and S. Grijalva, “A rolling-horizon unit commitment framework with flexible periodicity,” *I. J. of Electrical Power & Energy Systems*, vol. 90, pp. 280 – 291, 2017. 94, 109
- [25] P. Daly, D. Flynn, and N. Cunniffe, “Inertia considerations within unit commitment and economic dispatch for systems with high non-synchronous penetrations,” in *IEEE PowerTech*, June 2015, pp. 1–6. 66
- [26] I. Dassios, “Stability and robustness of singular systems of fractional nabla difference equations,” *Circuits, Systems, and Signal Processing*, vol. 36, no. 1, pp. 49 – 64, 2017. 50
- [27] I. Dassios and D. Baleanu, “Caputo and related fractional derivatives in singular systems,” *Applied Mathematics and Computation*, vol. 337, pp. 591–606, 2018. 49, 52
- [28] I. Dassios, T. Kërçi, and F. Milano, “Fractional-order dynamical model for electricity markets,” *Mathematical Methods in the Applied Sciences*, Wiley, 2021. 45

- [29] I. Dassios, G. Tzounas, and F. Milano, “Generalized fractional controller for singular systems of differential equations,” *Journal of Computational and Applied Mathematics*, vol. 378, p. 112919, 2020. 52
- [30] J. P. Deane, G. Drayton, and B. Ó Gallachóir, “The impact of sub-hourly modelling in power systems with significant levels of renewable generation,” *Applied Energy*, vol. 113, pp. 152 – 158, 2014. 66
- [31] S. Delikaraoglou, A. Papakonstantinou, C. Ordoudis, and P. Pinson, “Price-maker wind power producer participating in a joint day-ahead and real-time market,” in *2015 12th International Conference on the European Energy Market (EEM)*, 2015, pp. 1–5. 31
- [32] V. Di Dio, S. Favuzza, D. La Cascia, F. Massaro, and G. Zizzo, “The evolution of the FIT mechanism in Italy for PV systems: A critical analysis,” in *2013 International Conference on Renewable Energy Research and Applications (ICRERA)*, 2013, pp. 890–895. 121
- [33] R. Doherty, G. Lalor, and M. O’Malley, “Frequency control in competitive electricity market dispatch,” *IEEE Trans. on Power Systems*, vol. 20, no. 3, pp. 1588–1596, Aug 2005. 66
- [34] EirGrid & SONI, “Balancing Market Principles Statement. A Guide to Scheduling and Dispatch in the Single Electricity Market,” 2020. [Online]. Available: [https://www.eirgridgroup.com/site-files/library/EirGrid/EirGrid-and-SONI-Balancing-Market-Principles-Statement-V4-0-\(final\).pdf](https://www.eirgridgroup.com/site-files/library/EirGrid/EirGrid-and-SONI-Balancing-Market-Principles-Statement-V4-0-(final).pdf) 25
- [35] EirGrid Group, “System and Renewable Data.” [Online]. Available: <http://www.eirgridgroup.com/how-the-grid-works/renewables/> 88
- [36] A. M. Elshurafa, S. R. Albardi, S. Bigerna, and C. A. Bollino, “Estimating the learning curve of solar PV balance-of-system for over 20 countries: Implications and policy recommendations,” *Journal of Cleaner Production*, vol. 196, pp. 122–134, 2018. 134
- [37] ENTSO-E, “An overview of the european balancing market and electricity balancing guideline,” 2018. [Online]. Available: <https://eepublicdownloads.entsoe.eu/clean-do>

cuments/Network%20codes%20documents/NC%20EB/entso-e\_balancing\_in%20\_europe\_report\_Nov2018\_web.pdf 3

- [38] ENTSO-E, “Continental Europe significant frequency deviations – January 2019 ,” 2019. [Online]. Available: [https://eepublicdownloads.entsoe.eu/clean-documents/news/2019/190522\\_SOC\\_TOP\\_11.6\\_Task%20Force%20Significant%20Frequency%20Deviations\\_External%20Report.pdf](https://eepublicdownloads.entsoe.eu/clean-documents/news/2019/190522_SOC_TOP_11.6_Task%20Force%20Significant%20Frequency%20Deviations_External%20Report.pdf) 3, 96
- [39] EPEX SPOT, “Trading on EPEX spot 2019-2020,” 2020. [Online]. Available: [https://www.epexspot.com/sites/default/files/download\\_center\\_files/Trading%20Brochure.pdf](https://www.epexspot.com/sites/default/files/download_center_files/Trading%20Brochure.pdf) 24
- [40] G. C. Evans, *Mathematical introduction to economics*. New York: McGraw-Hill, 1930. 45
- [41] Fraunhofer ISE, “Energy-charts,” 2021. [Online]. Available: <https://energy-charts.info/index.html?l=en&c=DE> xvi, 132, 155
- [42] Y. Fu, Z. Li, and L. Wu, “Modeling and solution of the large-scale security-constrained unit commitment,” *IEEE Trans. on Power Systems*, vol. 28, no. 4, pp. 3524–3533, Nov 2013. 65
- [43] Y. Fu, M. Shahidehpour, and Z. Li, “Security-constrained unit commitment with ac constraints,” *IEEE Trans. on Power Systems*, vol. 20, no. 3, pp. 1538–1550, Aug 2005. 66
- [44] H. Gangammanavar, S. Sen, and V. M. Zavala, “Stochastic optimization of sub-hourly economic dispatch with wind energy,” *IEEE Transactions on Power Systems*, vol. 31, no. 2, pp. 949–959, Mar 2016. 66
- [45] R. F. Gantmacher, *The Theory of Matrices I, II*. New York: Chelsea, 1959. 53
- [46] A. Gómez Expósito, A. J. Conejo, and C. Cañizares, *Electric energy systems: analysis and operation*. CRC press, 2018. ix, 1, 2, 91, 93
- [47] Y. Gu and L. Xie, “Stochastic look-ahead economic dispatch with variable generation resources,” *IEEE Transactions on Power Systems*, vol. 32, no. 1, pp. 17–29, 2017. 81

- [48] X. Guo and X. Guo, “China’s photovoltaic power development under policy incentives: A system dynamics analysis,” *Energy*, vol. 93, pp. 589–598, 2015. 144
- [49] L. Gurobi Optimization, “Gurobi optimizer reference manual.” [Online]. Available: <http://www.gurobi.com> 7
- [50] A. Held, M. Ragwitz, C. Huber, G. Resch, T. Faber, and K. Vertin, “Feed-in systems in Germany, Spain and Slovenia: A comparison,” *International Feed-in Cooperation*, 2007. 121
- [51] E. Hillberg, A. Zegers, B. Herndler, S. Wong, J. Pompee, J.-Y. Bourmaud, S. Lehnhoff, G. Migliavacca, K. Uhlen, I. Oleinikova, H. Pihl, M. Norström, M. Persson, J. Rossi, and G. Beccuti, “Flexibility needs in the future power system,” ISGAN, Tech. Rep., 2019, discussion paper. 66
- [52] J. Hoppmann, J. Huenteler, and B. Girod, “Compulsive policy-making-The evolution of the German feed-in tariff system for solar photovoltaic power,” *Research Policy*, vol. 43, no. 8, pp. 1422–1441, 2014. 121
- [53] C.-W. Hsu, “Using a system dynamics model to assess the effects of capital subsidies and feed-in tariffs on solar PV installations,” *Applied Energy*, vol. 100, pp. 205 – 217, 2012, clean Energy for Future Generations. xvi, 123, 124, 134, 144, 155
- [54] M. Håberg, “Fundamentals and recent developments in stochastic unit commitment,” *International Journal of Electrical Power & Energy Systems*, vol. 109, pp. 38–48, 2019. 90
- [55] A. Ibanez-Lopez, J. Martinez-Val, and B. Moratilla-Soria, “A dynamic simulation model for assessing the overall impact of incentive policies on power system reliability, costs and environment,” *Energy Policy*, vol. 102, pp. 170 – 188, 2017. 2, 119, 144, 145
- [56] IEA-WIND, “Design and operation of power systems with large amounts of wind power,” 2019. [Online]. Available: <https://www.vttresearch.com/sites/default/files/pdf/technology/2019/T350.pdf> 83
- [57] Illinois Center for a Smarter Electric Grid (ICSEG), “IEEE 39-Bus System,” URL: <http://publish.illinois.edu/smartergrid/ieee-39-bus-system/>. 29, 71, 77, 94, 151

- [58] Illinois Center for a Smarter Electric Grid (ICSEG), “WSCC 9-Bus System,” URL: <http://publish.illinois.edu/smartergrid/wsc-9-bus-system/>. 16
- [59] IRENA, “Renewable power generation costs in 2014,” 2015. [Online]. Available: [https://irena.org/-/media/Files/IRENA/Agency/Publication/2015/IRENA\\_RE\\_Power\\_Costs\\_2014\\_report.pdf](https://irena.org/-/media/Files/IRENA/Agency/Publication/2015/IRENA_RE_Power_Costs_2014_report.pdf) xvi, 154
- [60] S. A. Kazarlis, A. G. Bakirtzis, and V. Petridis, “A genetic algorithm solution to the unit commitment problem,” *IEEE Trans. on Power Systems*, vol. 11, no. 1, pp. 83–92, Feb 1996. 77
- [61] T. Kërçi, M. T. Devine, M. A. A. Murad, and F. Milano, “Impact of the aggregate response of distributed energy resources on power system dynamics,” in *2020 IEEE Power Energy Society General Meeting (PESGM)*, 2020, pp. 1–5. 39, 40
- [62] T. Kërçi and F. Milano, “A framework to embed the unit commitment problem into time domain simulations,” in *IEEE International Conference on Environment and Electrical Engineering*, June 2019, pp. 1–5. 82
- [63] T. Kërçi and F. Milano, “Sensitivity analysis of the interaction between power system dynamics and unit commitment,” in *2019 IEEE Milan PowerTech*, 2019, pp. 1–6. 82
- [64] T. Kërçi, M. A. A. Murad, I. Dassios, and F. Milano, “On the impact of discrete secondary controllers on power system dynamics,” *IEEE Transactions on Power Systems*, pp. 1–1, 2021. 48, 57
- [65] T. Kërçi, G. Tzounas, I. Dassios, M. A. A. Murad, and F. Milano, “A short-term dynamic electricity market model with memory effect,” in *2021 IEEE Power Energy Society General Meeting (PESGM)*, 2021, pp. 1–5. 45
- [66] T. Kërçi, J. Giraldo, and F. Milano, “Analysis of the impact of sub-hourly unit commitment on power system dynamics,” *International Journal of Electrical Power & Energy Systems*, vol. 119, p. 105819, 2020. 26, 109
- [67] J. Kiviluoma, M. O’Malley, A. Tuohy, P. Meibom, M. Milligan, B. Lange, H. Holttinen, and M. Gibescu, “Impact of wind power on the unit commitment,

- operating reserves, and market design,” in *IEEE PES General Meeting*, July 2011, pp. 1–8. 66, 69
- [68] P. Kundur, *Power System Stability and Control*. New York: McGraw-Hill, 1994. 39, 83
- [69] P. Kundur, J. Paserba, V. Ajjarapu, G. Andersson, A. Bose, C. Cañizares, N. Hatziargyriou, D. Hill, A. Stankovic, C. Taylor, T. Van Cutsem, and V. Vittal, “Definition and classification of power system stability IEEE/CIGRE joint task force on stability terms and definitions,” *IEEE Transactions on Power Systems*, vol. 19, no. 3, pp. 1387–1401, Aug 2004. 82
- [70] T. Kërçi, J. S. Giraldo, and F. Milano, “Sensitivity analysis of the impact of the sub-hourly stochastic unit commitment on power system dynamics,” *Energies*, vol. 13, no. 6, 2020. 108
- [71] E. Lannoye, D. Flynn, and M. O’Malley, “Evaluation of power system flexibility,” *IEEE Transactions on Power Systems*, vol. 27, no. 2, pp. 922–931, 2012. 3
- [72] P. Lazzeroni, S. Olivero, and M. Repetto, “Economic perspective for PV under new Italian regulatory framework,” *Renewable and Sustainable Energy Reviews*, vol. 71, pp. 283–295, 2017. 120, 139, 145
- [73] Y. Lee and R. Baldick, “A frequency-constrained stochastic economic dispatch model,” *IEEE Trans. on Power Systems*, vol. 28, no. 3, pp. 2301–2312, Aug 2013. 66
- [74] C. Leepa and M. Unfried, “Effects of a cut-off in feed-in tariffs on photovoltaic capacity: Evidence from Germany,” *Energy Policy*, vol. 56, pp. 536–542, 2013. 121
- [75] M. D. Leiren and I. Reimer, “Historical institutionalist perspective on the shift from feed-in tariffs towards auctioning in german renewable energy policy,” *Energy Research & Social Science*, vol. 43, pp. 33–40, 2018. 121
- [76] I. D. López, D. Flynn, M. Desmartin, M. Saguan, and T. Hinchliffe, “Drivers for sub-hourly scheduling in unit commitment models,” in *IEEE PES General Meeting*, Aug 2018, pp. 1–5. 66

- [77] J. Luo, F. Teng, and S. Bu, “Stability-constrained power system scheduling: A review,” *IEEE Access*, vol. 8, pp. 219 331–219 343, 2020. 66
- [78] I. MacGill, “Electricity market design for facilitating the integration of wind energy: Experience and prospects with the Australian national electricity market,” *Energy Policy*, vol. 38, no. 7, pp. 3180 – 3191, 2010. 3, 94, 101
- [79] A. MacGillivray, H. Jeffrey, M. Winkler, and I. Bryden, “Innovation and cost reduction for marine renewable energy: A learning investment sensitivity analysis,” *Technological Forecasting and Social Change*, vol. 87, pp. 108–124, 2014. 122, 152
- [80] A. Mahalingam and D. Reiner, “Energy subsidies at times of economic crisis: A comparative study and scenario analysis of Italy and Spain,” *Cambridge Working Paper in Economics*, 2016. xvi, 154
- [81] A. Masini and E. Menichetti, “The impact of behavioural factors in the renewable energy investment decision making process: Conceptual framework and empirical findings,” *Energy Policy*, vol. 40, pp. 28–38, 2012. 124
- [82] L. Meegahapola, P. Mancarella, D. Flynn, and R. Moreno, “Power system stability in the transition to a low carbon grid: A techno-economic perspective on challenges and opportunities,” *WIREs Energy and Environment*, p. e399, 2021. 3
- [83] F. M. Mele, Á. Ortega, R. Zárate-Miñano, and F. Milano, “Impact of variability, uncertainty and frequency regulation on power system frequency distribution,” in *2016 Power Systems Computation Conference (PSCC)*, Jun. 2016, pp. 1–8. 78
- [84] F. Milano, *Power System Modelling and Scripting*. London: Springer, 2010. 13, 15, 83
- [85] F. Milano, “A Python-based software tool for power system analysis,” in *2013 IEEE Power Energy Society General Meeting*, 2013, pp. 1–5. 7, 71
- [86] F. Milano, F. Dörfler, G. Hug, D. J. Hill, and G. Verbič, “Foundations and challenges of low-inertia systems (invited paper),” in *Power Systems Computation Conference (PSCC)*, June 2018, pp. 1–25. 14, 66, 81

- [87] F. Milano and R. Zárate-Miñano, “A systematic method to model power systems as stochastic differential algebraic equations,” *IEEE Transactions on Power Systems*, vol. 28, no. 4, pp. 4537–4544, Nov 2013. 75, 82, 83
- [88] F. Milano and Á. Ortega, *Converter-Interfaced Energy Storage Systems: Context, Modelling and Dynamic Analysis*. Cambridge University Press, 2019. 32
- [89] C. A. Monje, Y. Chen, B. M. Vinagre, D. Xue, and V. Feliu, *Fractional-order Systems and Controls, Fundamentals and Applications*. Springer, 2010. 57, 58
- [90] J. M. Morales, A. J. Conejo, and J. Perez-Ruiz, “Economic valuation of reserves in power systems with high penetration of wind power,” in *IEEE PES General Meeting*, July 2009, pp. 1–1. 87, 99
- [91] G. Morales-España, J. M. Latorre, and A. Ramos, “Tight and compact milp formulation for the thermal unit commitment problem,” *IEEE Transactions on Power Systems*, vol. 28, no. 4, pp. 4897–4908, Nov 2013. 40
- [92] S. Movilla, L. J. Miguel, and L. F. Blázquez, “A system dynamics approach for the photovoltaic energy market in Spain,” *Energy Policy*, vol. 60, pp. 142–154, 2013. 4
- [93] J. Nutaro and V. Protopopescu, “The impact of market clearing time and price signal delay on the stability of electric power markets,” *IEEE Transactions on Power Systems*, vol. 24, no. 3, pp. 1337–1345, 2009. 23
- [94] Á. Ortega and F. Milano, “Generalized model of VSC-based energy storage systems for transient stability analysis,” *IEEE Transactions on Power Systems*, vol. 31, no. 5, pp. 3369–3380, 2016. 32
- [95] V. Pandurangan, H. Zareipour, and O. Malik, “Frequency regulation services: A comparative study of select north american and european reserve markets,” in *2012 North American Power Symposium (NAPS)*, 2012, pp. 1–8. 14, 15
- [96] V. Pavlovsky and A. Steliuk, *Modeling of Automatic Generation Control in Power Systems*. Cham: Springer International Publishing, 2014, pp. 157–173. 16
- [97] K. Poplavskaya, J. Lago, S. Strömer, and L. de Vries, “Making the most of short-term flexibility in the balancing market: Opportunities and challenges of voluntary

bids in the new balancing market design,” *Energy Policy*, vol. 158, p. 112522, 2021.

44

- [98] A. Pyrgou, A. Kylili, and P. A. Fokaides, “The future of the feed-in tariff (FiT) scheme in Europe: The case of photovoltaics,” *Energy Policy*, vol. 95, pp. 94–102, 2016. 121, 125, 133, 139, 152
- [99] Y. G. Rebours, D. S. Kirschen, M. Trotignon, and S. Rossignol, “A survey of frequency and voltage control ancillary services—Part I: Technical features,” *IEEE Transactions on Power Systems*, vol. 22, no. 1, pp. 350–357, 2007. 15, 24
- [100] S. Saberi Oskouee, S. Kamali, and T. Amraee, “Primary frequency support in unit commitment using a multi-area frequency model with flywheel energy storage,” *IEEE Transactions on Power Systems*, pp. 1–1, 2021. 66
- [101] G. Scerrato, “Solar PV feed-in tariff: the distortion of Italian power market,” in *XX Summer School ”Francesco Turco” - Industrial Systems Engineering*, 2015, pp. 1–10. 120, 137
- [102] B. Schafer, M. Timme, and D. Witthaut, “Isolating the impact of trading on grid frequency fluctuations,” in *2018 IEEE PES Innovative Smart Grid Technologies Conference Europe (ISGT-Europe)*, 2018, pp. 1–5. 96
- [103] H. Schwarz, H. Schermeyer, V. Bertsch, and W. Fichtner, “Self-consumption through power-to-heat and storage for enhanced PV integration in decentralised energy systems,” *Solar Energy*, vol. 163, pp. 150–161, 2018. xvi, 155, 156
- [104] F. Spertino, P. Di Leo, and V. Cocina, “Economic analysis of investment in the rooftop photovoltaic systems: A long-term research in the two main markets,” *Renewable and Sustainable Energy Reviews*, vol. 28, pp. 531–540, 2013. xvi, 121, 124, 134, 152, 153
- [105] T. Stegink, C. De Persis, and A. van der Schaft, “A unifying energy-based approach to stability of power grids with market dynamics,” *IEEE Transactions on Automatic Control*, vol. 62, no. 6, pp. 2612–2622, 2017. 3

- [106] H. Sun, Y. Zhang, D. Baleanu, W. Chen, and Y. Chen, “A new collection of real world applications of fractional calculus in science and engineering,” *Communications in Nonlinear Science and Numerical Simulation*, vol. 64, pp. 213–231, 2018. 45
- [107] V. E. Tarasov, “Generalized memory: Fractional calculus approach,” *Fractal and Fractional*, vol. 2, no. 4, p. 23, 2018. 44
- [108] V. E. Tarasov, “On history of mathematical economics: Application of fractional calculus,” *Mathematics*, vol. 7, no. 6, p. 509, 2019. 44
- [109] V. E. Tarasov, “Fractional econophysics: Market price dynamics with memory effects,” *Physica A: Statistical Mechanics and its Applications*, vol. 557, p. 124865, 2020. 45, 47
- [110] V. V. Tarasova and V. E. Tarasov, “Concept of dynamic memory in economics,” *Communications in Nonlinear Science and Numerical Simulation*, vol. 55, pp. 127 – 145, 2018. 44
- [111] F. Teng, V. Trovato, and G. Strbac, “Stochastic scheduling with inertia-dependent fast frequency response requirements,” *IEEE Transactions on Power Systems*, vol. 31, no. 2, pp. 1557–1566, March 2016. 66
- [112] F. Tilli and G. Maugeri, “National survey report of PV power applications in Italy,” 2018. [Online]. Available: [https://iea-pvps.org/wp-content/uploads/2020/01/NSR.Italy\\_2018.pdf](https://iea-pvps.org/wp-content/uploads/2020/01/NSR.Italy_2018.pdf) xvi, 132, 153, 154
- [113] N. Troy, D. Flynn, and M. O’Malley, “The importance of sub-hourly modeling with a high penetration of wind generation,” in *IEEE PES General Meeting*, July 2012, pp. 1–6. 66, 73
- [114] A. Tuohy, P. Meibom, E. Denny, and M. O’Malley, “Unit commitment for systems with significant wind penetration,” *IEEE Transactions on Power Systems*, vol. 24, no. 2, pp. 592–601, May 2009. 81, 90
- [115] G. Tzounas, I. Dassios, M. A. A. Murad, and F. Milano, “Theory and implementation of fractional order controllers for power system applications,” *IEEE Trans. on Power Systems*, vol. 35, no. 6, pp. 4622–4631, 2020. 49, 58

- [116] R. Vacca, “Forecasting growths and declines with Volterra equations,” 2014. [Online]. Available: [https://www.academia.edu/4238459/Forecasting\\_Growths\\_and\\_Declines\\_with\\_Volterra\\_Equations](https://www.academia.edu/4238459/Forecasting_Growths_and_Declines_with_Volterra_Equations) 148
- [117] R. Villanueva, P. C. d. Granado, I. Oleinikova, and H. Farahmand, “A minute-to-minute unit commitment model to analyze generators performance,” in *2019 16th International Conference on the European Energy Market (EEM)*, 2019, pp. 1–6. 66
- [118] P. Vorobev, D. M. Greenwood, J. H. Bell, J. W. Bialek, P. C. Taylor, and K. Turitsyn, “Deadbands, droop, and inertia impact on power system frequency distribution,” *IEEE Trans. on Power Systems*, vol. 34, no. 4, pp. 3098–3108, July 2019. 110
- [119] R. Wand and F. Leuthold, “Feed-in tariffs for photovoltaics: Learning by doing in Germany?” *Applied Energy*, vol. 88, no. 12, pp. 4387–4399, 2011. 121, 122
- [120] B. Wang and B. F. Hobbs, “Real-time markets for flexiramp: A stochastic unit commitment-based analysis,” *IEEE Transactions on Power Systems*, vol. 31, no. 2, pp. 846–860, 2016. 81
- [121] J. Wang, M. Shahidehpour, and Z. Li, “Security-constrained unit commitment with volatile wind power generation,” *IEEE Transactions on Power Systems*, vol. 23, no. 3, pp. 1319–1327, Aug 2008. 88
- [122] Q. Wang, C. Zhang, Y. Ding, G. Xydis, J. Wang, and J. Østergaard, “Review of real-time electricity markets for integrating distributed energy resources and demand response,” *Applied Energy*, vol. 138, pp. 695 – 706, 2015. 58
- [123] X. Wang, H. Chiang, J. Wang, H. Liu, and T. Wang, “Long-term stability analysis of power systems with wind power based on stochastic differential equations: Model development and foundations,” *IEEE Transactions on Sustainable Energy*, vol. 6, no. 4, pp. 1534–1542, 2015. 82
- [124] D. Watts and F. L. Alvarado, “The influence of futures markets on real time price stabilization in electricity markets,” in *Procs. of the 37th Annual Hawaii Int. Conf. on System Sciences*, 2004, pp. 1–7. 59
- [125] T. P. Wright, “Factors affecting the cost of airplanes,” *Journal of the aeronautical sciences*, vol. 3, no. 4, pp. 122–128, 1936. 122

- [126] K. Yamashita *et al.*, “Modelling of inverter-based generation for power system dynamic studies,” *CIGRE, Technical Brochure C*, vol. 4, May 2018. 81, 106
- [127] B. Yuan, M. Zhou, G. Li, and X. Zhang, “Stochastic small-signal stability of power systems with wind power generation,” *IEEE Transactions on Power Systems*, vol. 30, no. 4, pp. 1680–1689, 2015. 82
- [128] M. Zhang, Z. Yang, W. Lin, J. Yu, W. Dai, and E. Du, “Enhancing economics of power systems through fast unit commitment with high time resolution,” *Applied Energy*, vol. 281, p. 116051, 2021. 66
- [129] Q. P. Zheng, J. Wang, and A. L. Liu, “Stochastic optimization for unit commitment—A review,” *IEEE Transactions on Power Systems*, vol. 30, no. 4, pp. 1913–1924, 2015. 91, 114